Republic of Iraq
Ministry of Higher Education
& Scientific Research
University of Baghdad
College of Education for pure science
Ibn-Al-Haitham

New Study for Nanocomposite Hydrogels for Biomedical Applications and Drug Delivery: Synthesis, Characterizations and Electrical Properties

A Thesis
Submitted to the College of Education
(Ibn-AL-Haitham) University of Baghdad
in Partial Fulfillment of the Requirements
for the Degree of Ph.D. of Science in Chemistry

By
Ma'ida Hameed Saleem
B.Sc.In Chemistry 2003
M.Sc. In Chemistry 2012
University of Baghdad

Supervisors
Ass. Prof. Dr. Issam Abdulkreem
Ass. Prof. Dr. Hilal M. Abdullah

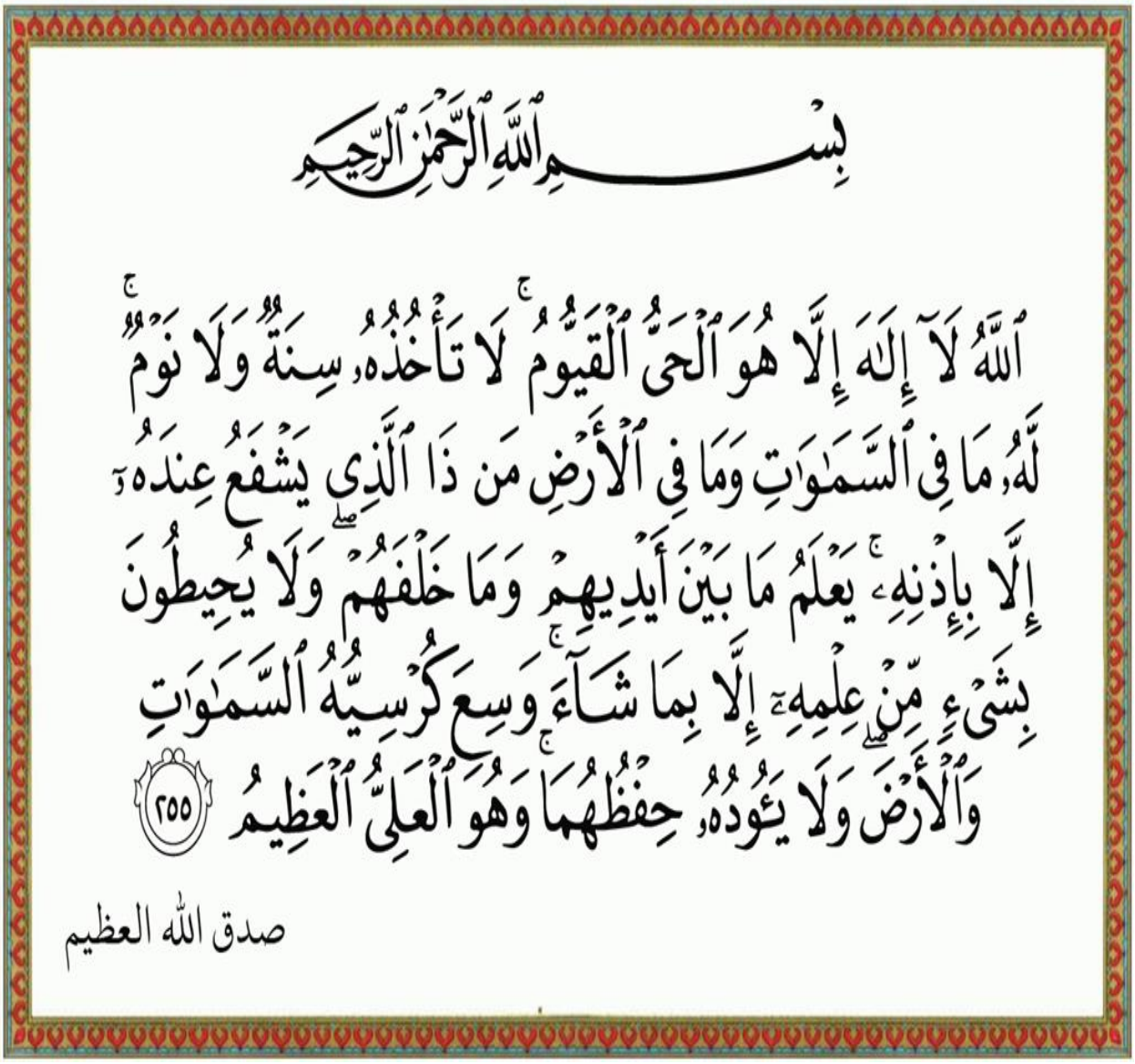

(آية الكرسي، سورة البقرة)

Supervisors Certification

We certify that this thesis was prepared under our supervision at Department of Chemistry, College of Education for Pure Science (Ibn Al-Haitham) Baghdad University, as a partial fulfillment of the requirements for the Degree of Doctor of philosophy in Science Chemistry.

Supervisor:
Signature:
Asst. Prof. Dr. Issam Abdulkreem
Date : / / 2016

Supervisor:
Signature:
Asst. Prof. Dr. Hilal M.Abdullah
Date : / / 2016

In View of the available recommendation, I forward this thesis for debate by examination committee.

Signature:
Asst. Prof. Dr. Najwa Issac Abdulla
Head of Department of Chemistry
Date : / / 2016

Examination Committee Certification

We chairman and members of the discussion committee, certify that we have studied this thesis "**New Study for Nanocomposite Hydrogels for Biomedical Applications and Drug Delivery: Synthesis, Characterizations and Electrical Properties**" presented by the student (**Ma′ida Hameed Saleem)** and examined her in it's contents and that, we have found its worthy to be accepted for the Degree of Doctor of Philosophy of Science in chemistry with (Excellent)

Signature:
Chairman**: Prof. Dr. Emaad T. Bakir**
Date: / /2016

Signature:
Prof. Dr. Najat J. Saleh
(Member)
Date: / /2016

Signature:
Prof. Dr. Khalid F. Ali
(Member)
Date: / /2016

Signature:
Assist. Prof. Dr. Maha T. Sultan
(Member)
Date: / /2016

Signature:
Assist. Prof. Dr. Nada E. Fairouz
(Member)
Date: / /2016

Signature:
Assist. Prof. Dr. Issam Abdulkreem
(Supervisor)
Date: / /2016

Signature:
Assist. Prof. Dr. Hilal M. Abdullah
(Supervisor)
Date: / /2016

I have certified upon the decision of the discussion committee
Signature:
Name: **Prof. Dr. Khalid F. Ali**
Address: Dean of the College of Education for Pure Science (Ibn Al-Haitham)
University of Baghdad
Date: / /2016

ACKNOWLEDGEMENTS

First of all, I acknowledge my deep gratitude to the clement Allah for his blessing, benefaction, and generosity.

I wish to express my gratitude to my supervisors Ass. Prof. Dr. Issam Abdulkreem and Ass. Prof. Dr. Hilal M. Abdullah for suggesting the problem and their continued support, advice and encouragement.

Sincerely thanks are also to Dean of College of Education for Pure Science Ibn Al-Haitham and the Head of Chemistry Department.

My thanks to all the staff members of Chemistry Department at College of Education for Pure Science Ibn Al-Haitham.

My thanks to all the staff members of The Central Service Laboratory at College of Education for Pure Science Ibn Al-Haitham.

I thank all my friends who helped me during the time of my study especially (Azhar Farouq) and (Zainab Abbas).

Finally, I am deeply indebted to my family for their support and patience during the years of my study.

Ma'ida

DEDICATIONS

This thesis is dedicated

To all those who

Supported me, helped me

To end this thesis dedicate them the fruit my hard work of humble with high respect and

Appreciation

Ma'ida

CONTENTS

LIST OF FIGURES

LIST OF SCHEMES

LIST OF TABLES

ABSTRACT

Six different hydrogels were prepared and they were ; (CPG) from crosslinking between chitosan and poly(vinyl alcohol)by glutaraldehyde as crosslinker agent, (CPM) from crosslinking between chitosan and poly (vinyl alcohol) by maleic anhydride, (PPM) from also crosslinking between pectin and poly (vinyl alcohol) by maleic anhydride, (PgA) by grafted polymerization of acrylic acid monomer on poly(vinyl alcohol) backbone under N_2 with free radical polymerization, (CgA) synthesis with same method by grafted polymerization of acryl amide monomer on chitosan backbone , and (IPN) by interpenetrating chitosan-poly(acrylic acid-co-acryl amide)hydrogel. The thermal properties of hydrogel were studied by Thermogravimetric Analysis (TGA), Differential Scanning Calorimetry (DSC), and characterization by Fourier Transform Infrared Spectroscopy (FTIR), X-ray diffraction (XRD), and used Atomic Force Microscopy(AFM) for studying surface topography.

Conductive poly aniline was prepared by oxidation of aniline with ammonium persulfate and different nanomatrials were prepared which include, graphene oxide nanosheets (GO) was prepared by Hummer's method by oxidation of graphite with concentrated H_2SO_4, $NaNO_3$, $KMnO_4$. Graphene nanosheets (G) were prepared by reduction GO with hydrazine hydride. Fe_3O_4 MNPs was prepared by co-precipitation method followed by coating with conductive hydrogel (CPG/PANI) which synthesis from crosslinking between chitosan and poly (vinyl alcohol) by glutaraldehyde as crosslinker agent to form (CPG) hydrogel during poly aniline (PANI) polymerization. The coated form (CPG/Fe_3O_4/PANI) was obtained. This coated magnetite form (CPG/Fe_3O_4/PANI) has magnetic-electro sensitive. Fe_3O_4 MNPs pure and coated form (CPG/Fe_3O_4/PANI) were characterized by

XRD, TEM, SEM, AFM & EDS. The average size of nanoparticles was found to be about (11-13) nm for uncoated and (12-14)nm for coated forms. Magnetic properties were studied for coated and uncoated magnetite by vibrating sample magnetometer (VSM) for study hysteresis loop, the hysteresis loop is completely reversible, the hysteresis has an "S" shape where both the descending and ascending loops coincide and yield zero coercivity, indicating that the magnetite nanoparticles are superparamagnetic .

Also multiwall carbon nanotube (MWCNTs) was purchased from CheapTubes Company to prepared conductive hydrogel composite.

Then was prepared the conductive hydrogels composite which include (hydrogel/PANI), (hydrogel/G) and (hydrogel/MWCNTs). All of hydrogels and hydrogel composite were characterized by FTIR spectroscopy, X-ray diffraction, AFM and some nanocomposite was characterization by SEM.

Hydrogel and hydrogel composite were swelled with water at different periods. It was found the PgA hydrogel has the highest degree of swelling equals to S=15.1314, for PANI composite, the PPM/PANI hydrogels composite has the highest degree of swelling (S= 2.2515), for G composite, the PPM/G has the highest degree of swelling (S=5.1151), for MWCNTs composite, the PPM/MWCNTs has the highest degree of swelling (S=11.6776).

The conductivity properties for hydrogel and hydrogel composite were studied by LCR meter over the frequencies range (100Hz-100 KHz) at room temperature. LCR measurement indicated that, all hydrogels have insulation electric properties while when they were modified with PANI, G, MWCNTs, they were transformed to be semi conductors. For nanomatrials, MWCNTs has the highest electric conductivity (σ=2.5305 S/m at 100 KHz), while for nanocomposite hydrogels, CPG/MWCNTs has the highest electric conductivity (σ=1.9669 S/m at 100KHz).

The conductive hydrogel nanocomposites were loaded with indigo carmine dye, which was used as drug model and tested for drug release with

times by UV-Vis spectrophotometer at room temperature and applied voltages 8V for PANI composite, 2 V for G & MWCNTs composite in phosphate buffer solution (pH=7.4). It was found that CPG composite has the highest value of drug release, the maximum drug release of CPG/PANI was 13.026%, maximum drug release of (CPG/G) was 33.097%, and maximum drug release of CPG/ MWCNTs was 55.072%.

Repeat the study of drug release with doxorubicin, methotrexate anticancer drug in addition to indigo carmine was carried for the best composite hydrogel (CPG/PANI), (CPG/Fe_3O_4/PANI), (CPG/G), & (CPG/MWCNTs) with voltages (3, 5, 8) V for PANI composite, (1,2,3)V for G and MWCNTs nanocomposite and different temperatures (35.5, 37, 38.5ºC). The drug release was increased with increasing voltages for all composite at 37ºC. Doxorubicin hydrochloride loaded on (CPG/MWCNTs) was found to have the highest value of drug release (62.257%) at 2volt and 38.5ºC while Methotrexate loaded on (CPG/MWCNTs) have the highest value of release equal to (43.668%) at 2volt and 38.5ºC.

The percentage ratio of drugs release from all nanocomposite hydrogels was found to have the following order:

(CPG/MWCNTs) > (CPG/G) >(CPG/PANI) >(CPG/Fe_3O_4/PANI).

1. Preface

Nanocomposite polymers have biomedical applications exciting, such as carrying with drugs for cancer treatment. They have main objective in cancer therapy through destroying cancer cells without damaging normal cells. For example, strategy is directed to site at tumor magnetically carriers using external magnetic field. It can then be released to the drug carriers by any activity of enzyme and changes in physiological circumstances like, pH, temperature, etc.. Contrary traditional methods of cancer treatment such as surgery, radiation and chemotherapy have unpleasant side effects of treatment[1].

1.1 Drug Delivery Systems

Effective drug therapy need a drug to be delivered to target tissue, cell or receptor of interest at a sufficient concentration to give its preferred effect for an enough amount of time before diluted of drug, deactivated and/or rejected by the body. Drug therapy is most commonly accomplished through pills or injections, which result in systemic delivery of the drug during the body. Controlled, local drug delivery is a striking alternative because it allows for effective treatment with avoiding the unpleasant side effects and risk of toxicity related with systemic drug delivery. Hydrogel synthesis from biocompatible polymer systems has received wide-spread research attention for their potential use in localizing and controlling drug delivery.

Hydrogels are three-dimensional networks of water-soluble polymers created through crosslinking chemical or physical of different polymer precursors [2].

They have considerable potential as controlled drug delivery systems because hydrogels can be implanted neighboring to the target tissue and designed to release drug slowly for a long time. Hydrogel networks can also be made to illicit a minimal immune response, because of their high water content and our ability to engineer networks with similar chemical and

mechanical properties to native body tissues [3]. However, the medical applications of hydrogels are limited by their highly elastic mechanical properties which make them difficult to implant in a minimally invasive fashion (i.e. via injection), so their use generally necessitates surgical implantation [4]. By co-injecting reactive polymers that spontaneously form a macroscopic hydrogel when mixed, surgical intervention can be avoided.

Despite the ability of hydrogels alone to provide slowed release, improved control over drug release from hydrogel matrices can be carried out by co-incorporation of nanoparticles with variable chemical or physical characteristics [2].

Drug delivery system built on nanostructured is one of the rapidly promising areas currently that has acquired many researcher interests because of the suitable means of both side specific and time controlled drug delivery. Currently drug delivery systems built on nanostructured fabricate many commercially available products that is patient conformity and no side effect. Present drug delivery system built on nanostructured many features, some of which include; (1) they can move through the smallest and narrow capillary vessels as a result of their ultra-tiny volume; (2) they can enter cells and tissue hole to arrive at target organs for example, liver, spleen, lungs, spinal cord and lymph; (3) they can provide controlled- release for prolong time. These rare properties makes drug delivery system based on nanostructured better choice to delivery drug compare to convectional drug delivery system.

Lately, merged of polymeric system with drug delivery system built on nanostructured provides prolonged drug release. Among different kind of polymeric system, hydrogel regard as a suitable drug carrier for controlled drug release. Hydrogel is crosslinked with a three dimensional network that able to absorb huge quantity of water due to the hydrophilic group in the network such as carboxylic, hydroxyl group and others. Hydrogel can considerably use in drug delivery system. Hydrogel can be a suitable carrier for drug delivery system owing drug release from its matrix based on

swelling/ or deswelling, the solubility of the drug in the release media, and the interaction between drug with the polymers. Hydrogel have capability to defend drugs from aggressive environment such as presence of enzymes and extreme pH in the inner organs like stomach. In addition, hydrogels physical characteristic make them as good selector for drug carrier. For example, hydrogels porosity permit drug loading into gel network and accordingly drug release at desired site. Hydrogel has able to appearing significant volume changes in response to small changes in pH, temperature and other environmental stimuli [5].

Unfortunately, triggering thermal transitions inside the body is challenging, restrictive the application of these release vehicles in vivo. For example, this challenge is to physically entrap magnetic nanoparticles along with hydrogel in the hydrogel matrix. When the composite is force by an oscillating magnetic field, the magnetic nanoparticles produced heat by hysteresis heating [6], raising the composite temperature, causing hydrogel collapse and driving on-demand drug release using a highly penetrative but non-invasive signal. Removing the magnetic field would permit convective cooling, returning the composite to its first state and slowing drug release [7].

There are three major factors that determine whether drug therapy will be effective:

(1) The drug must be delivered to the target tissue, cell or receptor of interest; (2) concentration of the drug at the tissue must be sufficient to exert the desired effect; and (3) this concentration must be maintained for a sufficient period of time before the drug is diluted, damaged and/or rejected by the body.

Whether a drug reaches its target tissue within the body is highly relied on the nature of the drug and its way of administration [8]. The drug's chemical and physical properties determine its mobility within the body and into which tissues it will preferentially diffuse [9]. For example, substances injected into the blood stream (intravenous injection) with a hydrodynamic

diameter below 10nm will be filtered by the kidney and will accumulate in the renal system or bladder until voided [10]. This characteristic is useful if the purpose of the administered drug is to therapy a urinary tract infection, but would be quite dangerous if the drug caused renal toxicity or damage.

Use of an improper delivery technique could result in ineffective treatment and/or toxicity to the body, making the method of drug administration pivotal in determining drug efficiency. The most frequent method of drug administration is oral ingestion, either in the appearance of a pill or solution. It is beneficial because of its ease of use and convenience; however, the caustic nature of the digestive system can deactivate or denature drugs. Drugs that are absorbed intact along the digestive tract subsequently move through the liver which can further deactivate, degrade and/or eliminate (through bile) the drugs, limiting the probability of the drug reaching its target tissues in sufficient concentrations. Other methods of administration such as intravenous injection or rectal or sublingual administration avoid first path metabolism by the liver, increasing the bioavailability of the drug. However, they also result in systemic delivery throughout the circulatory system, which can result in significant risks of overdose or other toxic effects [8].

1.2 Biodegradable polymeric nanoparticles as drug delivery devices

Over the last few years, there has been considerable attention in developing biodegradable polymeric nanoparticles (NPs) as activated drug delivery systems. Different polymers have been utilized in drug delivery research as they can successfully deliver the drug to a target site and thus raise the therapeutic advantage, while reducing side effects [11].

The controlled release of drug active agents to the exact site of action at the therapeutically optimal rate and dose schedule has been a major goal in planning such systems. Liposomes have been utilized as possible drug carriers

rather than conventional dosage forms because of their rare advantages which include ability to protect drugs from degradation, target the drug to the position of action and decrease the poisons or undesired effects [12]. However, evolution work on liposomes has been restricted to inherent troubles such as poor storage stability, low encapsulation efficiency, and rapid leakage of water-soluble drug in the existence of blood components. On the other side, polymeric nanoparticles submit some specific advantages over liposomes. Such as, nanopaticles help to increase the stability of drugs /proteins and possess useful controlled release features.

Furthermore release average can also be affected by ionic interaction of the drug and supplement of helpful components. When the drug is involved in interaction with helpful components to form a less water soluble complex, then the drug release can be very slow with almost no burst release effect; whereas if the addition of helpful component e.g., addition of (ethylene oxide)-(propylene oxide) block copolymer (PEO-PPO) to chitosan, decreased the interaction of the model drug bovine serum albumin (BSA) with the matrix polymer (chitosan) as a result of vying electrostatic interaction of(PEO-PPO) with chitosan, then an enhance in drug release could be observed. Hezaveh used methylene blue as model drug to test the drug release from nanocomposite hydrogel. It can be realize that by increasing the (MgO) content of nanocomposites, methylene blue release is appreciably increased. By increasing nanoparticles concentration from (0.1 g to 0.2 g), the maximum methylene blue release increases from (0.174 to 0.267 mg/mL). Also, compared to bare hydrogel, the addition of MgO NPs has increased the collective release up to (52%), which means that more methylene blue release is achieved [13].

Nanoparticles generally differ in size from (1-100) nm. The drug is entrapped, encapsulated, dissolved or linked to a nanoparticle matrix accordingly the method of preparation; NPs, nanospheres or nanocapsules can be obtained [14].

A number of various drug delivery compounds such as liposomes, microspheres, and hydrogels, which respond to stimuli, for examples, temperature, pH, electric fields, light, ultrasound, magnetic field etc., are presently used to investigate in an attempt to improve drug therapy [15].

1.3 Biodegradable polymers

1.3.1 Chitosan

Chitosan is naturally obtained by deacetylation of chitin in alkaline conditions, which is one of the most available natural polymers, being second only after cellulose in the amount generated annually by biosynthesis. Chitin is a significant ingredient of the exoskeleton in animals, particularly in crustaceans, molluscs and insects. It is also the major fibrillar polymer in the cell wall of certain fungi. (Fig. 1.1) show, chitosan is a polysaccharide has chain linear, composed of glucosamine and *N*-acetyl glucosamine units linked by β (1–4) glycosidic bonds. The unit of glucosamine is determined the degree of deacetylation (DD). In fact, in a general way, it is considered that when the DD of chitin is higher than about50% (depending on the source of the polymer and on the allocation of acetyl groups along the chains), it will be soluble in an aqueous acidic solution. In these conditions it is named chitosan [16].

Chitosan is currently getting huge interest for medicinal and pharmaceutical applications as a result of its nontoxic odorless, biocompatible in animal tissues and biodegradable properties [17].

Effective methods of improving the physical and mechanical features of chitosan include blending of chitosan with further polymers and crosslinking are both convenient for practical applications. Immunization studies executed on rats using glutaraldehyde crosslinked chitosan spheres displayed promising acceptance by the living tissues of the rat muscles [18, 19].

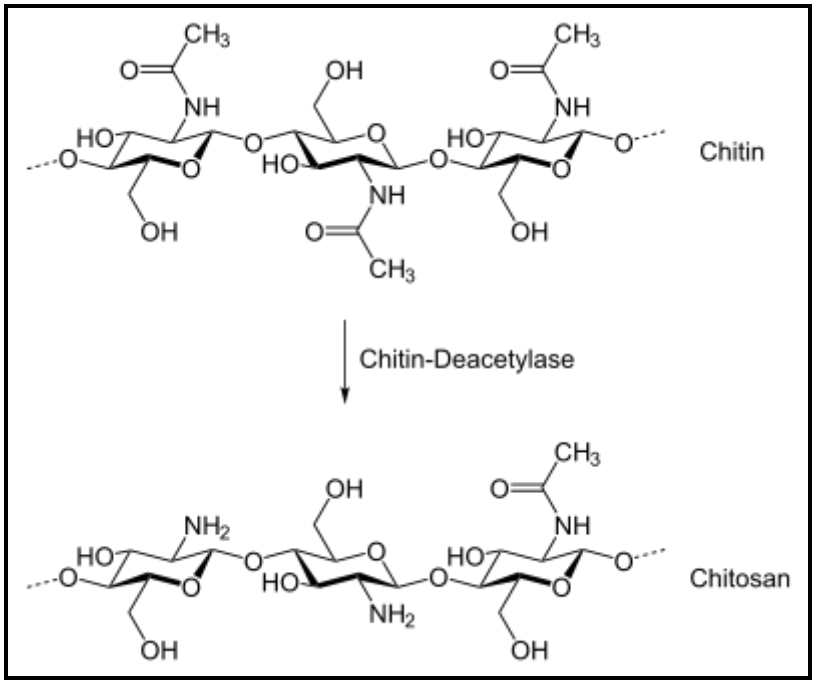

Figure (1.1): Chemical structure of chitin and chitosan [20]

Chitosan crosslinking with dialdehydes, one can get a hydrogel with a swelling capability in acidic media. When an anionic monomer for example acrylic acid is grafted onto chitosan (in the existence of a divinyl crosslinking agent like(N,N′-methylenebisacrylamide), an ampholytic hydrogel comprising both cationic and anionic charges, was prepared. Therefore, by entering anionic charges (-COO−) onto chitosan, a hydrogel with swelling ability at various pH was prepared [21].

1.3.2 Pectin

Pectin is heterogeneous, hydrophilic polysaccharide containing linear chains of poly (α-1-4 galacturonic acid), with varying degrees of methylation of carboxylic acid residues. Pectin is the methylated ester of poly galacturonic acid (fig.1.2). Commercially, under mildly acidic conditions, pectin is extracted citrus peels and apple pomace. Pectin such as any polysaccharide is generally, non-poisoned, biocompatible and biodegradable. Therefore, pectin

is extensively used as possible carrier for colon specific drug delivery [22, 23].

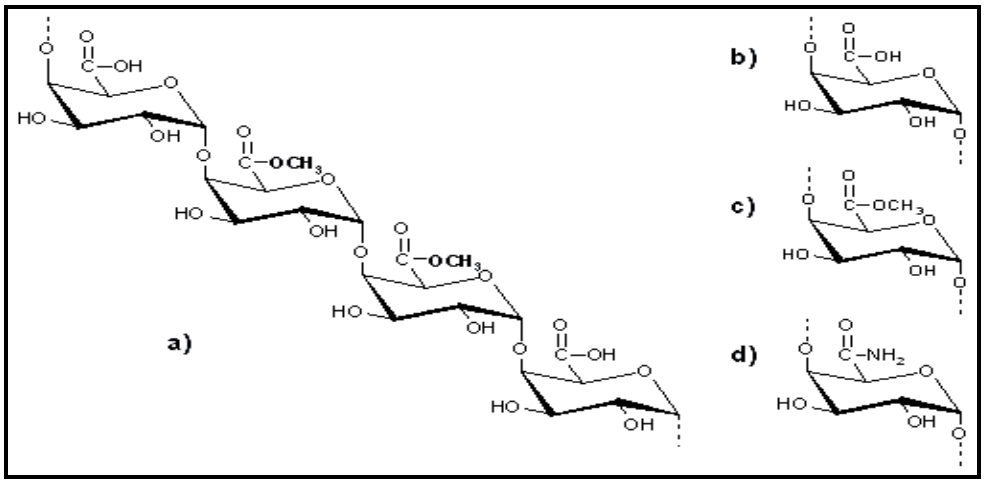

Figure (1.2): (a) A repeating segment of pectin molecule and functional groups: (b) carboxyl; (c) ester; (d) amide in pectin chain [24]

The polygalacturonic acid chain is partly esterified with methyl groups and the free acidic groups may be partly or completely equalize with sodium, potassium or ammonium ions [25].

Pectin accumulation tends to dissociate and expand and is digested by much of colonic microflora at neutral pH. To overcome the trouble of high dissolution of pectin in the upper gastrointestinal tract, pectin has been blended with other polymers [26].

1.3.3 poly (vinyl alcohol) (PVA)

Poly (vinyl alcohol) (PVA) is synthetic polymer has linear chain, prepared by part or complete hydrolysis of poly (vinyl acetate) to eliminate the acetate groups. The quantity of hydroxylation determines the physical characteristics, chemical properties, and mechanical features of the PVA. The resulting PVA polymer is highly soluble in water unlike resistant to most organic solvents. The higher hydroxylation degree when polymerization of the PVA, the lower the solubility in water and the more difficult it is to crystallize. Because of its water solubility, PVA requires to be crosslinked to

form hydrogels for employ in several applications. The crosslinks, either physical or chemical, provide the structural stability of PVA by configuring the hydrogel, which swells in water or biological fluids. PVA has excellent mechanical strength, good film forming, and temperature and pH stability. Furthermore, PVA is bio-compatible and nontoxic, and exhibits minimal cell adhesion and protein absorption, as desired in bio-medical applications requiring contact with bodily fluid [27, 28].

1.4 Hydrogels

Three-dimensional lattice structures obtained from synthetic and/or natural polymers that can absorb and keep large quantity of water describes the term hydrogel. The hydrogel structure is built by the hydrophilic groups or domains present in a polymeric network upon the hydration in an aqueous medium [29].

1.4.1 Classification of Hydrogel

Hydrogels are broadly classified into two categories:

Permanent / chemical gel: they are called ‘permanent' or ‘chemical’ gels when they are covalently, or ionically cross-linked (exchanging hydrogen bond by a stronger and stable covalent or ionic bonds) networks. Depends on the polymer-water interaction parameter and the crosslinking density, they reach an equilibrium swelling state.

Reversible / physical gel: they are called ‘reversible’ or ‘physical’ gels when the networks are held together by molecular entanglements, and / or secondary forces including, hydrophobic interactions or hydrogen bonding. In physically cross-linked gels, dissolution is banned by physical interactions, which present between different polymer chains. All of these interactions are

reversible, and can be collapsed by changes in physical conditions or application of stress [30].

1.4.2 Methods to Produce Hydrogel

1.4.2.1 Physical cross-linking

There has been an increased attention in physical or reversible gels due to prorated ease of production and the advantage because not using cross-linking agents. The various methods to obtain physically cross-linked hydrogels are:

1.4.2.1.1 Heating/cooling a polymer solution

Physically cross-linked gels are formed when cooling hot solutions of gelatine or carrageenan (is a class of linear sulphated polysaccharides that are extracted from red edible seaweeds). The gel creation is because of helix-creation, connection of the helices, and generating junction zones. Carrageenan is existing as random coil configuration in hot solution over the melting transition temperature. At cooling it convert to rigid helical rods. In existence of salt (K^+, Na^+, etc.), double helices further aggregate to structure stable gels due to sorting of repulsion of sulphonic group (SO^{-3}), (Fig.1.3) [31].

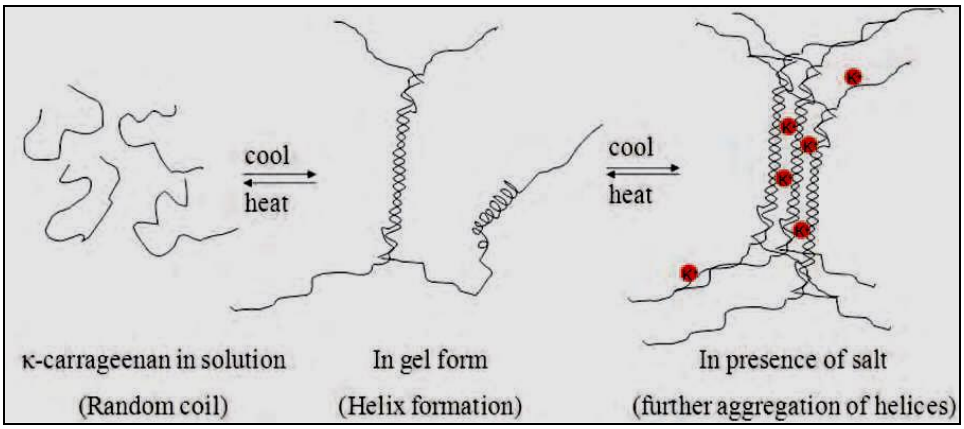

Figure (1.3): Gel formation due to aggregation of helix upon cooling a hot solution of carrageenan [31].

1.4.2.1.2 Complex coacervation

The gels can be created by mixing of a polyanion with a polycation. The fundamental principle of this method is that polymers with opposite charges attach together and form soluble and insoluble complexes according to the concentration and pH of the own solutions (Fig.1.4). Coacervation polyanionic xanthan with polycationic chitosan is the best example [32].

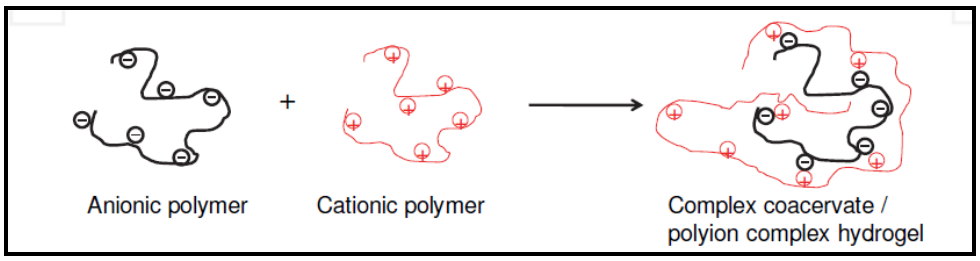

Figure (1.4): Complex coacervation between polyanion and polycation [32]

1.4.2.1.3 H-bonding

H-bonded hydrogel can be gained in acidic aqueous solution of polymers containing carboxyl groups. For example of such hydrogel is (carboxymethyl cellulose (CMC)) network formed by adding (CMC) into (0.1M)HCl. Hydrogen bonding can be formed by replacing the sodium in (CMC) with hydrogen in acidic solution (Fig.1.5) because hydrogen bonds lead to a reduce of (CMC) solubility in water and cause the configuration of flexible hydrogel. Hydrogels can also formed by crosslinking of (carboxymethylated chitosan) in acids or poly functional monomers [33].

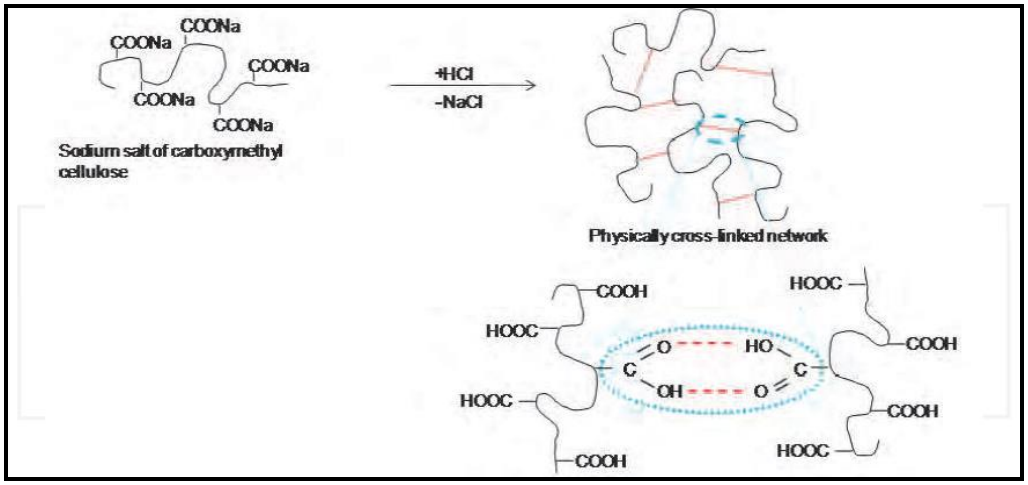

Figure (1.5): Hydrogel network formation due to intermolecular H-bonding in CMC at low pH [33]

1.4.2.1.4 Maturation (heat induced accumulation)

This hydrogel can be formed in arabic gum (acacia gums) which is mostly carbohydrate but contain (2-3%) protein as an integral fraction of its structure. Three major kinds with various molecular weights and protein content have been recognized following partition by "hydrophobic interaction chromatography" with various molecular weights and protein content. These are glycoprotein (GP), arabinogalactan (AG), and arabinogalactan protein (AGP). Heat treatment induced aggregation of the proteinaceous components by, increases the molecular weight and consequently produces a hydrogel structure with improved mechanical properties and water binding capability. The molecular changes which go together with the maturation process show that a hydrogel can be obtained with exactly structured molecular dimensions. The controlling feature is the aggregation of the proteinaceous components inside the molecularly disperse system that is present in of the naturally going on gum. Growing of the gum leads to transfer of the protein connected with the lower molecular weight components to give larger concentrations of high molecular weight section (AGP) (Fig.1.6). By same way other gums such as

gum ghatti and Acacia kerensis have been utilized for application in denture care [34, 35].

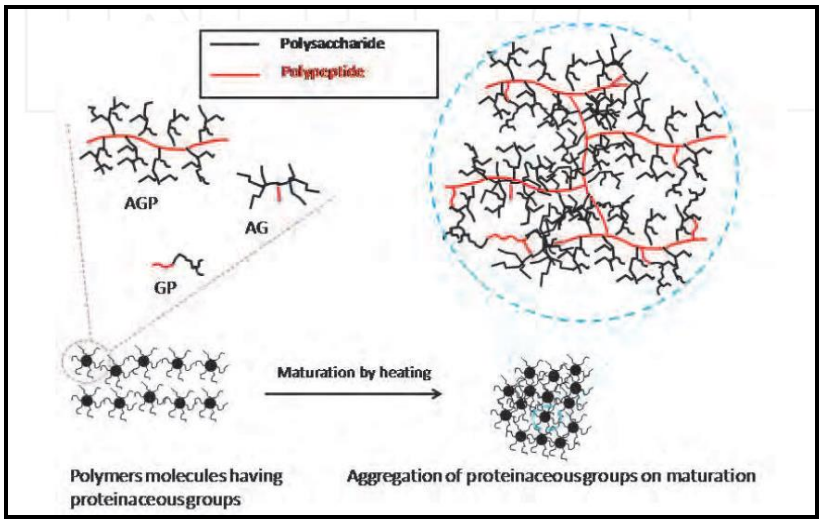

Figure (1.6): Maturation of Arabic gum causing the aggregation of proteinaceous part of molecules leading to cross-linked hydrogel network [34].

1.4.2.1.5 Freeze-thawing

By employing freeze-thaw cycles, physical crosslinking of polymers to form their hydrogels can also be achieved. The mechanism involves the configuration of microcrystals in the structure as a result of freeze-thawing cycles. Examples of this type of gelation are freeze-thawed gels of poly (vinyl alcohol) and xanthan [36, 37].

1.4.2.2 Chemical cross-linking

This method involves grafting of monomers on the backbone of the polymers or adding crosslinking agent to link two polymer chains. The crosslinking can be obtained through the reaction of functional groups (such

as OH, COOH, and NH_2) of natural or synthetic polymers with cross-linkers such as aldehyde (e.g. glutaraldehyde). To obtain chemically cross-linked permanent hydrogels, there are many methods mentioned in literature. For example, interpenetrating network (IPN) structure can be form by polymerization one or two monomer in presence polymer has polar groups, to form network. The major chemical methods (crosslinker, and grafting) used to formed hydrogels [30].

1.4.2.2.1 Chemical crosslinking using crosslinker agent

Cross-linkers such as glutaraldehyde, epichlorohydrin, maleic anhydride, and (N, N´-methylenebisacrylamide (MBA)), etc have been usually utilized to obtain the crosslinking hydrogel network of different polymers(natural or synthetic). The technique chiefly involves enter of new molecules between the polymeric chains to form crosslinking chains (Fig.1. 7). The reaction is happened of corn starch and poly (vinyl alcohol) with (glutaraldehyde) as a crosslinker agent as good example of hydrogel. The membrane of this hydrogel could be utilize in many applications like, artificial skin; various healing/ nutrients factors and drugs may be delivered to the site of action [38].

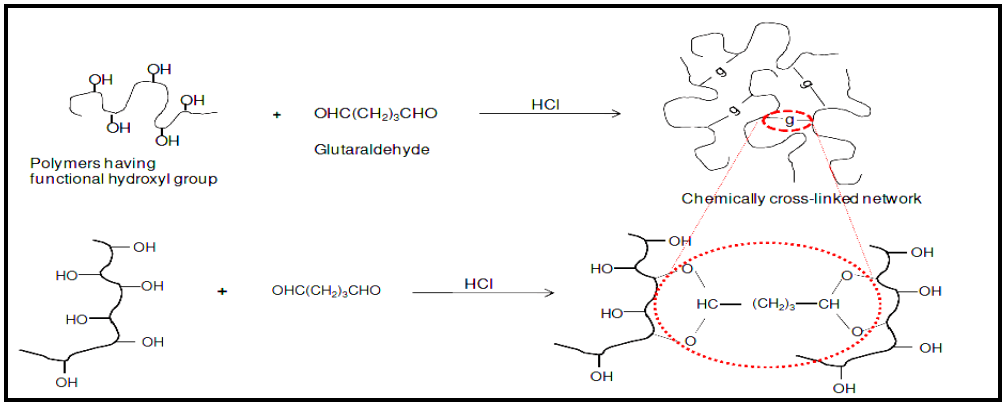

Figure (1.7): Schematic illustration of using chemical cross-linker to obtain cross-linked hydrogel network [38]

1.4.2.2.2 Ionic interaction

Crosslinking of ionic polymers can be by adding of divalent or trivalent counterions. This method depending on the principle of gelling of a polyelectrolyte solution (e.g. Na^+ alginate$^-$) with calcium chloride salt (Fig.1.8) [39].

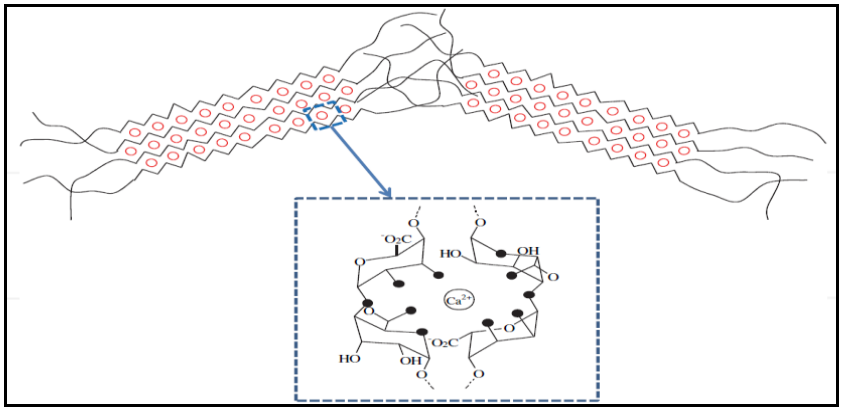

Figure (1.8): Ionotropic gelation by interaction between anionic groups on alginate (COO^-) with divalent metal ions (Ca^{2+}) [39]

1.4.2.2.3 Grafting

This can be defining of polymerization of a monomer on backbone of a polymer (fig.1.9).

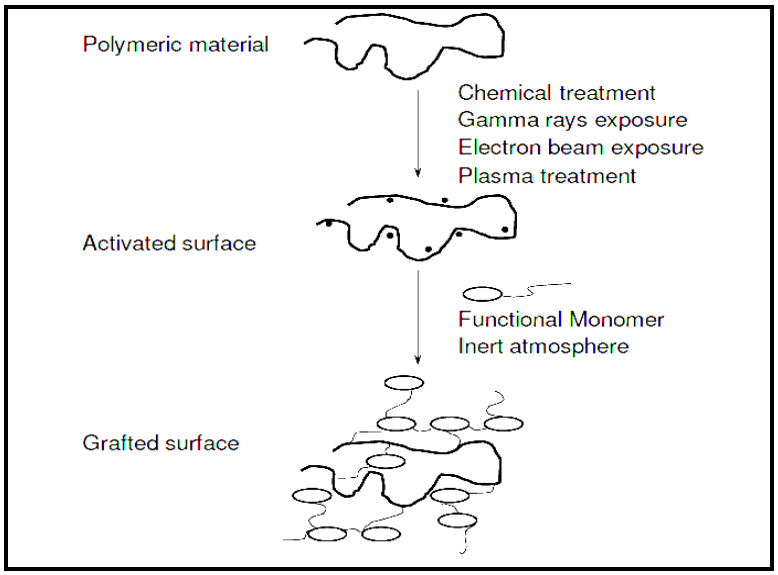

Figure (1.9): Grafting of a monomer on preformed polymeric backbone leading to infinite branching and cross-linking [40]

Chemical materials, or high radiation energy treatment are used to active of the polymer chains. The propagation of functional groups of monomers on activated macroradicals induced branching and further to crosslinking [40].

1.5 Nanocomposite Hydrogels

Nanocomposite hydrogels, also famous as hybrid hydrogels, may be defined as hydrated polymeric networks, either covalently or physically crosslinked with each other and/ or with nanostructures or nanoparticles. Although there are numerous appropriateness for nanocomposite biomaterials, such as carbon-based nanomaterials (carbon nanotubes, graphene, nano diamonds), inorganic/ceramic nanoparticles (silica, silicates, calcium phosphate, hydroxyapatite), polymeric nanoparticles (dendrimers, polymer nanoparticles, hyperbranched polyesters), and metal/metal-oxide nanoparticles (iron oxide, gold, silver) are shared with the polymeric network to get nanocomposite hydrogels (Fig. 1.10) [41].

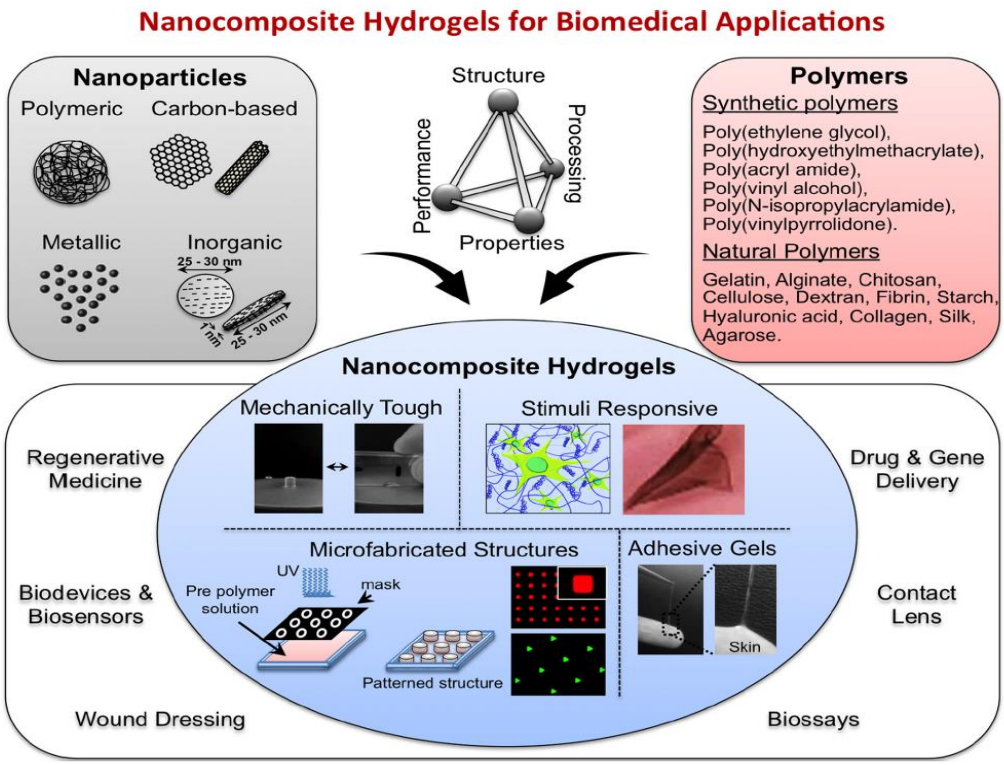

Figure (1.10): Engineered nanocomposite hydrogels, a range of nanoparticles such as carbon-based nanomaterials, polymeric nanoparticles, inorganic nanoparticles, and metal/ metal-oxide nanoparticles are combined with the synthetic or natural polymers to obtain nanocomposite hydrogels with desired property combinations [41]

1.6 Conductive hydrogel nanocomposite

Percolation theory explained the electrical conductivity of composites made of a conductive phase dispersed in an insulating matrix, critically based on the filler loading [42]. The fillers are existed as small aggregation or signal elements at a low filler concentration; since the average distance between the filler elements overrun their size, the conductivity of the nanocomposite is so close to that of the pure insulating matrix. When a sufficient amount of filler is loaded, a ‘‘percolation’’ path of connected fillers forms and allows charge transport through the sample. At this critical concentration, term the “percolation threshold”, the conductivity unexpectedly and quickly increases. Depend on geometrical structure; the value of the “percolation threshold” is prospective to be strongly impacted by the aspect ratio (ratio of length-to-diameter) of the particles filler. Considering a filler system having a specific filler orientation, the “percolation threshold” reduced with rising aspect ratio

of the filler. Carbon nanotubes (CNTs) are striking filler for forming electrically conductive nanocomposites, where, (CNTs) have an outstanding conductivity (10^5–10^8S /m) [43], combined with a large aspect ratio reaching (100–1000) for (mm) lengthy single-wall and multi-wall carbon nanotubes [44]. These composites are striking for use in, electromagnetic interference (EMI) shielding, (at low CNT contents) transparent conductors etc [45].

Superior electrical conductivity is the mainly significant features of graphene. Conductive polymer composites can be form when graphene fills the insulating polymer matrix. The different polymers, including, PVA, PVC (poly vinyl chloride), PS (poly styrene) etc. have been utilized as matrices to synthesis electrically conductive graphene/polymer composites. Composite materials usually appeared a non-linear increment of the electrical conductivity as a function of the filler concentration. The electric conductivity of nanocomposite is influenced with two parameters, electrical conductivity and "percolation threshold". At a certain filler loading fraction, which is called "percolation threshold (*pc*)", the fillers in a network induced an unexpected increase in the electrical conductivity of the composites. Sometimes presence of a very low quantity of conducting particles can make filler connect to form impact conducting paths and thus making the whole composite conductive [46, 47].

"Xie et al". [48] reported that graphene is more effective for conductivity improvement than competing nanofillers such as (CNTs) because of their large specific surface area. A wonderful electrically conductive graphene/polymer composite is probable to have lower "percolation threshold" and higher conductivity at a lower graphene loading, which can not only decrease the cost of filler but also maintain the processability of the composite. "Ruoff et al." [49] prepared graphene/PS composites and they noticed a low "percolation threshold" at (0.1) vol% of graphene. The electrical conductivity difference in composites occurs in three stages, as illustrated in (Fig. 1.11). Here the process is explained with a graphene filled

polymer. At first, the conductivity is quite low (Fig. 1.11a) because of a smaller number of additives, but large clusters gradually begin to form (Fig. 1.11b) with a little raise in conductivity. At this stage, tunneling effects take place between neighboring graphene flakes, making it practical in sensing materials.

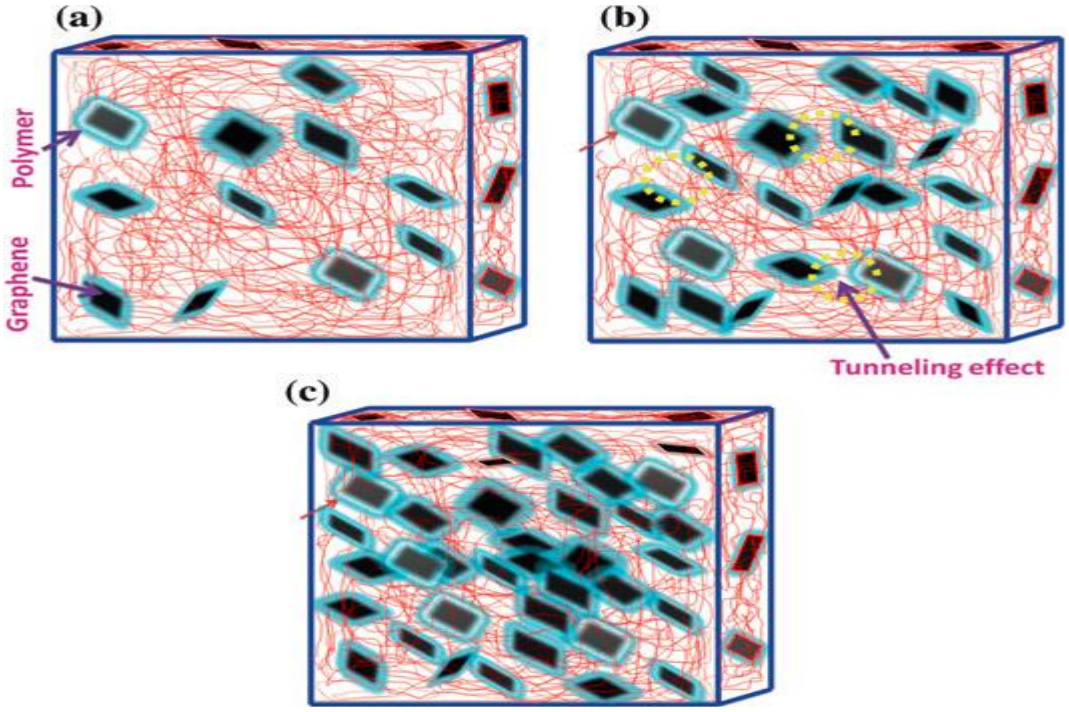

Figure (1.11): Percolation process in conductive composites [49]

As the graphene flakes increases, a complete conductive path (red) is formed by the contacting flakes (Fig. 1.11c) at the percolation, and further increase in the conducting particles enhances the number of conducting networks, (Fig. 1.11c), until the conductivity levels off. This interpretation based on the method those nanoparticles form conducting network when dispersed in polymer matrix is named “percolation theory”. Divers factors affected the electrical conductivity and the “percolation threshold” of the composites such as aggregation of filler, concentration of filler, processing methods, functionalization and aspect ratio of graphene sheets, dispersion in the matrix, inter-sheet junction, crinkle and warp etc. [50].

1.7 Introduction to nanotechnology

Research on new materials technology is attracting the look of researchers from around the world. Developments are being made to enhance the features of the materials and to find replacement precursors that can give desirable properties on the materials.

Nanotechnology, which is one of the new technologies, refers to the evolution of devices, structures, and systems whose size varies from (1 - 100) nm. The last century has seen progression in every side of nanotechnology such as: nanoparticles and powders; nanostructured biological materials, nanolayers and coats; electrical, optic and mechanical nanodevices. Currently, nanotechnology is evaluated to be influential in the next 20-30 years, in all fields of science and technology.

Nanotechnology is acquiring a lot of attention of late across the globe. The term nano originates derivatively from the Greek, and it means “dwarf.” The term indicates physical dimensions that are in the range of one-billionth of a meter. This scale is called popularly nanometer scale, or also nanoscale. One nanometer is approximately two hydrogen atoms length. Nanotechnology links to the utilization, creation, and design of materials whose component structures be present at the nanoscale; these constituent structures can, by conference, reach to (100) nm in size. Nanotechnology is a developing field that explores electrical, optical, and magnetic activity as well as structural performance at the molecular and submolecular level [51].

1.8 Nanomaterials

1.8.1 Magnetic Nanoparticles (MNPs)

Magnetic nanoparticles are a group of engineered particulate materials of <(100)nm that can be played under the action of an external magnetic field. MNPs are commonly consisted of magnetic elements, like as iron, nickel, cobalt, chromium and their oxides like magnetite (Fe_3O_4), maghemite (γ-Fe_2O_3), cobalt ferrite(Fe_2CoO_4), chromium dioxide(CrO_2) [52].

MNPs are a major kind of nanoscale materials with the power to revolutionize current clinical diagnostic and therapeutic techniques [53-57]. Moreover, other applications of (MNPs) are widely studied including magnetically helped gene therapy; magnetically stimulate hyperthermia and magnetic-force-based tissue engineering [58].

Iron oxide magnetic nanoparticles show a higher performance at the level of chemical stability and biocompatibility compared with metallic nanoparticles [59]. Nanoparticles have a large surface which can be adjusted to connect biological agents [60].

Among superparamagnetic nanoparticles, iron oxide nanoparticles such as magnetite (Fe_3O_4) or its oxidized form maghemite (γ-Fe_2O_3) are by far the most usually used in biomedical applications, as their biocompatibility has already been assured [61]. Highly magnetic materials such as nickel and cobalt are toxic, capable to oxidation therefore are of little importance. Nanoparticles of magnetic iron oxides, are frequently modified through the formation of few atomic layers of polymer/surfactant or inorganic metallic (such as gold) or oxide surfaces (such as silica or alumina), which prevents conglomeration and also allows further functionalization by attaching various biomolecules [62, 63]. MNPs with appropriate surface characteristics have effort applications both in vitro and in vivo. To determining particles size distribution and morphology, their surface chemistry and, obviously, magnetic properties need information about the preparation method of magnetic particle system and its modified surface must be accompanied by its full characterization. All these features are crucially important, if the material is planned and estimated for application in medical practices [64].

1.8.2 Graphene Oxide (GO)

Graphene oxide, a graphite derivative with hydroxyl, carboxyl, and epoxy groups covalently bond to its layers. The most frequent approach to words graphite exfoliation is the use of strong oxidizing agents to obtained graphene oxide (GO), a nonconductive hydrophilic carbon material [65, 66].

Although the precise structure of GO is difficult to determine, it is clear that (GO) contained of contiguous aromatic lattice of graphene is interspersed, alcohols, ketone carbonyls, carboxylic and epoxides groups [67, 68]. The disruption of the layers is reflected by a raise in interlayer spacing from (0.335) nm for graphite to more than (0.625) nm for GO [69]. Brodie [70] first confirmed the synthesis of GO in 1859 by adding amount of $KClO_3$ to a slurry of graphite in fuming HNO_3. In 1898, Staudenmaier[71] improved this method by using mixture of concentrated H_2SO_4 and fuming HNO_3 subsequently gradual addition of chlorate to the reaction mixture. This small change in the procedure provided a simple technique for the production of GO. In 1958, Hummers reported an alternative method for the synthesis of graphene oxide by using potassium permanganate and sodium nitrate in concentrated sulfuric acid [72]. Graphene oxide synthesized by this method could be used for preparing large graphitic film [73]. In the present thesis, attempts have been made to synthesize graphene oxide with few layers by modifying the hummer's methods.

Though it has been advanced for over a century, the precise chemical structure of GO is still not completely clear, which contributes to the complication of GO due to its partial amorphous nature. Several early searches have proposed structural models of GO with an uniform lattice composed of discrete repeat units [74], and the widely accepted GO model proposed by Lerf and Klinowski [66,67] is a nonstoichiometric model (Fig. 1.12), where in the carbon plane is designed with hydroxyl and epoxy (1,2-ether) functional groups. Carbonyl groups are also present, most likely as carboxylic acids along the sheet edge but also as organic carbonyl defects within the sheet.

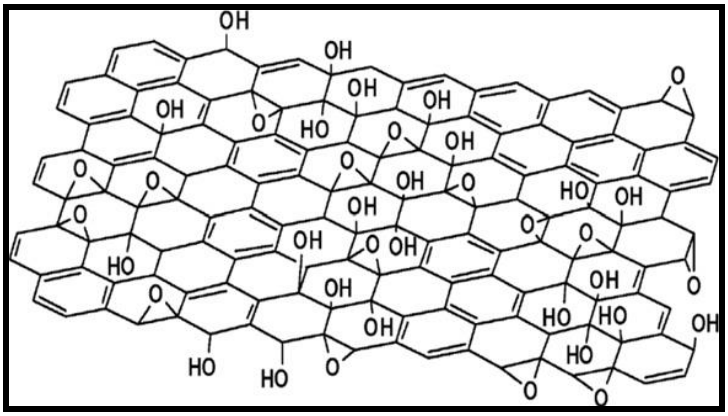

Figure (1.12): Lerf–Klinowski model of GO with the omission of minor groups (carboxyl, carbonyl, ester, etc.) on the periphery of the carbon plane of the graphitic platelets of GO [66, 67]

1.8.3 Graphene (G)

Graphene, also called as 'super carbon'[75], is one-atom thick two-dimensional sheet of carbon atoms fashioned in a honeycomb lattice (fig. 1.13) and considered as the future rebellious material [76]. Graphene has rare electronic properties like the absence of charge localization, half-integer quantum Hall effect, ultrahigh mobility as well as terrific mechanical properties compared to other carbon materials, has attention huge interest.

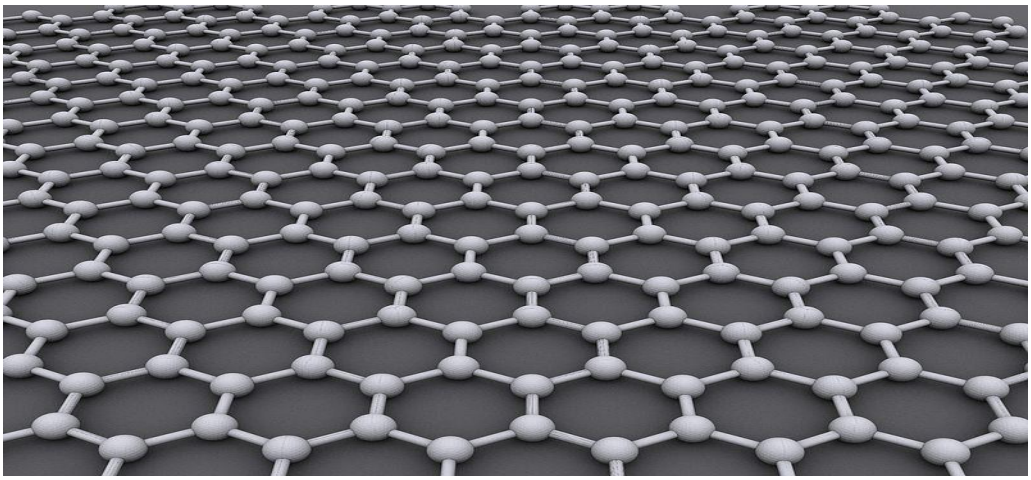

Figure (1.13): Honeycomb lattice of graphene [75]

The electronic properties of graphene are resulting mainly from the π-electrons, which make it an ideal 2D system where the π -states form the

valence band and the π * states form the conduction band. In the conduction band structure these two bands overlap at six points in *k*-space, which are called as Dirac points (zero band gaps) [77]. The conduction electrons in graphene called “Dirac fermions” can move near the speed of light and have zero effective mass. Graphene is that's why known as a Dirac solid. The other noticeable electrical and optical properties are its ballistic transfer over ~ (0.4) μm length, thermal conductivity of(> 5000 W/(mK)), high carrier mobility at room temperature [78] (15,000 cm^2 V^{-1} s^{-1}), wideband absorption (from visible to near-infrared (NIR) regions) combined with good visual transparency, single-molecule field-effect sensitivity [79], and “quantum Hall effect” at room temperature. Graphene has so huge surface area [80], the area (about ~ 2600 m^2/g) is interested for sensors, where all the carbon atoms can participate in the sensing and interaction with foreign molecules/species. Graphene can be important for potential applications in both emerging and conventional fields like field-effect transistors [81, 82], electrochemical devices, electromechanical resonators, polymer nanocomposites, biosensors, ultracapacitors, batteries, and light-emitting devices [83-86]. Graphene-based flexible conducting electrodes are important for soft electronic devices [87].

They have been applied for “organic light-emitting diodes (OLED)”, capacitive sensors in touch-screen displays and for “organic photovoltaic (OPV) “devices. Graphene and graphene-based hybrids can be thinking as possible nominee for replacing Si-based technologies as a result of their exceptional properties. Outstanding, ultimate thinness (atomic level) good transconductance of graphene devices, carrier mobility, and stability of the material are the main attention of graphene. Graphene can be a revolting material for living beings as it is less toxic, which can be tampered chemically and, more importantly, it is biodegradable [88, 89]. Graphene has been prepared by different methods, comprised, “chemical vapour deposition (CVD)”, “metal-organic chemical vapour deposition (MOCVD)” and

“mechanical exfoliation”, wet chemical and solid-state methods. “Novoselov *et al*.” [78] mentioned a simple mechanical exfoliation technique using Scotch Tape to obtain supported single layer graphene from graphite. The most followed gram scale wet chemical prepare of graphene from graphite powder by oxidation and reduction followed by exfoliation is known as Hummer’s method [72].

1.8.4 Carbon nanotubes (CNTs)

Carbon nanotubes are molecular-scale tubes of graphitic carbon with wonderful properties. The simplest carbon nanotube is created from a single sheet of a honeycomb network of carbon atoms, called graphene; it is rolled up easily into a tubular form. Carbon nanotubes as multi-tubes (MWCNTs) form-nest in a concentric pattern were discovered in (1991), however, Single-wall carbon nanotubes (SWCNTs) were discovered in (1993) by Iijima [90, 91]. SWCNTs have diameter from (0.4 to 2.0) nm and length in the extent of (20–1000) nm, while MWCNTs are bigger objects with diameter in the range of (1.4–100) nm and length from 1 to several μm. The exact structure of a nanotube depends on the different angles and curvatures in which a graphene sheet can be rolled into a tube and is determined by a vector, which is called a chiral vector and discriminates CNTs into “zigzag”, “arm chair”, and “chiral” forms(fig.1.14). The electronic properties of a nanotube change in correspondence to its structure; thus armchair nanotubes are metallic, while zigzag and chiral can be either metallic or “semiconducting” [92]. In general, SWCNTs are a mixture of metallic and semiconducting material, based on their geometrical features, while MWCNTs are considered as metallic conductors.

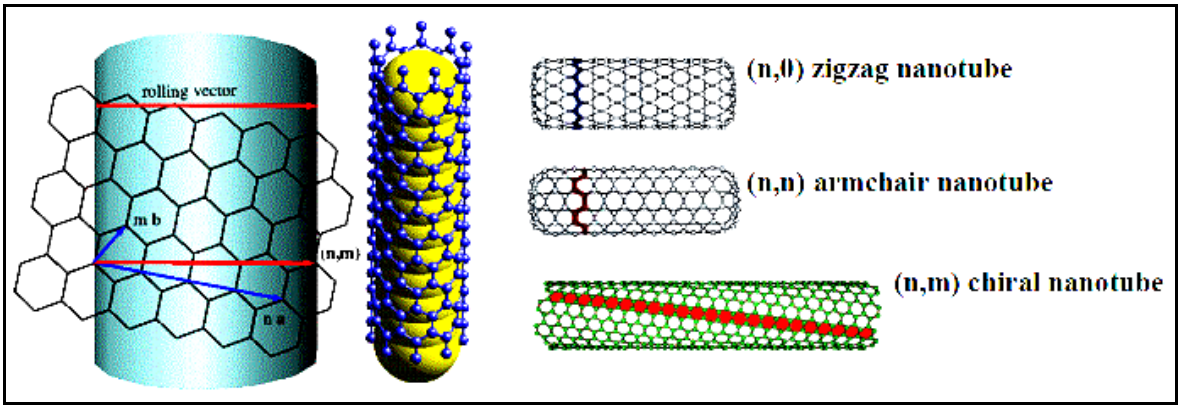

Figure (1.14): Types of nanotube according to rolling vector (n, m) [92]

In particular, some mechanical properties of carbon nanotubes have been mentioned to be outstanding. For example Young's modulus in about of (1TPa) contrast with diamond (1.2 TPa) while reported tensile strengths (≈200 GPa) are about of steel provided (CNTs) density is taken into account [93-95].

1.9 Polyaniline(PANI) [96-99]

The polyaniline, probably the earliest known synthetic polymer, refer to a large class of conducting polymers which have the following general formula**:**

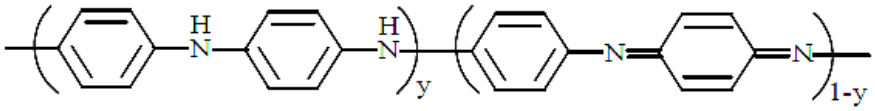

It contains y (reduced) and (1-y) oxidizing units. The existence of nitrogen atoms as imine (in sp2) or amine (in sp3 hybridized state) forms, and their relative proportion in the overall polymer backbone chain determines the resulting structure and the different properties of polyaniline.

A large variety of derivatives can be prepared through substitution in the ring or on the N atoms. One of the particular features of polyaniline is that it can be doped by protonic acids. Thus, the properties of the doped polymer can be turned by incorporating different dopant anions.

It has been found that polyaniline can presence in three different state, They are the “leucoemeraldine” oxidation state, the “emeraldine” oxidation state, and the “pernigraniline” oxidation state. Other oxidation states are the result of physical mixture of these oxidation states.

(i) Leucoemeraldine base: the fully reduced form of non-doped polyaniline. It is composed solely of reduced units.

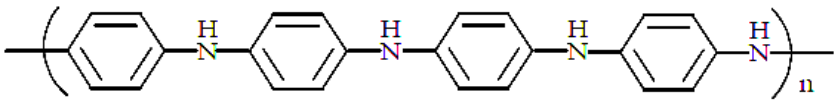

(ii)Pernigraniline base: the fully oxidized form of non-doped polyaniline. It is composed solely of oxidized base unites.

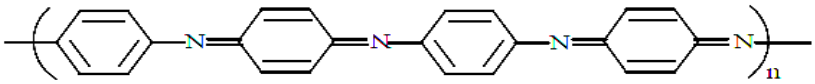

(iii)Emeraldine base: the intermediate oxidation state of polyaniline. It is composed of equal amounts of alternating reduced base and oxidized base units.

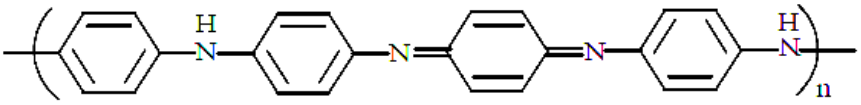

Polyaniline can be “chemically” or “electrochemically” synthesized by the oxidative polymerization of aniline monomer in aqueous acid e.g., 1M HCl solution. The formed polymer is called an emeraldine salt. For chemical synthesis, there are many different oxidizing agents, including: ammonium peroxydisulfate, hydrogen peroxide, ferric chloride and ceric nitrate and

sulfate. Polyaniline can also be synthesized electrochemically by the oxidation of aniline on an inert metallic (e.g., Pt) electrode.

In both case, the polymerization method proceeds via the following mechanism:

The first step is the formation of the radical cation by an electron transfer from the 2*s* energy level of the aniline nitrogen atom, (Figure 1.16). The obtained of aniline "radical cation" has several resonant forms, in which (c) is the more reactive one because of its important substituent inductive effect and its absence of steric hindrance.

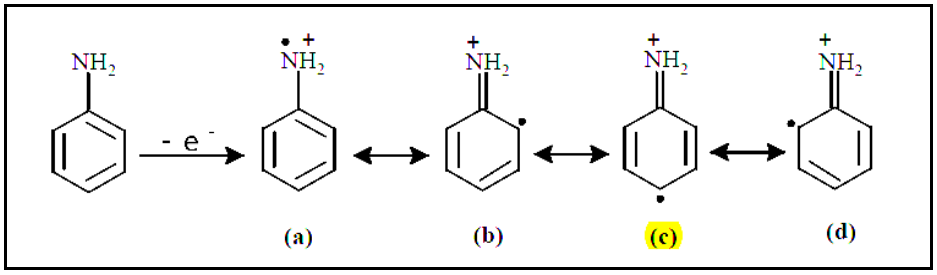

Figure (1.15): The formation of the aniline radical cation and its different resonant structures

The next step corresponds to the "dimer" formation by the so-called "head-to tail" reaction between the" radical cation" and its resonant form (most probably form (c)) in acidic medium. Then the "dimer" is oxidized to form a new "radical cation dimer", (Fig. 1.16).

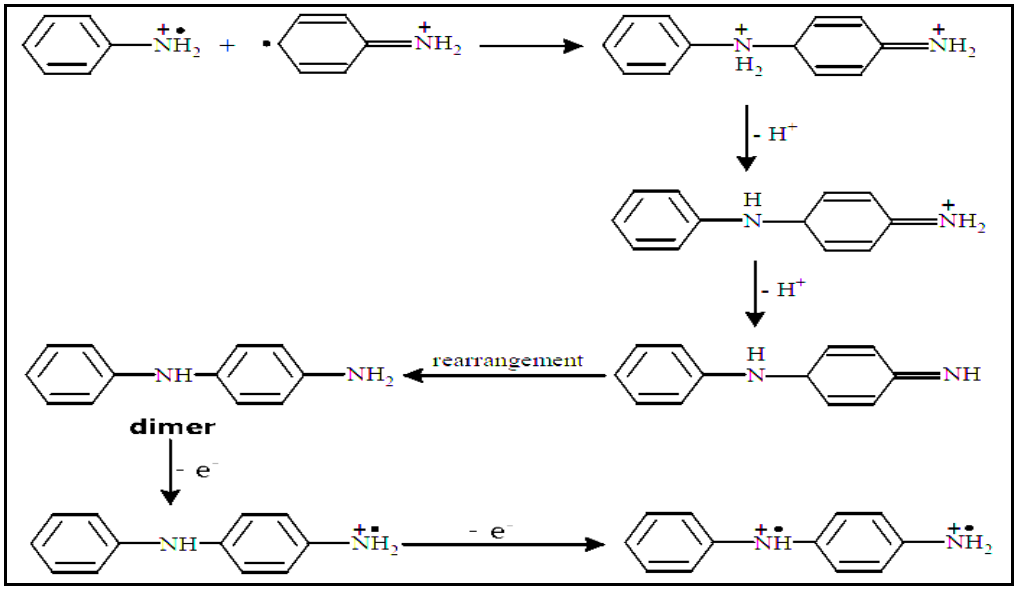

Figure (1.16): Formation of the dimer and its corresponding "radical cation"

Next, the formed radical can react either with the radical cation monomer or with the radical cation dimer to form, respectively, a trimer or a tetramer. If this continues, similar to the above steps, the polyaniline (PANI) polymer is finally formed (Fig.1.17).

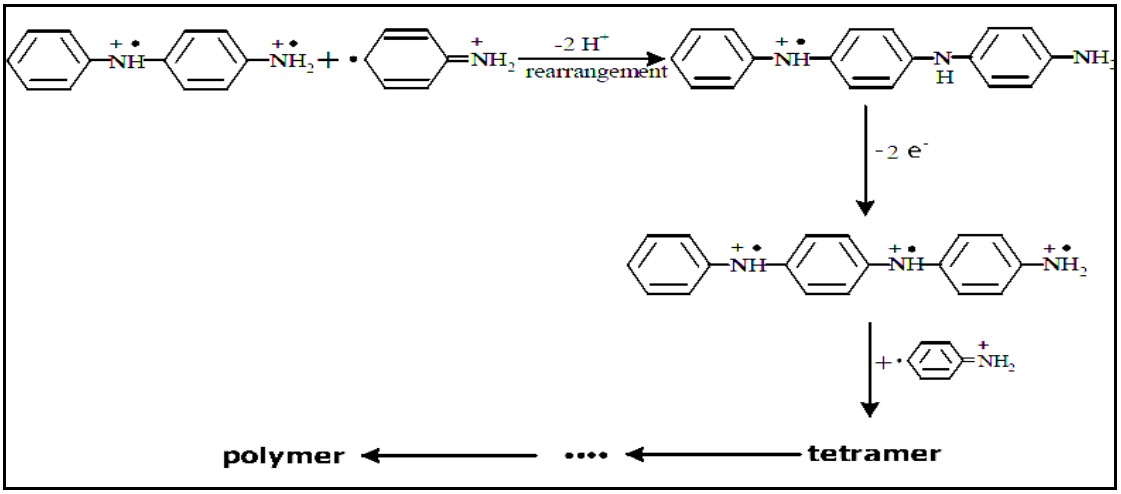

Figure (1.17): Mechanism of PANI formation

1.10 Types of Electroactive Materials and Band Theory[100, 101]

Any material can, in principle, be classified as an insulator, semiconductor or metal, frequently based on its electrical resistivity. Insulators have high resistivities ($>10^{10}$ ohm.cm); metals have low resistivities ($<10^{-3}$ ohm.cm); semiconductors have intermediate resistivities. The range of resistivities from insulators to metals is enormous. A good insulator such as quartz can have a resistivity as high as (10^{18} ohm.cm); a good metal such as copper can have a resistivity as low as (10^{-6} ohm.cm). It should be noted that, at a certain critical temperature, pressure and magnetic field, either insulators or semiconductors or metals can become superconductors with resistivities as low as (10^{-25} ohm.cm). The electronic conductivity is dependent on the migration of electrons or their counterpart holes. The conductivity (σ) is given by the equation:

$$\sigma = n.e.\mu \qquad (1.1)$$

Where n is the number of charge, e the charge and μ the mobility of the charge carriers. For metals, n is large and essentially unchanged with temperature. The only variable in σ is μ and since μdecreases slightly with increase of temperature due to collisions between the moving electrons and lattice atoms, σ also decreases with increase of temperature. For semiconductors and insulators, n usually increases exponentially with temperature. The effect of this dramatic increase in n more than outweighs the effect of the small decrease in μ. Hence, σ increases rapidly with temperature.

The electronic structures of metals, semiconductors and many solids may be described in terms of band theory. The “chemical approach” to band theory is to take “molecular orbital theory”, as it is usually applied to small, finite-sized molecules and to extend the treatment to infinite, three-dimensional structures. In the molecular orbital theory of diatomic molecules, an atomic orbital from an atom 1 overlaps with an atomic orbital on atom 2, resulting in the formation of two molecular orbitals (either σ orbitals or π

orbitals) that are delocalized over both atoms. One of the molecular orbitals is “bonding” and has lower energy than that of the atomic orbitals. The other is “antibonding” and is of higher Extension of this approach to large molecules leads to an increase in the number of molecular orbitals. For each atomic that is put into the system, one molecular orbital is created. As the number of molecular orbitals increases, the average “energy gap” between adjacent molecular orbitals must decrease as shown in (Fig. 1.18). The gap between bonding and antibonding orbitals also a decrease until the situation is reached in which there is essentially a continuum of energy levels.

The energy band resulted from bonding orbitals of a molecule is called the valence band. The energy band resulted from antibonding orbitals of a molecule is called the conduction band. The width of individual bands across the range of energy levels is called band width. The gap between the highest filled energy level and lowest unfilled energy level is called band gap *Eg*. There is no band gap in metals, i.e., *Eg*=0 eV. At absolute zero temperature (0K), when the electrons all occupy the lowest available energy state, the energy in the middle of the highest occupied state and the lowest unoccupied is the Fermi level . This energy level separates the occupied from unoccupied electron levels. The corresponding energy is the “Fermi energy E_F.”

The location of the “Fermi level” in relation to the allowed energy state is crucial in determined the electrical properties of a solid. As can be seen from (Fig. 1.18), metals always have a partially filled free-electron band, so that the “Fermi level” corresponds to a level in the middle of the band and this makes the metals electrical conductors. Semiconductors and insulators always have completely empty electron bands at (0K). This means that the “Fermi energy” lies between the bands, and consequently they are poor electrical conductors at ambient temperatures.

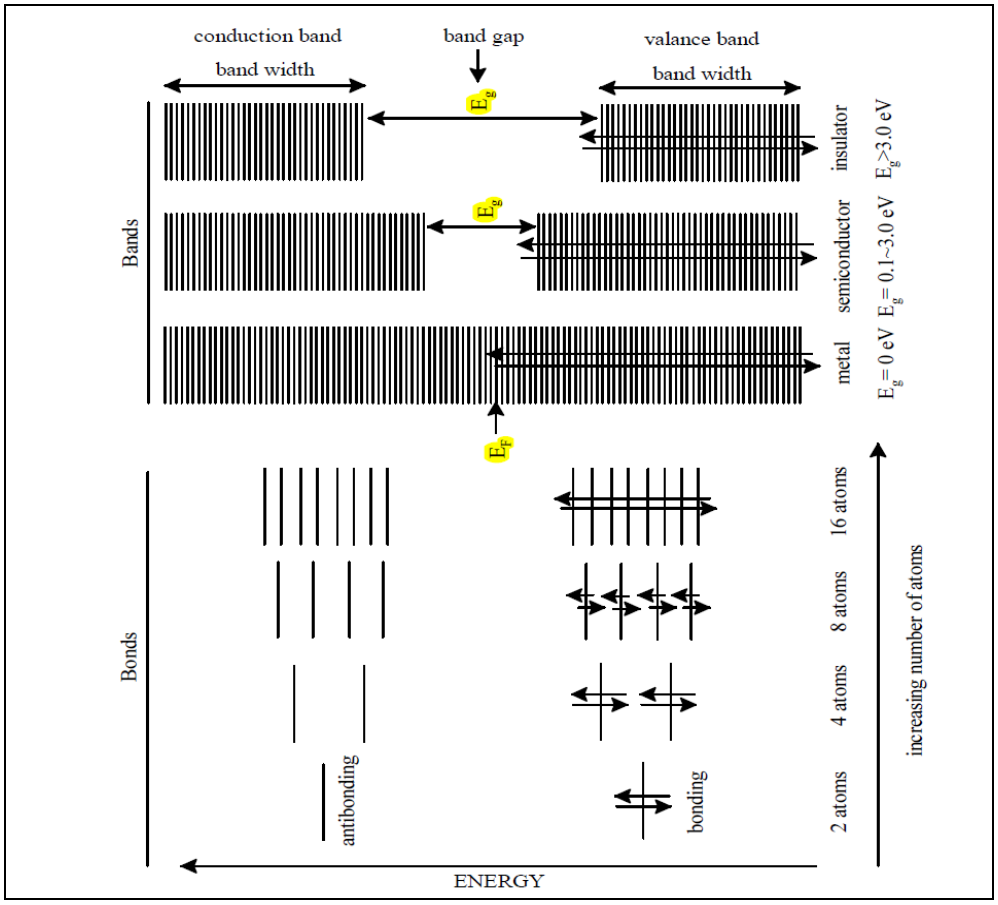

Figure (1.18): Bonds in molecules and bands in solids

1.11 Smart Hydrogel

Living systems respond to external stimuli adjustment themselves to changing conditions. Polymer scientists have been trying to imitate this behaviour for the last twenty years creating the so called “smart hydrogel”. These are defined as hydrogels that suffer reversible large, physical or chemical changes in response to small external changes in the environmental circumstances, such as temperature, pH, light, electric field, magnetic field, ionic factors, biological molecules, etc (fig 1.19). Smart hydrogels have very promising applications in the biomedical field as delivery systems of therapeutic agents, tissue engineering scaffolds, cell culture supports, bio separation devices, actuators or sensors systems [102].

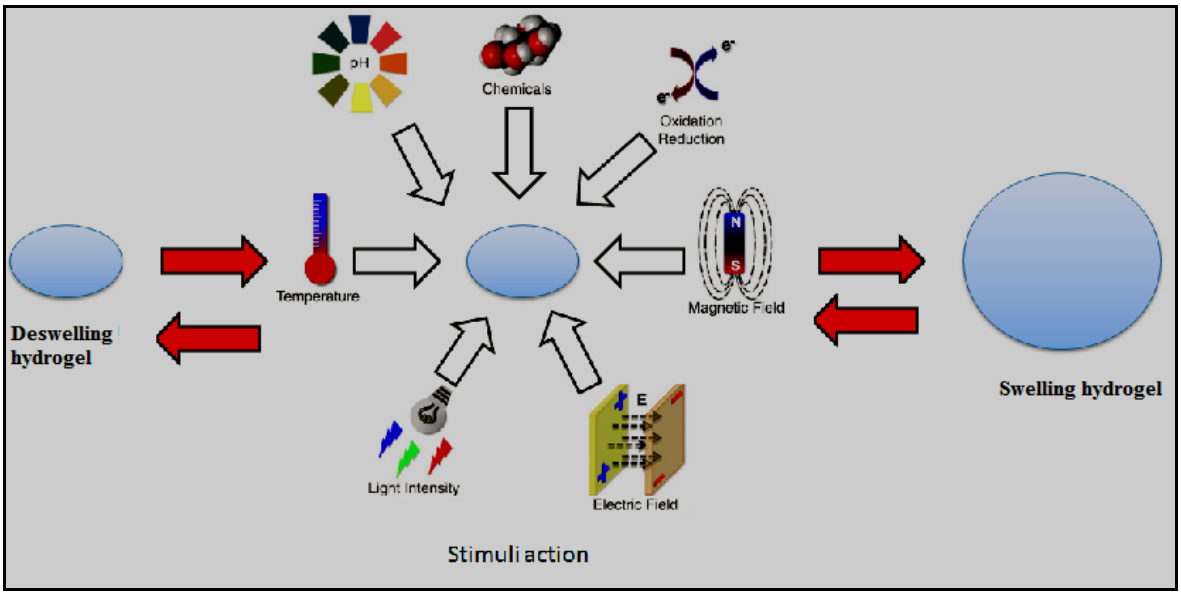

Figure (1.19): Stimuli responsive hydrogel [102]

Smart hydrogel have been divided into following types according to stimuli:

1.11.1 Temperature-sensitive hydrogels

Temperature-sensitive hydrogels are the most studied kind of stimuli sensitive polymer in drug delivery system. These hydrogels have ability to swell or de-swell due to vary in the temperature of the surrounding fluid. They are divided into three types: “negatively thermosensitive”, “positively thermosensitive” and “thermally reversible gels”[103].

“Negative temperature-sensitive hydrogels” have a lower critical solution temperature (LCST); means the critical temperature below which the polymer swells in the solution while above it the polymer shrinks. Below the LCST, the enthalpy factor, related to the hydrogen bonding between the polymer and the water molecules, is responsible for the polymer swelling. When the temperature is raised above the LCST, the entropy factor (hydrophobic interactions) dominates and polymer contraction may occur.

The polymers, which are used to prepare temperature-sensitive hydrogel, respond to a lower critical solution temperature (LCST) are Poly (*N*-isopropylacrylamide) (PNIPAM), Poly (*N*,*N*-diethylacrylamide) (PDEAM), Poly (*N*-ethylmethacrylamide) (PNEMAM), Poly (methyl vinyl ether) (PMVE), Poly (2-ethoxyethyl vinyl ether) (PEOVE), Ploy (*N*-vinylcaprolactam (PNVCa), Poly (*N*-vinylisobutyramide) (PNVIBAM) , & Poly (*N*-vinyl-*n*-butyramide) (PNVIBAM).

" Positive temperature-sensitive hydrogels" have an upper critical solution temperature (UCST). At cooling below the UCST, contraction may occur. Polymer networks of poly (acrylic acid) (PAA) and polyacrylamide (PAAm) or poly (acrylamide-co-butylmethacrylate) exhibit positive temperature dependence of swelling [104].

"Thermo responsive copolymer hydrogel", this copolymer is a composite stimuli-responsive polymer which has both an UCST and a LCST within changes temperature, and also responds to change of pH. For example utilize keto-enol tautomerization to form this kind of hydrogel. Accordingly, it can be effectively used for separation, chemovalve, drug delivery systems, artificial muscles, catheters, etc [105].

1.11.2 pH-sensitive hydrogels

Polymers sensitive to change pH are mainly water soluble with ionizing functional groups. Their physical properties like solubility vary in terms of pH. Hydrogels sensitive to pH have two main divides; cationic hydrogels and anionic hydrogels. "*Cationic hydrogels"* at a lower pH environment of stomach are swelling and drug release. They are mainly used for the advance of self-regulated insulin delivery system, which releases the insulin in response to change in the glucose concentration. "*Anionic hydrogels"* at a higher pH environment are swelling and drug release so swelling of this type of hydrogels is minimal in the stomach and the drug

release is also minimal. They are used in the preparation of smart controlled release systems for site specific drug delivery of therapeutic proteins to the large intestine, where the biological activity of the proteins are prolonged, Most commonly used ionic polymers for pH-responsive properties are poly (acrylamide) (PAAm), poly (acrylic acid) (PAA), poly (methacrylic acid) (PMAA), poly (diethylaminoethyl methacrylate) (PDEAEMA) and poly (dimethylaminoethyl methacrylate) (PDMAEMA) [106].

1.11.3 Dual pH-thermal sensitive systems

Some hydrogels are also known which have both pH and thermal sensitivities. It was synthesized by copolymerizing of monomer sensitive to change temperature, frequently, *N*-isopropylacrylamide, with a monomer sensitive to change pH like acrylic acid. Hydrogels prepared from poly (*N*-isopropylacrylamide) PNIPAAm and PAA exhibited dual sensitivities, PNIPAAm shows temperature-sensitivity, whereas PAA shows pH sensitive swelling. This hydrogels was able to respond quickly to both temperature and pH changes. “liu *et al.”* planned their use for controlled drug release [107].

1.11.4 Magnetic Field Sensitive Hydrogels

Gels sensitive magnetic field, or as we call them "ferrogels", are typical representatives of smart materials.

A ferrogel is a chemically crosslinked hydrogel swollen via a ferrofluid. A ferrofluid, or a magnetic fluid, is a colloidal dispersion of magnetic particles [108]. Their usual size is about (10 nm) and they have superparamagnetic behaviour. In the ferrogel, the finely dispersed magnetic particles are situated in the swelling liquid and linked to the flexible network chains of hydrogel by adhesive forces. The solid particles of colloidal size are the primary carriers of a magnetic moment. The moments are oriented

randomly in the absence of an applied field, so the gel has no net magnetization. The magnetic moments tend to align with the magnetic field to produce a bulk moment as soon as an external field is applied. The trend of the dipole moments to align with the application field is partially overcome by thermal agitation ordinary with field strengths, such as the gas molecules paramagnetic. All these particles are ultimately align their moments along the direction of the field with increases field strength, and as a result, the saturation magnetization. The magnetic dipole moments randomize quickly if the field is turned off, so the bulk magnetization to be again reduced to zero. A mechanical behavior ferrogel presents very close to that of the swollen network filled with non-magnetic colloidal particles when magnetic field equal zero. Preparation of ferrogel is similar to that of other networks hydrogel. One can precipitate well-dispersed particles in the polymeric matrix. The "in situ" precipitation is carried out before, during or after crosslinking reaction [109]. Preparation and characterization of magnetic colloidal particles are made separately, and the cross-linking occurs after the polymer solution and the magnetic sol are mixed together according to another method. [110].

The principle of the ferrogels shape conversion and motility deceit in a unique magneto-elastic behaviour. The magnetic field controls and drives the motion, and the final shape is set by the balance of magnetic and elastic interactions.

Magnetic hydrogels thus offer ways to selectively target, detect, and potentially treat cancer tissue via inductive heating and magnetic resonance imaging [111].

1.11.5 Electrical Field Sensitive Hydrogels

Electro-conductive hydrogels (ECHs), consists mainly of conducting polymer inherent within tridimensional network crosslinked hydrogel of

polymer-based tunable electrical properties. They are dynamic and flexible for various medical purposes [112], such as implantable drug delivery systems, allowing for controlled release of drugs on a patient when they need directly into the target area due to a combination of conductive properties of electro-active polymers (EAPs) and the swelling/de-swelling capabilities of the hydrogel (Fig.1.20).

There are different (EAPs) which may be used as conducting polymers, such as polypyrrole, polythiophene, poly (3,4-ethylenedioxythiophene) (PEDOT) and polyaniline (PANI) [113-116].

Usually, polymers with freely held electrons in their backbones can be called conducting polymers. On the backbone, each atom has link with a π bond, which is much weaker than the σ bonds in the backbone. These atoms have always a conjugated backbone with highly overlap of π-orbital [117]. It is known that the polymer chain can be reduced or oxidized to become either negatively or positively charged through doping process [118]. It is also known that conducting polymers could not be completely conductive without using dopants, and doping of π-conjugated polymers results in high conductivity [119]. The doping process is affected by different factors such as chain length, conjugation length, polaron length, and charge transfer to adjacent molecules. There have been various dopants for the addition of H^+ (protonation) to the polymers. Such as, strong inorganic hydrochloric acid (HCl), organic and aromatic acids containing diverse aromatic substitution has been used as dopants for (PANI) [117].

The application of PANI as (EAPs) has attracted much attention in a wide range of areas such as, technological applications such as electromagnetic interference shielding, rechargeable batteries, radar absorbing materials, microwave, biosensors, and anti-static coatings and anti-corrosive biomedical application such as artificial muscles [120-123]. This is attributed to the simplicity of its synthesis, either chemically or electrochemically method, easy doping process, and high chemical stability[124]. Polyaniline, the

intrinsically conductive polymer, has been shown also to be biocompatible and, is therefore, the (EAPs) choice for the synthesis of Electro-conductive hydrogel (ECH) [125]. When (EAPs) as PAIN or polypyrrole (PPy) are used alone, they demonstrate a lack of solubility and fragility, so it requires the blending of the (EAPs) into a system of co-matrix making it a necessary step for the synthesis of (ECH) [126].

1.11.6 Other stimuli-sensitive hydrogels

Several stimuli, other than effects above, can also stimulate the release of some therapeutically active agent from a depot. These include physical stimuli, such as ultrasound and light, which can be applied to the systems externally.

Ultrasound : is commonly used as a penetration enhancer drugs through biological barriers. For example, can release drugs Pulsatile available by on/off applied of ultrasonic device to ultrasound-sensitive hydrogel. Pulsatile release of insulin was achieved only after ultrasonic exposure for 1 minute, which causes the release of insulin [127].

Light-responsive hydrogels are utilized in developing photo-responsive devices, especially in ophthalmic drug delivery systems. These have a potential of becoming really biomimetic sensors. Light induced self-healing polymers can imitative the biological systems in which damage triggers a self-healing response. These hydrogels can be used to repair fiber fracture, delamination or propagation of microcracks of polymeric components used in a diversity of applications, extending the functional life and safety of the polymeric components [128].

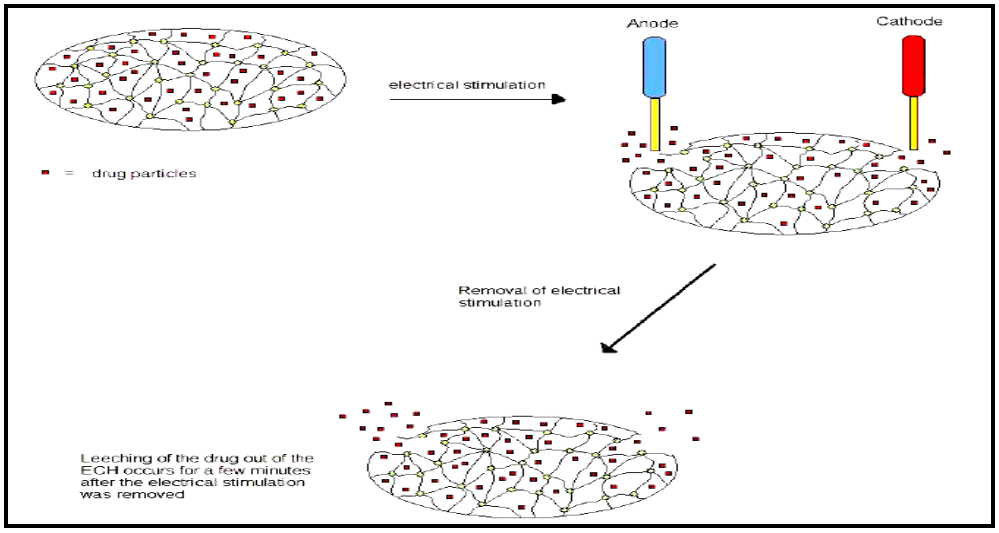

Figure (1.20): Schematic depicting the potential mechanism of drug release from the ECH [112]

1.12 Indigo Carmine as drug model

It is a dark blue powder; aqueous solutions are blue or bluish purple (the structural formula represented in fig 1.21). Indigo carmine is primary use as a pH indicator. It is an indigoid dye used to color oral and topical pharmaceutical preparations. It is utilized as a dye in the manufacturing of capsules. It is also utilized to color nylon surgical sutures and diagnostically as (0.8% w/v) injection [129].

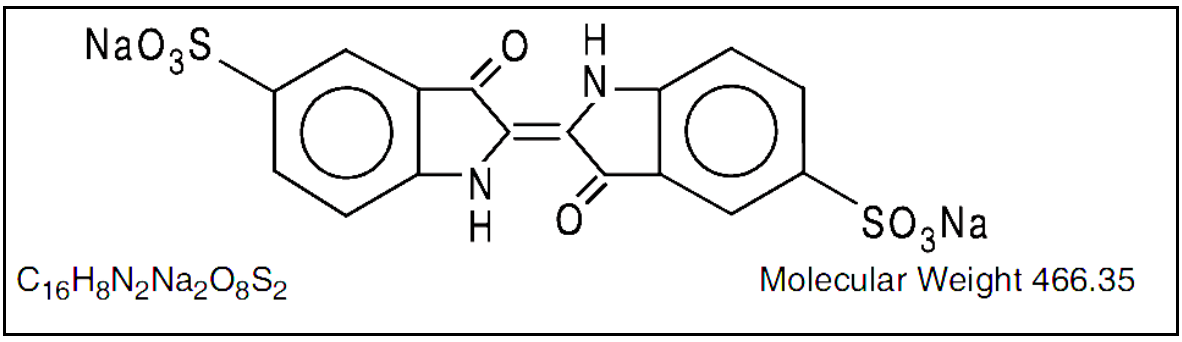

Figure (1.21): Structural formula for indigo carmine dye

It is frequently used to support assess ureteral patency, therefore indigo carmine used in female pelvic reconstructive surgery. It is given intravenously and largely renally excreted. Urine is colored blue and is consequently more easily visualized cystoscopically as blue efflux is noted from the ureteral orifices. The dye is visible after about (10) minutes, being half-life (4-5)

minutes in patients with normal renal function and adequate hydration. It is secreted primarily rather than re-absorption, and keeps its color blue as it passes through the body because of its molecular size. Indigo carmine can have a gentle pressor effect and should be used with care in patients with cardiac or vascular disease [130].

Indigo carmine is a deep-blue contrast stain that is used primarily in the colon for enhancing the detection or differentiation of colorectal neoplasms. Indigo carmine staining is often used in conjunction with high-resolution or magnification endoscopy [131]. The staining technique consists of either pancolonic or lesion-targeted spraying of (0.1% to 0.8%) indigo carmine, followed by immediate observation of mucosal irregularities and cavity patterns. The staining patterns are generally categorized by the Kudo pit pattern classification; nonneoplastic tissues are characterized by regular, rounded, or stellar pits, whereas neoplastic tissues are characterized by irregular, tubular, or villous pits (Fig. 1.22) [132].

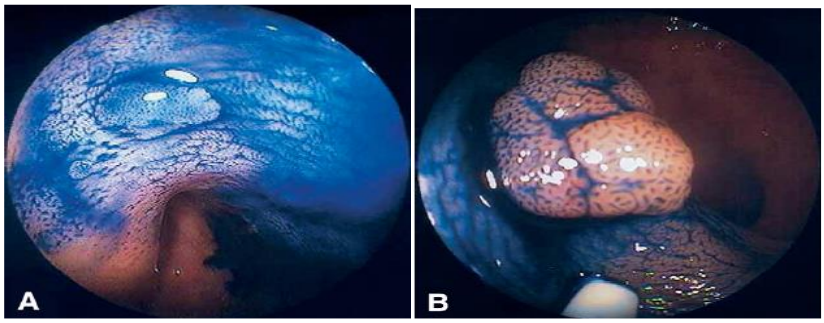

Figure (1.22): A, Colonoscopic view of hyperplastic polyp stained with 0.9% indigo carmine dye, B, Colonoscopic view of adenomatous polyp stained with 0.9% indigo carmine dye [132]

1.13 Anti-Cancer drug

1.13.1 Doxorubicin hydrochloride drug

The drug chosen for this study was doxorubicin hydrochloride, which belongs to the family of anti-tumor drugs (Fig. 1.23). It is anthracycline cytotoxic antibiotic, is widely used in the treatment of acute lymphoblastic leukemia, lymphoma not Hodgkin's lymphoma, breast carcinomas and many

other types of cancer [133]. It is hygroscopic crystalline powder, orange-red water-soluble and little soluble in methanol. It has to be administered by the intravascular route (intravenous or intra-arterial) because the drug is extremely irritating to tissues also is not absorbed by the gastrointestinal tract. Intravesical administration has been demonstrated as possible; following such administration, drug crossing to the systemic circulation is minimal.

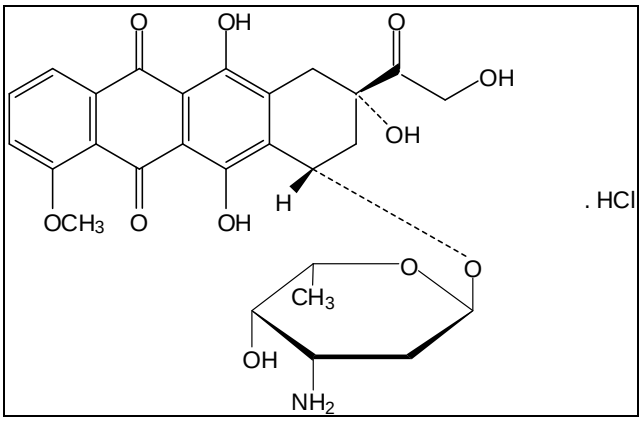

Figure (1.23): schematic of doxorubicin hydrochloride

Dosage is generally calculated on the basis of body surface area (mg/m^2). The schedule of doxorubicin dose to be delivered is changing depending on the therapeutic indication (e.g. solid tumors or acute leukemia) as well as on its use within a specific routine (e.g. as a single agent or in combination with other cytotoxics or as a part of multidisciplinary systems which include combination with surgery and/or radiotherapy and/or hormonotherapy).

Intravenous administration of doxorubicin should be performed with care. It is recommended to control its into the tubing of a freely flowing IV infusion (isotonic 5% glucose solution or sodium chloride) over a period of (3 to 5) minutes. Plasma levels of doxorubicin is followed decrease multiphasic, with a terminal half-life was reported in the range of hours (20 to 48). In the range of (8 to 20) ml/min/kg, plasma clearance and biliary excretion and metabolism mainly is due. In patients with impaired liver function could slow

elimination of plasma can be long now. By metabolic conversion to several products less active or inactive clearing doxorubicin occurs to a significant extent. The dose administered is recovered (40-50) percent in the bile or in the faeces in seven days. Renal excretion is modest, accounting for only (5% to 10%) of the administered dose in five days [134].

1.13.2. Methotrexate drug

Methotrexate is required for DNA synthesis, acts as an antagonist of folic acid and has a therapeutic effect on many types of cancer cells overexpress folate receptors on their surfaces [135]. It is widely used at present as a chemotherapeutic agent for major human malignancies as leukemia, malignant lymphoma, acute lymphoblastic, breast cancer, osteosarcoma, neck and head cancer [136]. An encapsulation of antitumor drugs in nanoparticulate systems such as polymeric nanoparticles, a higher drug concentration is kept within the cell, may overcome the shortcomings associated with conventional drug delivery strategies[137].

Methotrexate is yellow to orange brown crystalline powder (fig. 1.24). Practically is insoluble in water, alcohol, chloroform and ether but dissolved in dilute solution of mineral acids and alkali hydroxides and carbonates.

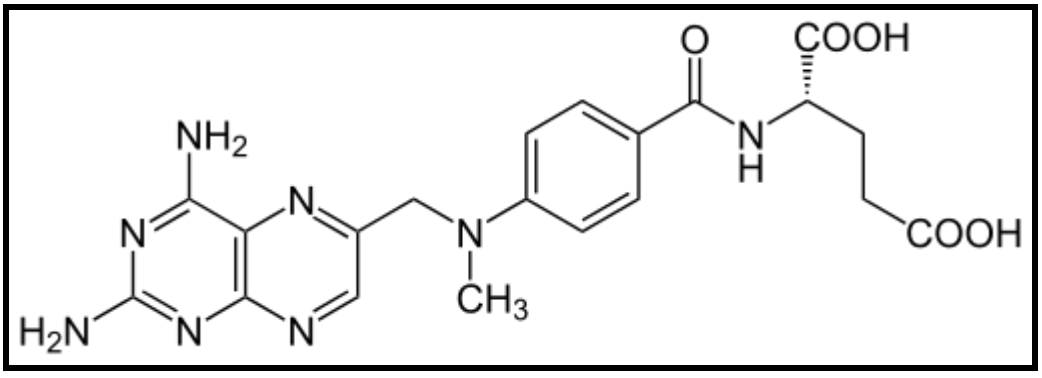

Figure (1.24): Schematic of methotrexate

Methotrexate dosage may be given orally as the base or sodium salt, or by injection as methotrexate sodium. The half-life reported for methotrexate is about (3 to 10) hours for patients receiving treatment for rheumatoid

arthritis or psoriasis, or low dose antineoplastic therapy (less than 30 mg/m^2). While patients are receiving high doses of methotrexate, the terminal half-life is eight to 15 hours [138].

1.14. Mechanism of Electro-responsive Drug Release from Hydrogels

Hydrogels sensitive to an electrical field are usually made of both synthetic and natural polyelectrolytes, separately or in combination. Electro-responsive hydrogels generally deswell or bend under the influence of an electric field, depending on the shape and the orientation of the gel between the electrodes [139].

Electrically responsive drug release occurs through a number of different mechanisms, such as, a charged drug migrates toward the oppositely charged electrode or, more commonly, hydrogel contraction results in ejection of drugs out of the gels on electrical stimulation (fig 1.25). Three main mechanisms have been suggested for electro-induced gel deswelling: (i) the development of a stress tendency in the hydrogel; (ii) differ in local pH around the electrodes as a result of the electrolysis of water (an increased pH in the cathode and a decreasing pH in the anode); and (iii) electro-osmosis of water coupled to electrophoresis. Electro-osmosis is defined moving fluid out of or through a porous material or a biological membrane induced by electric field. Although electrophoresis is to be happening through migration molecules in solution applied electric field. In practice, based on the nature of the gel and on the used experimental conditions, deswelling anisotropic gel occurs through a combination of some or all of the mechanisms discussed above. However, the major limitations of these systems are slow response times, nonlinear control between stimulation and drug release, and gel fatigue with time and electrical stimulations [140, 141].

In a recent study, an amphiphilic chitosan-silica hybrid hydrogel has been prepared for electrically modulated release of an anticonvulsant drug, Ethosuximide. Drug release was restricted by applying voltage to the

composite hydrogel. In this case, the electrical stimulation causes the release profiles in vitro modulation drugs ranging from burst-like patterns to slow-elution due to the combination of electro-osmotic and electrophoretic mechanisms [142].

Graphene also has attracted attention because of its attractive properties, such as high electron mobility, thermal conductivity and mechanical stability. "Reduced graphene oxide (rGO)" has been employed in the preparation of a drug releasing electrical system responsive. Lidocaine hydrochloride with the use of a hydrophilic substance as a model, drug release behavior of reduced graphene oxide-poly (vinyl alcohol) (PVA-rGO) hydrogels have been investigated. When larger amounts of (rGO) were incorporated, the (rGO-PVA) polymeric network became more negatively charged, which enhanced the action of electro-osmosis and reduced the intermolecular interactions between Lidocaine and (rGO). Accordingly, the Lidocaine release rate was increased [143].

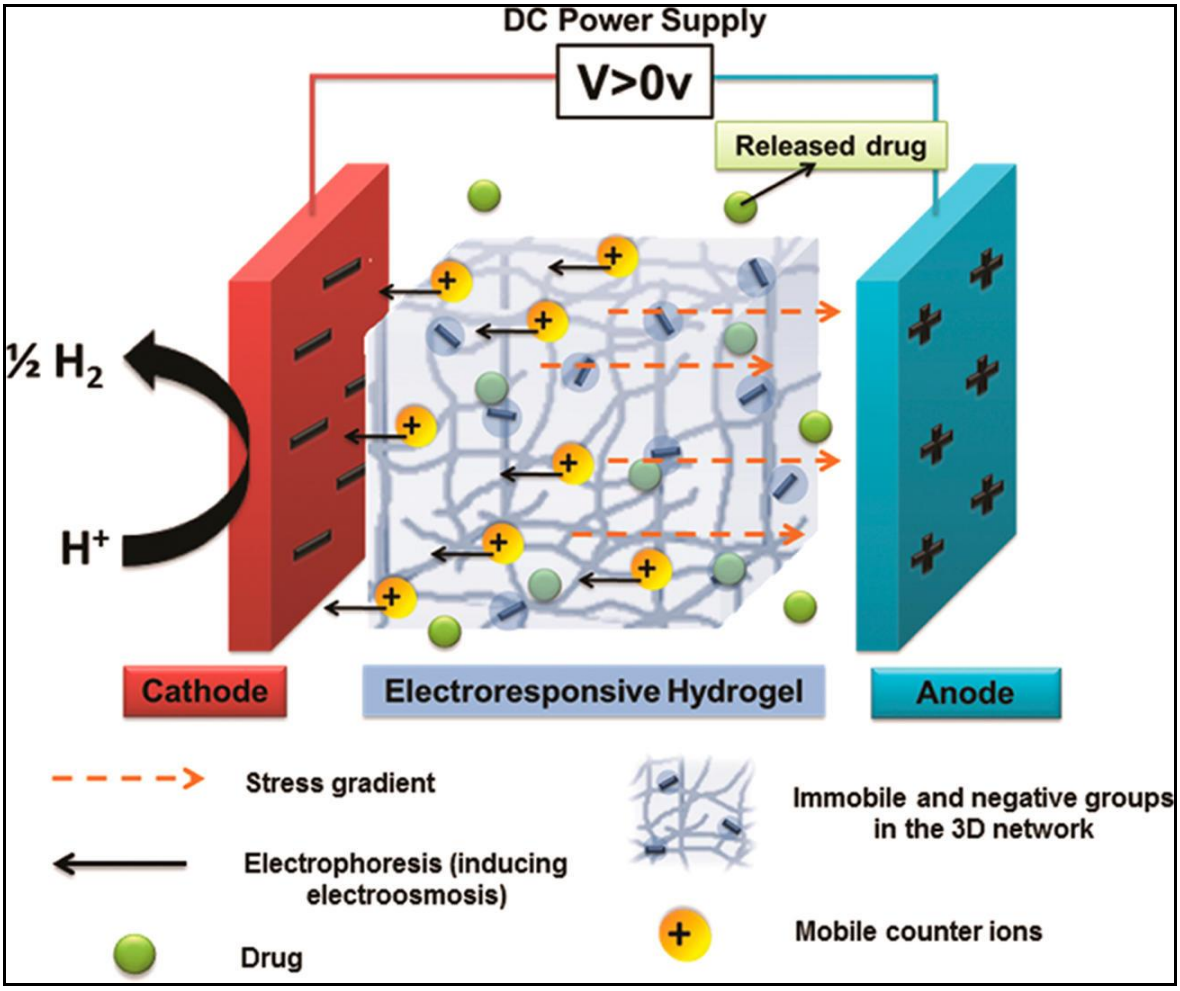

Figure (1.25): Schematic illustration showing the main mechanisms for electro-induced gel deswelling [140]

The response of polyelectrolyte hydrogels to an applied electric field can be used to control drug release from these hydrogels. Drugs can be integrated into the hydrogels either during or after the formation of hydrogel. This has been formed by impregnating the hydrogels in a solution and allowing drug molecules diffuse into the polymer network. Drug is released when an electric field is applied and stopped or reduced when the electrical induced will be removed in most cases.

Other types of drug release are pulsatile drug release system. The main mechanisms of pulstile drug release from hydrogels containing increasing amounts drug release are forced convection (heat transfer is complicated since it involves fluid motion as well as heat conduction) of drug out of the

hydrogel along with syneresed water (the contraction of a gel accompanied by the separating out of water)., diffusion, electrophoresis of charged drugs and release of drugs upon erosion of electroerodible hydrogels [144]. These different pathways of drug release are discussed in more detail response to electrically-induced changes in local pH below.

1.Forced convection of drug as hydrogel deswells

Ejection of a drug from the hydrogel is the most important release of drugs seem to be as the hydrogel deswelling and water syneresis under electrical stimulation. The electro-stimulation of the drug release from hydrogel reflecting profile deswelling hydrogel [143]. Anionic hydrogels are being contract at the anode [146]. While cationic hydrogels are be contract at the cathode [144]. Where volume changes of responsive hydrogels are be usually diffusion–controlled. The deswelling equilibrium is reached gradually[147].

When the electric field is switched off, drug release is stopped. Thus a pulsatile ‘‘on’’ and ‘‘off’’ profile of drug release can be got by switching the electric field ‘‘on’’ and ‘‘off’’ (Fig. 1.26)[148].

Sometimes, the back-flow of the drug into the hydrogel environment is observed as an electrical field is switched off, in this case hydrogel swells and absorbs some of the medium release or syneresis liquid because the back-flow of a drug into the hydrogel occurs through convection, rather than through diffusion (which would have led one to expect back-flow occur when the drug concentration in the hydrogel was lower than in the release medium.

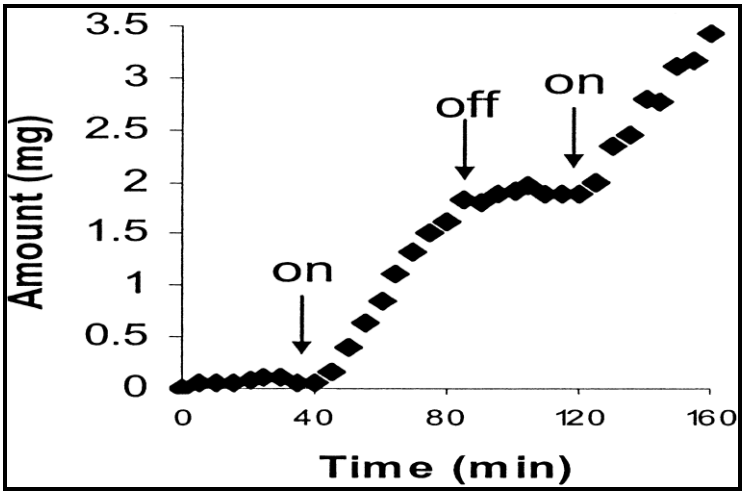

Figure (1.26): Pulsatile drug release profile from hydrogel when an electric field was switched "on" and "off "[148]

The size of the drug molecule is important, however. The smaller drug molecule [Aprotinin, molecular mass (Mr) 6512] back-flowed into the gel, but the larger one (lysozyme, (Mr) 14400) did not. Entry of the larger molecule into the hydrogel was restricted by the ‘‘pores’’ of the polymeric gel network [149].

2.Drug Diffusion out of hydrogel

Drug diffusion out of hydrogel also is an important mechanism of drug release and release profiles have been obtained when an interesting diffusion becomes an important mechanism of drug release. In contacting electrodes induced all the part of hydrogel deswelling while non-contacting electrodes only caused deswelling of the hydrogel surface. Consequently, the electrically-induced drug release profiles differed when contacting (set-up a) or non-contacting (set-up b) electrodes were used (fig. 1.27). In contacting electrodes, under induced electric field increased drug release due to bulk hydrogel deswelling which resulted in drug and water syneresis simultaneously were expelled from hydrogel caused by squeezed of hydrogel. In contrast, in non-contacting devices where the effects of the electric

current are first felt at the hydrogel surface, hydrogel deswelling at the surface (the formation of a ‘‘skin’’ with small reticular size around the bulk hydrogel) inhibited drug diffusion out of the bulk hydrogel under electrical stimulation. Drug release increased as drug diffusion could become unhindered when the electric field was removed [150]. As the hydrogel deswelled and the reticular size of the polymer network was reduced, the macromolecule’s pathway of the hydrogel became more tortuous and drug diffusion out of the molecules, in relation to the hydrogel was decreased. It is likely that the large size ‘‘pore’’ size of the polymeric network hindered their expulsion from the hydrogel when the latter syneresed.

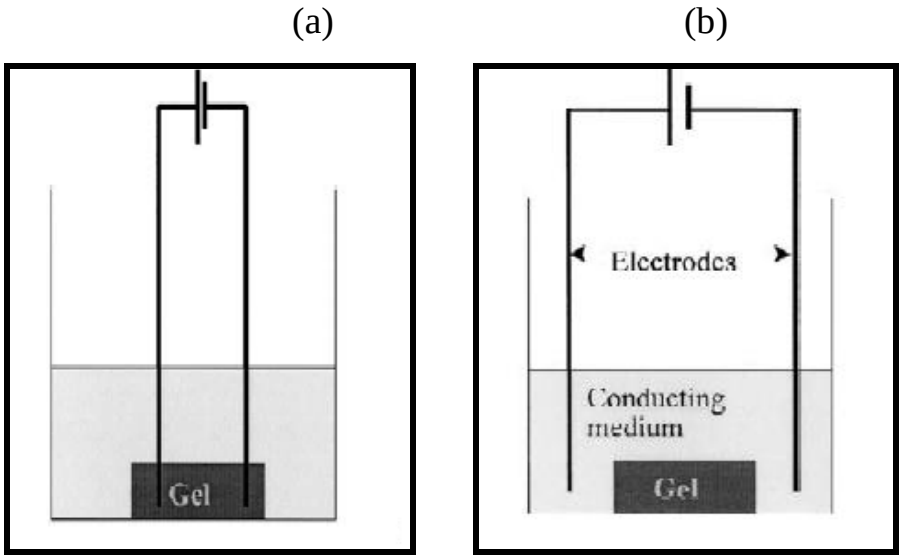

Figure (1.27): (a) set-up of contacting electrodes,(b) none contacting electrodes to study electro-responsive drug delivery from hydrogels [150]

When the electric current is switched off, pulsatile release drug is still achieved, while the release is suspended or reduced when the electric field is switched on. Suggested, when the current is switched off; releasing the drug was stopped when the polymeric hydrogel shrank tighter network and prevent diffusion of the macromolecule out of the hydrogel. Contrary when the current was switched on, electro-responsive release of macromolecules is desired, because hydrogels which swell in response to an electric field may be more

suitable drug carriers. A pulsatile release was thus demonstrated when the electric field was switched ‘‘on’’ and ‘‘off’’ sequentially. The response of the hydrogel was sharp and no leakage of drug occurred during the ‘‘off’’ periods due to electrostatic interactions between the largely ionized drug and the groups of the polymer [151].

3.Drug electrophoresis

Charged drugs may also be electro-released from hydrogels when charged ions migrate towards opposite charge of electrode. Such an additional pathway of drug release has significant effects on the amount of drug that is electro-released. The release of positively charged (Edrophonium drug) ion from anionic hydrogel was found to have higher degree than release of neutral drug (hydrocortisone) which could only be released by convection enforcement causes of hydrogel deswelled. This explained by positively charged drugs were displaced from their interactions with negative charges on the polymer network by (H^+) ions be of water electrolysis at the anode at electrical stimulation. Subsequently, the ‘‘free’’ Edrophonium ions was electrophoresed towards the cathode and diffused out of the hydrogel. It is important that (H^+)ions produced at the anode exchange with the Edrophonium ion so that the latter are ‘‘free’’ to be released from the gel. When electric current was increased, drug release increased, but not linearly. The average increase in drug release decreases with increasing current. Kwon et al., Suggests (H +) ions production could migrate faster toward the cathode, resulting in less opportunity for (H +) to exchange with Edrophonium ion connected with polymer network at higher voltages. Thus, drug release increases with increasing electric field, it is not linearly proportional [152].

4.Drug Liberation when hydrogel Erodes

Drug release can also be happened by gel erosion mechanism; this

mechanism can be occurred to kind of gels that erode in response to an electric stimulus. On electrical stimulation, the polymer complex breaks up to small part when attached to an electrode and drug release due. “Kwon et al.,” suggested pulsatile release behavior of insulin from poly (ethyloxazoline)-poly(methacrylic acid) which reflected the pulsatile electrical stimulation (Fig. 1.28). Insulin was released in such a stepwise manner until (70%) of the load had been released. The large deviations in the rate of release can be attributed to irregular erosion of hydrogels that were due to deficiencies in the hydrogel matrix [153].

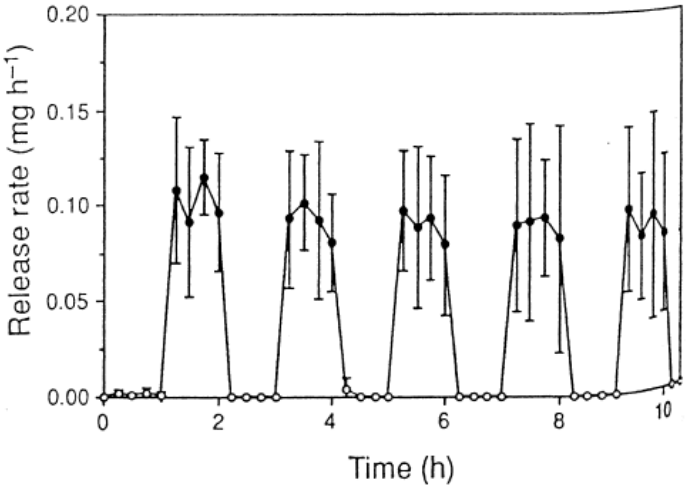

Figure (1.28): Pulsatile release of insulin from electro-erodible polymer complexes (•—current on 5 mA, o—current off) [153]

1.15 Literature Survey

S. Mohammadi-Samani et. al.,[154] have prepared and characterized chitosan-coated superparamagnetic Fe_3O_4 nanoparticles for controlled delivery of methotrexate. They used transmission electron microscopy (TEM) to know the average size of iron oxide alone (10nm) while Zetasizer was applied to calculated average size of coated Fe_3O_4 with chitosan which carrying with drug. From this method was being obvious change in particle size after coating (152 nm).

Doina Hritcu et. al.,[155] synthesized magnetic chitosan nanosphere, by co-precipitation method. They synthesized Fe_3O_4 and crosslinked with chitosan by sodium tripolyphosphate (STPP). It was characterized by (TEM) and other techniques.

Dena Dorniani et. al.,[156] preparation of magnetic nanoparticles with average size(6nm) and coated with chitosan carrying drug (prindopril erbumine)then characterization by (X-ray diffraction, TEM, magnetic measurements, thermal analysis and infrared spectroscopic studies). They have observed the change in size to (15 nm) after coating.

S. Asgari et. al., [157], used grafted copolymerization to prepare N-sodium acrylate-O-carboxymethyl chitosan [CMCH-g-PAA (Na)] bound with Fe_3O_4 nanoparticles, and by XRD through applied Debye-Scherre equation, they calculated different in size before and after coated Fe_3O_4 was (26 and 33nm,) respectively.

Jude Namanga, et. al., [158], prepared magnetic nanocomposites composed of superparamagnetic magnetite nanoparticles in a pectin matrix by "in situ" coprecipitation method. X-ray diffraction (XRD), scanning electron microscopy (SEM), transmission electron microscopy (TEM), energy dispersive X-ray spectroscopy (EDX), & Fourier-transform infrared (FT-IR) spectroscopy were used to characterize the nanocomposite. The mean diameters of Fe_3O_4 and pectin-Fe_3O_4 were 9 and 13 nm, respectively.

Foba-Tendo J. Ngenefeme, et.al. [159], prepared Fe_3O_4 MNPs with co-precipitation method by using two differences precipitating agent (NH_4OH, NaOH) and studying differences between them. Then coated with pectin and characterization with (TEM), (FT-IR), scanning electron microscopy (SEM), (XRD), and zeta-potential.

Reyhan Omidirad, et. al. , [160], Prepared poly (acrylic acid)-coated Fe_3O_4 MNPs composite loading with doxorubicin. Fe_3O_4 has spherical shape with (6nm). The drug delivery study in vitro with two pH values (4.2 and 7.4)

for (8h.). Drug release was (100%) in pH=4.2 larger than in pH=7.8 found (78%).

S. Kayal, & R.V. Ramanujan [161], studied drug delivery in vitro to doxorubicin drug carrying on (PVA-Fe_3O_4). This composite was characterized with X-ray diffraction, TEM, TGA, FTIR and VSM techniques.

Xing-ping Qiua and Francoise Winnikb [162], have prepared composite (PVA-Fe_3O_4). This iron oxide was obtained by co-precipitation of Polyvinyl alcohol coated magnetic particles (PVA ferrofluid) have been synthesized by chemical co-precipitation of Fe(II)/Fe(III) salts in (1.5 mol/L) NH_4OH solution at 70°C in the presence of PVA.

Hailong Fan, et.al. [163], prepared graphene with few layer by direct current arc-discharge method and (NH_3) as buffer gases and then doping with chitosan.

Lulu Ren, et. al. [164], synthesized (graphene/polyacrylamide) with responsive pH.

I. Tantis, et.al. [165], made modification of graphene with PVA and characterized with SEM which appeared graphene was inserted PVA backbone by adsorption on PVA backbone.

Jangho Kim, et. al. [166], synthesized nanotopographic substrate by using graphene incorporated chitosan for stem cell engineering.

Yeon-YiKim et. al. [167], synthesized conductive hydrogel composite (Multi-walled carbon nanotube/poly (vinyl alcohol) (PVA)) by freezing-thawing method. This composite was responsive to electric field and has outstanding of mechanical properties.

Sajjad Sedaghat [168], was synthesized and characterized (chitosan-graft-polyaniline) by using formaldehyde as crosslinking agent. This composite was characterized by (FT-IR), UV-visible, scanning electron microscopy (SEM), and differential scanning calorimetry (DSC) techniques.

Tong-Sheng Tsai, et.al. [169], synthesized electro-conductive hydrogels from crosslinking between PVA and diethyl acetamidomalonate and doping

by using PANI. Then loading with indomethacin drug and studying electro-actuable release of it.

A. K. Bajpai, et.al. [170], synthesized hydrogel (poly (vinyl alcohol) (PVA)-g-poly (acrylic acid) (PAA)) and impregnated with PANI to obtain conductive composite. LCR meter was using to study electric properties of this composite.

Prabhaker and kumar [171], synthesized conductive hydrogel composite poly (acrylate-co-acrylamide)/polyaniline by interpenetrating of PANI inside hydrogel matrix by using N, N´ –methylene bis acrylamide as crosslinking agent.

Aims of the Present Work

The aim of this work is to use new electric field stimulus responsive nanocomposite hydrogels for drug delivery program through loading the nanocomposite hydrogels with drug and study releasing of the drug. Weak external Ac field is preferred to control the releasing the drug, approaching a novel interactive drug delivery system that can show an externally tailored release profile with an excellent spatial, temperature, and dosage control.

Conductive nanocomposite hydrogels will be synthesis by mixing conductive nanomaterials (graphene, multi-wall carbon nanotubes) with hydrogels or coating magnetite nanoparticle with conductive hydrogel to obtain electro-magnetic nanocomposite.

Magnetite nanoparticle (Fe_3O_4) will be synthesis by co-precipitation method and coating with conductive hydrogel, where conductive hydrogel will be synthesis by mixing conducting polymer inherent as polyaniline within tridimensional network crosslinked hydrogel, while graphene (G) will be synthesis by hummer method.

Hydrogels will be synthesis from biodegradable polymers by crosslinking method as chitosan crosslinking with poly (vinyl alcohol) by glutaraldehyde [CPG], by maleic anhydride [CPM], pectin crosslinking with poly(vinyl alcohol) by maleic anhydride [PPM]. Free radical polymerization method also will be use to synthesis hydrogels as poly (vinyl alcohol)-graft-poly acrylic acid [PgA], chitosan-graft-poly acrylamide [CgA], and interpenetrating chitosan-poly (acrylic acid-co-acrylamide) [IPN].

Hydrogel and nanocomposite hydrogel will be characterization by FTIR, X-ray diffraction, AFM, SEM,TEM, TGA, and DSC.

Electric properties of conductive nanomaterials and their composite will be study by LCR meter.

Magnetic properties of uncoated and coated magnetite will be study by vibrating sample magnetometer (VSM).

Drug release will be study by UV-Vis spectrophotometer in phosphate buffer solution (pH=7.4) with different voltage at room temperature or different temperature at constant voltage to determine the effect of voltages and temperature on drug release ratio from nanocomposite hydrogel.

Anti cancer drugs will be select as (doxorubicin hydrochloride and methotrexate) to study how be reduce the side effect of these drugs through loading on smart hydrogel or stimuli responsive hydrogel.

2.1 Materials

Chemical materials used in the present work are given in (Table 2.1) for liquid and (2.2) for solid together with their purity and suppliers. All were used without further purification except aniline.

Table (2.1): Chemicals Liquid, purity and suppliers

Chemicals	**percentage**	**Supplier**
Acetic acid	99%	Sigma-Aldrich
Acetone	99.7%	ROMIL LTD
Acrylic acid	99%	HIMEDIA
Ammonium hydroxide solution	30%	BioSolve BV
Aniline		CDH
Diethyl ether	99.8%	ROMIL LTD
Glacial acetic acid	99.8%	Sigma-Aldrich
Glutaraldehyde solution	25%	Sigma-Aldrich
Hydrazine hydrate solution	80%	Scharlab S.L.
Hydrochloric acid	37%	BDH
Hydrogen Peroxide	50%	Sigma-Aldrich
Sulphuric acid	98%	ROMIL LTD
N,*N*,*N*′,*N*′Tetramethylethylene diamine (TEMED)	99 %	HIMEDIA

Table (2.2): Chemicals solid, purity and suppliers

Chemicals	Purity	Supplier
Acryl amide	≥99%	Sigma-Aldrich
Ammonium Persulphate	97%	Hopkin & Williams LTD
Chitosan(medium molecular weight)		Sigma-Aldrich
Di Sodium hydrogen phosphate	≥99%	Sigma-Aldrich
Doxorubicin hydrochloride		Sigma-Aldrich
Ferric Chloride anhydrous	98%	Thomas Baker
Graphite rod(low density)	99.99%	Sigma-Aldrich
Indigo carmine		Hopkin & Williams LTD
Iron(II) Sulphate 7-Hydrate	99.5%	BDH
Maleic anhydride	≥99%	Sigma-Aldrich
Methotrexate		Sigma-Aldrich
N,N-methylene bis- acrylamide	99.5%	Thomas Baker
Multi-wall Carbon nanotubes*	>99%	CheapTubes
Pectin (30000-100000)		Sigma-Aldrich
Poly (vinyl alcohol) (175000)	99.9%	Panreac
Potassium chloride	≥99%	Sigma-Aldrich
Potassium dihydrogen phosphate	≥99%	Sigma-Aldrich
Potassium permanganate	≥99%	Sigma-Aldrich
Potassium persulphate	99.99 %	Sigma-Aldrich
Sodium chloride	≥99%	Sigma-Aldrich
Sodium dodecyl sulfate	≥99%	Sigma-Aldrich
Sodium Nitrate	≥99%	Sigma-Aldrich

*Multi-walled carbon nanotubes with characterization following, outer diameter (13-18) nm, length(1-12)μm, surface area(> 233)m^2/g, electric

conductivity(>10^2 S/cm), method of preparation (Catalytic chemical vapor deposition (CCVD)).

2.2 Instrumentation and Equipments

2.2.1 FT-IR Spectra

FT-IR spectra were characterized by using Shimadzu, Fourier Transform Infrared Spectrophotometer, model IR-Prestige 21, work in the range (4000–400) cm^{-1}. Using potassium bromide discs, carried out at Ibn Sina Company, Baghdad University.

2.2.2 X-Ray diffractometer (XRD)

The prepared materials are characterized by X-ray diffraction using (Shimadzu-XR-6000) device with Copper target (wave length =0.15406 nm), voltage (40 KV), and current (30mA). Scanning is done on the range (2θ= 5.000-80.000) continuously with speed (5 degree / min) and receiving slit (0.3 mm). The analysis was conducted at College of Education for Pure Science /Ibn -Al- Haitham / Baghdad University.

2.2.3 UV-Vis Spectrophotometer

Drug release from conductive hydrogels was studied by using (UV-Vis) spectrophotometer type T80 (PG Instruments Ltd U.K.) of the range (190-1100) nm, Supplied with a motorised (8 cell) changer and pre-aligned Tungsten and Deuterium lamps. The analysis was conducted at College of Education for Pure Science /Ibn -Al- Haitham / Baghdad University.

2.2.4 Atomic Force Microscope (AFM)

Compact Atomic Force Microscope (AFM) made by PHYWE (Germany) was used to study of surface topography of nanomaterials. This

analysis was carried out in the College of Education for Pure Science /Ibn-Al- Haitham /Baghdad University.

2.2.5 Scanning Electron Microscope (SEM) and Energy Dispersive X-Ray Spectroscopy (EDS)

SEM made by Zeiss (Oxford instruments) was used to study the surface topography of nanomaterials and hydrogel nanocomposite and from EDS was determined the element present in pure Fe_3O_4 MNPs and coating form (CPG/Fe_3O_4/PANI). This analysis was carried out in Sharif University of Technology, Tehran, Iran.

2.2.6 Transmission Electron Microscope(TEM)

TEM made by Zeiss (Jena, Germany) EM10C-80K was used to study of surface topography of coated and uncoated magnetite with examine particle size. This analysis was carried out in Sharif University of Technology, Tehran, Iran.

2.2.7 LCR Meters

LCR Electronic Test device was used to measure the Inductance (L), Capacitance (C), and Resistance (R), of a component.

The electric properties of the nano and nanocomposite films were measured by using Multi -Frequency LCR Meters (HEWLETT. PACKARD) device was made in Japan. This measure was carried out in College of Education for Pure Science /Ibn -Al- Haitham /Baghdad University.

2.2.8 TGA & DSC analysis

TGA and DSC analysis was performed thermogravimetric analysis (TGA) and differential scanning calorimetry (DSC) by Linseis model STA

PT-1000, made in Germany. This measure was carried out in College of Education for Pure Science /Ibn -Al- Haitham /Baghdad University.

2.2.9 Vibrating Sample Magnetometer (VSM)

The magnetic properties of pure Fe_3O_4 & coated form (CPG/Fe_3O_4/PANI) were measured with MDK vibrating sample magnetometer (VSM) with magnetic field strength equal to 1 tesla, made in Japan. This measure was carried out in Kashan University, Iran.

2.2.10 Ultra- sonic devices

For dispersion of nanomatrials (nanoparticles, nanosheets, nanotubes) in the solution a device of type soniprep 150 (Great Britain) was used while for dispersion and mixing nanocomposite was used ultrasonic water bath of type WiseClean model WUC-A06H made by DAIHAN Scientific Co. Ltd., Korea. This technique was carried out in College of Education for Pure Science /Ibn -al- Haitham Baghdad University.

2.2.11 Mechanical stirrer

For Mixing of nanocomposite was used mechanical stirrer of type WiseStir, HS300 by speed to 3000rpm made by DAIHAN Scientific Co., Ltd. (Korea).

2.2.12 Digital Multimeter

Digital Multimeter type DT 9208A, China was used for examining conductivity for samples.

2.2.13 Power Supply

To applied potential for studying drug release was used power supply model FMN TGL 10395 TL made by FEINWERKTECHNIK (Germany) with power SVG 220V~ 40VA.

2.2.14 Vacuum Drying Oven

The prepared materials were dried by vacuum oven model VO-27 made in Korea.

2.2.15 pH-meter

For measurement pH solution was used Professional Benchtop pH Meter, model BP3001 by Trans Instruments (Singapore) Pte. Ltd.

2.2.16 Micrometer

Nano composite films thickness was measured by micrometer (0-25mm) made by JIANGXI (China).

2.3 Synthesis of graphene oxide (GO)

Graphene oxide (GO) was synthesized from graphite powder using modified Hummer's method (scheme (2.1)). In brief, (3 g) of graphite was sieved to size (75μm) and (1.5 g) of sodium nitrate were mixed together followed by the addition of (69 ml) of concentrated sulphuric acid under constant stirring in ice bath (at 0ºC). Two hours after mixing, (9 g) of KMnO4 was added gradually to the above solution while keeping the temperature less than (20°C) to prevent overheating and explosion. The mixture was stirred also at (35 °C) for (1 h) and the resulting solution was diluted by adding (500 ml) of water drop wise under vigorous stirring. To ensure the completion of reaction with KMnO4, the suspension was further treated with (15 ml) of (50% H_2O_2) solution. [72]. graphene oxide was collected by decantation and filtration and washed with (300ml) of HCl (5%) and several time with distillated water respectively to remove residue material. The graphene oxide was dried in vacuum oven at (50ºC).

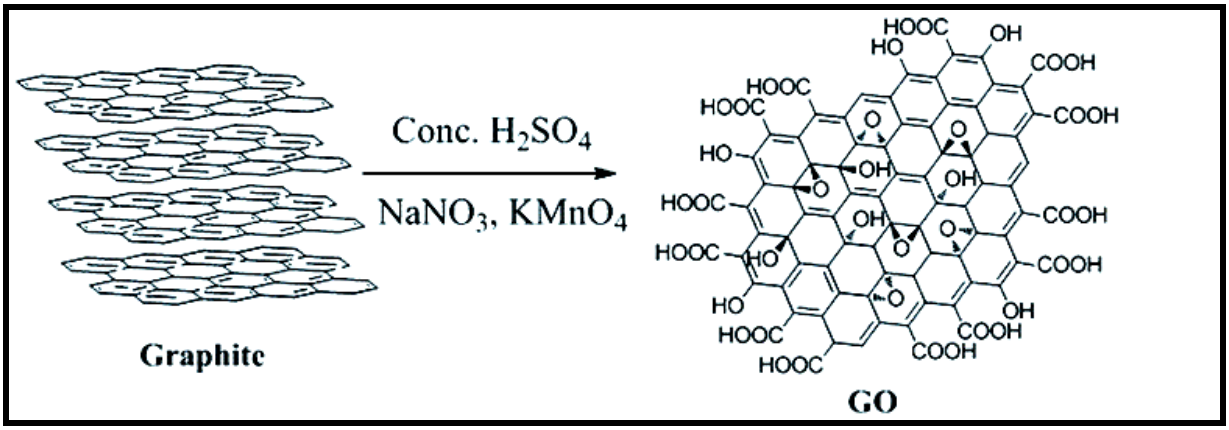

Scheme (2.1): Hummer's methods for synthesis GO[72]

2.4 Synthesis of graphene (G)

GO powder was added to a beaker containing (100ml) of distilled water to dispersion in ultrasonic for one hour. Immediately after that, dispersed GO was placed in a three neck round bottom flask was immersed in water bath set at (80ºC), then (5ml) of hydrazine monohydrate was added to it under reflux with stirring for (24 hrs). The resulting black powder was collected by decantation, filtered and washed several time with distilled water. The graphene was dried in vacuum oven at 50ºC overnight [172].

2.5 Synthesis of magnetic nanoparticles of Fe_3O_4 (MNPs)

Fe_3O_4 magnetic nanoparticles were synthesized by chemical co-precipitation method. In typical synthesis, a solution of $FeCl_3$ and $FeSO_4.7H_2O$ (molar ratio 2:1) was prepared by double distilled water treated with ultrasonic for (1 h). The solution of ferrous sulfate hydride was placed in a three neck round bottom flask was immersed in water bath set at (60ºC) with stirring under nitrogen for (30 min) followed by addition solution of ferric chloride and left to mix for one hr.

$$Fe^{+2} + 2Fe^{+3} + 8OH^- \rightarrow Fe_3O_4 + 4H_2O$$

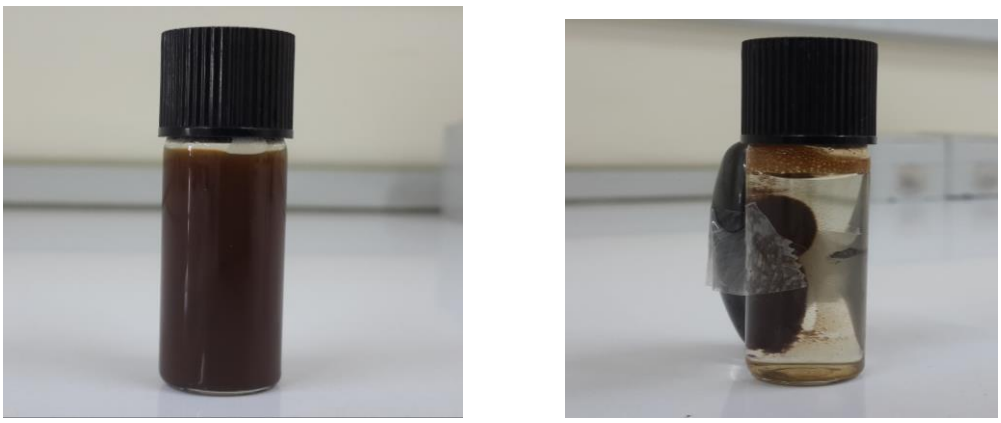

Figure (2.1): Image of dispered solution of magnetite, and collected with magnet

The temperature was raised to (80ºC) and enough ammonium hydroxide solution was added immediately with violently stirring until to pH=10 then was added (6ml) of solution of sodium dodecyl sulfate (0.4% $NaC_{12}H_{25}SO_4$) to avoid accumulation. The stirring was continued for another (2hrs) at same temperature [173]. The black brown precipitate was formed and washed several times with distillated water to purified where collection by magnet fig (2.1).

2.6 Synthesis of polyaniline (PANI)

Aniline hydrochloride was prepared by adding concentrated hydrochloric acid to freshly distilled aniline drop wise with molar ratio (2:1) in ice bath. The Precipitate of aniline hydrochloride was filtrated and washed with diethyl ether. The aniline hydrochloride was dried with the filter papers by desiccator to prevent exposure of light for 24hrs.

Aniline hydrochloride (1g) was dissolved in 5ml of distilled water. Ammonium persulfate (2g) was dissolved in (5 mL) of distilled water. First the solution was kept for (1 h) at (0-2 °C) in an ice bath. Polymerization reaction was started by drop wise addition of aqueous solution of ammonium persulphate (APS) for (1h) with stirring in beaker then left overnight in refrigerator. Next day, the PANI black green precipitate was collected on a

filter paper, washed three times with 100-mL of (0.2 M HCl), and similarly with acetone (scheme(2.2)).The precipitate PANI was washed with (0.2 M HCl) to remove residual monomer, oxidant, and its decomposition products. Polyaniline (emeraldine) powder was dried in vacuum oven at 50 °C. Under these conditions the polymer was obtained in a doped state (PANI-HCl) not soluble in water [174].

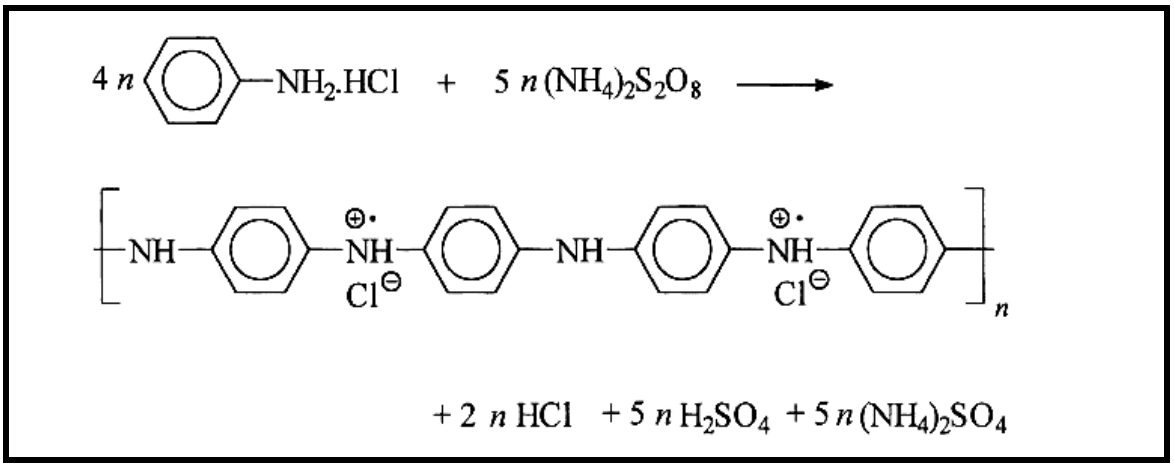

Scheme (2.2): Oxidation of aniline hydrochloride with ammonium persulfate yields polyaniline (emeraldine) hydrochloride[174]

2.7 Preparations of Hydrogels

PVA solution (10%w/v) was prepared by dissolving (10g) of PVA in (100ml) distilled water with stirring at 70ºC,while chitosan solution (1%w/v) was prepared by dissolving (1g) of chitosan in acetic acid solution (1%) with stirring at 60ºC, and Pectin solution (2.5 %w/v) was prepared by dissolving(0.5g) of pectin in (20ml) distilled water with stirring at 50ºC[175, 176].

2.7.1 Preparation of hydrogel (CPG) from crosslinking between chitosan and PVA by glutaraldehyde

CPG hydrogel was prepared by mixing equal volumes of PVA solution with chitosan solution. The mixture was stirred constantly until homogeneous at 60ºC and the appropriate amount of crosslinking agent (10 ml) of glutaraldehyde solution (1.25%) was added into the mixture under constant stirring with (2 drops) of concentrated H_2SO_4 [177].

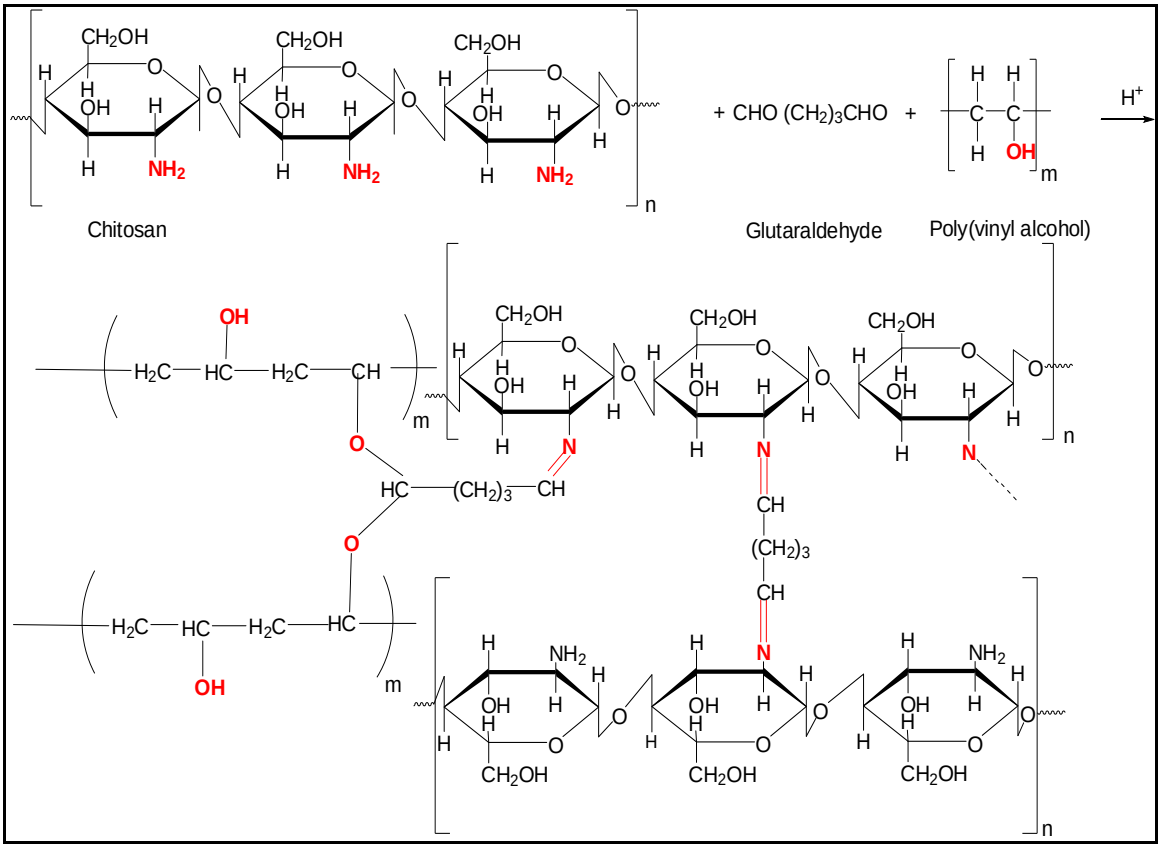

Scheme (2.3): Cross-linking of chitosan, PVA with glutaraldehyde[178]

2.7.2 Preparation of hydrogel (CPM) from crosslinking between chitosan and PVA by maleic anhydride

CPM hydrogel was prepared with a similar method as above (preparation of CPG hydrogel) except added (0.3g) of maleic anhydride instead of glutaraldehyde as crosslinker agent[175].

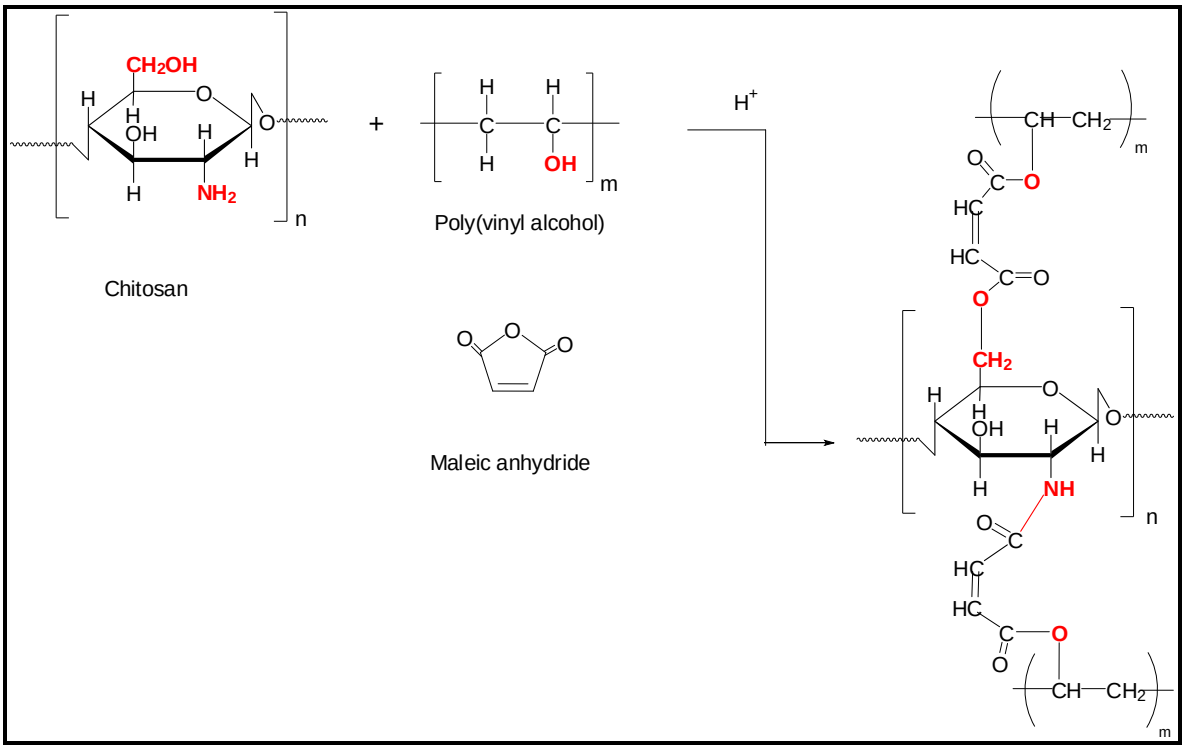

Scheme (2.4): Cross-linking of chitosan, PVA with maleic anhydride[179]

2.7.3 Preparation of hydrogel (PPM) from crosslinking between pectin and PVA by maleic anhydride

PPM hydrogel was prepared by mixing equal volumes of PVA solution with pectin solution. The mixture was stirred constantly until homogeneous at 60ºC and (0.3g) of maleic anhydride as crosslinker

agent was added to the mixture under constant stirring with (2 drops) of glacial acetic acid[180].

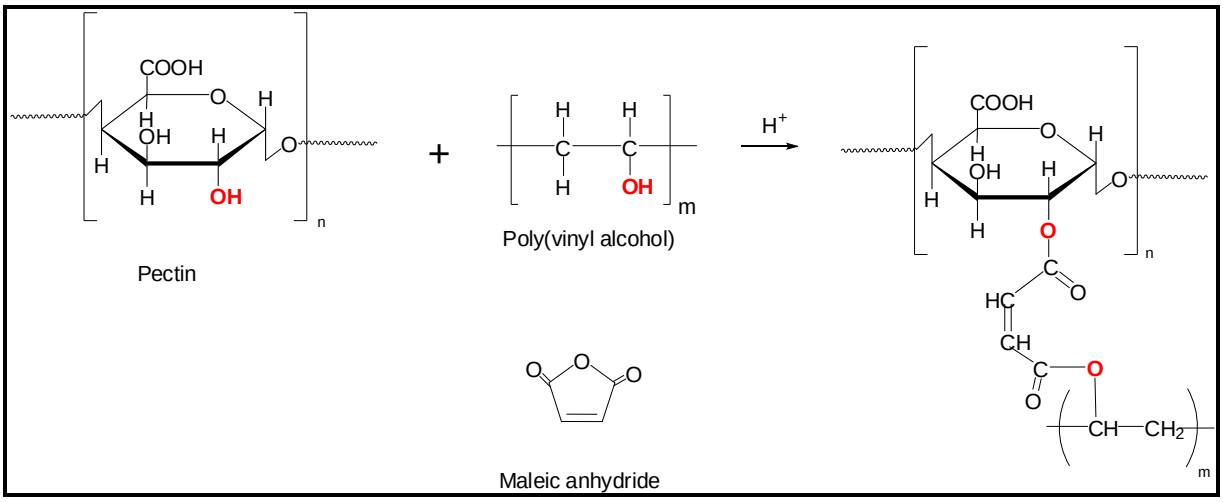

Scheme (2.5): Cross-linking of Pectin, PVA with maleic anhydride[181]

2.7.4 Preparation of hydrogel (PgA) from graft co-polymerization of acrylic acid on PVA

PgA hydrogel was prepared by mixing (20 ml) of PVA solution with (0.0375 g)of potassium persulphate (KPS) as initiator and (3.8ml)of acrylic acid under N_2 at 60ºC with (0.0375g) of (N,N´-methylenebisacrylamide(MBA)) as crosslinker at same temperature with stirring for (1h) [170].

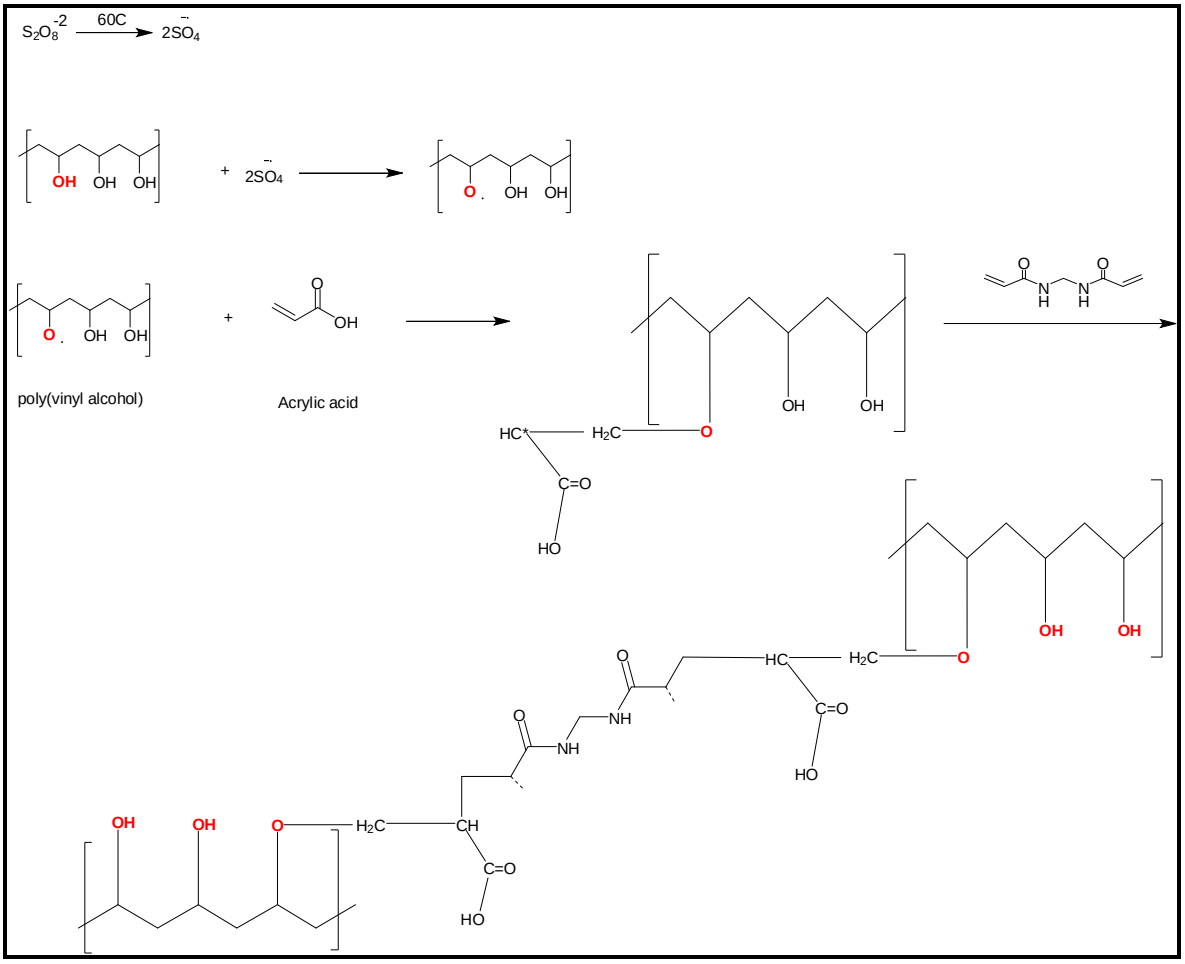

Scheme (2.6): grafted co-polymerization of Acrylic acid onto PVA[170]

2.7.5 Preparation of hydrogel (CgA) from graft co-polymerization of acryl amide on chitosan

CgA hydrogel was prepared by mixing (20 ml) of chitosan solution with (0.07 g) of ammonium persulphate (APS) as initiator and (1g) of acrylamide under N_2 at 60ºC with (0.07g) of (N,N´-methylenebisacrylamide(MBA)) at same temperature with stirring for (1h) [182].

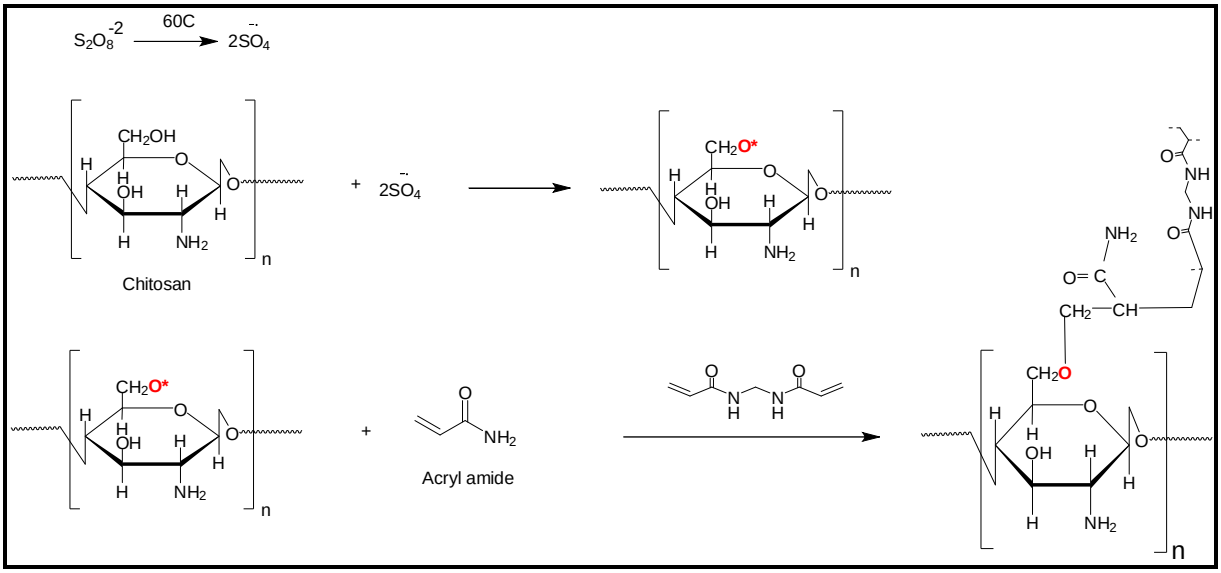

Scheme (2.7): APS-initiated graft copolymerization of acrylamide onto chitosan in the presence of MBA[182]

2.7.6 Preparation of hydrogel (IPN) from co-polymerization of acryl acid and acryl amide in presence chitosan

IPN Hydrogel was synthesized by free radical polymerization of acrylamide (AM) and acrylic acid (AA) in presence of the chitosan (CHI). A determined mass of AM and AA with ratio (CHI/AA/AM) equal to (10/10/80 w%), together with APS (1.2×10^{-3} mol/L), MBA (3.3×10^{-2} mol/L), and TEMED in a (1:1) molar ratio with APS, were added to chitosan solution and stirred for ten minutes at room temperature under N_2. Finally it was placed in a water bath at 60°C for 6 h [183].

For all hydrogels after homogeneous mixing, the hydrogels were formed and poured in to glass mold (10x5x2cm) and left to dry in air.

The whole mass converted into a transparent film and they were purified by equilibrating in double distilled water for a week. The hydrogel products were dried at 40 ºC in a vacuum oven overnight

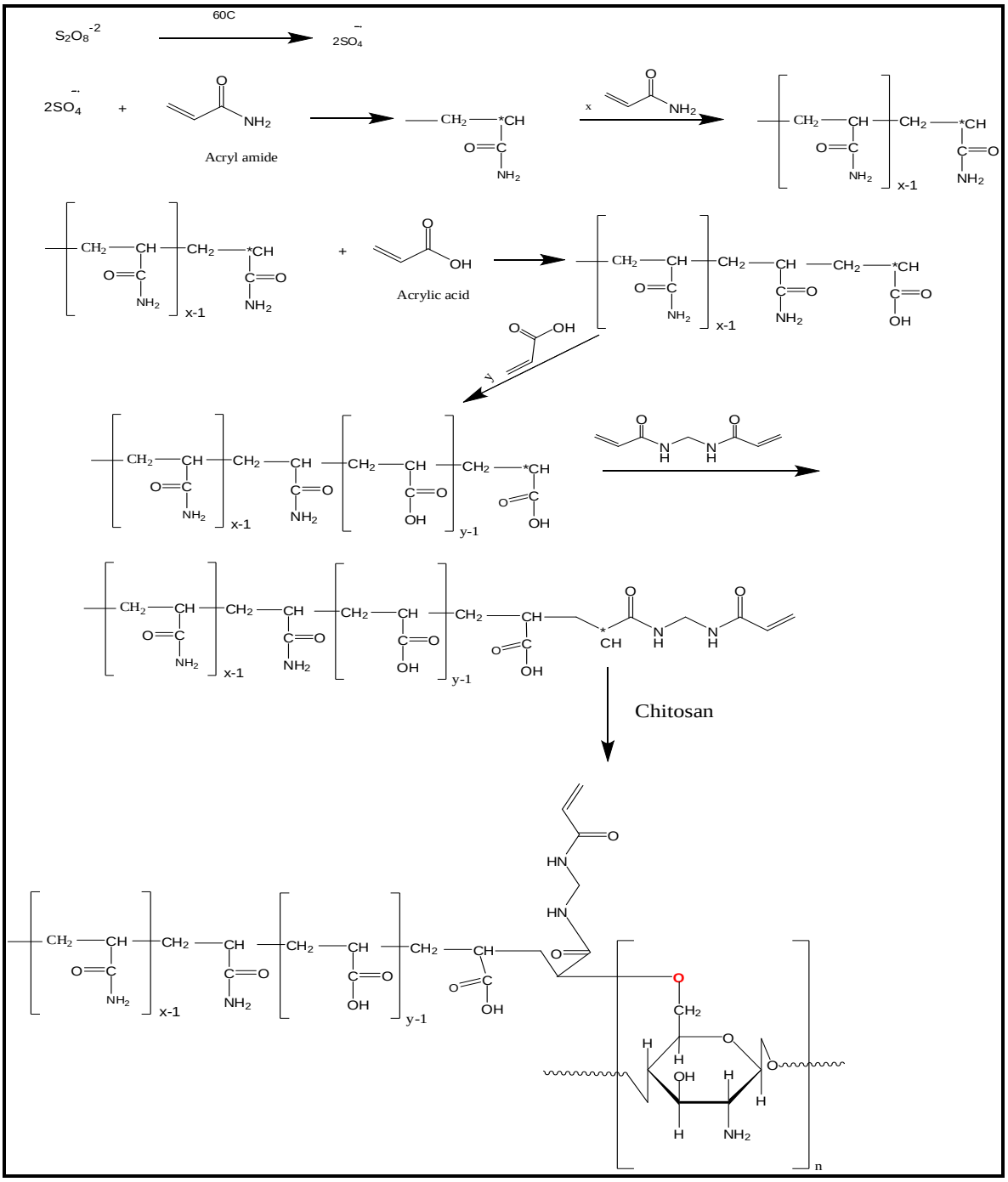

Scheme (2.8): Interpenetrating chitosan-poly (acrylic acid-co-acryl amide) hydrogel (IPN)[184]

2.8 Synthesis of conductive hydrogels

2.8.1 Synthesis of conductive hydrogels /PANI

An appropriate amount of prepared hydrogel as in (2.7) was provided and all steps of poly aniline synthesis were carried out within the hydrogel solution at a temperature between (0-2)° C and mixed with mechanical stirring (1500rpm) until color of solution convert to black green then added crosslinker agent with continuous mixing with mechanical stirring for (1h). Black green dispersion of conductive composite hydrogel poured in to glass mold(10x5x2cm) and left to dry in air, and washed with three 100-mL portions of (0.2 M HCl), and similarly with acetone. Then it was dried in vacuum oven at (40ºC) overnight.

2.8.2 Synthesis of conductive hydrogels /G

An appropriate amount of the prepared hydrogel as in (2.7) was provided and mixed with dispersion solution of G (0.25w/v %) with mechanical stirring for (1h) at (2500 rpm.). To make sure get dispersion solution of composite the mixture after added crosslinker agent placed in ultrasonic water bath for another hour. After completion of reaction, nanocomposite hydrogel was poured to glass mold (10x5x2 cm), then left to dry in air, washed with enough distilled water. Then it was dried in vacuum oven at (40ºC) overnight.

2.8.3 Synthesis of conductive hydrogels /MWCNTs

An appropriate amount of the prepared hydrogel as in (2.7) was provided and mixed with dispersion solution of MWCNTs (0.25w/v %) with mechanical stirring for (1h) at (2500 rpm.). To make sure get

dispersion solution of composite the mixture after added crosslinker agent placed in ultrasonic water bath for another hour. After completion of reaction, nanocomposite hydrogel was poured to glass mold (10x5x2 cm), then left to dry in air, washed with enough distilled water. Then it was dried in vacuum oven at (40ºC) overnight.

Figure (2.2): image of hydrogels, and hydrogel composites

2.9 Synthesis of Fe_3O_4 coating by hydrogels

An appropriate amount of the prepared hydrogel as in (2.7) was provided and mixed with dispersion solution of (Fe_3O_4 (2.5 w/v %)) with mechanical stirring for (1h) at (2500 rpm.). To make sure get dispersion solution of composite the mixture after added crosslinker agent placed in ultrasonic water bath for another hour. After completion of reaction, magnetite nanopaticles coated with hydrogels was collected by magnet and washed with enough distilled water and then dried in vacuum oven at (40ºC) for (5hrs).

2.10 Synthesis of coated Fe_3O_4 with conductive hydrogel (CPG/Fe_3O_4/PANI)

An appropriate amount of the prepared hydrogel as in (2.7.1) was provided and added dispersion solution of Fe_3O_4 MNPs (2.5 w/v %) then mixed together by mechanical stirring for (1h) at (2500 rpm.). with continuous mixing with mechanical stirrer was added poly aniline solution at (0-2) ° C until color of solution convert to black green then added glutaraldehyde crosslinking agent with continuous mixing with mechanical stirring for (1h).

To make sure get dispersion solution of magnetic conductive nanocomposite the mixture after added crosslinker agent placed in ultrasonic water bath for another hour. After completion of reaction, coated Fe_3O_4 were collected by magnet and wished several time with distilled water. It was dried in air and then dried in vacuum oven at (40ºC) for (5hrs).

2.11 Swelling of hydrogels

Swelling studies were done for most hydrogels. They were weighed with dry state and placed into (100mL) of water at room temperature. At time intervals, gently wiped with filter paper to remove surface water, reweighed, and then placed back into the beaker as quickly as possible. The mean weights were determined for each hydrogel. The degree of swelling (S) was calculated using eq. (2.1) [185].

$$S = \frac{Ws - Wd}{Wd} \quad \text{.....(2.1)}$$

Where Wd and Ws are the dry and swollen matrix weights, respectively, at immersion time (t) in the water.

2.12 Preparation of Phosphate Buffer Saline (PBS)

PBS (0.01M) was prepared in (1000mL) volumetric flask by dissolve (8g)NaCl, (0.2g) KCl, (1.44g)Na_2HPO_4 and (0.24g) KH_2PO_4 in (800mL) of distilled water. Adjust to pH 7.4 with HCl and the volume was completed with distilled water[186].

2.13 Preparation of drug solution

Indigo carmine, doxorubicin hydrochloride, and methotrexate were used as drugs models. A standard stock solution of indigo carmine (100 mg/L) was prepared by dissolving (0.01 g) in (100 ml) distillated water while standard solutions of doxorubicin and methotrexate (1000mg/L) were prepared by dissolving (0.1g) in (100 ml) of double distilled water and Phosphate buffer saline (PBS), respectively . The working solutions of indigo carmine and doxorubicin hydrochloride were prepared by diluting the stock solution with distilled water, while working solutions of methotrexate were prepared by diluting the stock solution with PBS.

2.14 Calibration Curve

2.14.1 Calibration curve of Indigo carmine

Solutions of different concentrations (0.5-5 mg/L) were prepared by dilutions from the standard stock solution (100 mg/L). Absorbance values of these solutions were measured at (λ_{max}= 610) nm, spectrum of indigo carmine in (fig. 2.3). The calibration curve for indigo carmine (absorbance vs. concentration) (Figure 2.4) was

showing the range of concentration that obeys Beers-Lambert law (Table (2.1).

Table (2.1): Data of calibration curve of indigo carmine

C(mg/L)	Absorbance
0.5	0.220
1	0.441
1.5	0.637
2	0.856
2.5	1.057
3	1.259
3.5	1.458
4	1.640
4.5	1.808
5	1.973

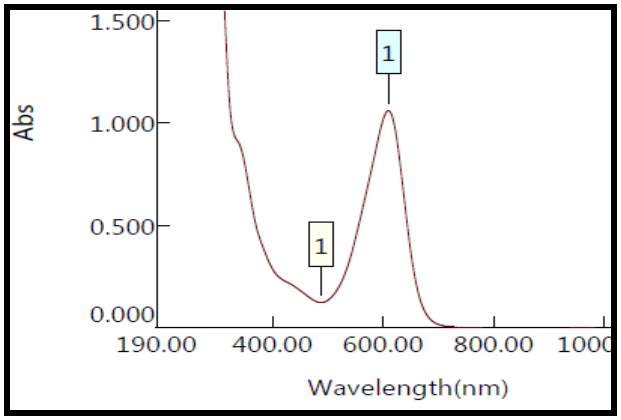

Figure (2.3): UV-Vis. Spectrum of indigo carmine

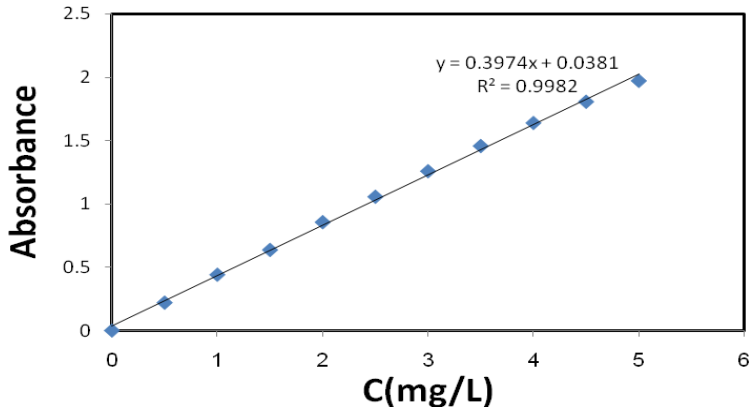

Figure (2.4): Calibration curve of indigo carmine

2.14.2 Calibration curve of Doxorubicin hydrochloride

Solutions of different concentrations (50-400 mg/L) were prepared by dilutions from the standard stock solution (1000 mg/L). Absorbance values of these solutions were measured at the (λ_{max}= 480) nm, spectrum of doxorubicin hydrochloride (fig. 2.5). The calibration curve for doxorubicin (absorbance vs. concentration) was appeared in (Figure 2.6) showing the range of concentration that obeys Beers-Lambert law (Table (2.2).

Table (2.2): Data of calibration curve of doxorubicin hydrochloride

C(mg/L)	Absorbance

50	0.124
100	0.257
150	0.396
200	0.497
250	0.654
300	0.76
350	0.926
400	1.003

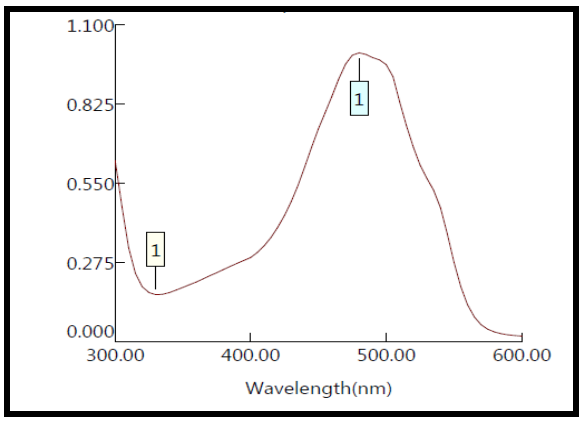

Figure (2.5): UV-Vis. Spectrum of doxorubicin hydrochloride

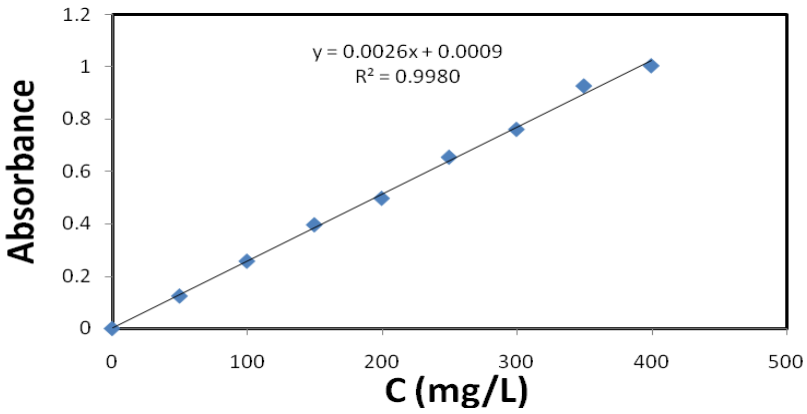

Figure (2.6): Calibration curve of doxorubicin hydrochloride

2.14.3 Calibration curve of methotrexate

Solutions of different concentrations (50-400 mg/L) were prepared by dilutions from the standard stock solution (1000 mg/L). Absorbance values of these solutions were measured at the (λ_{max}=360) nm, spectrum of methotrexate (fig. 2.7). The calibration curve for methotrexate (absorbance vs. concentration) in (Figure 2.8) was showing the range of concentration that obeys Beers-Lambert law(Table(2.3).

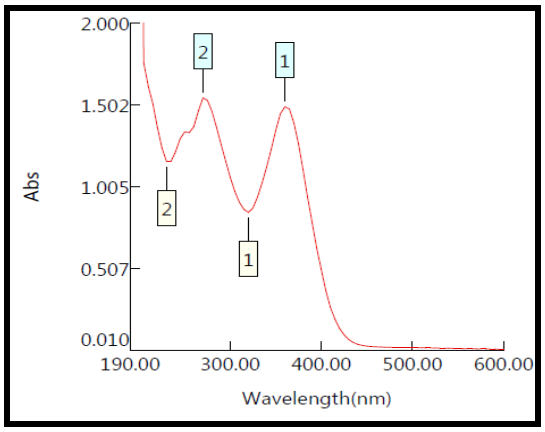

Figure (2.7): UV-Vis. Spectrum of methotrexate

Table (2.3): Data of calibration curve of methotrexate

C(mg/L)	Absorbance
50	0.262
100	0.458
150	0.666
200	0.877
250	1.060
300	1.241
350	1.492
400	1.732

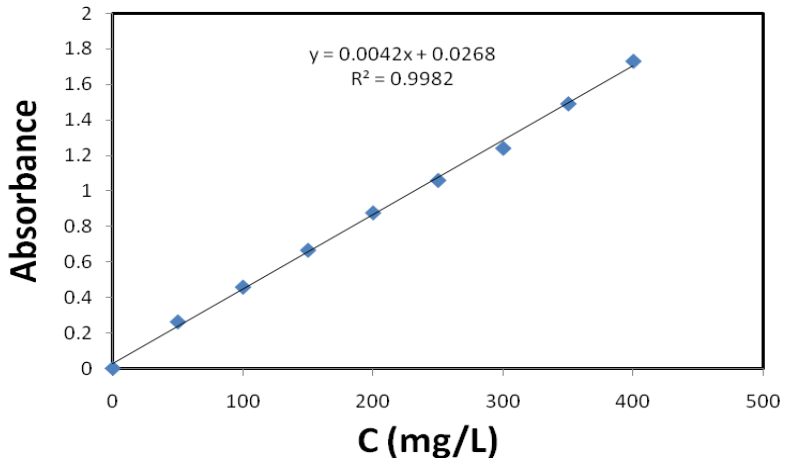

Figure (2.8): Calibration curve of methotrexate

2.15. Controlled release tests

2.15.1 Controlled release tests of indigo carmine

Conductive hydrogels were dried then were placed in an (5 mg/L) indigo carmine aqueous solution for 24 hrs. Composites were rinsed with distilled water and transported to electrochemical cell containing (65 mL) of a (0.01 M) of electrolytic solution (phosphate buffer saline (PBS)) with pH =7.4. The amount of indigo carmine dye released in the buffer solution was followed by absorbance measurements at (λ_{max} =610 nm) using UV-Vis spectrophotometer. Electro-liberation curves (concentration of indigo carmine vs. time) were obtained and the impact of the applied potential (2 for G, MWCNTs composites and 8 V for PANI composites) was analyzed.

The same procedure was followed using best hydrogel for indigo release (conductive CPG) at different temperature (35.5, 37, and 38.5)ºC and different voltage(1,2,3) V for (CPG/MWCNTs) and (CPG/G), while (3,5,8)V for (CPG/PANI) and (CPG/Fe_3O_4/PANI).

Figure below (2.9) show the picture of indigo release from conductive hydrogel at room temperature at onset release and at the end of release.

(a) (b)

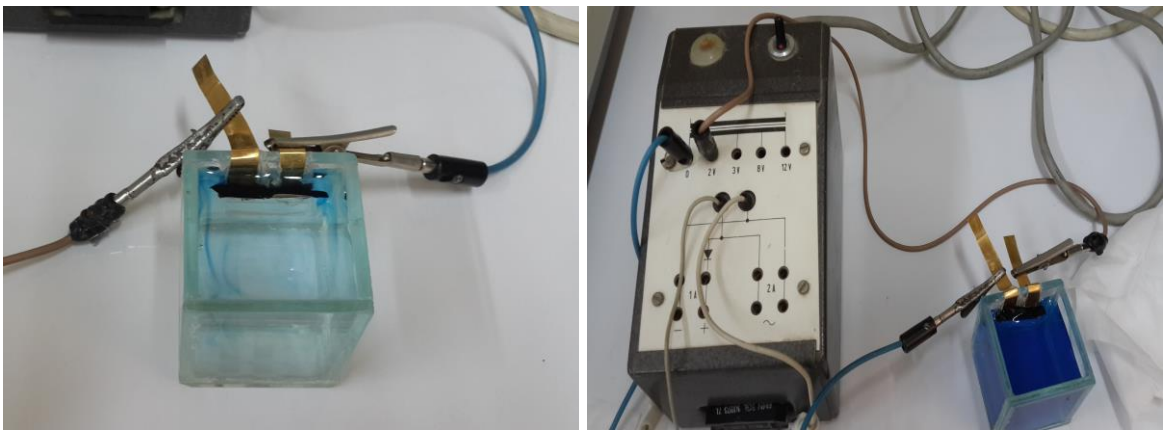

Figure (2.9): image of indigo release of conductive hydrogel at room temperature, (a): at first release and, (b): ending release

2.15.2 Controlled release tests of doxorubicin and methotrexate

Conductive CPG hydrogels were dried then were placed in a (100 mg/L) doxorubicin aqueous solution and methotrexate buffer solution, respectively, for 24 hrs. Composites were rinsed with distilled water and transport to electrochemical cell containing (65 mL) of a (0.01 M) of electrolytic solution (phosphate buffer saline (PBS)) with pH =7.4. The amount of drugs released in the buffer solution was followed by absorbance measurements at (λ_{max} =480 nm) for doxorubicin and (λ_{max} =360nm) for methotrexate using UV-Vis spectrophotometer. Electro-liberation curves (concentration of drugs vs. time) were obtained and the impact of different applied potential (1,2,3) for (G, MWCNTs composites) and (3,5,8) V for (PANI composites) with different temperatures(35.5,37,38.5)ºC were calculated.

2.16 Dielectric Constant Measurements [187]

All hydrogel films were cut into (2x1.5) cm^2 part to suitable a silver electrode for characterization by measuring dielectric properties using LCR meter with frequency range of (100Hz-100000 Hz). The dielectric constant as a function of frequency is described by the complex permittivity

$$\varepsilon*(\omega)=\varepsilon'(\omega)-\varepsilon''(\omega)------(2.2)$$

ε' & ε'' are real part and imaginary part represented energy storage and energy loss, respectively, in the presence electrical field. Using the following expression**,** where, capacitance (C) can be calculated by measuring the dielectric constant ε',

$$\varepsilon'=\frac{Cd}{\varepsilon_{\circ}A}-----(2.3)$$

Where, (A) : electrode area, (d): thickness between two electrodes (film thickness), $\varepsilon_{\circ}$: permittivity of a space, equals to (8.85 X 10^{-12} $F.m^{-1}$), ω: angular frequency; $(\omega=2\pi f)$, f is a applied frequency. While to calculate dielectric loss $\varepsilon''(\omega)$ can be used equation (2.4), $\tan\delta$: tangent delta.

$$\varepsilon''(\omega)=\varepsilon'(\omega).\tan\delta(\omega)----(2.4)$$

Electric conductivity ($\sigma_{a\,c}$) can be measured by equation(2.5).

$$\sigma=\varepsilon_{\circ}\varepsilon'\omega\tan\delta-----(2.5)$$

2.17 Magnetic Hysteresis

Hysteresis means the residual magnetization of ferromagnetic material, such as iron, behind the variations of magnetizing field. When ferromagnetic materials are placed within a coil of wire carrying an electric current, magnetizing field, or magnetic field strength (H), caused by the current forces some or all of atomic magnets in the material to align with the field. The net effect of this alignment is to increase magnetization (M). The alignment process does not take place at the same time or in step with magnetizing field but lags behind it.

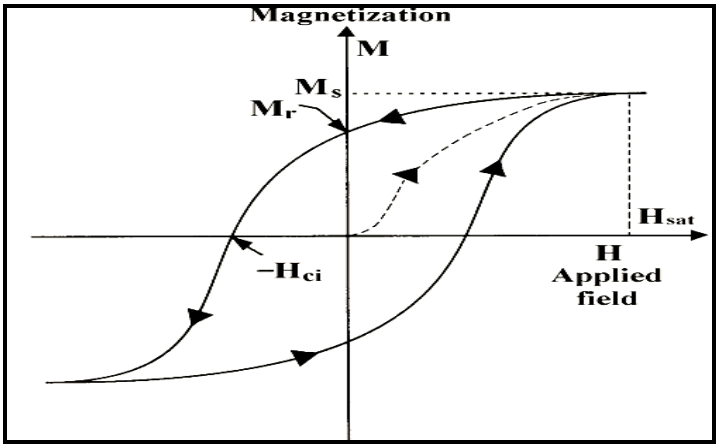

Figure (2.10): Schematic illustration of typical curve of a ferromagnetic material [188]

When intensity of magnetizing field is gradually increased, magnetization increases to a maximum, or saturation (Ms), where all of value of atomic magnets aligned in the same direction. Contrary, when magnetizing field is decreases, the magnetic flux density is decreased, again lagged behind change in the strength of the field (H). In fact, when (H) has fallen to zero, (M) is still a positive value called the remanence, residual induction, or retentivity (Mr) which has a high value for permanent magnets. (M) does not become zero until (H) has reached a negative value. The known value (H) in which M is zero coercive force (-Hci). A further increase in (H) (in the negative direction) causes magnetization to reverse and finally to reach saturation again, when all the atomic magnets are completely aligned in opposite direction. It may be the cycle continues so that the graph of the flux density lagged behind field strength seems like a complete loop, called "hysteresis loop" (fig (2.10). The energy lost as heat, which is known as hysteresis loss, reversed magnetization of the material proportional to the area of the hysteresis loop. Therefore, the basis of electricity transformer is made of materials with a narrow hysteresis loops so that very little energy is dissipated in the form of heat [189,190].

Magnetic materials have positive magnetic susceptibility is interested and divided to: (1) ferrimagnetic (2) ferromagnetic and (3)

superparamagnetic. The first two has hysteresis loop while last one has no loop that is no coercivity and no remanence. Fe_3O_4 nanoparticles when average size has smaller than about (20) nm often exhibit superparamagnetic manner at room temperature. At room temperature, the hysteresis should have an "S" shape (fig 2.11) where both the descending and ascending loops coincide and yield zero coercivity [191].

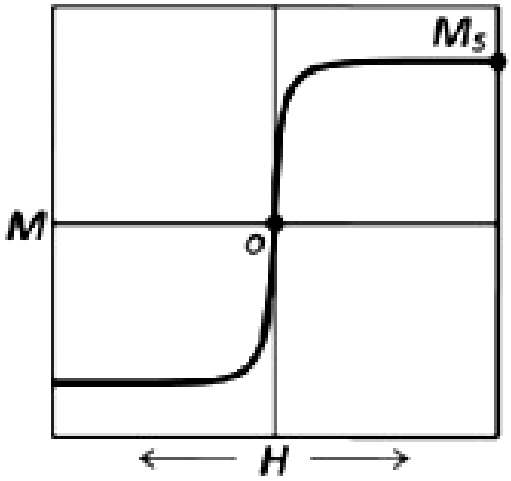

Figure (2.11): Schematic illustration of typical curve of a superparamagnetic material [191]

3.1 Characterization of Hydrogels and theirs Composites Form

3.1.1 FTIR Analysis of hydrogels

The FTIR spectrum of the pure chitosan is shown in Fig. (3.1). The spectrum showed a strong absorption band at 3429 cm^{-1} was due to OH and amine N-H symmetrical stretching vibrations. A peak at 2881 cm^{-1} was due to symmetric -CH_2 stretching vibration attributed to pyranose ring [192].
Peaks at 1654 and 1562 cm^{-1} were due to -C=O stretching (amide) and NH bending (amine), respectively. The sharp peaks at 1423 and 1377 cm^{-1} were assigned to CH_3 in amide group. The peaks at 1261, 1319 cm^{-1} were assigned to C—N groups [193]. Peak at 1157 cm^{-1} was due to secondary alcohol. The broad peak at 1080 cm^{-1} was indicated the C-O stretching vibration in chitosan. The peak at 894 cm^{-1} was assigned to the structure of saccharide [194].

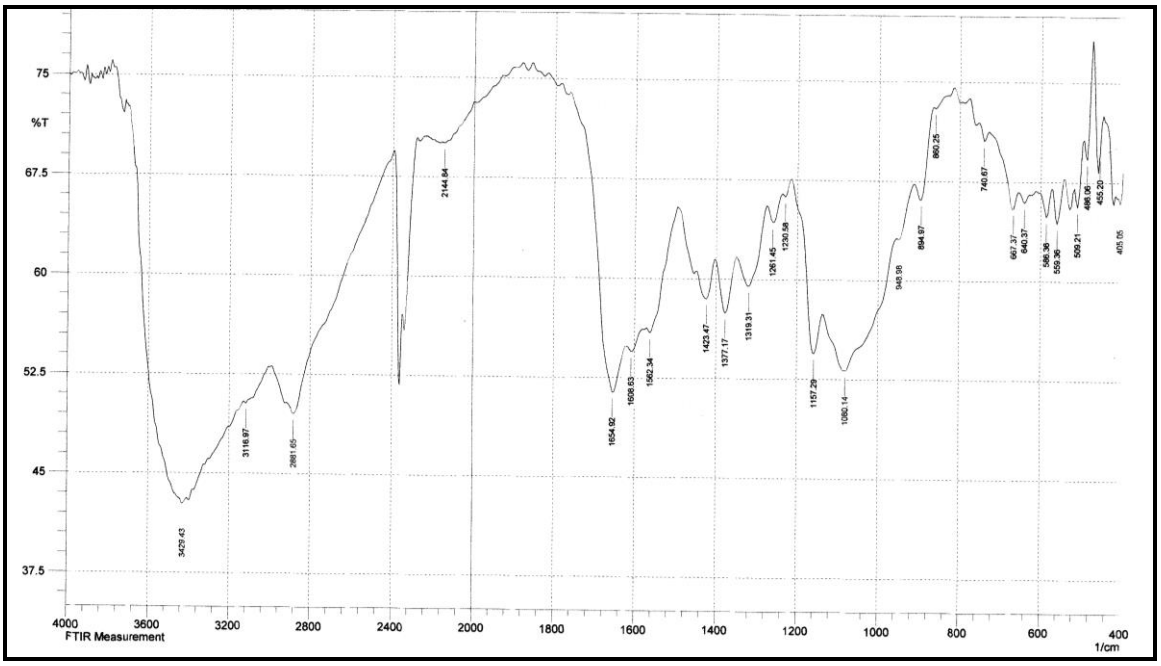

Figure (3.1): FT-IR spectrum of chitosan

Figure (3.2) shows the FTIR spectra relative to the pectin. The spectrum showed broad peak at 3410 and 3294 cm^{-1} was due to the stretching of —OH groups and stretching of —NH amide. The peak at 2943

cm^{-1} indicated C—H stretching vibration. The strong peak at1593 cm^{-1} was assigned to C=O (acidic)stretching vibration. The peaks at 1438, 1423 and 1388 cm^{-1} could be —OH bending vibration peaks and assigned to —CH_2 scissoring, respectively. The peaks at 1280, 1303 were assigned to C—N groups. The peak at 1149 cm^{-1} suggested the presence of —CH—OH in aliphatic cyclic secondary alcohol. The peaks at 1026 cm^{-1} was indicated the C-O stretching vibration in pectin [195, 196].

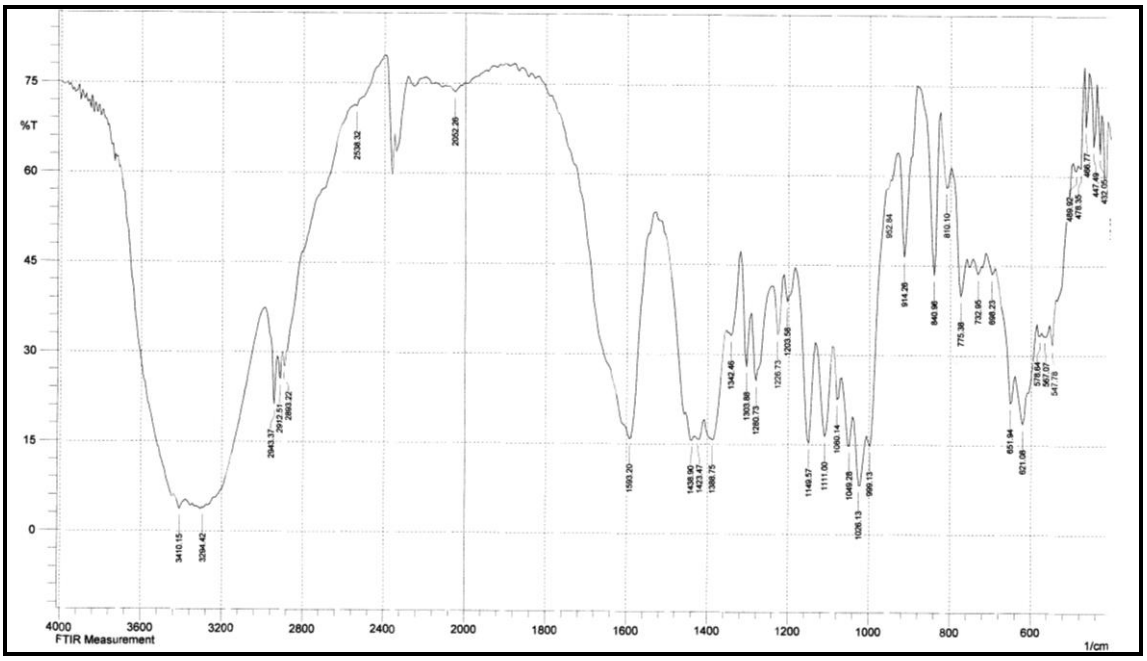

Figure (3.2): FT-IR spectrum of pectin

In Figure (3.3) shows the FTIR spectrum of PVA. The broad band observed at 3417 cm^{-1} was associated with the O–H stretching vibration .The vibrational band observed at 2939 and 2908 cm^{-1} were the result of the C–H stretch from alkyl groups and the peaks at 1712, 1651 and 1141 cm^{-1} were due to the C═O stretches from the remaining acetate groups in PVA and C–O alcoholic [197,198].

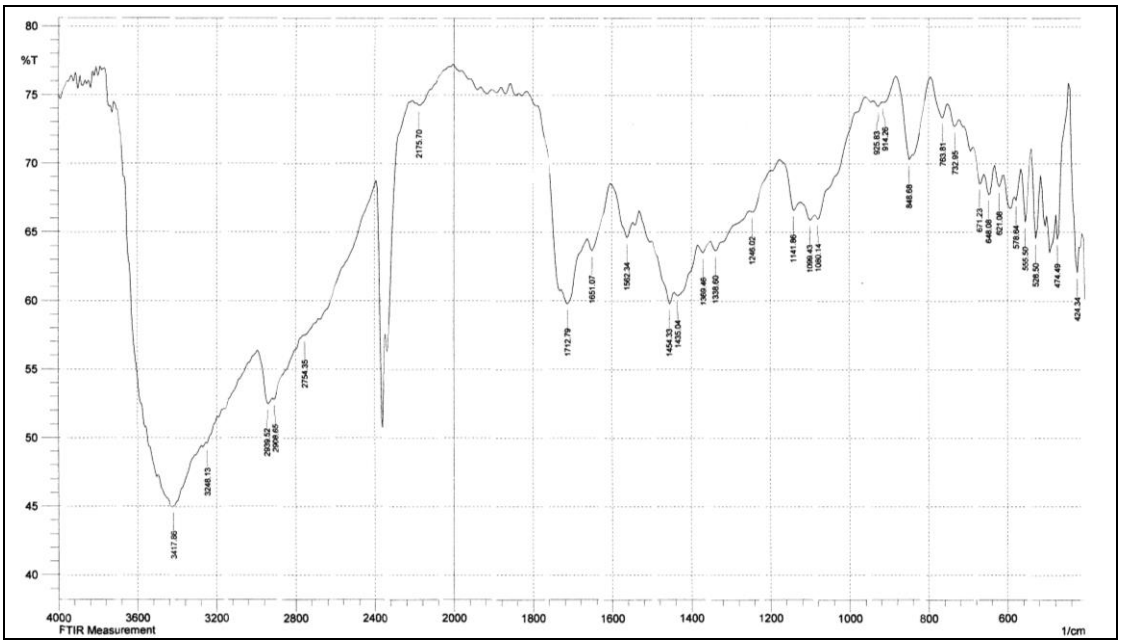

Figure (3.3): FT-IR spectrum of PVA

Fig (3.4) is represented of (PgA) film spectrum. The peak was returned to O-H stretching vibration of PVA was appeared sharper and shifted to 3402 cm^{-1}. The peak was returned to C-H group stretching vibration was appeared also at the same frequency (2939 &2908 cm^{-1}). The peaks were returned to C=O were appeared stronger, sharper and shifted to 1724cm^{-1}. The peak was returned to C-O alcoholic group stretching vibration was appeared in same frequency at 1141 cm^{-1} and new peak was appeared at 1192 was returned to C-O group of acrylic acid . The New peak appearance at 1296 cm^{-1} was returned to C-N group of bisacryl amide. The new peak appearance at 1192 cm–1 was due to the formation of acetal ring, which confirm the grafting of PAA in to PVA [170].

Fig (3.5) shows the spectrum of (PPM film). The overlap broad peak returned to O-H and N-H groups stretching vibration was shifted to (3429 cm^{-1}). The peak was shifted to 2939 cm–1 was returned to C-H stretching vibration. The peak was returned to C=O remaining acetate groups in PVA also appeared in the same frequency. The peak was returned to C=O stretching vibration to pectin was shifted to 1643 Cm^{-1} with broader. The two peaks was returned to C-N groups stretching vibration were weaker and shifted to 1261 Cm^{-1} for first peak and second peak at 1303 Cm^{-1} was disappeared. The peaks was returned to C-O group stretching vibration was broader and shifted to 1066 Cm^{-1} for pyranose ring in pectin and disappeared peaks at about (1149Cm-1) for cyclic secondary alcohol and C-O alcohol in PVA. This was suggested to get crosslinking between pectin and PVA with maleic anhydride [180].

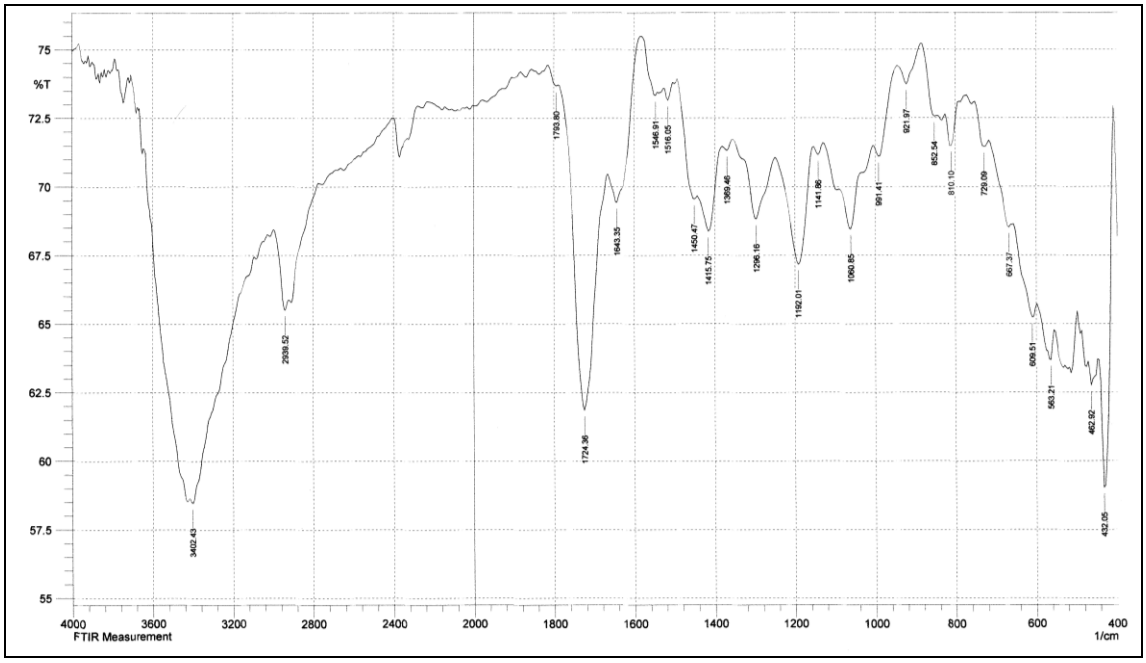

Figure (3.4): FT-IR spectrum of PgA film

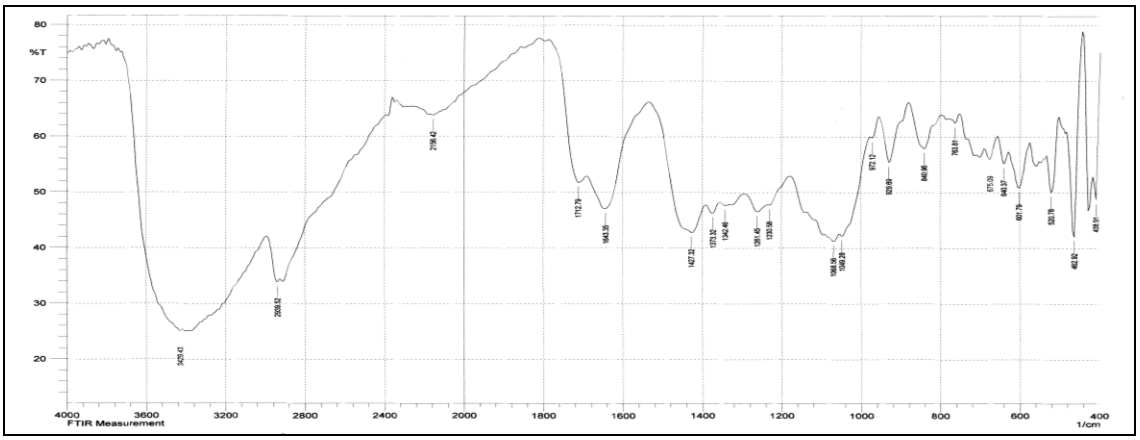

Figure (3.5): FT-IR spectrum of PPM film

Fig (3.6) appears of spectra of (CPG film). The peaks were returned to O-H and N-H stretching groups stretching vibration were overlapped, sharper, and shifted to 3398Cm-1. Two strong peaks at 2927 and 2858 Cm-1 were returned to C-H stretching vibration. The peaks were returned to C=O was disappeared. New peak was appeared at 1597 was returned to Schiff base (C=N). This was explained to get chemical crosslinking of chitosan and PVA by glutaraldehyde. The imine group was formed by the nucleophilic reaction of the amine group from chitosan with the carbonyl group from glutaraldehyde (see scheme 2.3). The two peaks was returned to C-N groups stretching vibration were weaker and shifted to 1246 Cm^{-1} for first peak and second peak at 1319 Cm^{-1} was disappeared. The peaks were returned to C-O ring in chitosan and cyclic secondary alcohol, alcoholic in PVA were shifted to 1045 and 1118, 1190 cm-1, respectively [199].

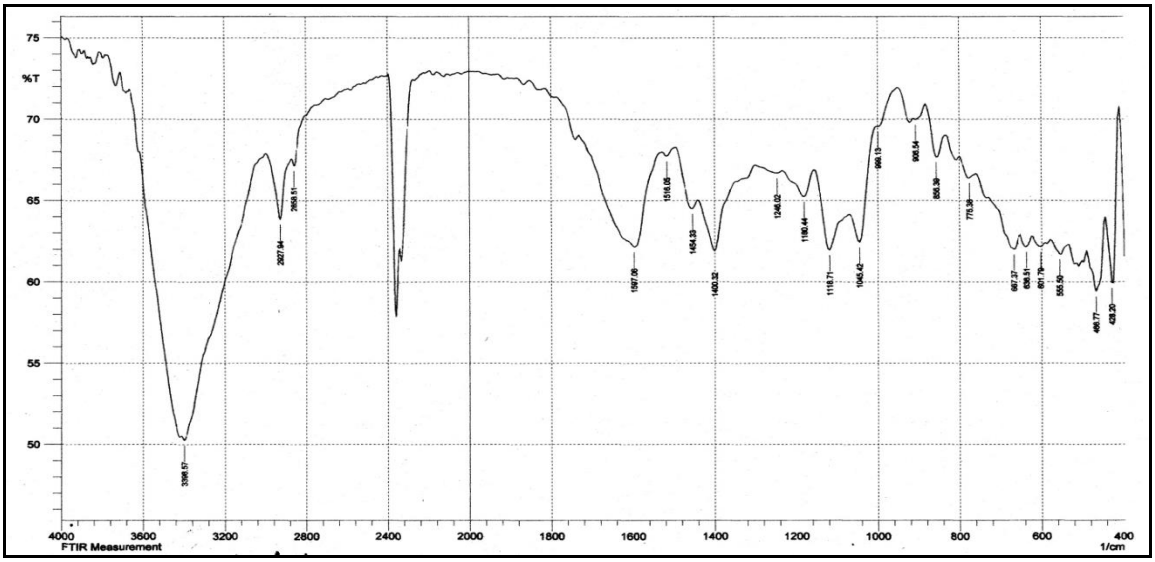

Figure (3.6): FT-IR spectrum of CPG film

Fig (3.7) shows FT-IR spectra of CPM hydrogel film. The strong peak was returned to O-H group stretching vibration was appeared at 3433Cm^{-1} .The peak at 3398 Cm^{-1} was assigned to N-H stretching vibration. The peak at 2943 Cm^{-1} was assigned to C-H stretching vibration. The peaks were returned to C=O amide of chitosan and remaining acetate group in PVA was shifted to 1643 and 1705 Cm^{-1} (weaker), respectively. The two peaks was returned to C-N groups stretching vibration were disappeared peak at 1261 Cm^{-1} for first peak and second peak at 1319 was shifted to 1319 Cm^{-1}. The peak was returned to C-O ring in chitosan was shifted to 1087 Cm^{-1} and disappeared peak for cyclic secondary alcohol and alcoholic in PVA.

It expect from mechanism scheme to get interaction between O-H groups from PVA and carbonyl groups from maleic anhydride to form unsaturated ester , this represented with appearance peaks at 1643 cm-1 , 1705 cm-1 returned to CH=CH stretching and ester carbonyl ,respectively. On the other may be form unsaturated amide by interaction between NH_2 groups from chitosan with C=O groups from

maleic anhydride, this represented with appearance peak at 1550 cm-1 returned to amide carbonyl stretching[179,181]

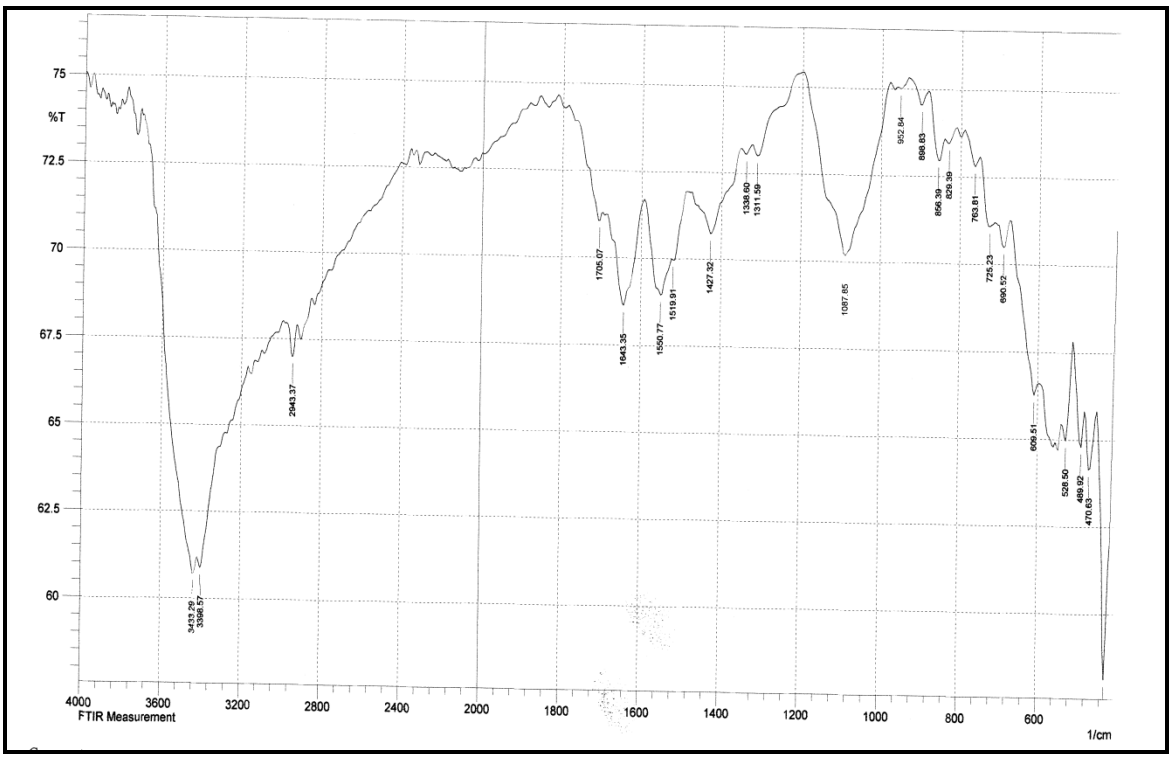

Figure (3.7): FT-IR spectrum of CPM film

The synthesis of chitosan-g-polyacrylamide hydrogel film was confirmed by comparing its FTIR spectrum with the spectrum of chitosan (Fig. 3.8). The chitosan spectrum shows the characteristic absorption bands at1654 cm-1 (C=O amide) and 1562 cm-1 (NH bending). These two peaks have a minor shift and are broader in the hydrogel spectrum, which is reconfirmed by two peaks at 1670cm−1 and 1616 cm−1 correspond to the C=O amide and NH bending vibration, respectively. Moreover, the C–H and O–H bending vibrations are observed in the 1300–1400 cm-1 with a sharp peak at 1400 cm-1. However, this sharp peak is related to the O–H group like two peaks at 1157 and 1080 cm-1 (alcoholic and etheric C–O stretching vibrations, respectively), which are decreased strength peaks in the hydrogel spectrum. This implies that the hydroxyl group of chitosan is the choose site for the reaction with the crosslinker and the grafting of acrylamide due to lower steric hindrance of the primary hydroxyl group [182].

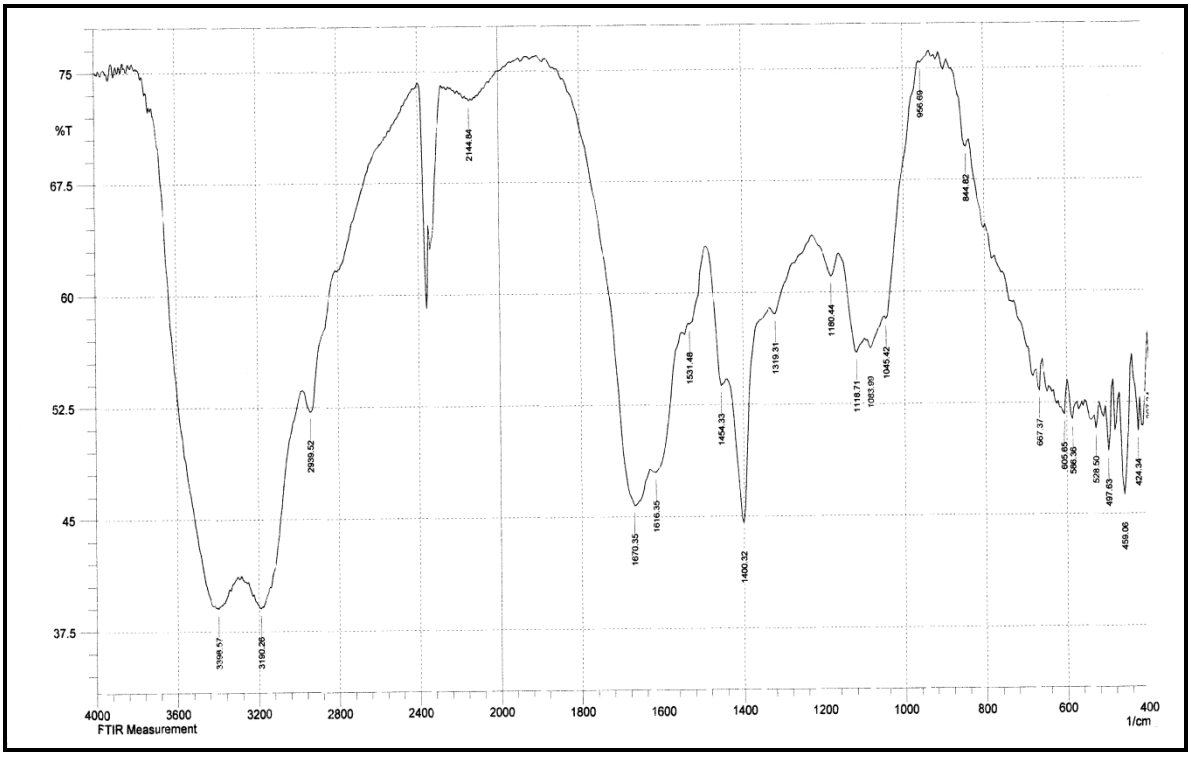

Figure (3.8): FT-IR spectrum of CgA film

Figure (3.9) show spectra of interpenetrated (chitosan-poly (acrylic acid-co-acrylamide) film. It shows the absorption band at 1720cm^{-1} due to the C=O stretching vibration of the carboxylic groups in poly acrylic acid. The intense band at 1674cm-1 corresponds to the C=O stretching vibration of amide group of poly acryl amide. The main absorption bands of the chitosan appeared also in this spectra [183].

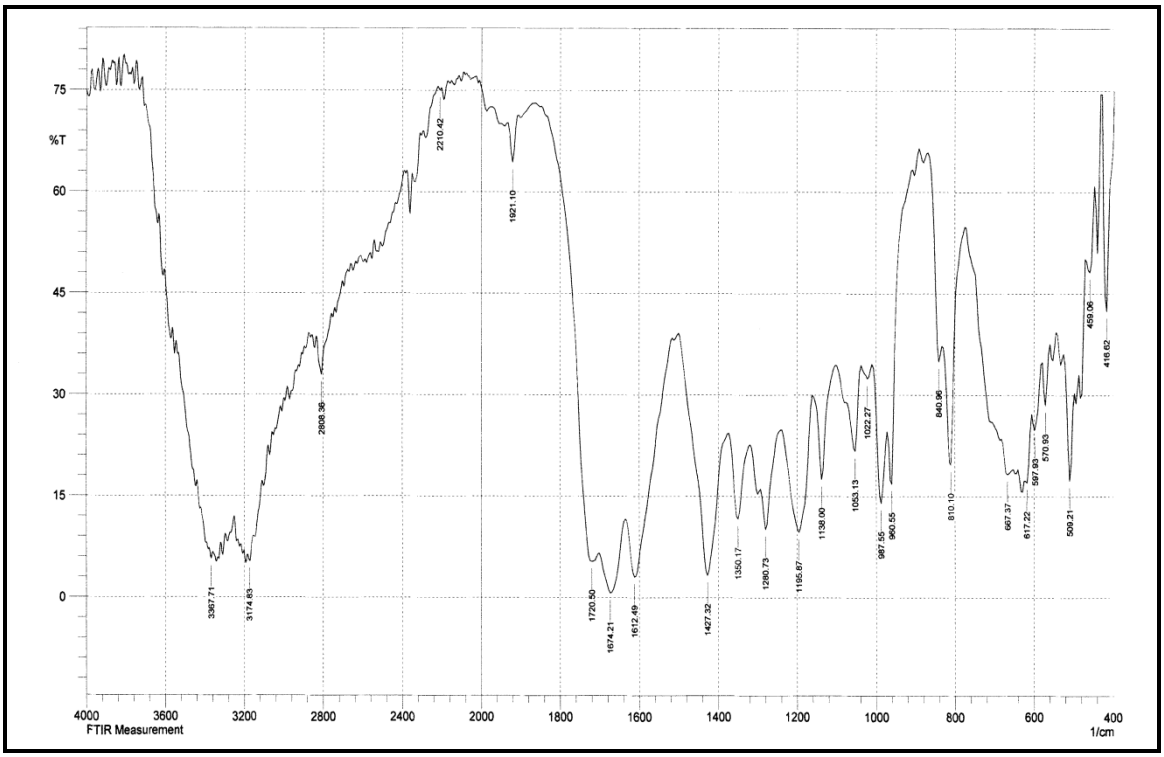

Figure (3.9): FT-IR spectrum of IPN film

3.1.1.2 FTIR Analysis of conductive hydrogels

3.1.1.2.1 FTIR Analysis of conductive PANI/ hydrogels

The FTIR spectrum of the pure polyaniline (PANI) is shown in Fig. (3.10). The peak at 3441 cm−1 is attributed to N-H stretching vibrations, the area of 1554 to 1743 cm−1 is related to NH flexural vibrations, and the peak at 1554 cm−1 is attributed to quinoid (Q) ring vibrations of PANI. The peak at 1481 cm−1 is due to benzenoid vibrations. Also, the vibrations of N=Q=N have characteristic absorption at 1134 cm−1. Aromatic C-N stretching vibrations appear at 1300 cm−1, and the area of 513 to 875 cm−1 is due to CH bending vibrations of substituted benzene ring [174].

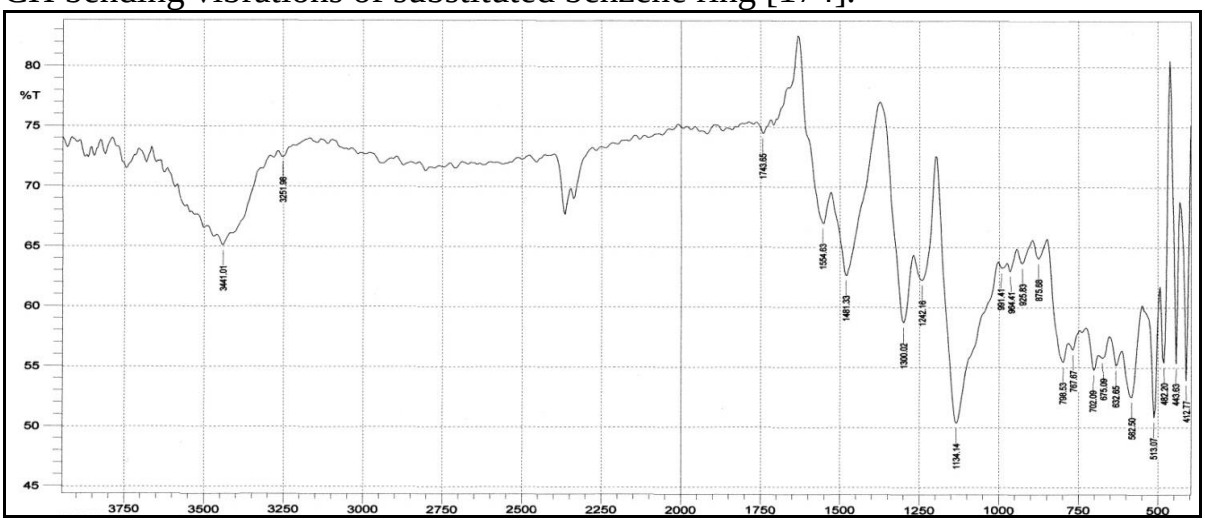

Figure (3.10): FT-IR spectrum of PANI

Characteristic peaks of PANI /hydrogels is showing in figures (3.11 - 3.16). It observed new peaks in spectrum of hydrogels returned to PANI represented to peaks at about 3000-3100 cm–1 corresponds to aromatic C–H stretching, 1543-1566 cm–1 (due to C=C stretching of quinoid (Q) rings), about 1462-1470 cm–1 (due to C=C stretching vibration of benzenoid (B) rings), at about 1300 cm–1 (due to C–N stretching). The absorption band at about 1111-1118 cm–1 was assigned to N=Q=N bending vibration to the PANI and at about 800-879 cm–1 was assigned to aromatic C–H bending vibration band due to the 1, 4-disubstituted benzene ring(see table (3.1).

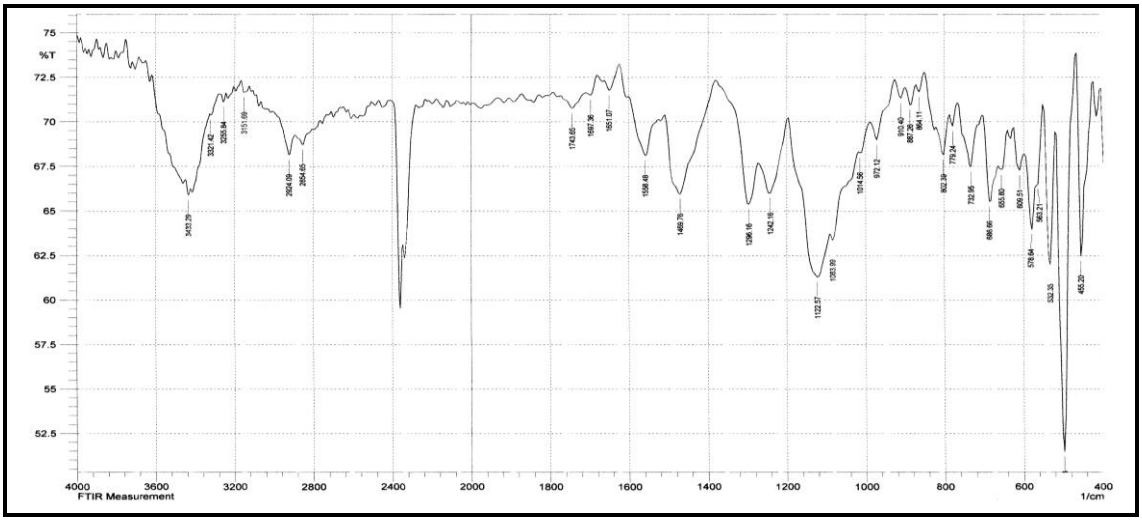

Figure (3.11): FT-IR spectrum of conductive hydrogel PgA/PANI film

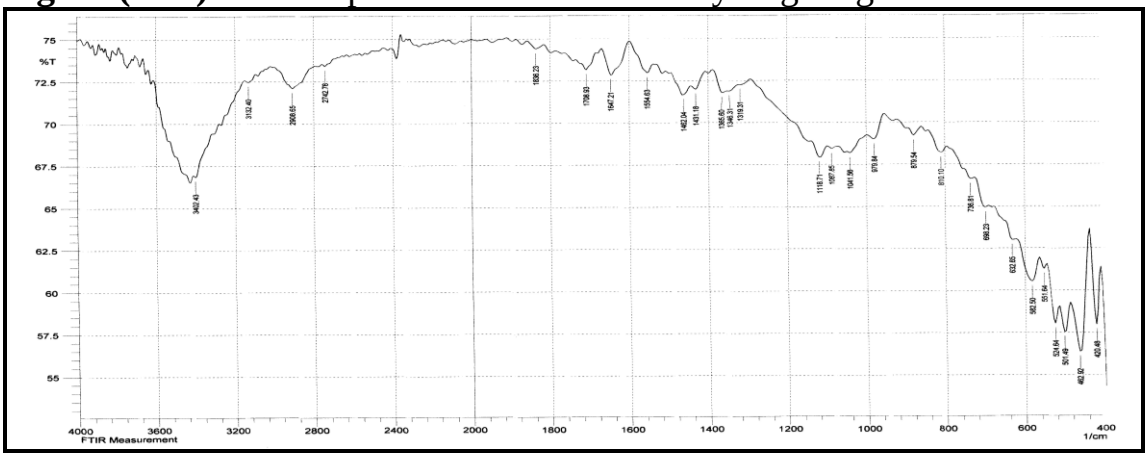

Figure (3.12): FT-IR spectrum of conductive hydrogel of PPM /PANI film

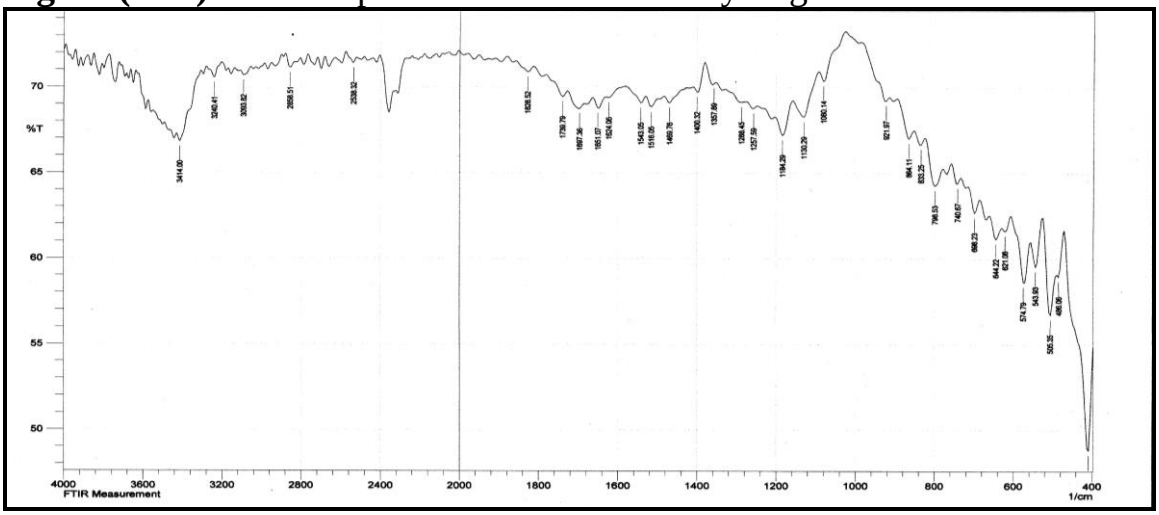

Figure (3.13): FT-IR spectrum of conductive hydrogel of CPG /PANI film

Table (3.1): Characteristics FTIR absorption bands (cm^{-1}) contain stretching vibrations& bending vibrations of hydrogels/PANI composite

Samples	O-H	N-H	CH-	C=O	C-O	C-N	peaks other
PgA/PANI	3433	New peak at 3255 to	2924,2854 aliphatic,	1743	1651	1242aliphatic ,	Q at 1558 B at 1469

		aromatic	New peak at 3151 to aromatic			New peak at 1296 for aromatic	N=Q=N at 1122overlap with C-O acetal
PPM/PANI	Stretching at 3402 ,bending at 1431	Overlaps with O-H	New peak for aromatic at 3132, aliphatic at 2908, bending at 1348	Shift to 1647 to pectin and 1708 to PVA	1087	Aliphatic at 1319, aromatic at 1365	Q at1554 B at 1482 N=Q=N at 1118
CPG/PANI	3414, bending at 1400	New peak at 3240 for aromatic, Bending shift to 1516 weak	2858aliphatic , new peak for aromatic at 3093	1697 (chitosan amide),1739(remaining acetate for PVA)	Shift to 1080, shift to 1130 for secondary alcohol, overlap with alcoholic of PVA	1257 aliphatic, new peak at 1288 for aromatic	Schiff base (C=N) shift to 1651, Q at 1543,B at 1449,N=Q=N at 1184
CPM/PANI	3487	3305 aliphatic , new peak at 3209 for aromatic, bending shift to1577	Shift to 2927, new peak at 3055 for aromatic	Shift to 1643 chitosan amide , shift and weaker to 1708 to PVA	Shift to 1041, disappeared peak for secondary alcohol	1215 for aliphatic, new peak at 1342 for aromatic	Q at 1543, B at 1482, N=Q=N at 1111
CgA/PANI	3421, bending at 1408	Overlap with O-H, bending at 1516	2881 aliphatic, new peak for aromatic at 3008	1678 and 1600	Weaker and shift to 1080, secondary alcohol peak shift and weaker to 1134	Overlaps between aliphatic and aromatic at 1288	Q at 1543, B at 1454, N=Q=N at 1176
IPN/PANI	3437	Stretching 3228, bending at 1608	2943	1670 for poly acryl amide, 1724 for poly acrylic acid	1083	1230 aliphatic, new peak for aromatic at 1300	Q at 1556, B at 1469, N=Q=N at 1118

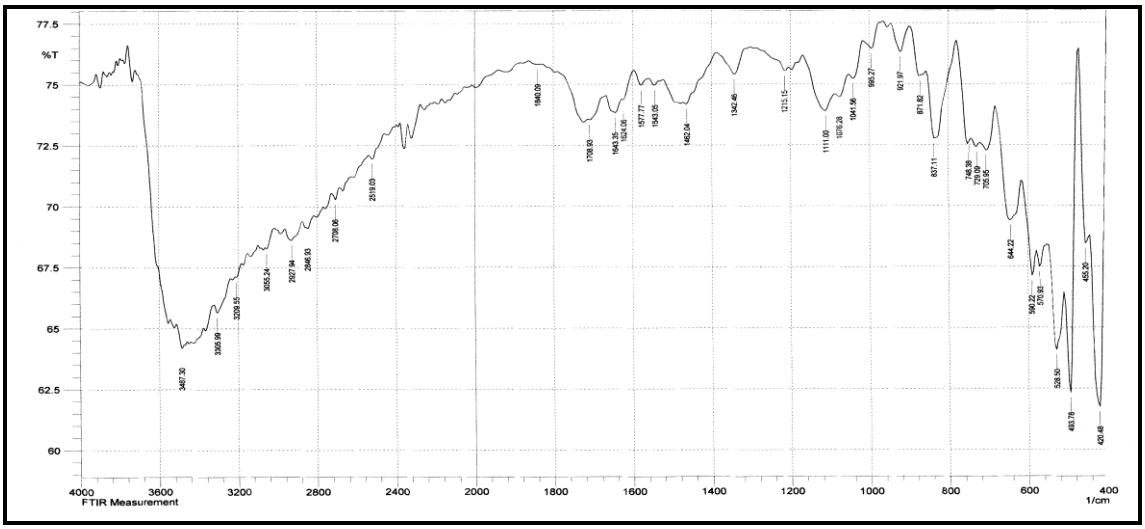

Figure (3.14): FT-IR spectrum of CPM/PANI film

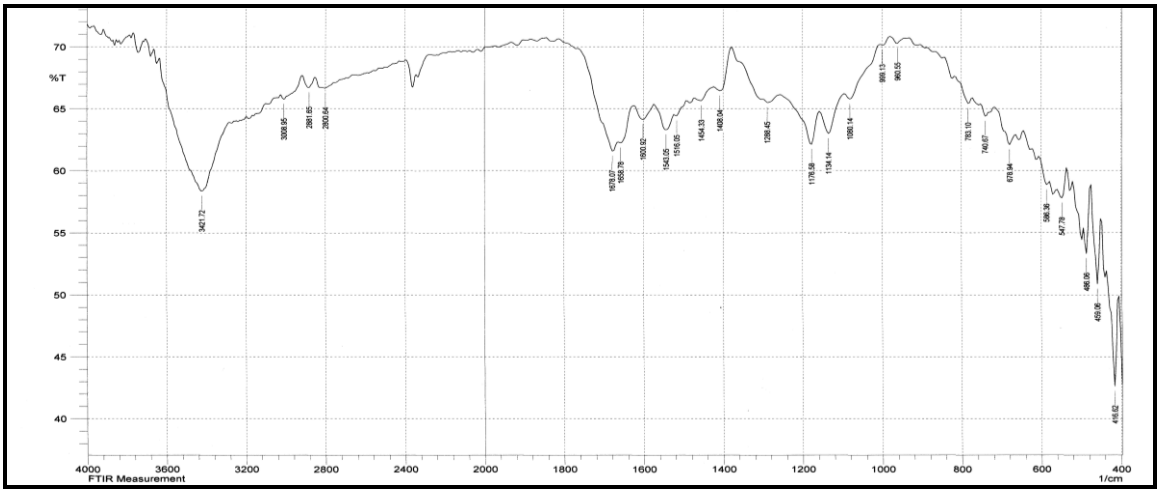

Figure (3.15): FT-IR spectrum of conductive hydrogel CgA/PANI film

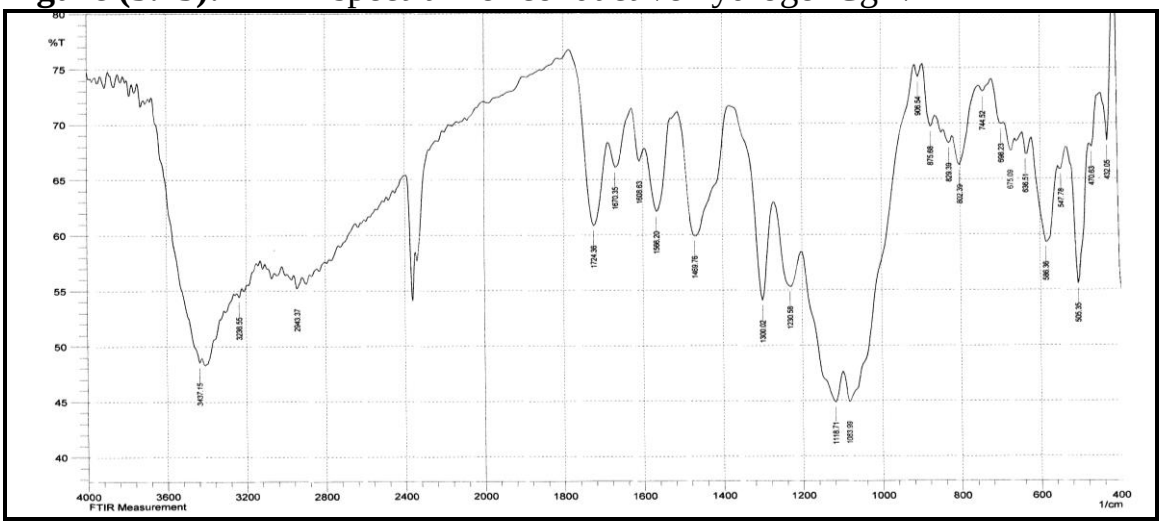

Figure (3.16): FT-IR spectrum of conductive hydrogel of IPN/PANI film

3.1.1.2.2 FTIR Analysis of conductive G/ hydrogels

In the spectrum of graphite (Fig 3.17), the absorption bands at 3444cm-1 was known to be the O-H stretching vibrations. The peaks located at 3043 and 2873 cm-1 could be attributed to aromatic and aliphatic C-H, respectively. The peak located at 1581 cm-1 could be attributed to the skeletal vibration of C=C aromatic [200].

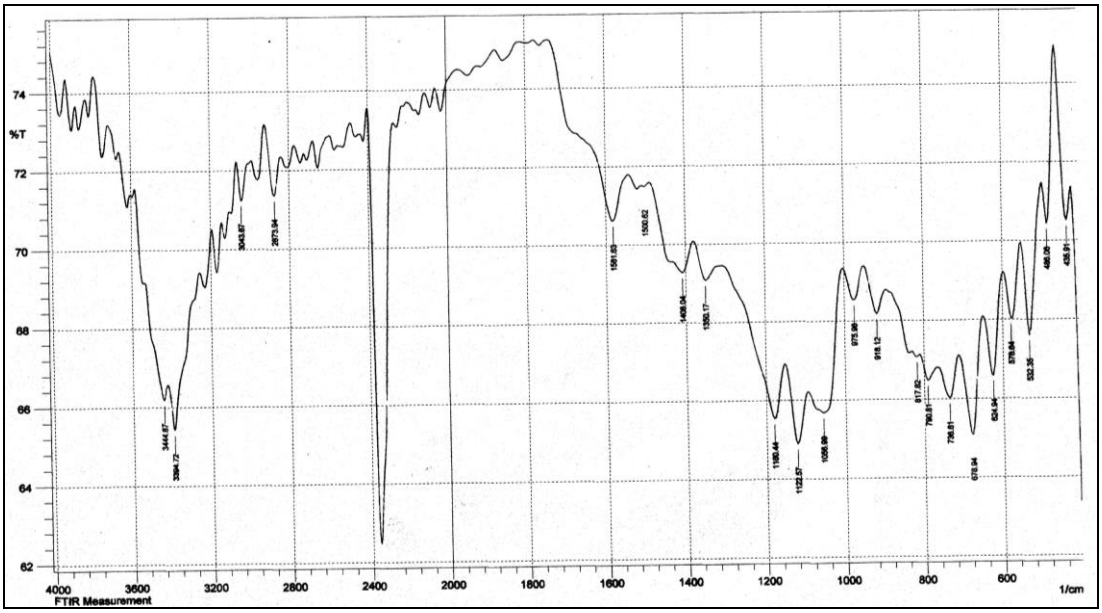

Figure (3.17): FT-IR spectrum of graphite

The FTIR spectrum of GO (Fig.3.18) shows a broad peak at 3402 cm-1 corresponding to the stretching vibration of OH groups of water molecules adsorbed on graphene oxide . Therefore, it can be concluded that the sample has strong hydrophilicity, while the presence of two absorption peaks observed in the medium frequency area, at 1616 cm-1 and 1712 cm−1 can be attributed to the stretching vibration of C=C and C=O of carboxylic acid and carbonyl groups present at the edges of graphene oxide . The absorption peaks at 1400 cm−1 and 1134 cm−1 are corresponding to the stretching vibration of C-O of carboxylic acid and C-OH of alcohol, respectively. Finally, the broad peak at 1068cm-1 is attributed to C-O of epoxy group.

The presence of these oxygen-containing groups reveals that the graphite has been oxidized. The polar groups, particularly the surface hydroxyl groups, result in the formation of hydrogen bonds between graphite and water molecules; this more explains the hydrophilic nature of graphene oxide [201].

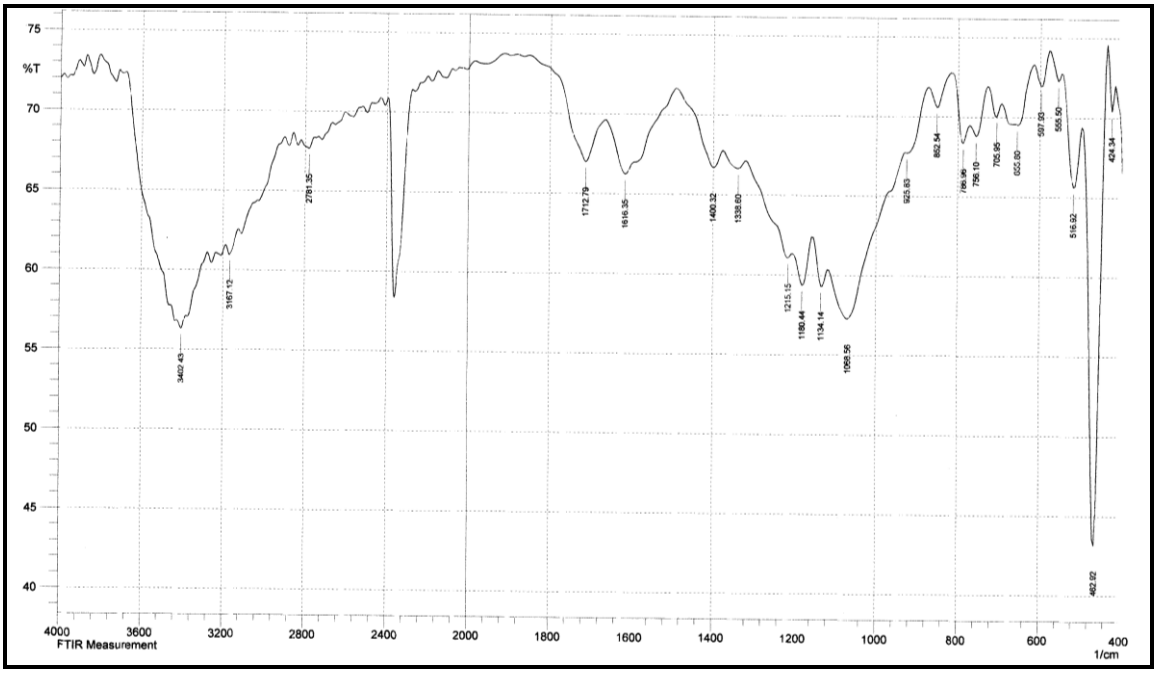

Figure (3.18): FT-IR spectrum of GO

The FTIR spectral assignment of graphene (G) provides information in fig (3. 19). FTIR peak of graphene presents that O-H stretching vibrations observed at about 3448 cm-1 was significantly reduced due to deoxygenating. However, stretching vibration for C=O was shifted to 1701 cm-1, it was still observed but weakness. On close observation, it appears that C=C aromatic stretching can be seen at 1647, and 1554 cm-1. Stretching vibration at 1068 cm-1 attributed to C-O (epoxy) was disappeared [202].

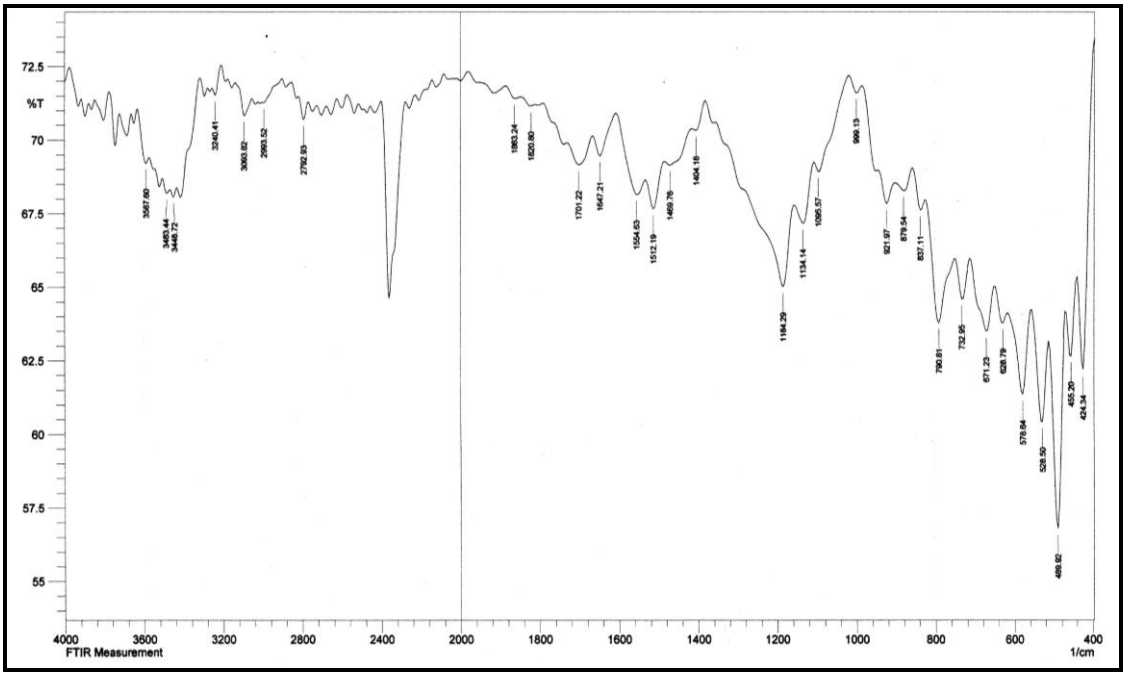

Figure (3.19): FT-IR spectrum of G

Characteristic peaks of G /hydrogels is showing in figures (3.20 -3.25). It observed new peaks in spectrum of hydrogels returned to G represented to peaks at about 3000-3100 cm–1 corresponds to aromatic C–H stretching, 1750-1700cm-1 (due to C=O of carboxylic acid), 1605-1500 cm–1 (due to C=C stretching of aromatic rings), 1400-1300 cm−1 and 1134-1100 cm−1 are corresponding to the stretching vibration of C-O of carboxylic acid and C-OH of alcohol, respectively, (see table 3.2).

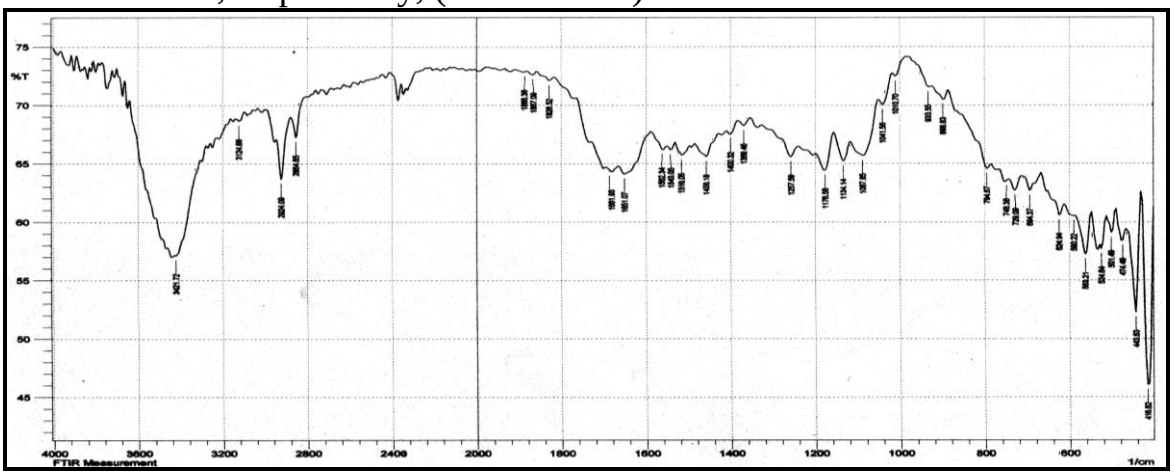

Figure (3.20): FT-IR spectrum of conductive hydrogel PgA/G film

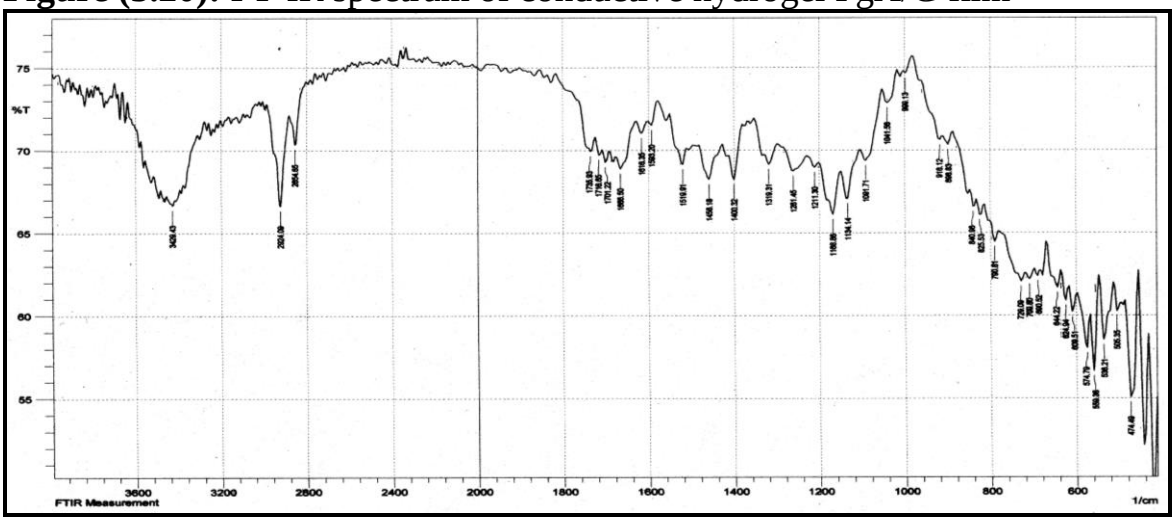

Figure (3.21): FT-IR spectrum of conductive hydrogel PPM/G film

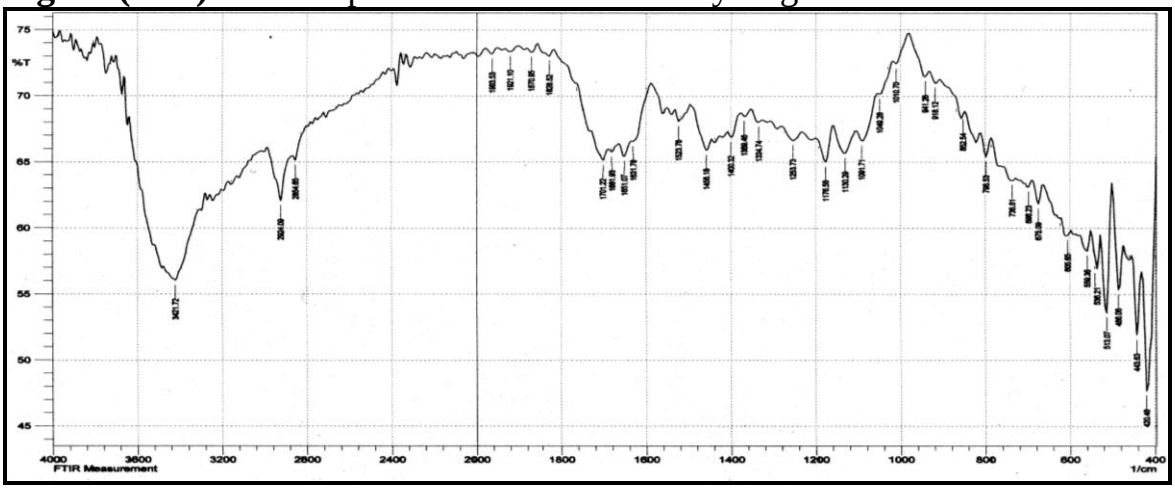

Figure (3.22): FT-IR spectrum of conductive hydrogel CPG/G film

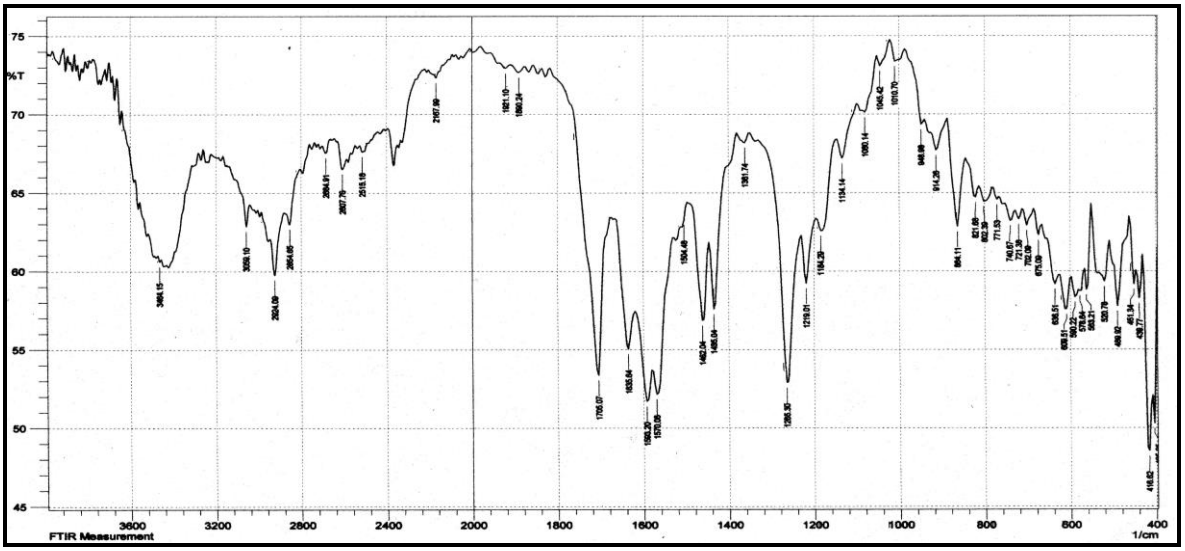

Figure (3.23): FT-IR spectrum of conductive hydrogel CPM/G film

Table (3.2): Characteristics FTIR absorption bands (cm^{-1}) contain stretching vibrations& bending vibrations of hydrogels/G composite

Samples	O-H	N-H	CH-	C=O	C-O	C-N	peaks other
PgA/G	3421	Overlaps with O-H	2924,2864 aliphatic, New peak at 3124 aromatic	1651, new peak at 1681 for G	1087 alcoholic, 1176 for acetal ring	1257 1309	C=C of G at 1562, 1543,1516
PPM/G	Stretching at 3429 ,bending at 1400	Overlaps with O-H	New peak for aromatic at 3132, aliphatic at 2924,2854 bending at 1319	Shift to 1716 to pectin and 1665 to PVA, 1735 for ester, new peak at 1701 for G,	Shift to 1091	1261,1319	C=C of G at 1616, 1593,1519
CPG/G	3421, bending at 1400	Overlaps with O-H	2924,2854	New peak at 1701 for G,	Shift to 1091, shift to 1130 for secondary alcohol	1253 , 1334	Schiff base (C=N) shift to 1651, C=C of G at 1661, 1560,1523
CPM/G	3464	Overlaps with O-H	2924,2854 new peak at 3059 for aromatic	1705, 1635	1080	1219 , 1265	C=C for G at 1593, 1570,1504
CgA/G	3433, bending at 1400	3410 , bending at 1454	2954, 2927,2860 aliphatic, new peak for G at 3174	1665 overlaps with C=O of G	1087	1215, 1249,1296,1323	C=C for G at 1604
IPN/G	3441	Overlaps with O-H	2924, 2854	1674 for poly acryl amide, 1712 for poly acrylic acid	1072	1265 , 1311	C=C for G at 1654,1558,1512

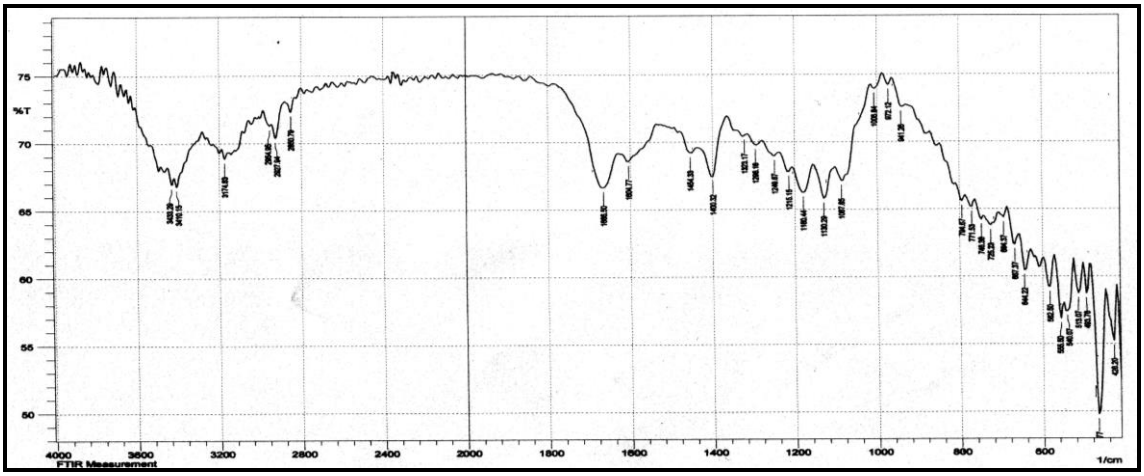

Figure (3.24): FT-IR spectrum of conductive hydrogel CgA/G film

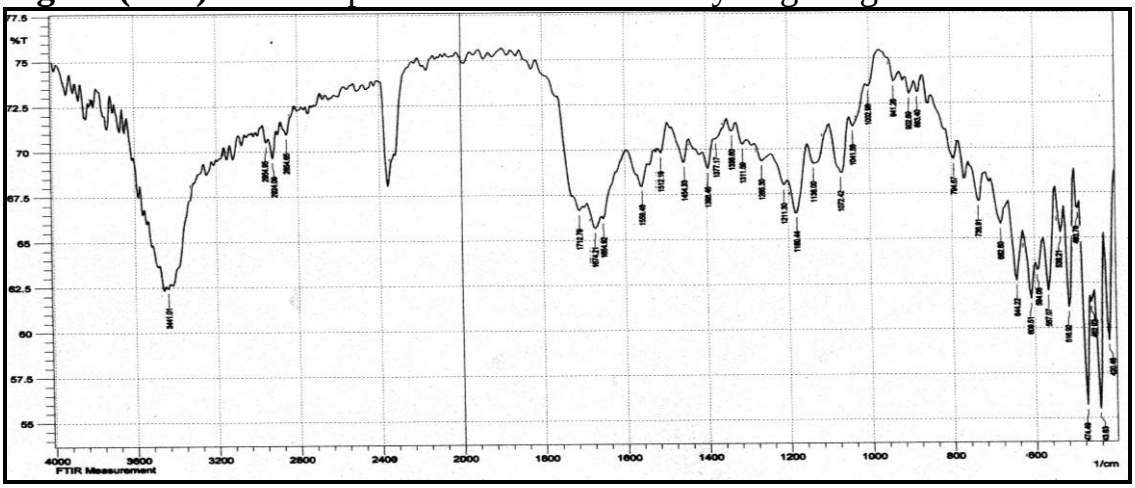

Figure (3.25): FT-IR spectrum of conductive hydrogel IPN/G film

3.1.1.2.3 FTIR Analysis of conductive MWCNTs/ hydrogels

Fourier transform infrared spectra of pristine multiwall carbon nanotubes (MWCNTs) is shown in (Fig. 3.26), C-O stretching at 1080 cm–1 , C=C at about 1605-1500 cm–1 , C-H stretching at 2978 cm–1 , C=O of carboxyl groups was very weakness at about 1750-1700 [203].

Characteristic peaks of MWCNTs /hydrogels are showing in figures (3.27-3.32). It observed new peaks in spectrum of hydrogels returned to MWCNTs represented to peaks at about 3000-3100 cm–1 corresponds to aromatic C–H stretching, 1750-1700cm-1 (due to C=O of carboxylic acid), 1605-1500 cm–1 (due to C=C stretching of aromatic rings), 1400-1300 cm−1 and 1134-1000 cm−1 are corresponding to the stretching vibration of C-O of carboxylic acid and C-OH of alcohol, respectively, (see table 3.3).

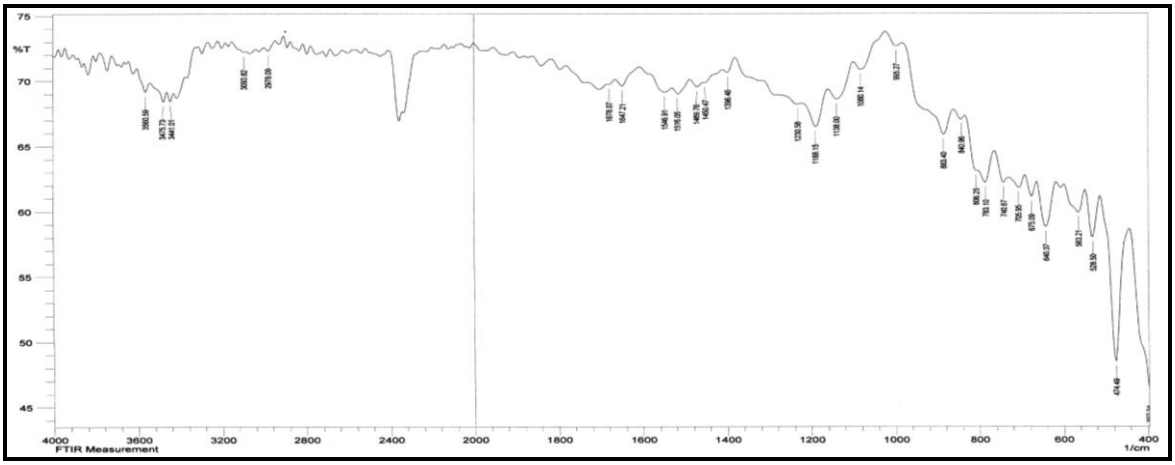

Figure (3.26): FT-IR spectrum of MWCNTs

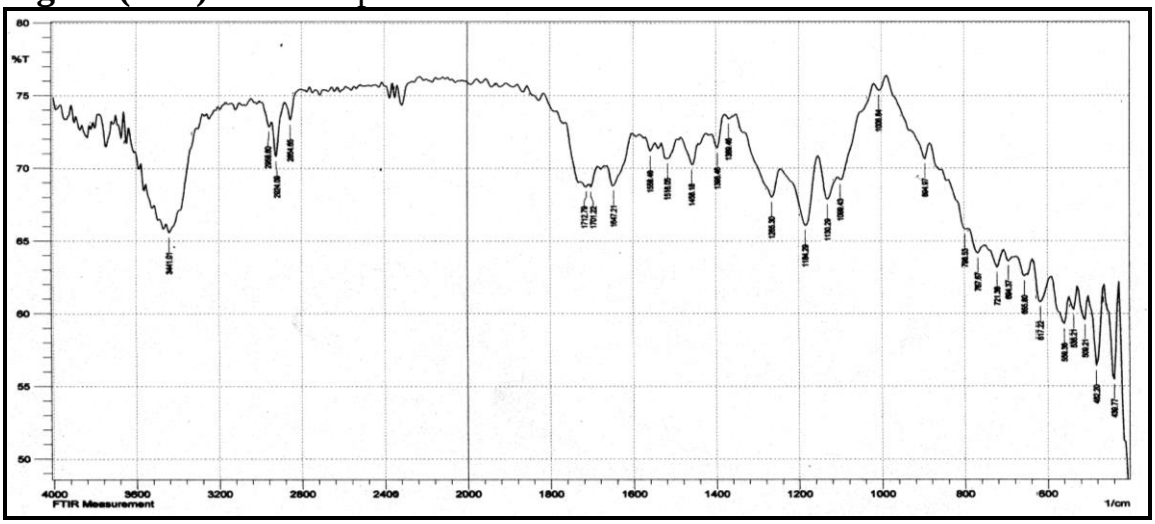

Figure (3.27): FT-IR spectrum of conductive hydrogel PgA/MWCNTs film

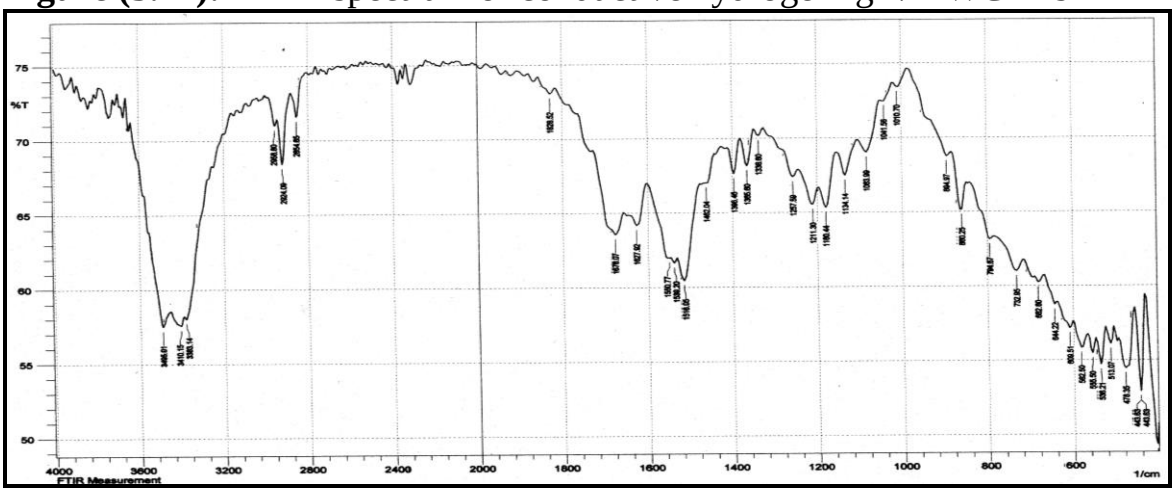

Figure (3.28): FT-IR spectrum of conductive hydrogel PPM/MWCNTs film

Table (3.3): Characteristics FTIR absorption bands (cm^{-1}) contain stretching vibrations& bending vibrations of hydrogels/MWCNTs composite

Samples	O-H	N-H	CH-	C=O	C-O	C-N	peaks other
PgA/MWCNTs	3441	Overlaps with O-H	2956,2924, 2864,	1712,1701	1099 overlaps with C-O for MWCNTs, 1184 for acetal ring	1265 1369	C=C of MWCNTs at 1647,1558 ,1516
PPM/MWCNTs	3495	3410	New peak for MWCNTs at	Shift to 1667 to pectin and	1041, new peak at 1083	1211,1257	C=C of MWCNTs at

			2958, 2924,2854	1627 to PVA,	for MWCNTs		1550, 1539,1516
CPG/MWCNTs	3471	Overlaps with O-H	3062, 2924	1701	Shift to 1045, shift to 1134 for secondary alcohol, new peak at 1087 for MWCNTs	1257 , 1334	Schiff base (C=N) shift to 1651, C=C of MWCNTs at 1681, 1620,1539 ,1512
CPM/MWCNTs	3441	Overlaps with O-H	2924,2854	1735, 1701,	Shift to 1041, new peak at 1083 for MWCNTs	1336,1257	C=C for MWCNTs at 1678,1651 ,1620, 1558, 1539, 1516
CgA/MWCNTs	3441	Overlaps with O-H, bending at 1456	2997, 2958 for MWCNTs, 2924,2864	1735,1701	1041 , new peak at 1087 for MWCNTs	1257,1369	C=C for MWCNTs at 1676, 1651,1556 ,1512
IPN/MWCNTs	3437	Overlaps with O-H	2927, 2856	1661for poly acryl amide, 1697 for poly acrylic acid	1045, new peak at 1083 for MWCNTs	1264 , 1396	C=C for MWCNTs at 1651,1620 ,1554,1516

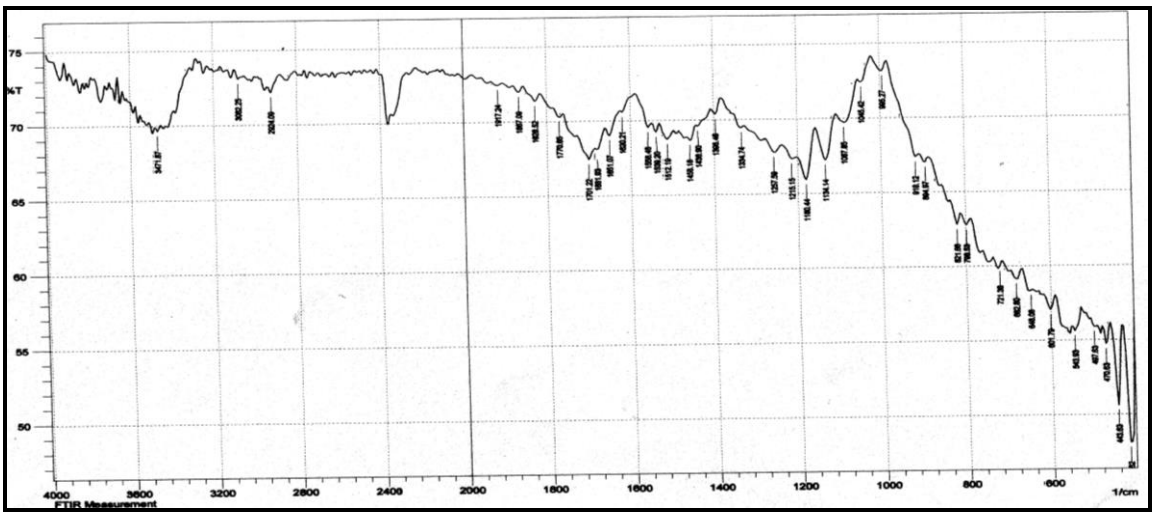

Figure (3.29): FT-IR spectrum of conductive hydrogel CPG/ MWCNTs film

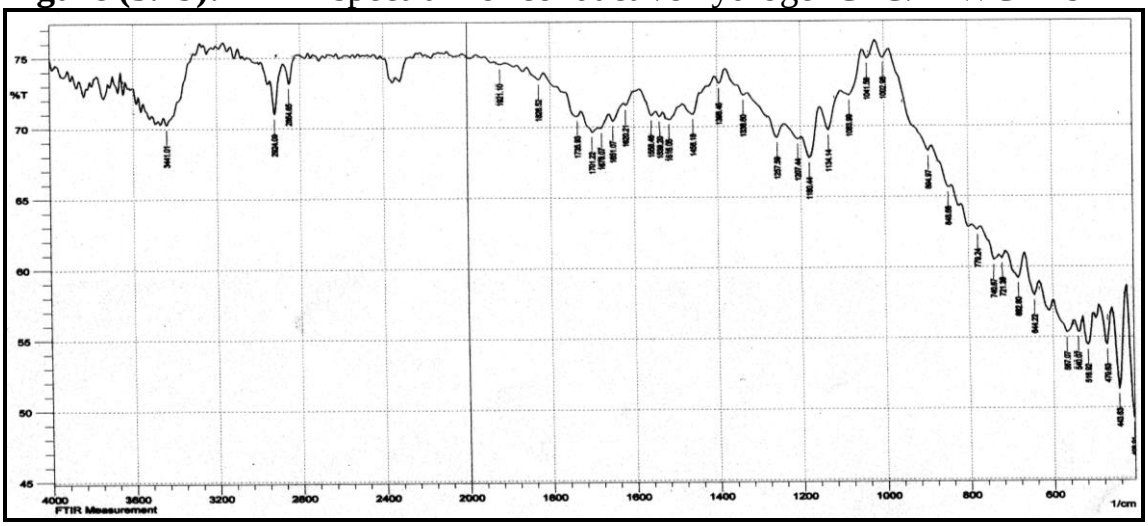

Figure (3.30): FT-IR spectrum of conductive hydrogel CPM/ MWCNTs film

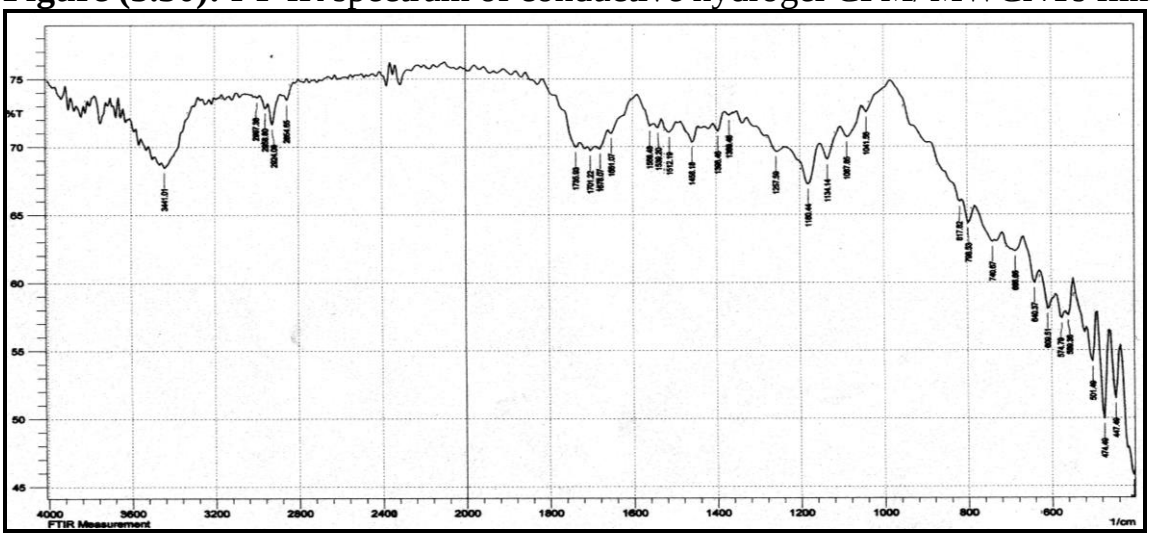

Figure (3.31): FT-IR spectrum of conductive hydrogel CgA/ MWCNTs film

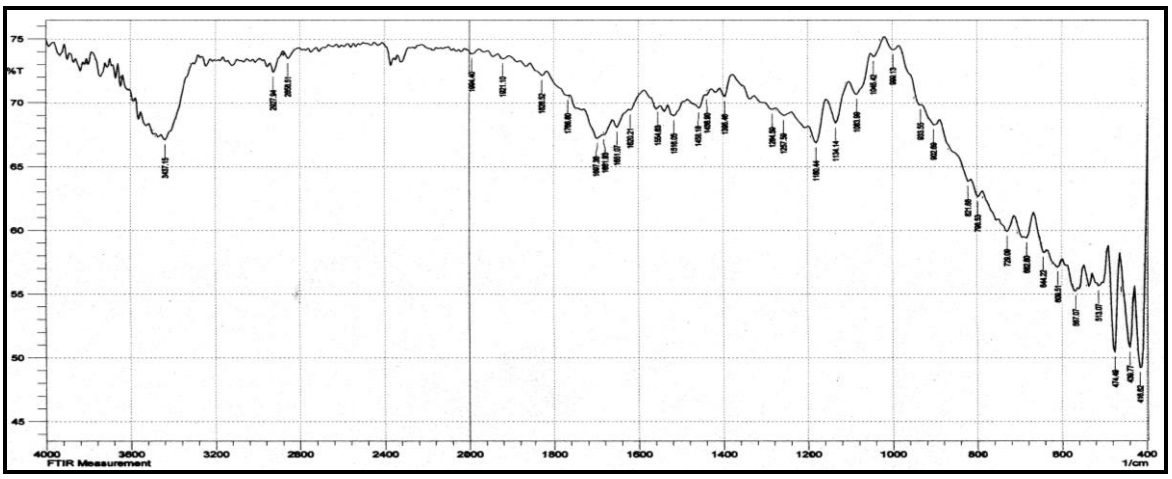

Figure (3.32): FT-IR spectrum of conductive hydrogel IPN/ MWCNTs film

3.1.1.3 FTIR Analysis of coating hydrogels

The absorption bands of iron oxide magnetic particles appear at 574 and 628 cm−1 (Fig. 3.33) are attributed to Fe–O deformation in the octahedral and tetrahedral sites. The bands OH stretching and HOH bending vibrational bands at 3412 cm−1 and 1631 cm−1are due to the adsorbed water in the sample [204].

Figures (3.34-3.39) are showing Fourier transform infrared spectra of coated magnetite with hydrogels. The spectrum of coated particles exhibits characteristic absorption bands of the functional groups of hydrogels as well as functional groups of Fe_3O_4 magnetic nanoparticles.

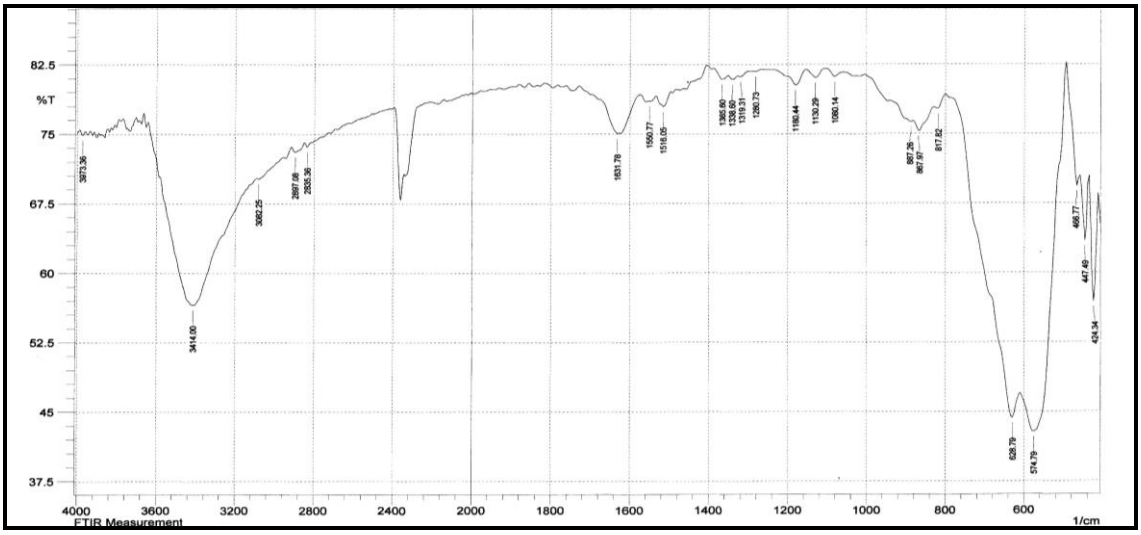

Figure (3.33): FT-IR spectrum of Fe_3O_4 MNPs

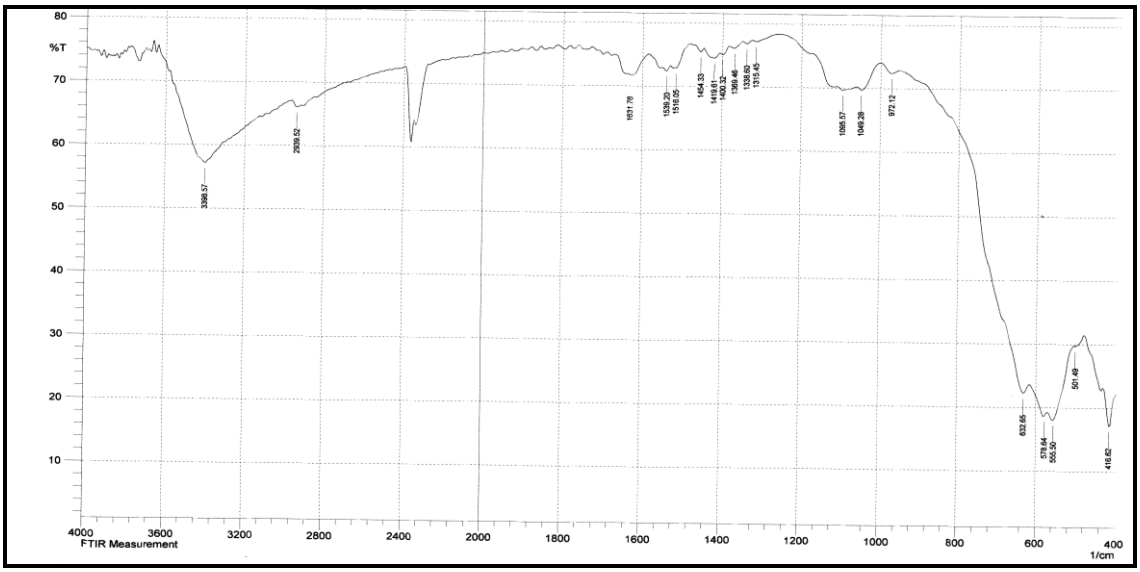

Figure (3.34): FT-IR spectrum of CPM/Fe_3O_4

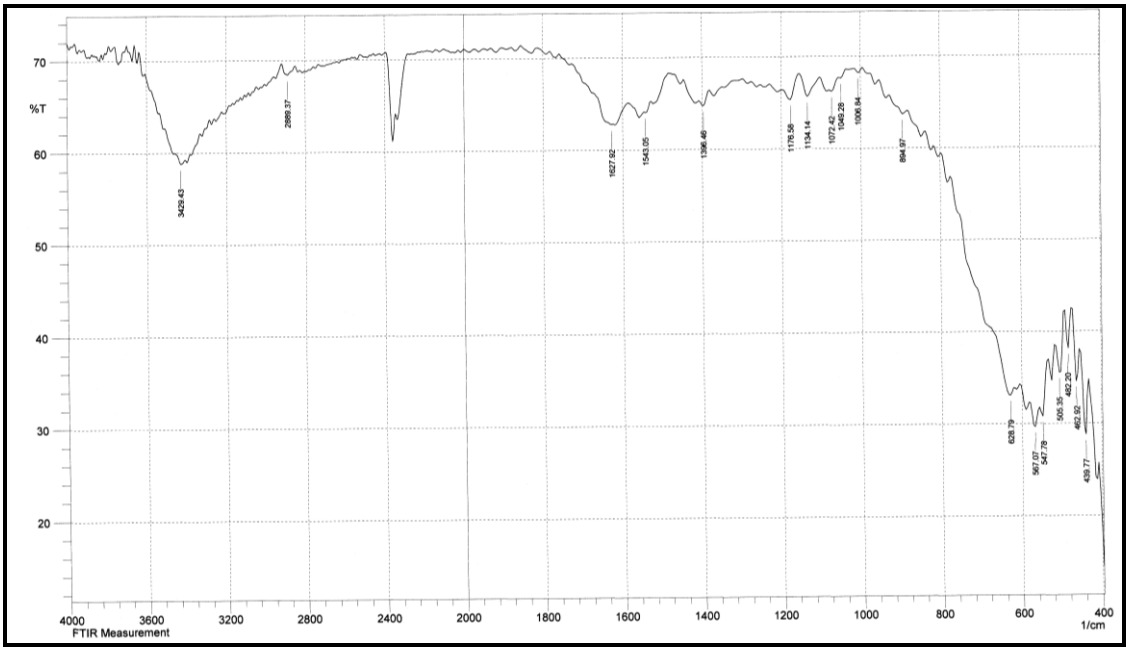

Figure (3.35): FT-IR spectrum of hydrogel of PPM/Fe_3O_4

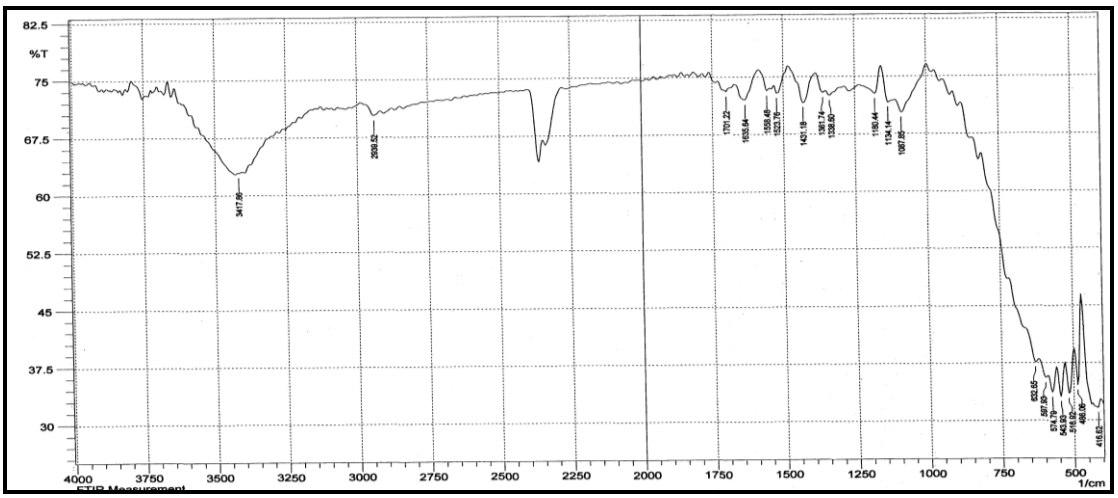

Figure (3.36): FT-IR spectrum of PgA/Fe_3O_4

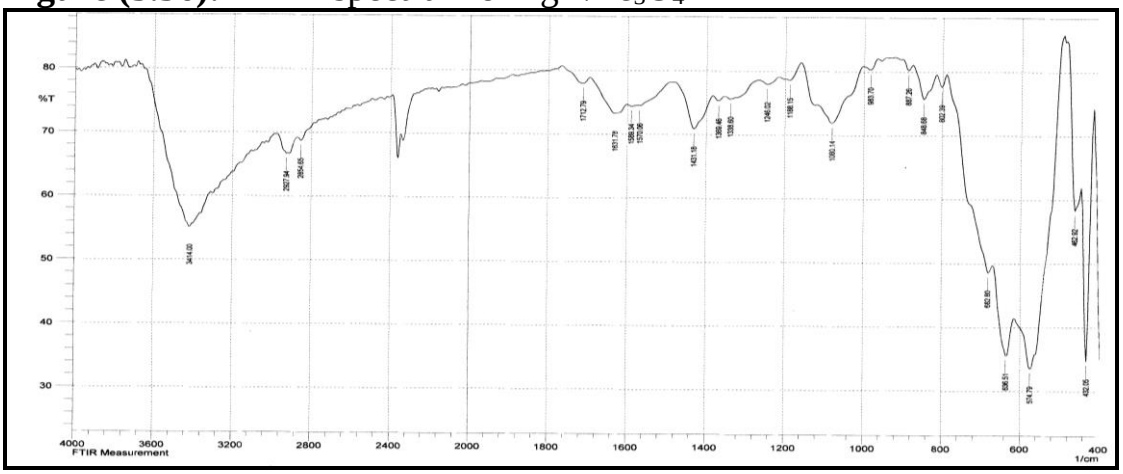

Figure (3.37): FT-IR spectrum of CPG/Fe_3O_4

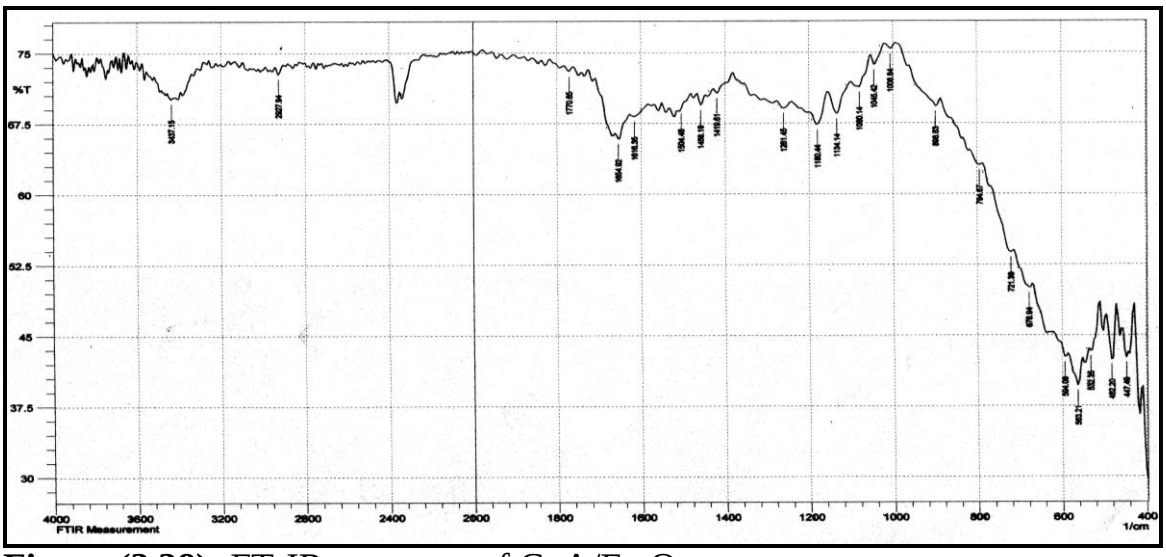

Figure (3.38): FT-IR spectrum of CgA/Fe_3O_4

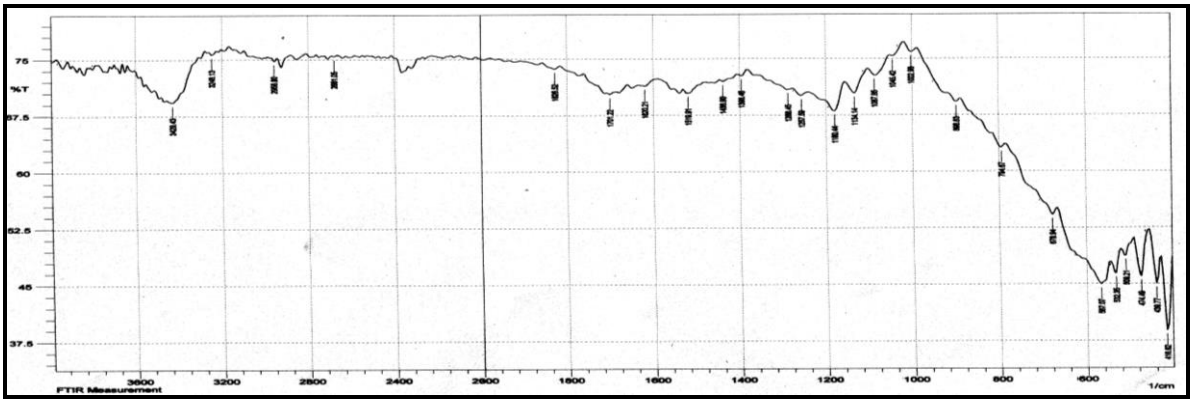

Figure (3.39): FT-IR spectrum of IPN/Fe_3O_4

Figure (3.40) is showing Fourier transform infrared spectra of coated magnetite with CPG/PANI conductive hydrogel. The spectrum of coated particles exhibits characteristic absorption bands of the functional groups of CPG/PANI as well as functional groups of Fe_3O_4 magnetic nanoparticles.

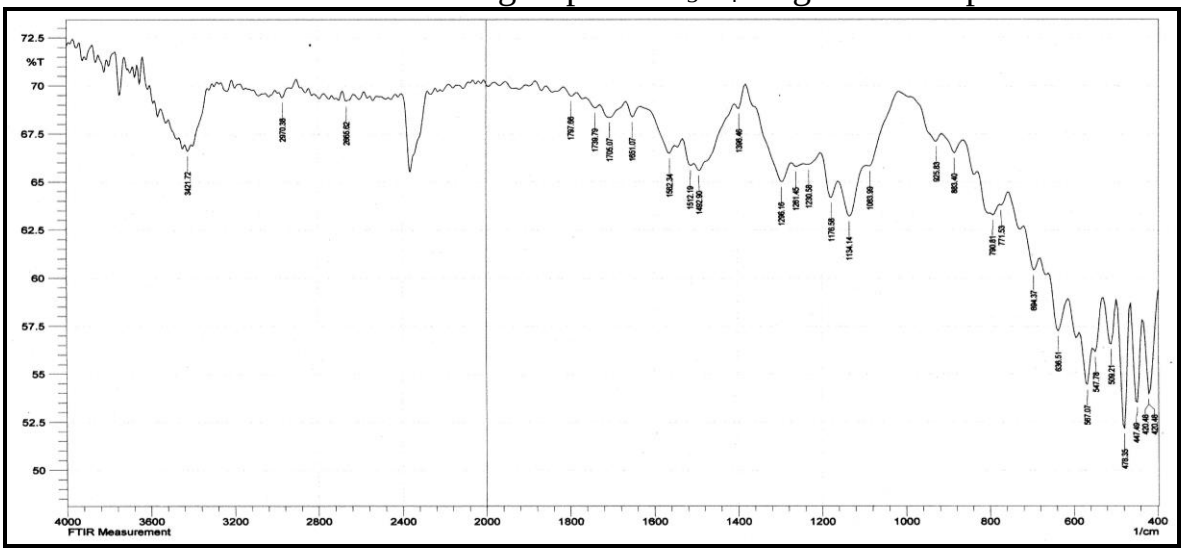

Figure (3.40): FT-IR spectrum of CPG/Fe_3O_4/PANI

3.1.2 XRD Analysis of hydrogels and hydrogel composite

3.1.2.1 XRD Analysis of hydrogels

X-ray diffraction patterns of hydrogels are shown in figures (3.41-3.46), from figure (3.41) is showing diffractive peaks of CPG hydrogel. The strongest peak in about 2θ= (20º) with the highest intensity of about 1500 counts. This diffractograph is similar to reference [205].

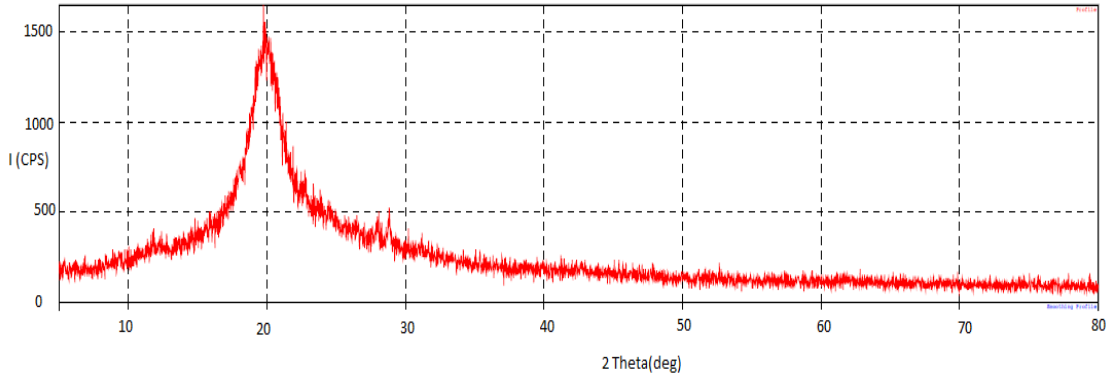

Figure (3.41): XRD for CPG hydrogel

Figure (3.42) shows X-ray diffraction of CPM hydrogel. The three strongest peaks in about 2θ= (19.3º, 18.7º, 24.7º) with the highest intensity of about 2000 counts.

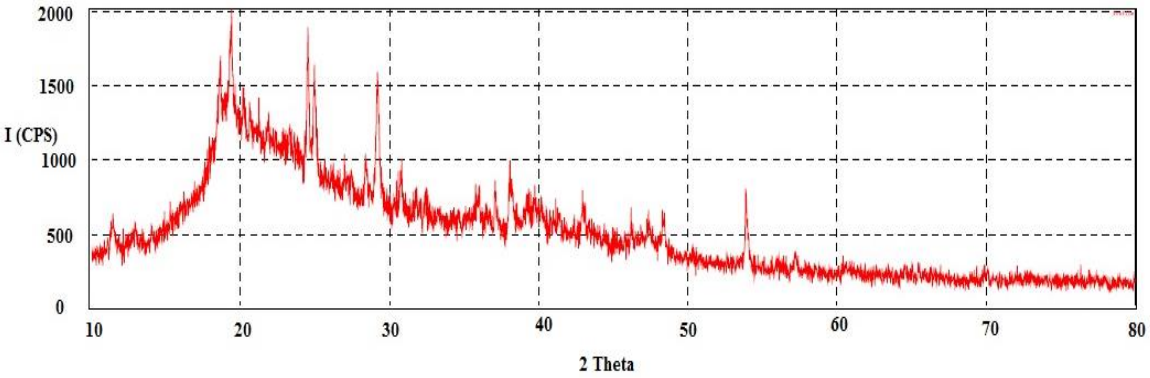

Figure (3.42): XRD for CPM hydrogel

Figure (3.43) shows X-ray diffraction of PPM hydrogel. The strongest peak in about 2θ= (20º) with the highest intensity of about 2000 counts.

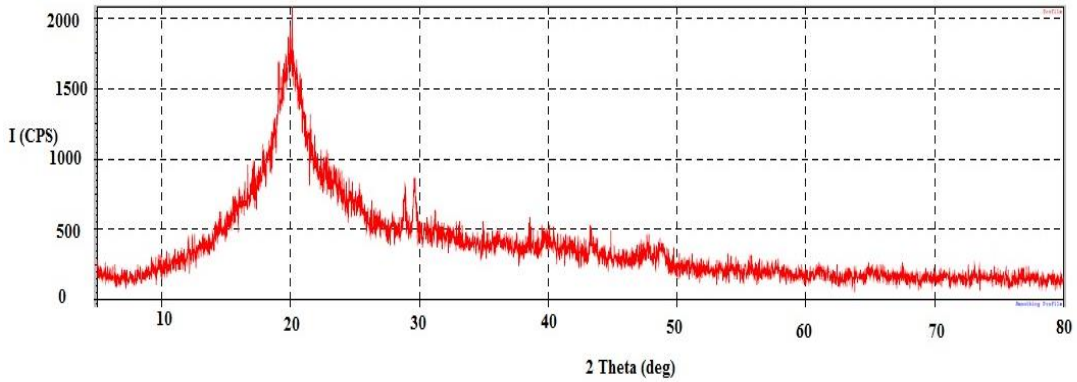

Figure (3.43): XRD for PPM hydrogel

Figure (3.44) shows X-ray diffraction of PgA hydrogel. The three strongest peak in about 2θ= (19.5º, 20.4º, 18.6º) with the highest intensity of about 1000 counts.

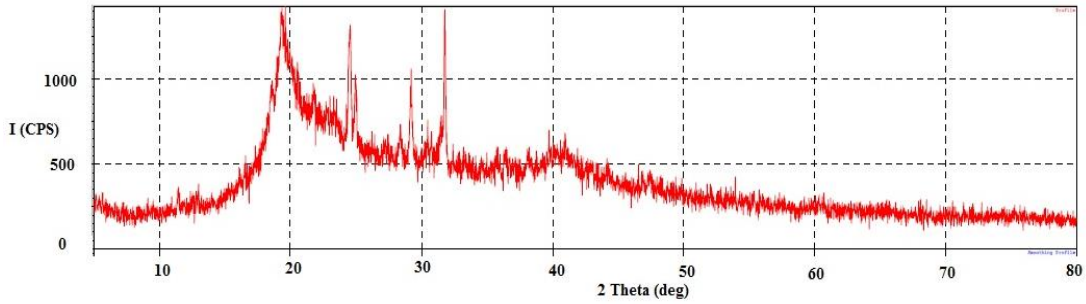

Figure (3.44): XRD for PgA hydrogel

Figure (3.45) shows X-ray diffraction of CgA hydrogel. The strongest peak in about 2θ= (24.5º) with the highest intensity of about 2000 counts.

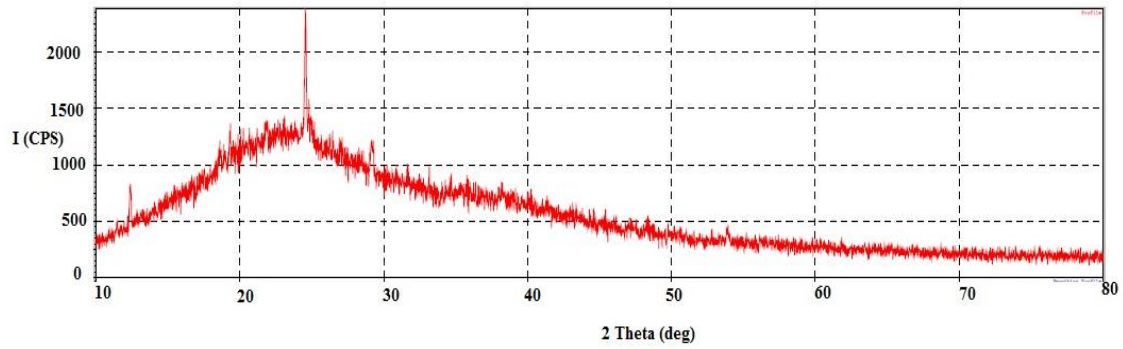

Figure (3.45): XRD for CgA hydrogel

Figure (3.46) shows X-ray diffraction of IPN hydrogel. The strongest peak in about 2θ= (21.2º) with the highest intensity of about 2000 counts.

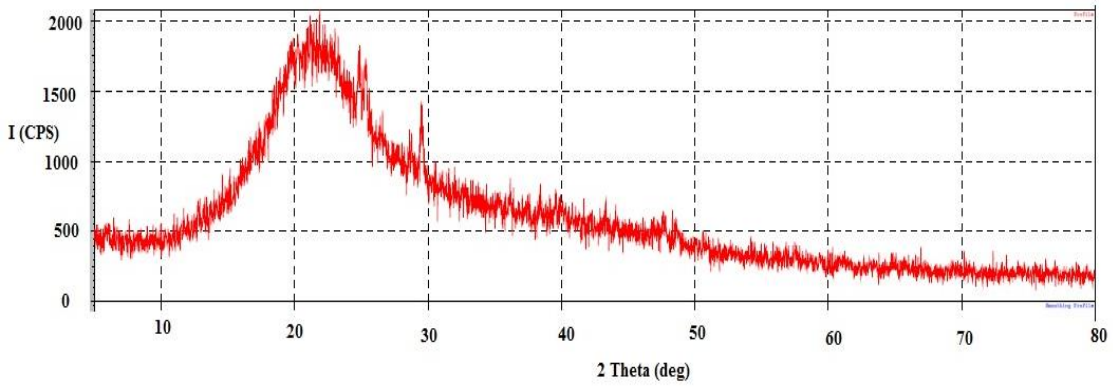

Figure (3.46): XRD for IPN hydrogel

From these diffractographs, it was obvious that CPG and PPM is more crystalline than others. The IPN hydrogel is more amorphous than others.

3.1.2.2 XRD Analysis of nano and nanocomposite

The crystal structures for Fe_3O_4 MNPs and MNPs composite were characterized by X-ray diffraction in Figures (3.47-3.53). For the pure Fe_3O_4 MNPs(fig. 3.47) as prepared in this work, seven characteristic peaks (2θ = 30.15°, 35.53°, 43.11°, 53.52°, 57.13°, 62.73° and 74.17 °) marked by their indices ((220),(311), (400), (422), (511), (440, and 533)) ascertained by comparison with Joint Committee on Powder Diffraction Standards(JCPDS card, File No. 79-0418) . Average size MNPs can be calculated from XRD data using the Debye–Scherrer equation.

$$D = \frac{K\lambda}{\beta \cos\theta} \quad \text{----------} \quad (3.1)$$

where, K (=0.89) is the Scherrer constant, λ is the X-ray wavelength(0.15406), β is the peak width at half-maximum height (FWHM) and θ is the Bragg diffraction angle[206]. The average size of the Fe_3O_4 MNPs was found to be about (11-13) nm.

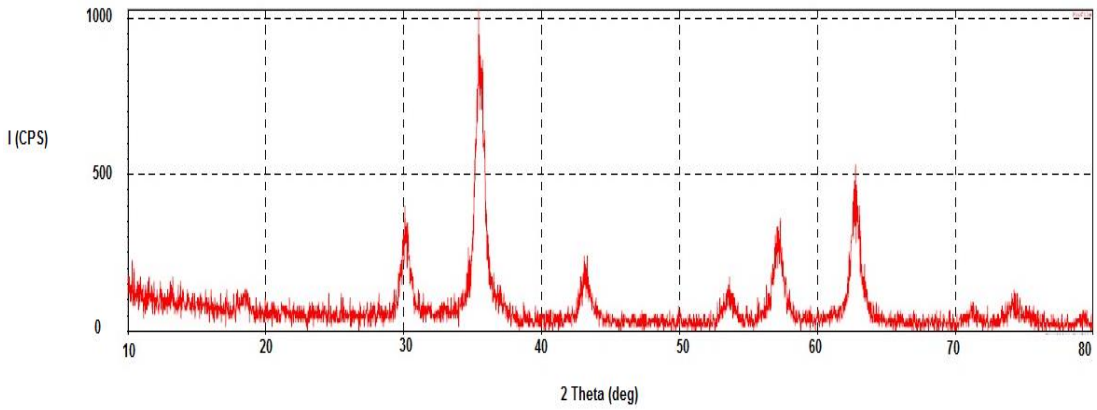

Figure (3.47): XRD for Fe_3O_4 MNPs

Figures (3.48-3.53) were showed XRD for MNPs composite, seven diffraction peaks of Fe_3O_4 MNPs were appeared also in MNPs composite. The peaks intensity of Fe_3O_4 MNPs composites is lower than pure Fe_3O_4 MNPs. The broad peak at 2θ = 17° to 27° in XRD MNPs composite was ascribed to hydrogels, which indicated the existence of an amorphous structure [207].

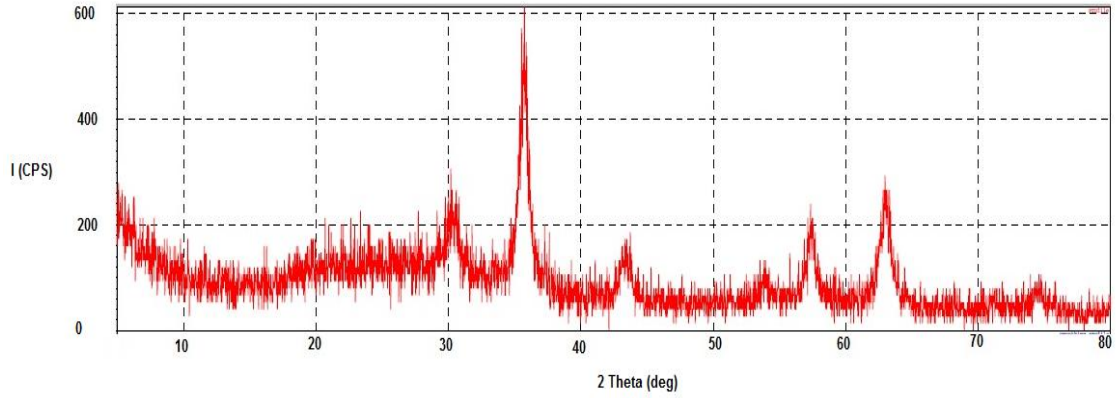

Fig (3.48): XRD for PPM/Fe_3O_4

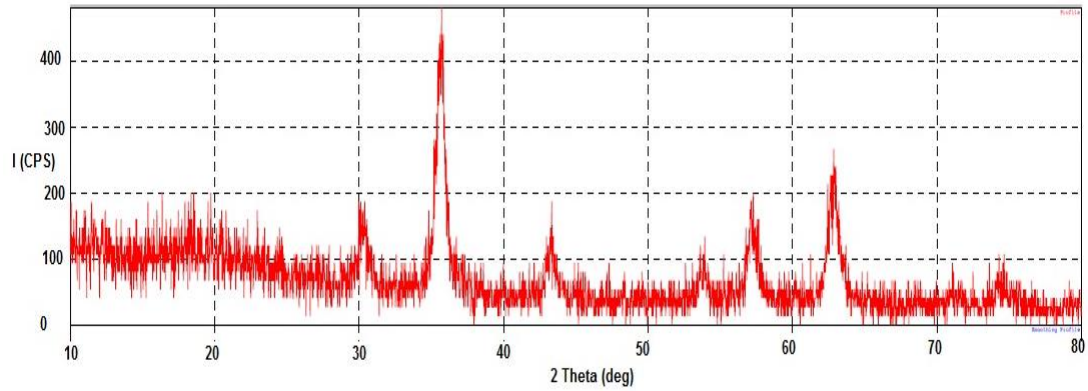

Fig (3.49): XRD for CPG/Fe_3O_4

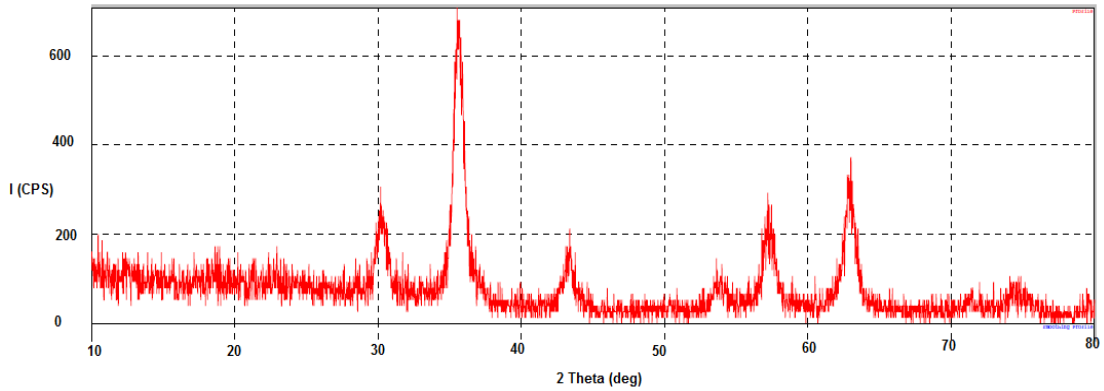

Fig (3.50): XRD for CPM/Fe_3O_4

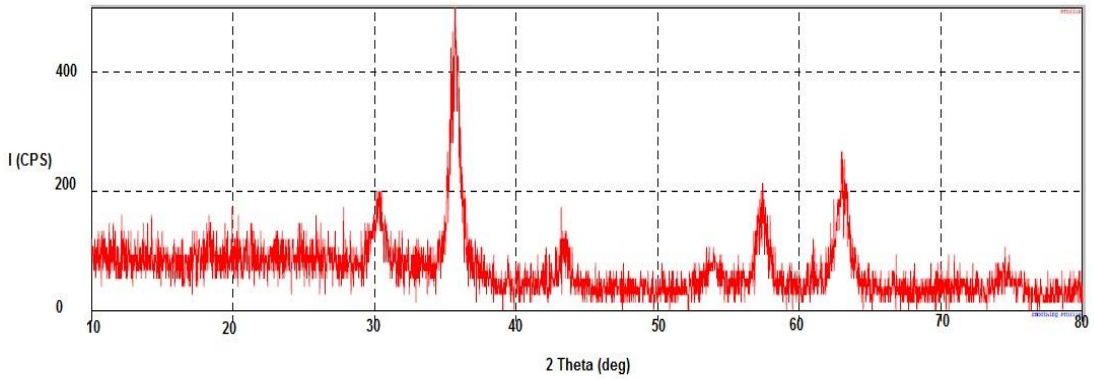

Figure (3.51): XRD for PgA/Fe_3O_4

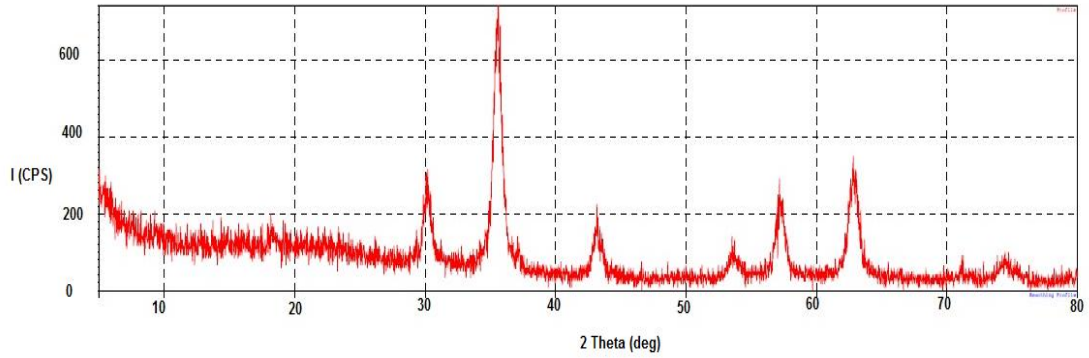

Figure (3.52): XRD for CgA/Fe_3O_4

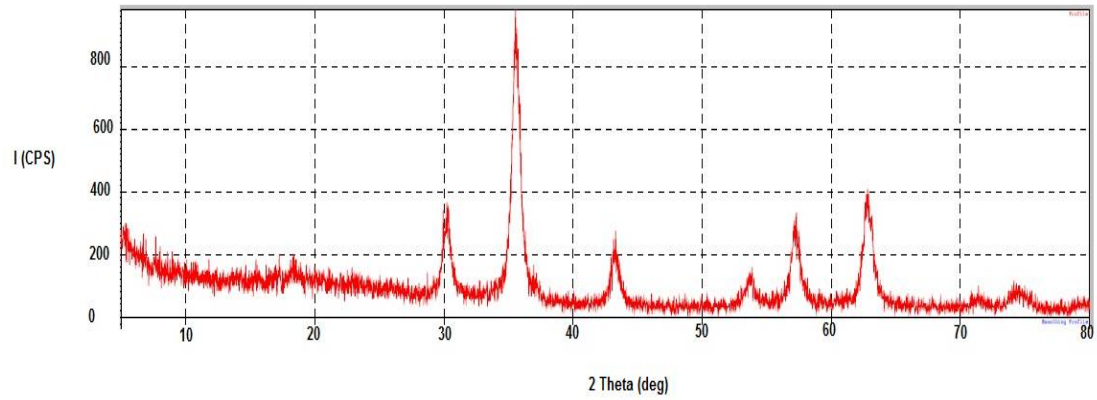

Figure (3.53): XRD for IPN/Fe_3O_4

The XRD of graphite (figure 3.54) shows a sharp peak at 2θ=26.4º. This peak corresponds to (002) reflection of graphite with interlayer spacing (d002) 3.36Å [168].

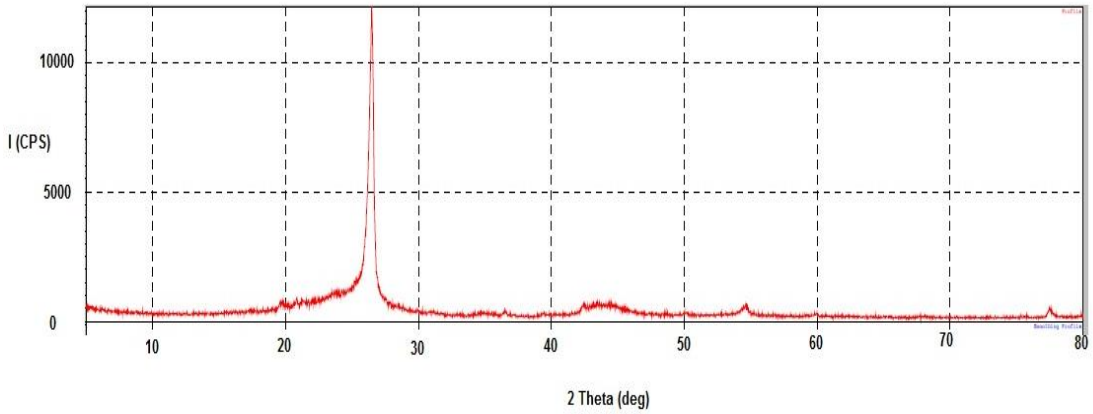

Figure (3.54): XRD for graphite

Figure (3.55) shows the X-ray diffraction pattern (XRD) of GO synthesized by modified Hummer's method, new diffraction peak observed at 2θ =10.77° with an interlayer distance of 8.20 Å corresponds to GO. While diffraction peak at 26.59 may be returned to graphite residue not oxidized. The d-spacing increases from 3.36 Å of pristine graphite to 8.20 Å for graphene oxide. The increased spacing indicates the presence of functional groups on the surface of graphene oxide [208].

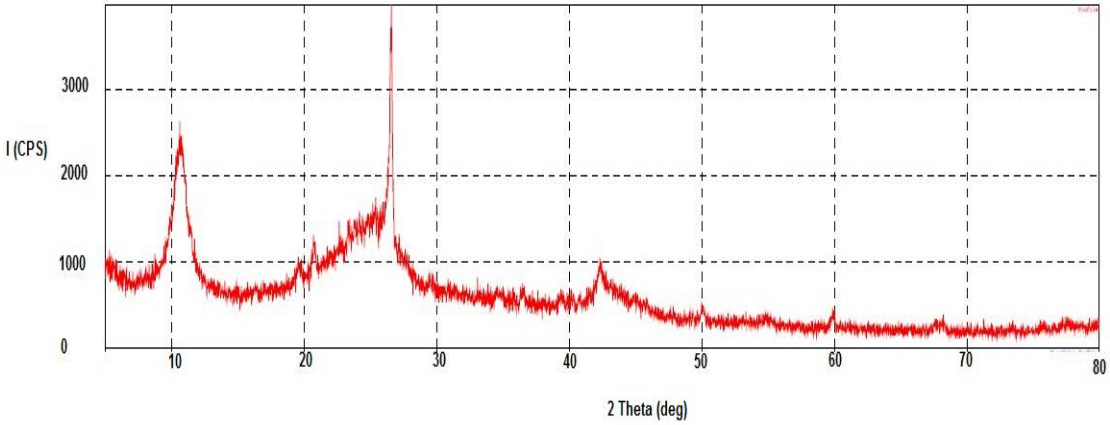

Figure (3.55): XRD for GO

In the X-ray diffraction (XRD) pattern of G (fig. 3.56), the peak at 10.77° corresponding to GO was disappeared in G with major peak is observed at about 23-26° . This gives an interlayer spacing of approximately 3.35 to 3.73 Å [209-211].

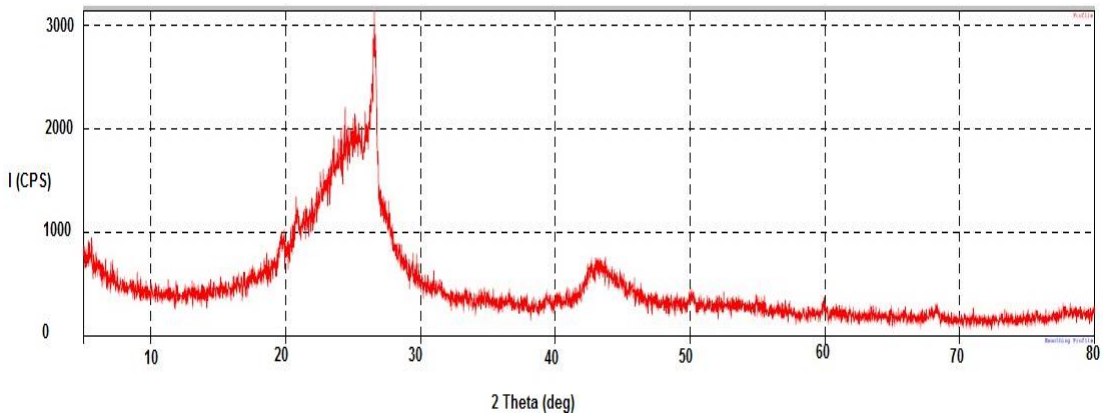

Figure (3.56): XRD for G

The XRD pattern (fig.3.57) of the MWCNTs was appeared the presence main peak at 26.50º corresponding to the interlayer spacing (0.34nm) of the nanotubes (d_{002}) and 42.49º (d_{100}) reflection of the carbon atoms, in good agreement with the literature [212].

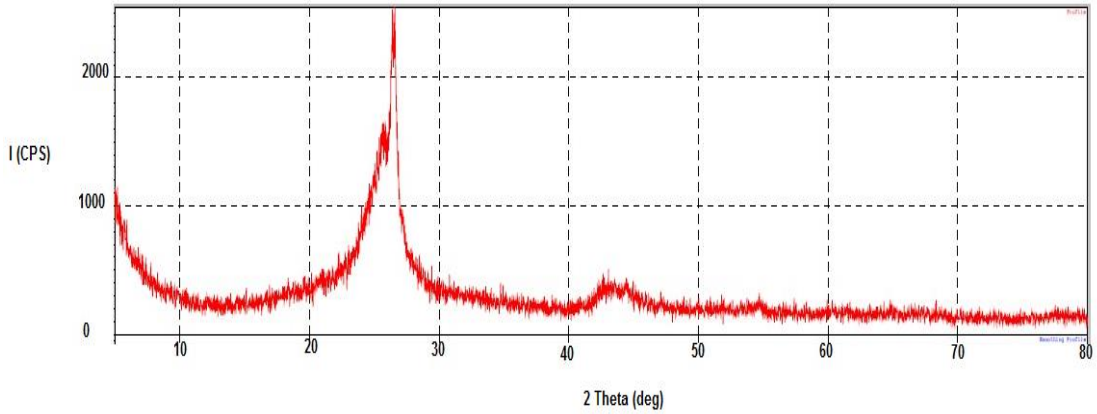

Figure (3.57): XRD for MWCNTs

The diffraction pattern of pure PANI has a broad peak around 2θ = 25.03º (fig. 3.58) which is a characteristic peak of PANI [213].

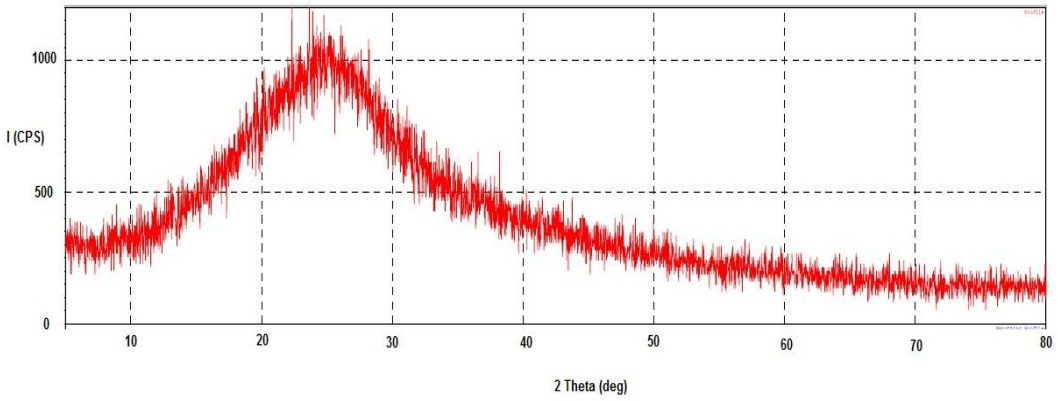

Figure (3.58): XRD for PANI

Figure (3.59) was showed XRD for (CPG/Fe_3O_4/PANI) composite, seven diffraction peaks of Fe_3O_4 MNPs were appeared also in composite. The peaks intensity of Fe_3O_4 MNPs composite is lower than pure Fe_3O_4 MNPs.

The broad peak at 2θ = 17° to 27° in XRD MNPs composite was ascribed to hydrogel with poly aniline, which indicated the existence of an amorphous structure. The average size of the coating form (CPG/Fe_3O_4/PANI) was found to be about (12-14) nm.

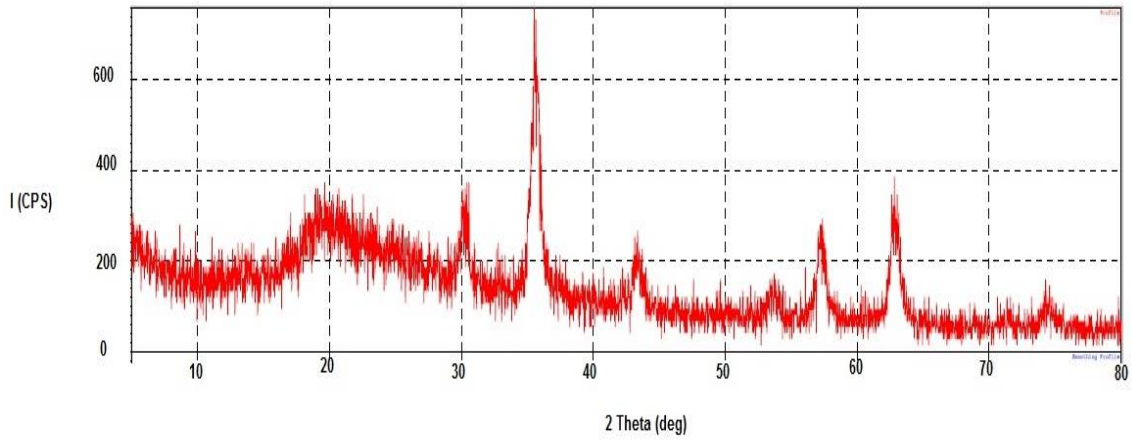

Figure (3.59): XRD for CPG/Fe_3O_4/PANI

Average size of nanoparticles was calculated from Debye–Scherrer equation represented in table (3.4) with three strongest peaks and FWHM.

Table (3.4): Average size of nanoparticles with strongest three peaks and FWHM was got from XRD graph

Samples	Strongest three peak 2 theta(deg)	FWHM (deg)	Average size(nm)
Fe_3O_4	35.5324, 62.7367, 57.1328	0.7700, 0.7467, 0.7750	11-13
CPG/Fe_3O_4	35.6339, 62.7734, 57.1253	0.6733, 0.6600, 0.5600	13-17
CgA/Fe_3O_4	35.5699, 62.8234, 57.2053	0.7350, 0.9600, 0.8000	10-12
IPN/Fe_3O_4	35.6054, 62.8200, 30.2363	0.7496, 0.8333, 0.7067	11-12
PPM/Fe_3O_4	35.7272, 62.8934, 57.3553	0.7000, 0.7000, 0.6200	12-15
CPM/Fe_3O_4	35.6050, 62.8800, 57.2600	0.8300, 0.8400, 0.8400	11-12
PgA/Fe_3O_4	35.6873, 62.9934, 57.3253	0.7800, 0.8600, 0.8400	11-12
CPG/Fe_3O_4/PANI	35.6298, 62.8334, 57.2453	0.7450, 0.8200, 0.6800	12-14

3.1.3. Thermal Studies

TGA and DSC analyses for the hydrogel are shown in figures (3.60 - 3.65), from graph of TGA is shown mass change with temperature. Table (3.5) is showing the real mass change (%) data of hydrogels at different temperature of TGA runs.

Many researchers have used the (DSC) analysis to find out of (glass transition temperature (Tg)) of some polymers, (Tg) is the temperature where the polymer undergoes the structural change form glassy state to rubbery state. Below (Tg), films are rigid and brittle, whereas above it blends become flexible and pliable [214].

Figure (3.60) shows the DSC thermogram of CPG hydrogel, (Tg)of hydrogel (CPG) is observed at about 226.5°C. In addition to this a broad endothermic peak was obtained at 111.3°C showing the crystallization of the blend of polymers in different form. No exothermic peak was obtained below 480°C showing that the there was no decomposition of hydrogel was occur in this temperature range.

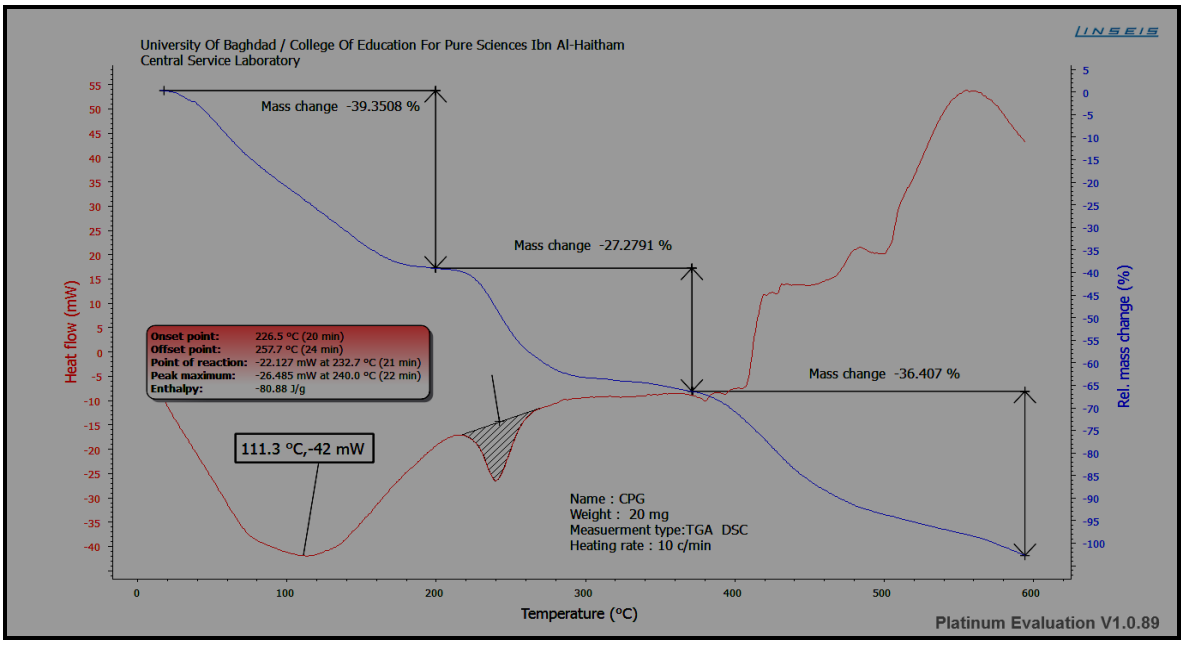

Figure (3.60): TGA and DSC of CPG hydrogel film

Figure (3.61) shows the DSC thermogram of CPM hydrogel. The glass transition temperature of hydrogel (CPM) is observed at about 194.7ºC. Exothermic peaks was obtained above 500ºC showing decomposition of hydrogel was taking place in this temperature range.

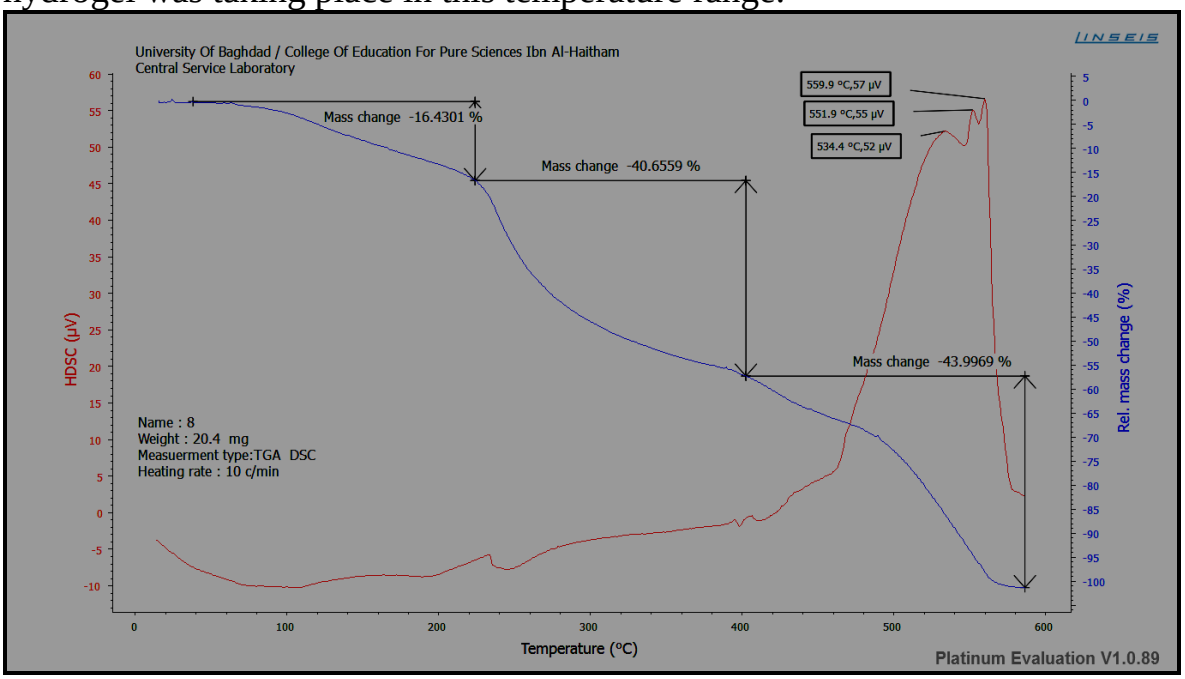

Figure (3.61): TGA and DSC of CPM hydrogel film

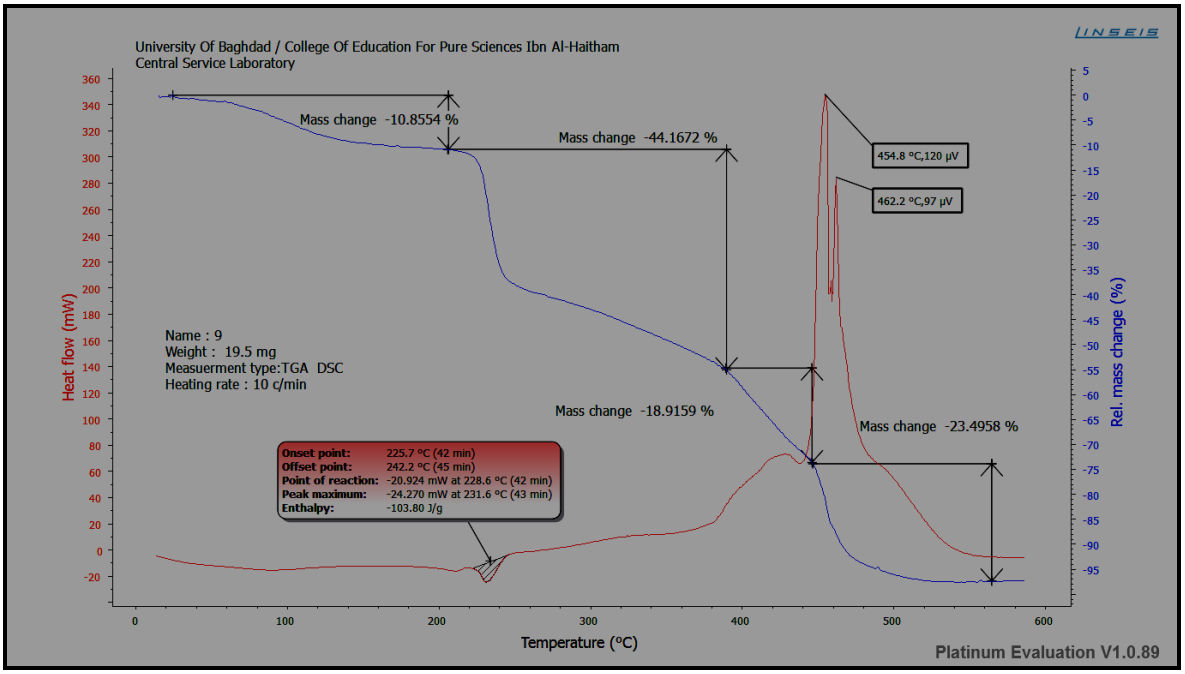

Figure (3.62): TGA and DSC of PPM hydrogel film

DSC thermogram of (PPM) hydrogel is showing in figure (3.62), the glass transition temperature of hydrogel (PPM) is observed at about 210ºC. Exothermic peak was obtained at about 455.3ºC. At this temperature, decomposition of hydrogel was taking place.

DSC thermogram of (PgA) hydrogel is showing in figure (3.63), the glass transition is observed at about 190ºC. Exothermic peaks was obtained at about 107.8ºC may be returned to thermal effect due to moisture evaporation from the sample. Also were observed exothermic peaks at above 380ºC. At this temperature, decomposition of hydrogel was taking place.

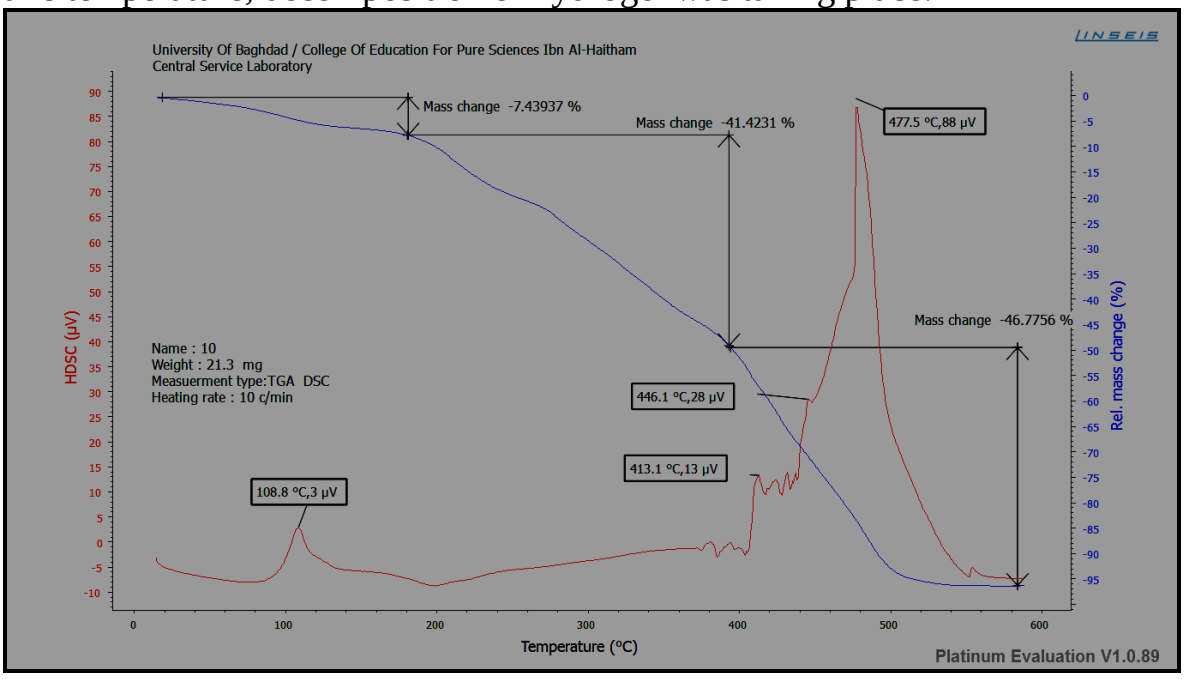

Figure (3.63): TGA and DSC of PgA hydrogel film

DSC thermogram of CgA hydrogel is showing in figure (3.64), the glass transition is observed at about 219.8ºC. In addition to this a broad endothermic peak was obtained at 200.4 °C showing the crystallization of the blend of polymers in different form. Exothermic peak at about 560ºC was returned to decomposition of hydrogel.

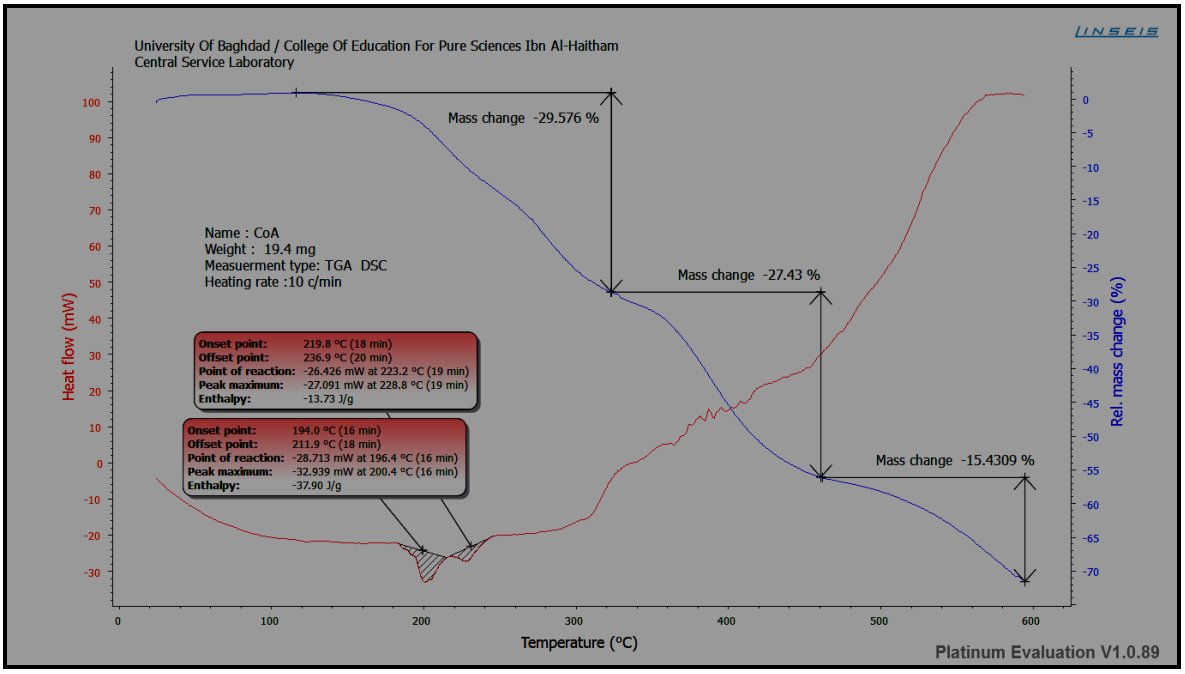

Figure (3.64): TGA and DSC of CgA hydrogel film

Finally DSC thermogram of IPN hydrogel is showing in figure (3.65), the glass transition is observed at about 209.8ºC. In addition to this endothermic peak was obtained at 69.1 °C showing the crystallization of the blend of polymers in different form. Exothermic peak at about 560ºC was returned to decomposition of hydrogel.

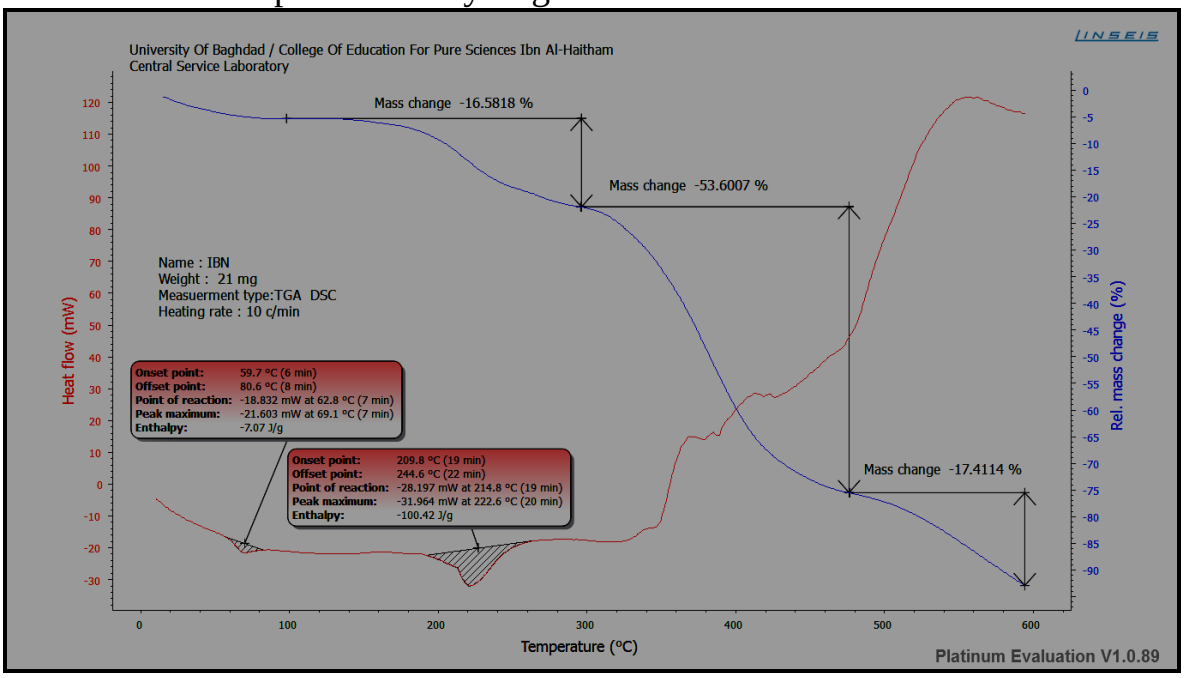

Figure (3.65): TGA and DSC of IPN hydrogel film

Table (3.5): Real mass change (%) of hydrogels at different temperature of TGA runs

T (ºC)	CPG	CPM	PPM	PgA	CgA	IPN
100	-21.1097	-2.6505	-5.4824	-4.2932	0.7999	-5.4749
200	-39.0355	-13.3074	-10.7776	-10.0161	-4.1583	-9.2820
300	-63.2153	-46.0063	-42.9447	-28.9665	-25.1609	-22.195
400	-70.848	-57.0865	-58.558	-51.0839	-45.2911	-59.5786
500	-93.4882	-72.8942	-96.0754	-92.8968	-58.2593	-77.2452
Max.	574 , -100	565.5, -100	586.7, -97.2593	589, -96.338	594.8, -71.6346	594.6, -93.0131

The glass transition and melting point of hydrogel is showing in table (3.6).

Table (3.6): Glass transition (Tg) & melting point (Tm) of hydrogel

	CPG	CPM	PPM	PgA	CgA	IPN
Tg (ºC)	226.5	194.7	210	190	219.8	209.8
Tm(ºC)	240	246.1	231.1	198.1	228.8	222.6

TGA data showed the thermal stability of the prepared hydrogels change within the reactions of crosslinking. The thermal degradation is completed in different steps for different crosslinked hydrogels samples, (CgA) was (50%) mass decomposed at about (400) ^{o}C, and show the best thermal stability than the other hydrogel.

3.1.4 Surface Morphology/ SEM Analysis

3.1.4.1 SEM analysis of PANI and composite

The surface morphology of PANI and its composite form (CPG/PANI) was studied by using electron microscope (SEM). The scanning electron micrographs of PANI and its composite form were obtained. Figure (3.66) gives clear picture of the surface morphology of PANI at 50 KX magnifications, presented in figure (3.67) at similar magnification, show modification of the surface texture of PANI.

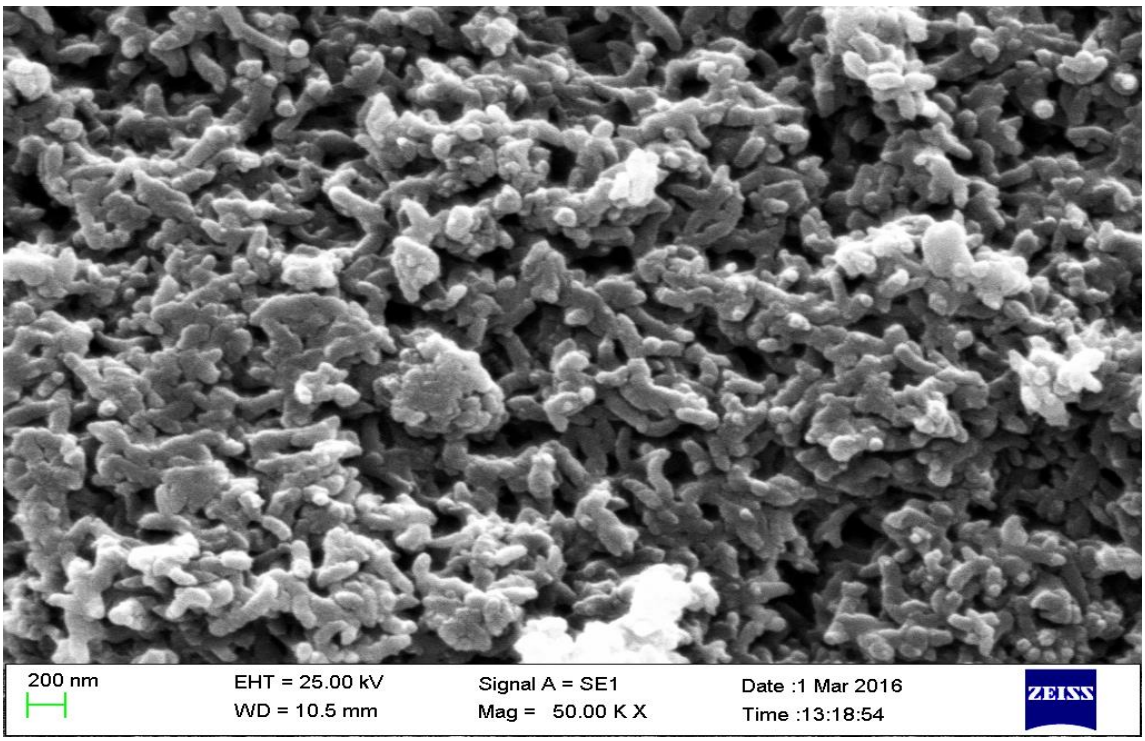

Figure (3.66): SEM photomicrograph of PANI with magnification 50 KX

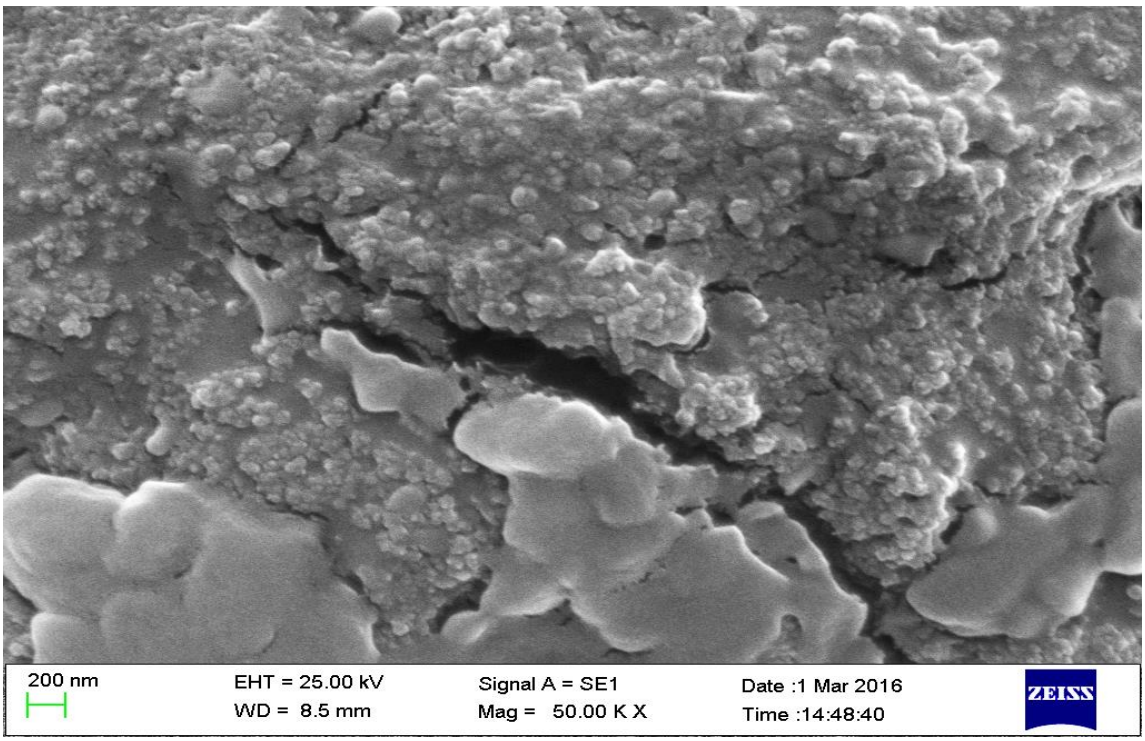

Figure (3.67): SEM photomicrograph of (CPG/PANI) with magnification 50 KX

3.1.4.2 SEM analysis of Fe_3O_4 pure and coated form

The surface morphology of uncoated Fe_3O_4 and its coated form (CPG/Fe3O4/PANI) was studied by using scanning electron microscope (SEM). The scanning electron micrographs of Fe_3O_4 and its coated form were obtained. Figure (3.68) gives clear picture of the surface morphology of Fe_3O_4 at 50 KX magnifications, presented in Figure (3.69) at similar magnification, show coated of the surface texture of magnetite.

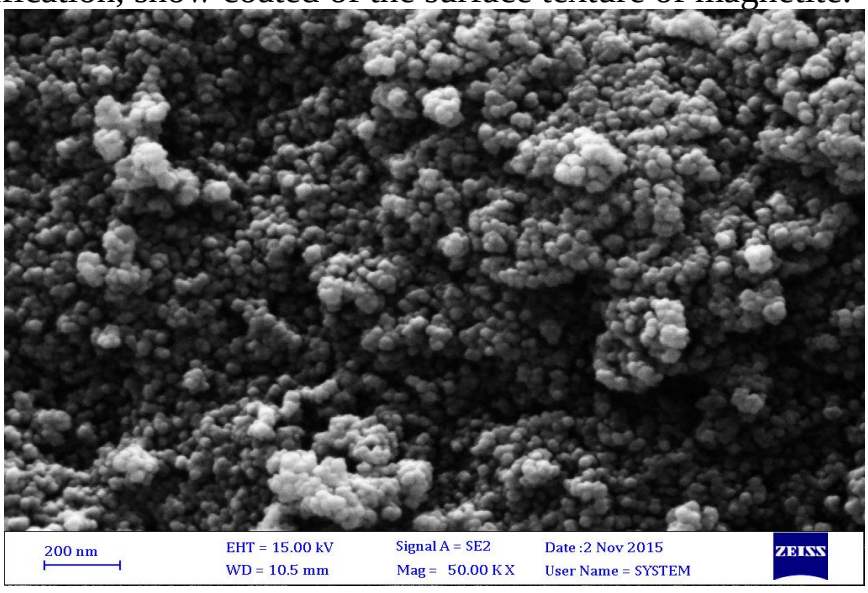

Figure (3.68): SEM photomicrograph of Fe_3O_4 with magnification 50 KX

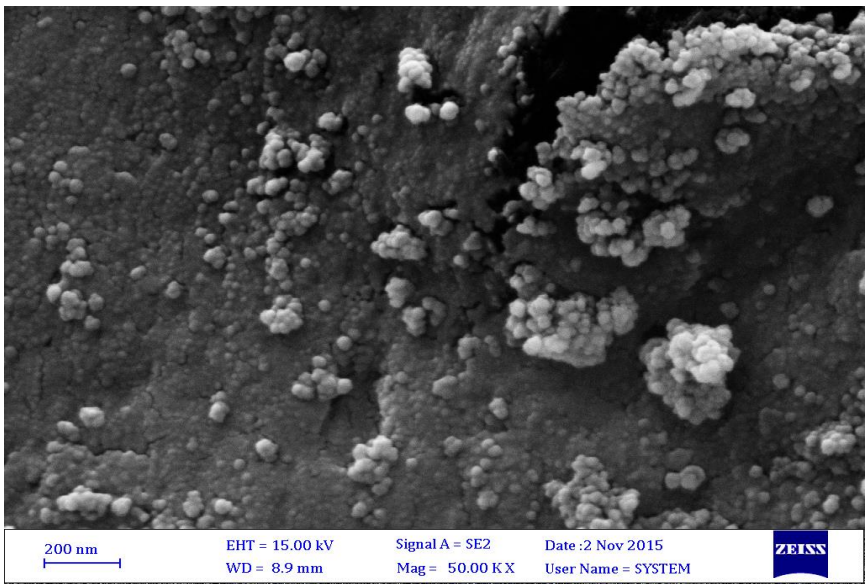

Figure (3.69): SEM photomicrograph of Coated Fe_3O_4 form (CPG/Fe_3O_4/PANI) with magnification 50 KX

3.1.4.3 SEM analysis of G and its composite

For showing the difference between the surface morphology of GO and G, it was studied by SEM. Figure (3.70) is show the surface morphology of GO at 50 KX, from this figure it appeared the d-spacing of sheet of GO is greater than G (fig 3.71) at same magnification.

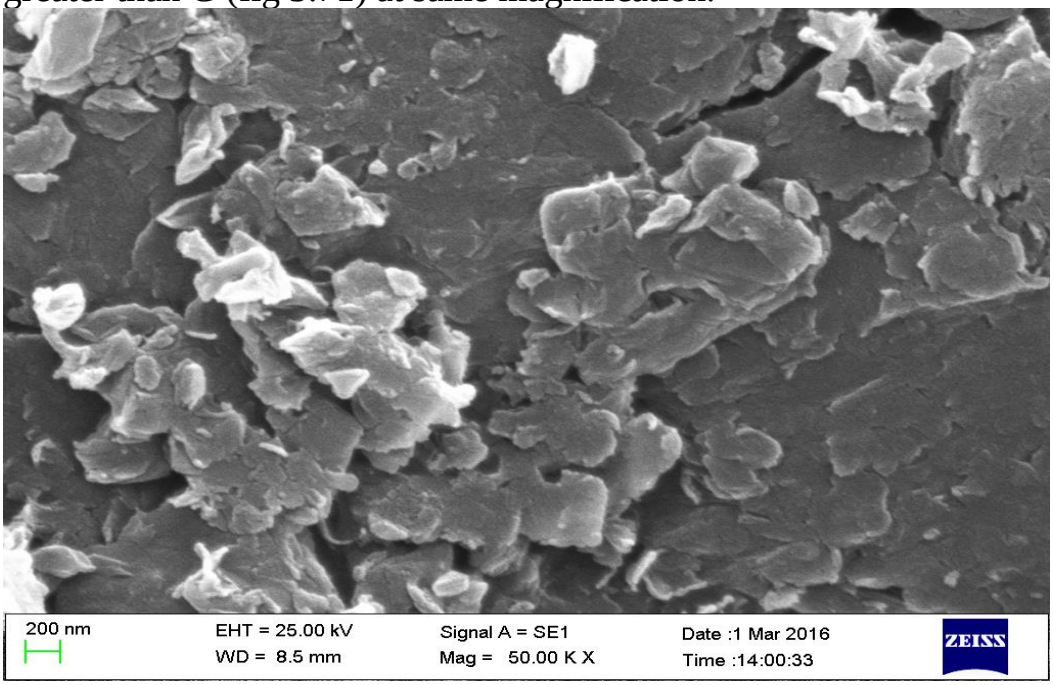

Figure (3.70): SEM photomicrograph of GO with magnification 50 KX

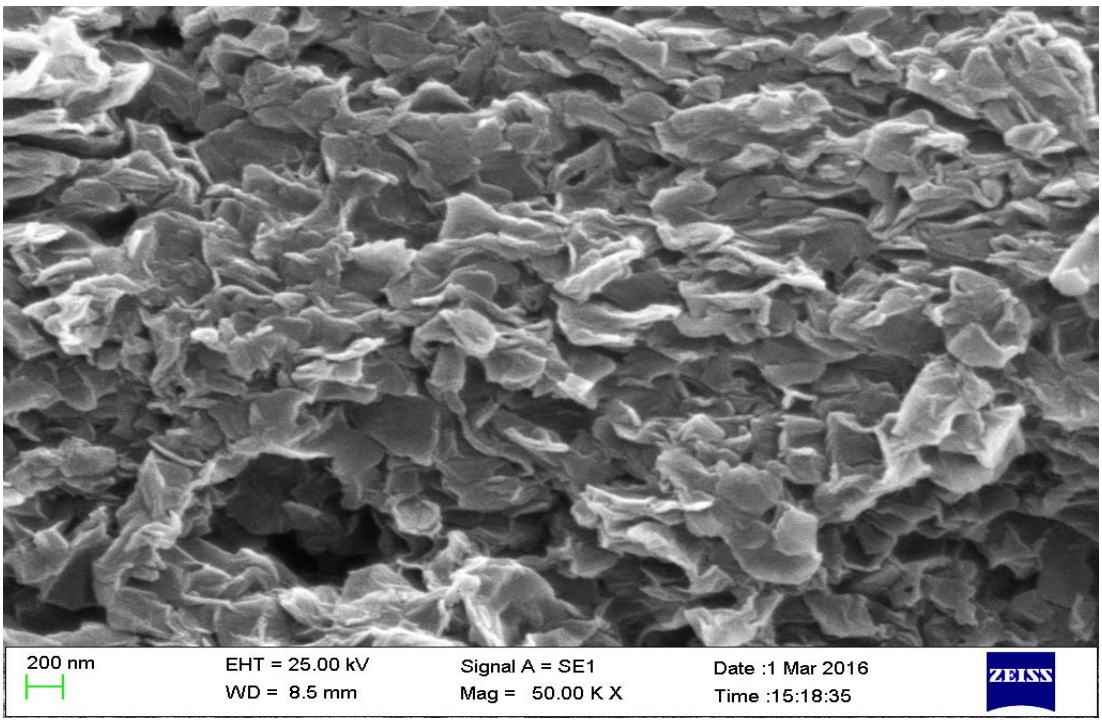

Figure (3.71): SEM photomicrograph of G with magnification 50 KX

The G composite form (CPG/G) also was characterized by SEM analysis. Figure (3.72) is show the surface morphology of CPG/G at 15 KX magnifications; it clear was dispersion of G sheet within hydrogel matrix.

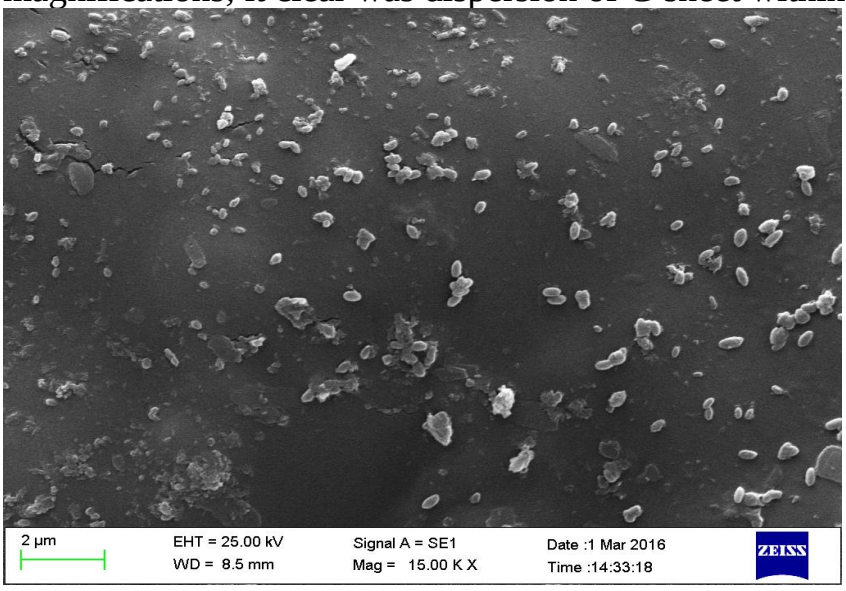

Figure (3.72): SEM photomicrograph of CPG/G with magnification 15 KX

3.1.4.4 SEM analysis of MWCNTs and composite

SEM analysis of MWCNTs is showing in fig (3.73) at 50 KX magnifications while SEM analysis of (CPG/ MWCNTs) at 10 KX is showing in fig (3.74). From figure (3.74) is showing the dispersion of MWCNTs within the hydrogel matrix.

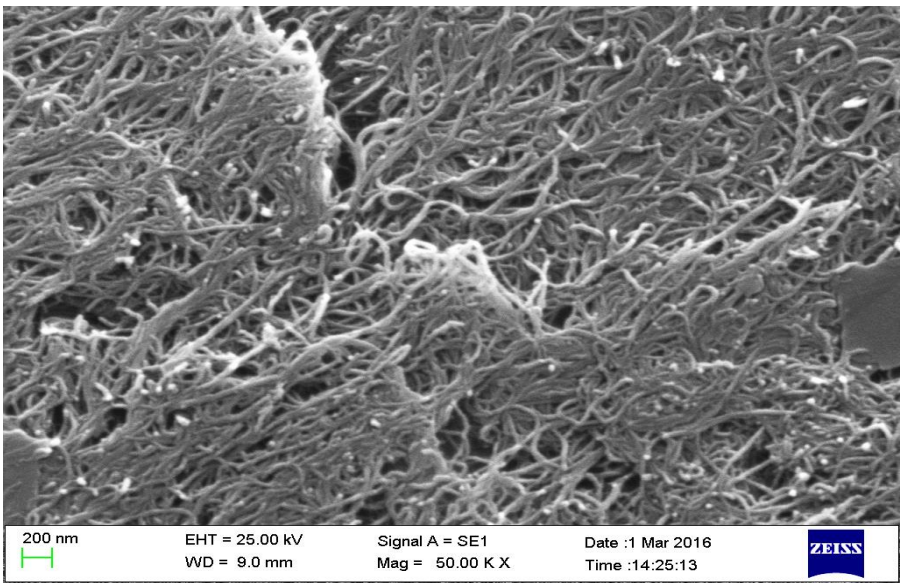

Figure (3.73): SEM photomicrograph of MWCNTs with magnification 50 KX

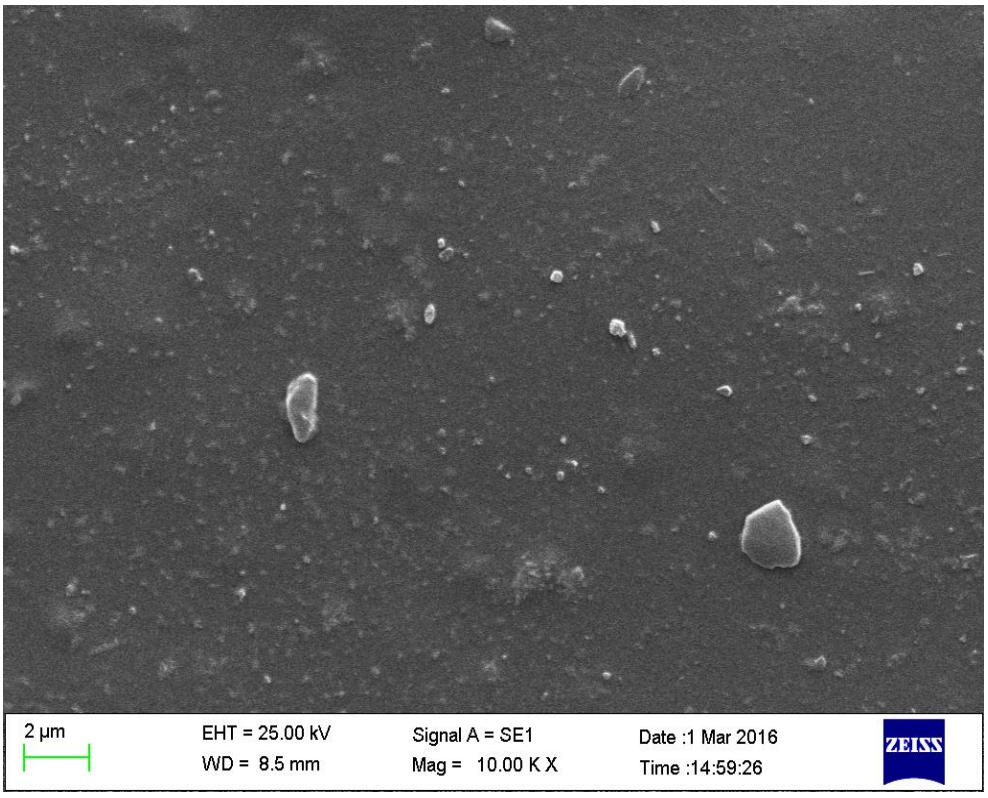

Figure (3.74): SEM photomicrograph of CPG/ MWCNTs with magnification 10 KX

3.1.5 Energy dispersive X–ray spectroscopy (EDS) of both uncoated and coated Fe_3O_4

The EDS for uncoated Fe_3O_4 and coated form (CPG/Fe_3O_4/PANI) were done. The EDS results are shown in Figures (3.75) and (3.76). The EDS give the type and weight percent of each element present in the selected point of sample at SEM micrographs.

According to the definition of Fe_3O_4, it consists of Fe and O. Same results were obtained from EDS analysis. We can notice the differences between EDS analysis of uncoated Fe_3O_4 and the coated by CPG/PANI hydrogel, the appearance of new element (C, N, Cl) due to conductive hydrogel, which resulted in the decrease in the percentage of O, Fe. Also it was appeared other element(S) with small amount returned to residue of persulfate which was used as an oxidizing agent in PANI polymerization.

a)

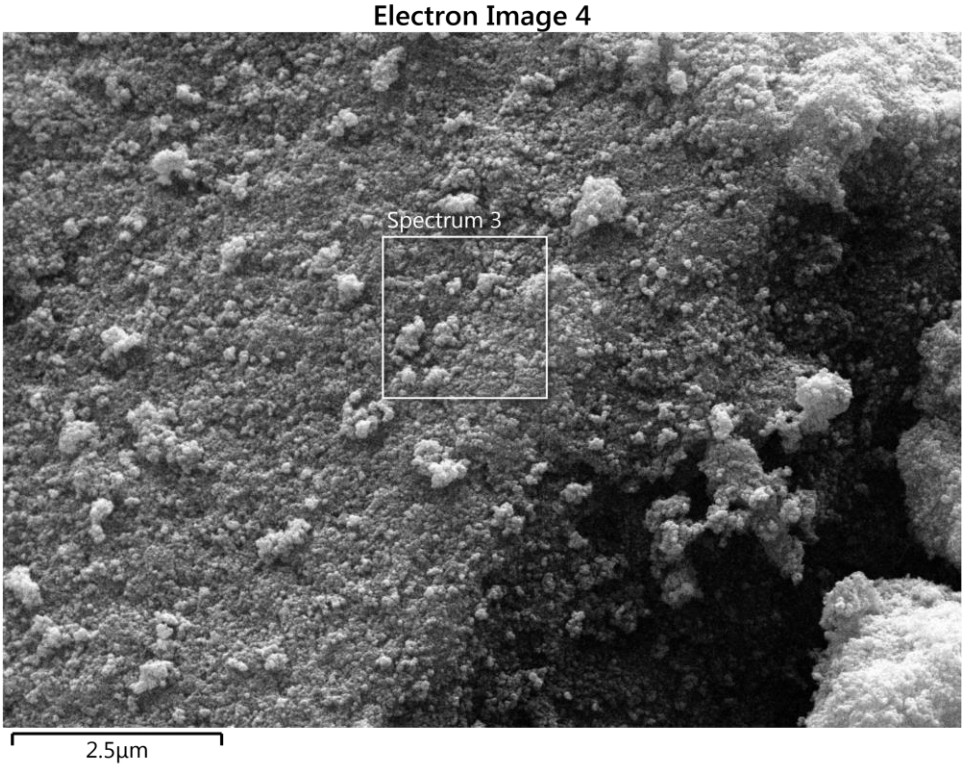

b)

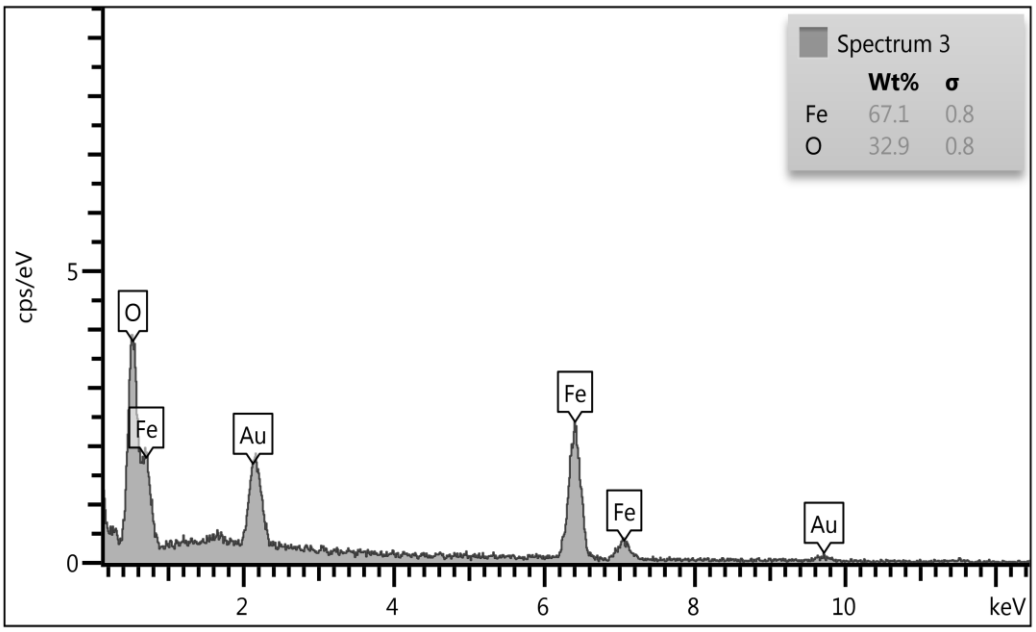

Figure (3.75): (a) SEM and (b) EDS for uncoated Fe_3O_4

(a)

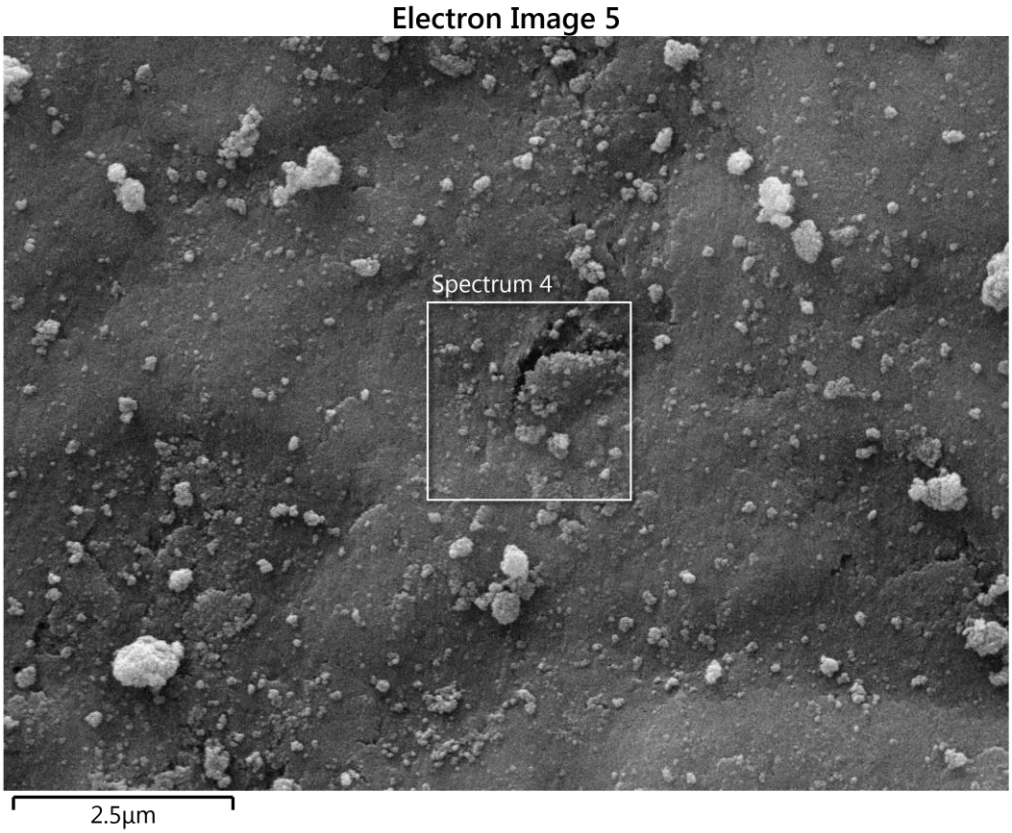

(b)

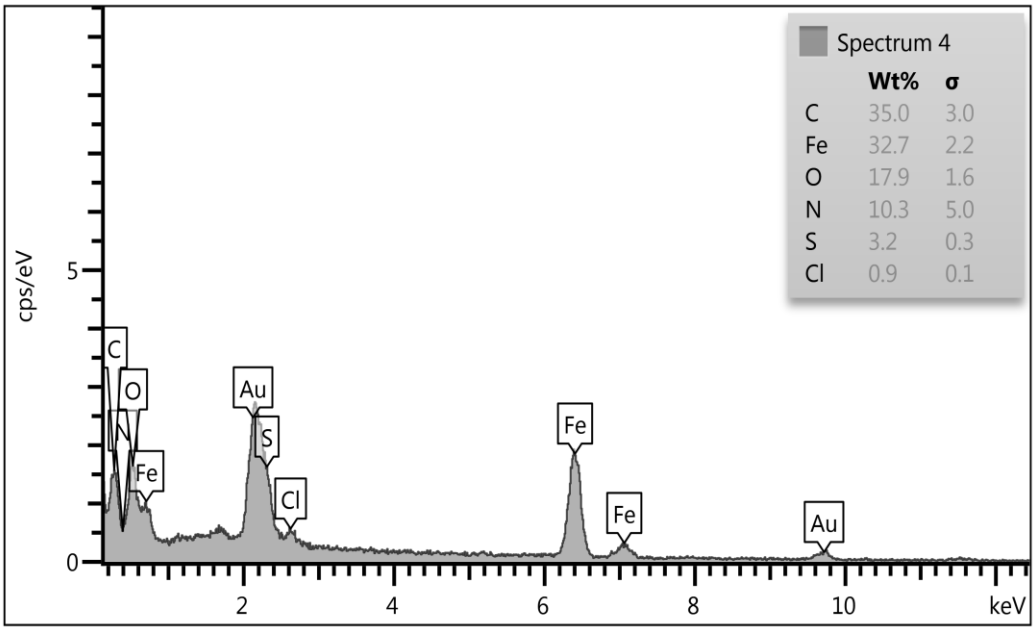

Figure (3.76): (a) SEM and (b) EDS for coated Fe_3O_4 form (CPG/Fe_3O_4/PANI)

3.1.6 Surface Morphology/ TEM Analysis

The surface morphology of uncoated Fe_3O_4 and its coated form (CPG/Fe_3O_4/PANI) was studied by using transmission electron microscope (TEM). The transmission electron image of Fe_3O_4 and its coated form were obtained. The uncoated Fe_3O_4 nanoparticles (Fig. 3. 77) tend to aggregate owing to their large specific surface area, high surface energy and magnetization effect. After coated (Fig. 3.78), the (CPG/Fe_3O_4/PANI) were almost spherical in shape, and the Fe_3O_4 nanoparticles were well coated with hydrogel. The Fe_3O_4 MNPs was coated with hydrogel (brighter region around the magnetic nanoparticles).

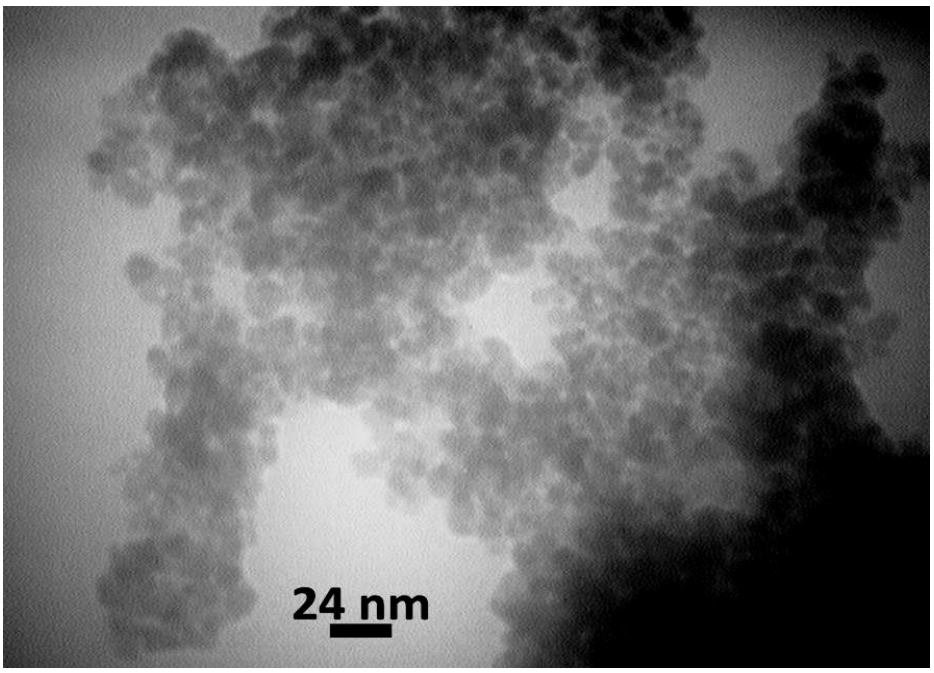

Figure (3.77): TEM photomicrograph of uncoated Fe_3O_4

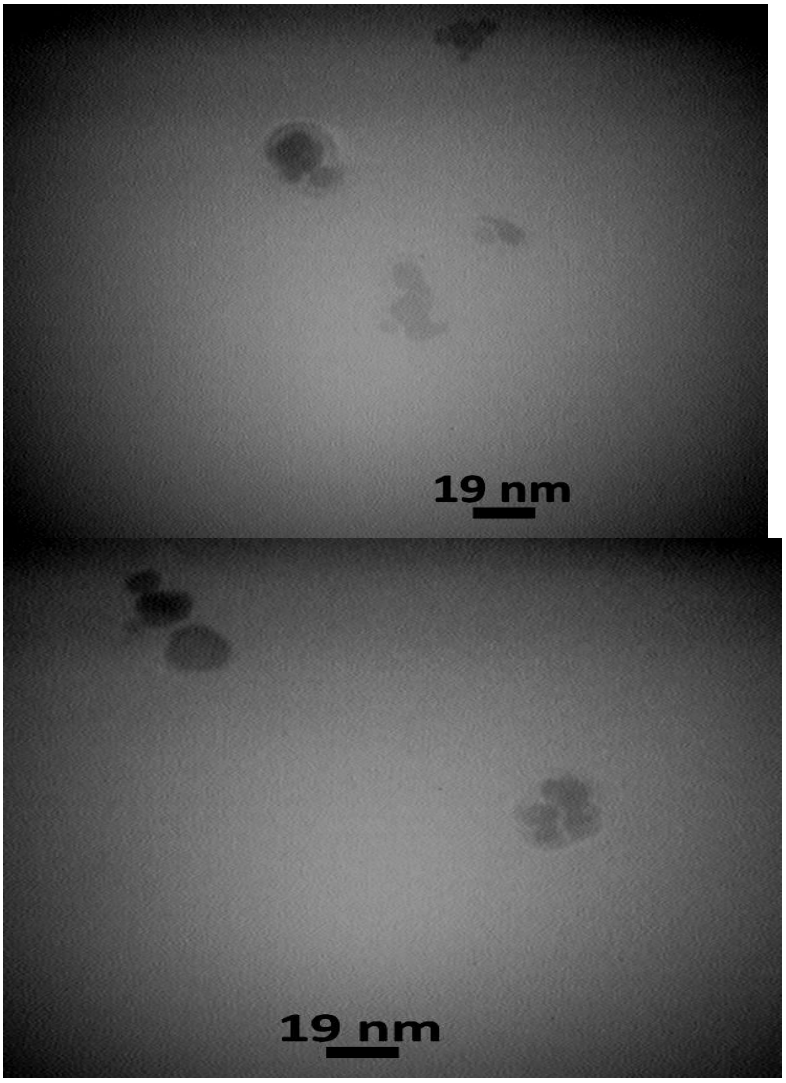

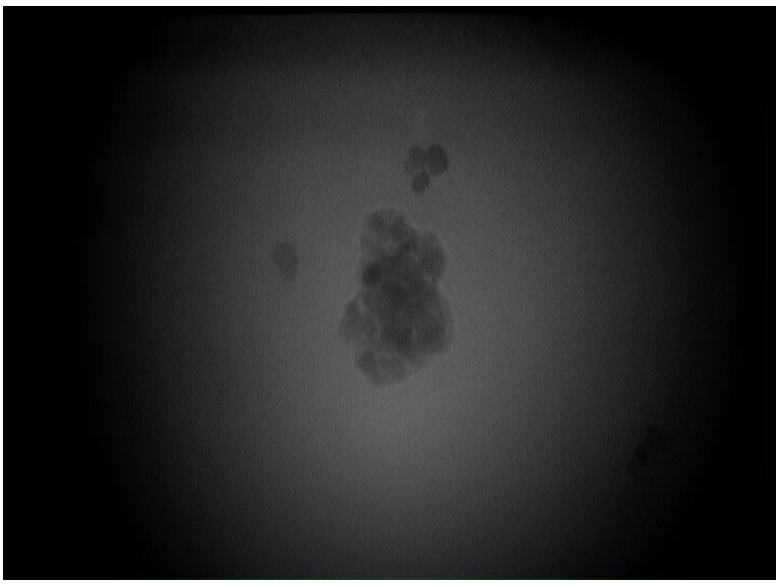

Figure (3.78): TEM photomicrographs of Coated Fe_3O_4 form (CPG/Fe_3O_4/PANI)

3.1.7 Surface Morphology/AFM analysis

3.1.7.1 Surface Morphology/AFM analysis of hydrogel

Hydrogels were investigated by (AFM), the (AFM) picture were analyzed. The pictures of topography are shown in figures (3.79 -3.84).

(a) (b)

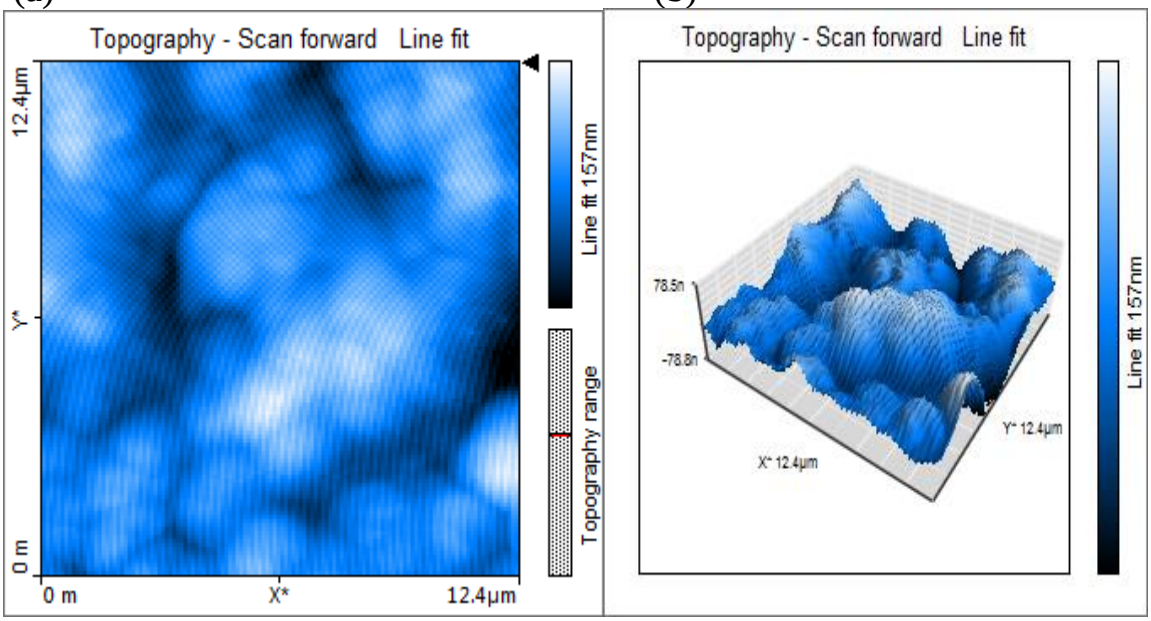

(c)

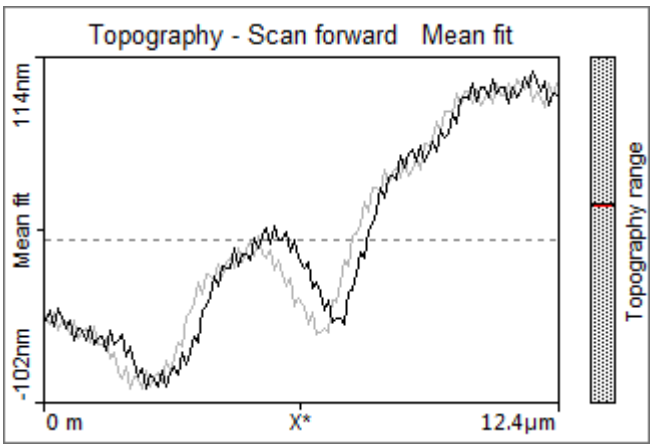

Figure (3.79): AFM photomicrograph of CPG , (a): scan topography, b: 3D topography, & (c): line graph topography

(a)

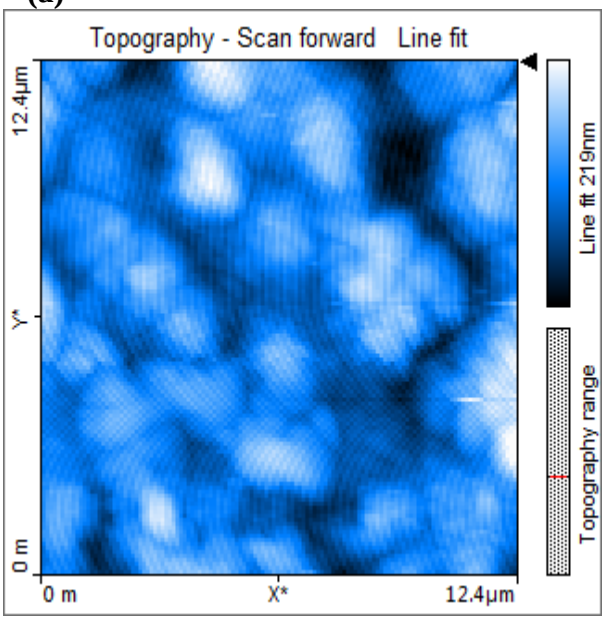

(b)

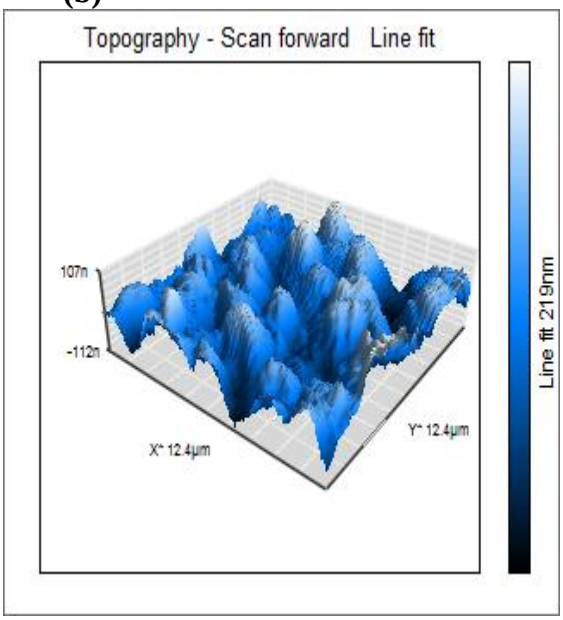

(c)

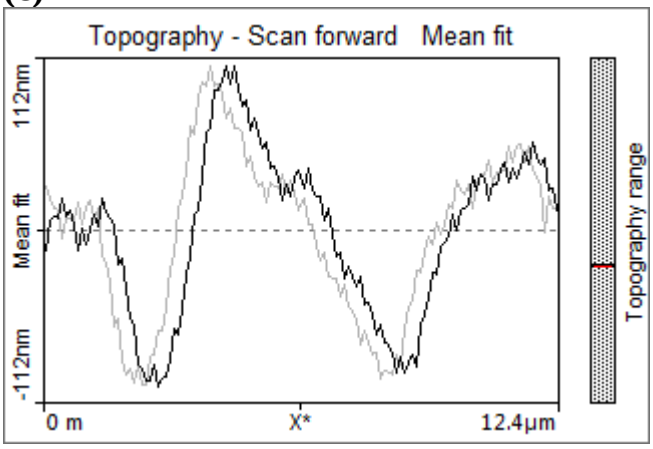

Figure (3.80): AFM photomicrograph of CPM , (a): scan topography, b: 3D topography, & (c): line graph topography

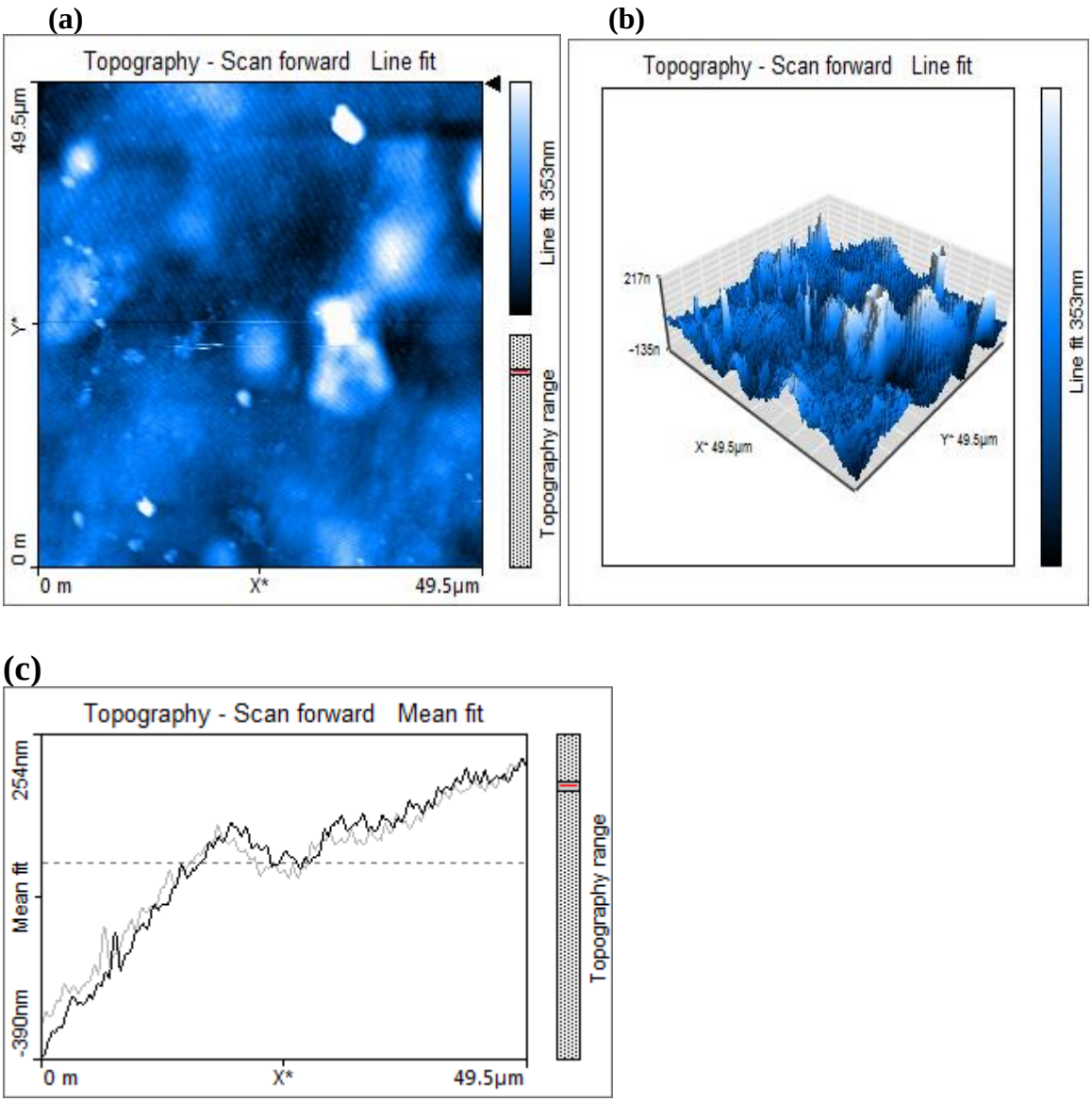

Figure (3.81): AFM photomicrograph of PPM , (a): scan topography, b: 3D topography, & (c): line graph topography

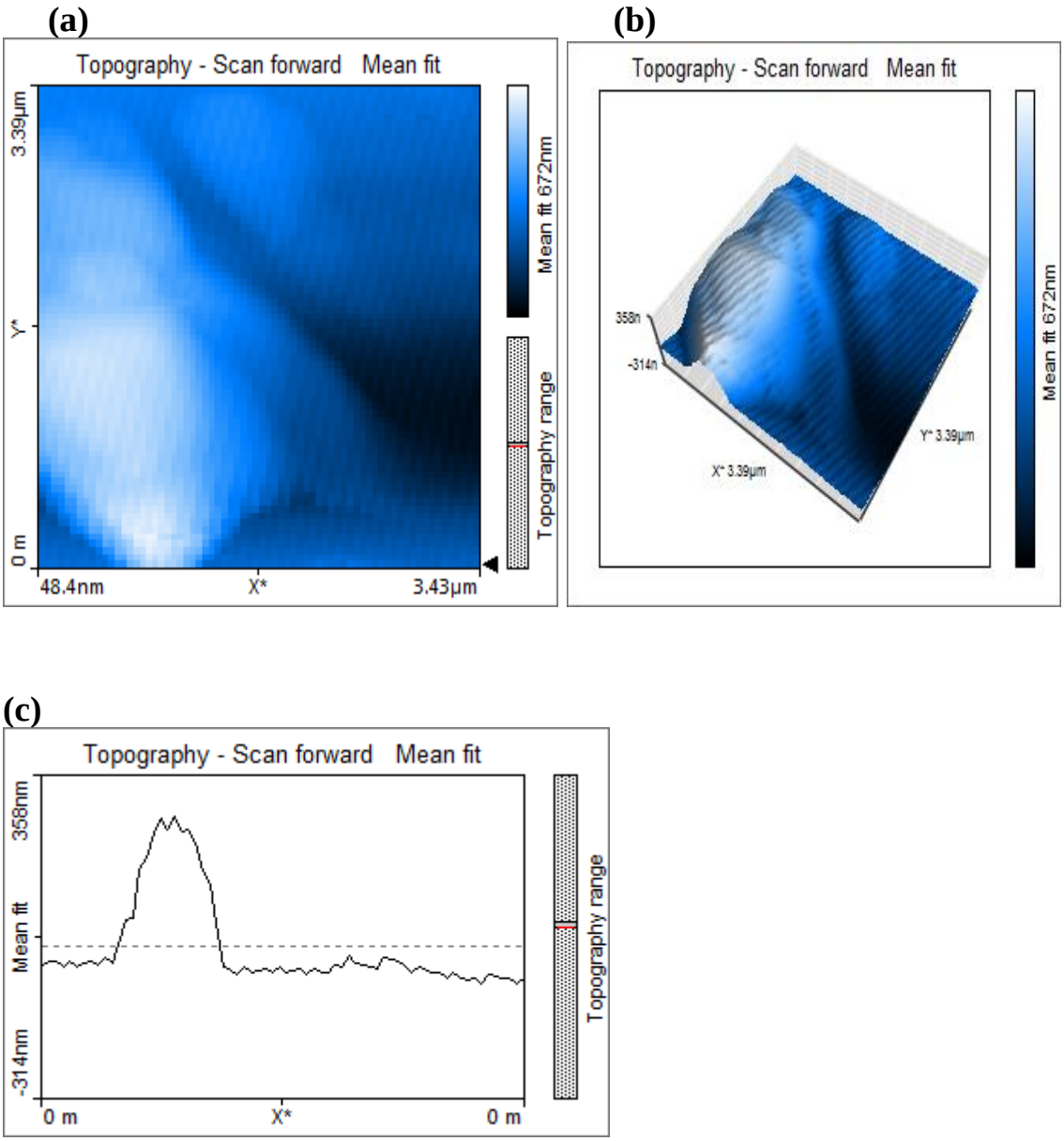

Figure (3.82): AFM photomicrograph of PgA , (a): scan topography, b: 3D topography, & (c): line graph topography

(a) **(b)**

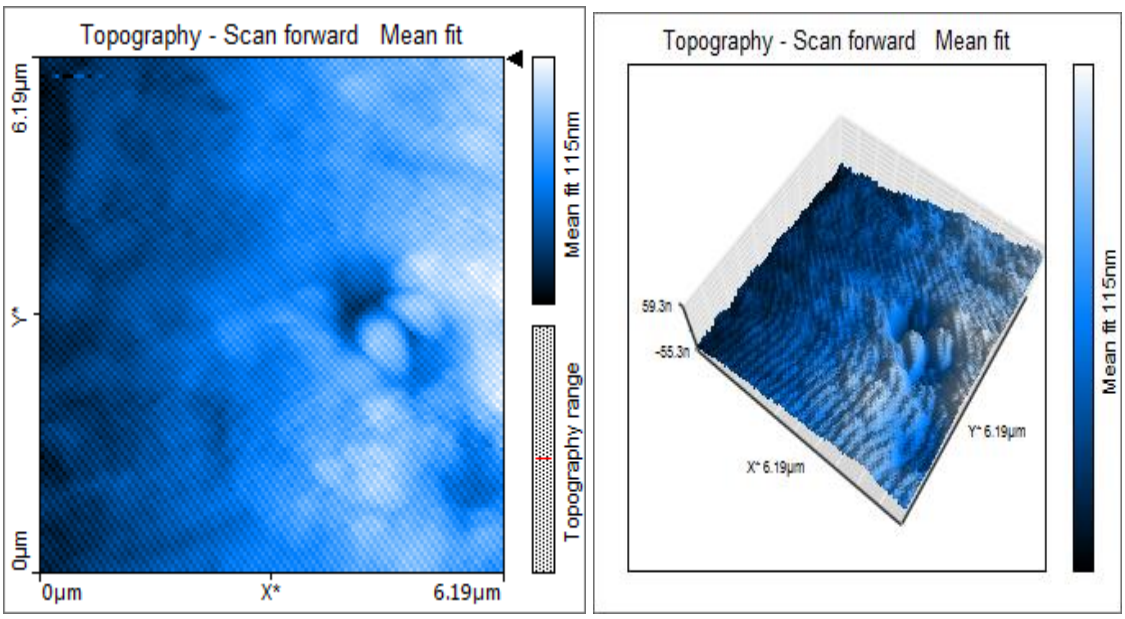

(c)

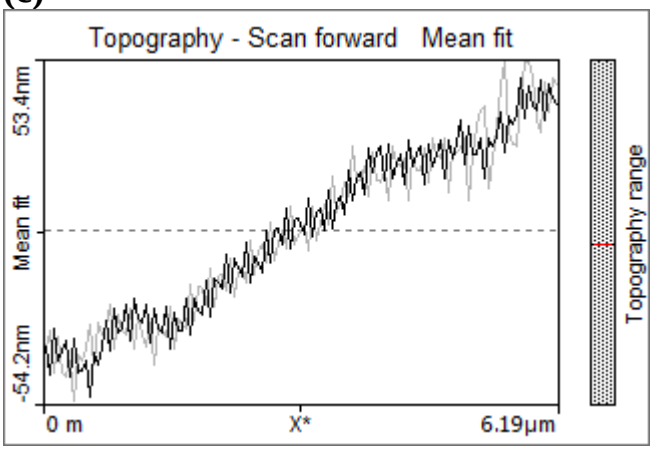

Figure (3.83): AFM photomicrograph of CgA , (a): scan topography, b: 3D topography, & (c): line graph topography

(a) **(b)**

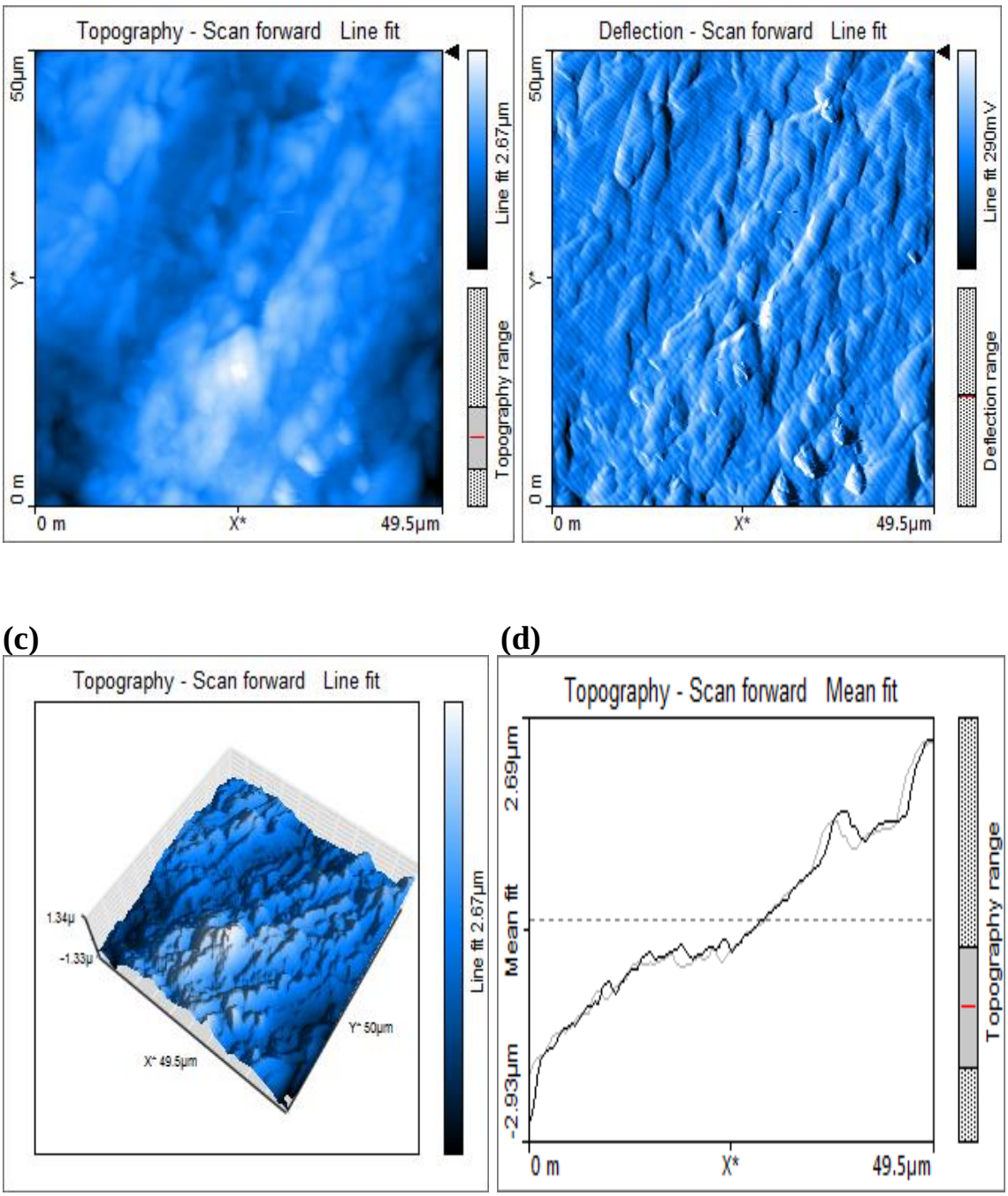

Figure (3.84): AFM photomicrograph of IPN , (a): scan topography, (b) : deflection scan, (c): 3D topography, & (d), line graph topography

3.1.7.2 Surface Morphology/ AFM Analysis of Nanomatrials

The nanomatrials were synthesized (Fe_3O_4 MNPs, GO, G nanosheets), and MWCNTs which was purchased from CheapTubes were investigated by (AFM). Picture of topography are shown in figures (3.85-3.89). AFM of Fe_3O_4 MNP figure (3.85) is shown accumulation of magnetite nanoparticles, while figure (3.86) is shown a little number of nano particle of magnetite and with nanoparticles size about (10.8-13.1nm). This size was approximately to size which was measured from XRD analysis.

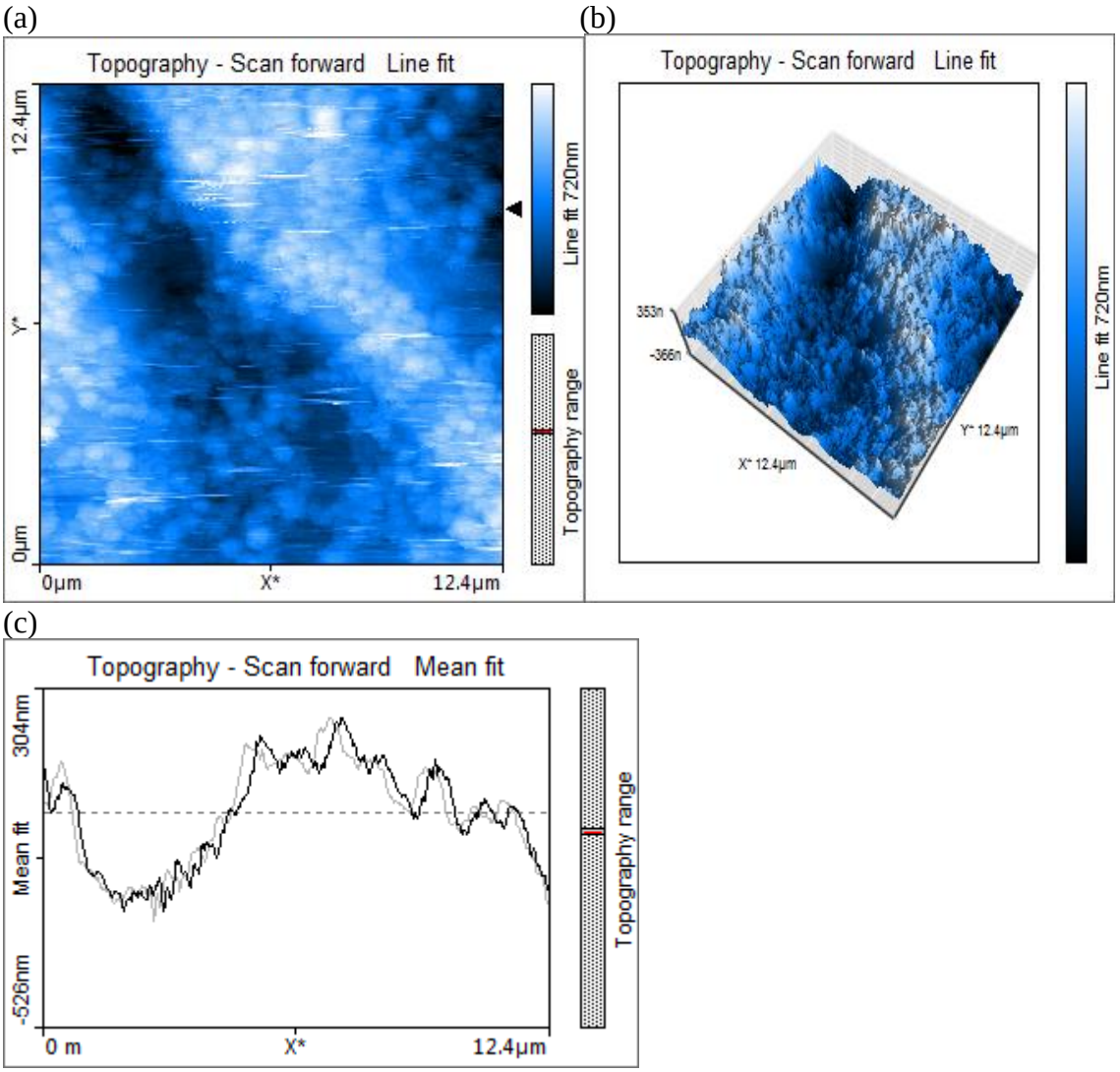

Figure (3.85): AFM photomicrograph of accumulation of Fe_3O_4 MNPs , (a): scan topography, b: 3D topography, & (c): line graph topography

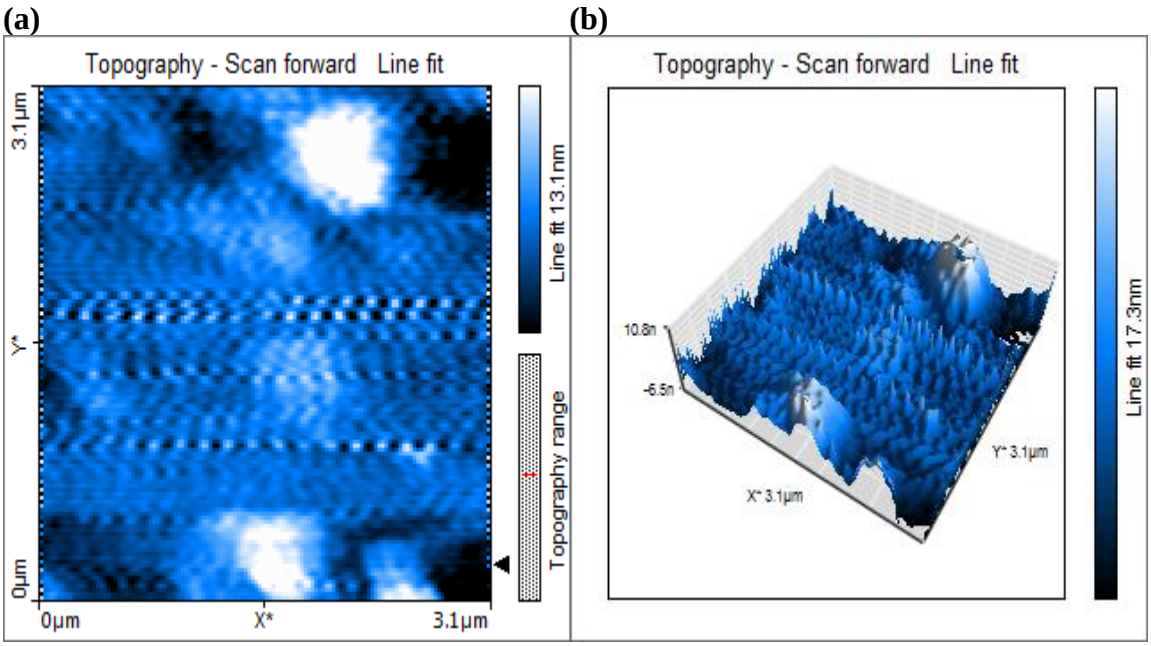

(c)

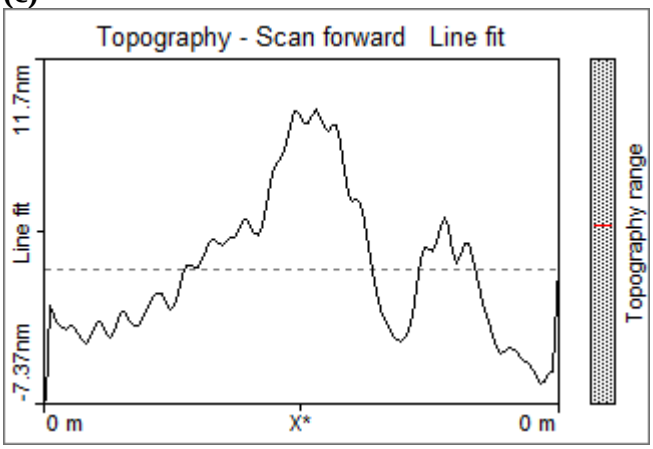

Figure (3.86): AFM photomicrograph of Fe_3O_4 MNPs , (a): scan topography, (b): 3D topography, & (c): line graph topography

(a) (b)

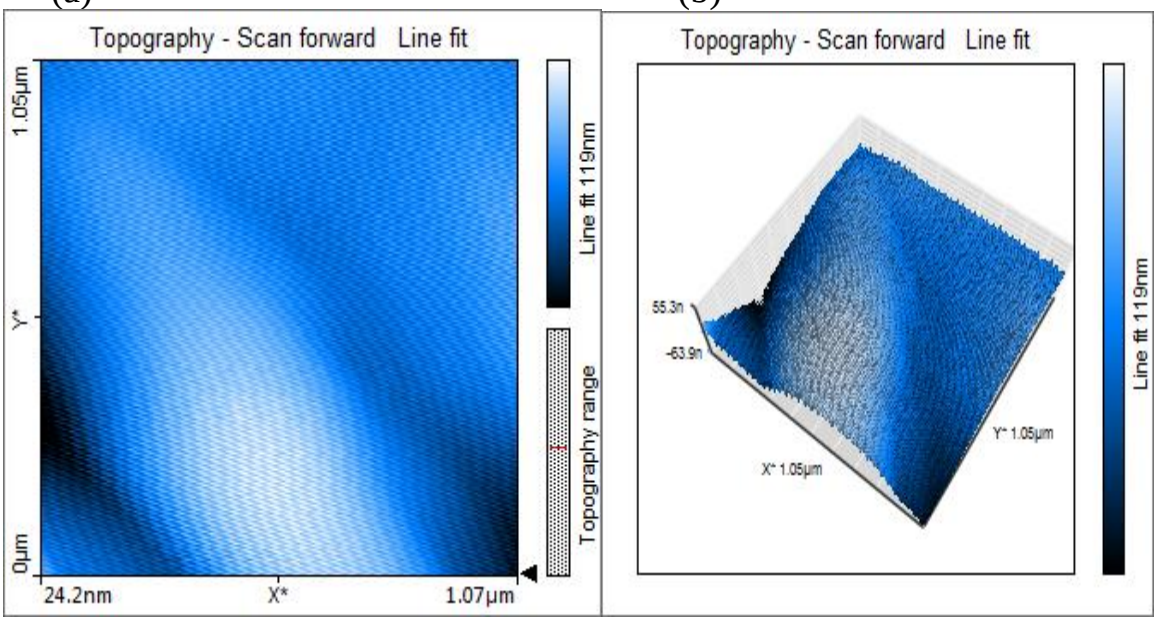

(c)

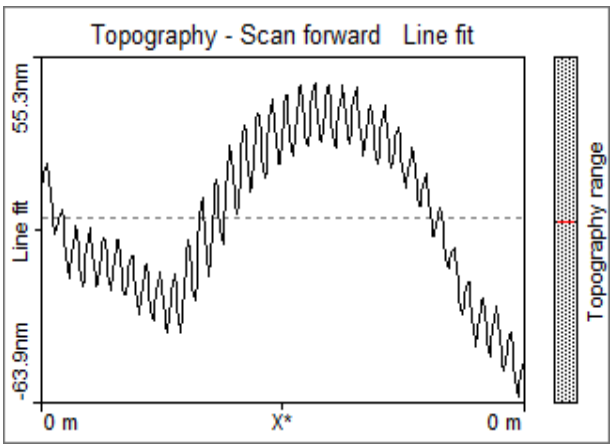

Figure (3.87): AFM photomicrograph of GO nanosheets, (a): scan topography, b: 3D topography, & (c): line graph topography

(a) **(b)**

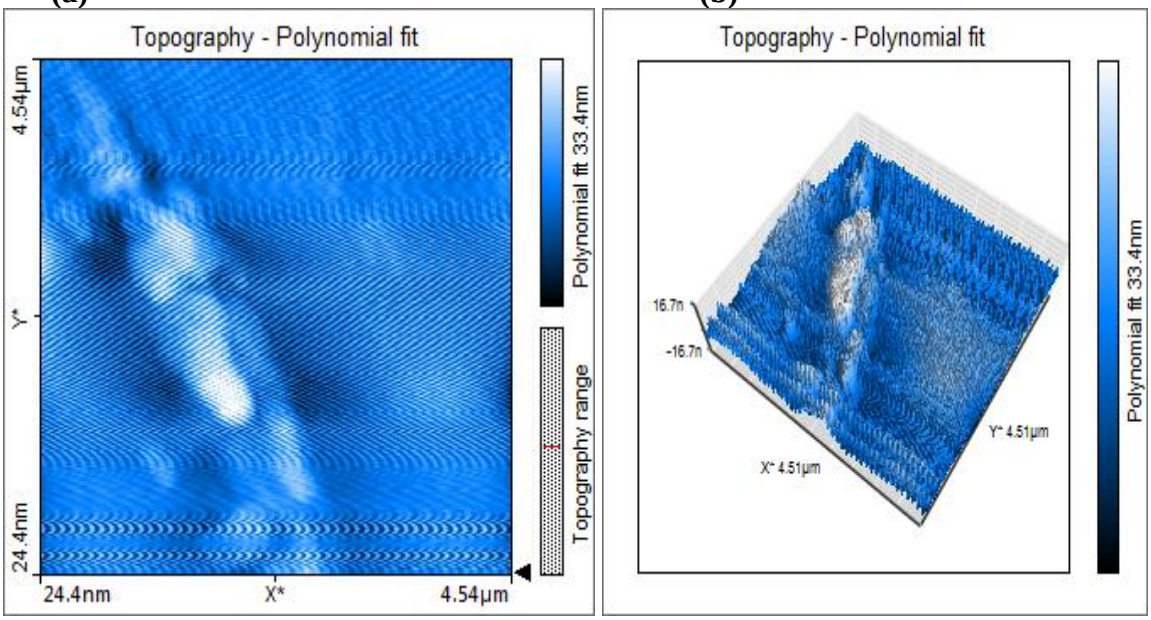

(c)

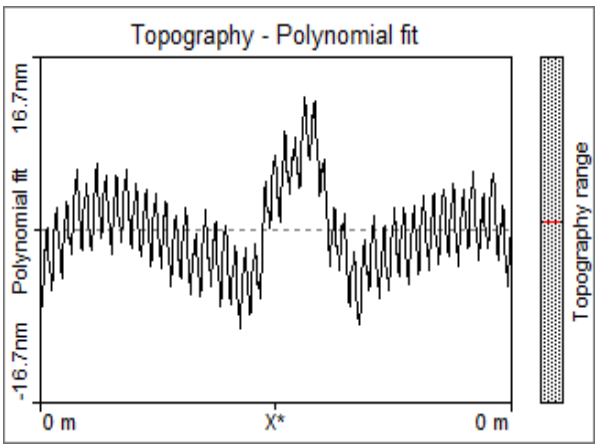

Figure (3.88): AFM photomicrograph of G nanosheets, (a): scan topography, b: 3D topography, & (c): line graph topography

(a) **(b)**

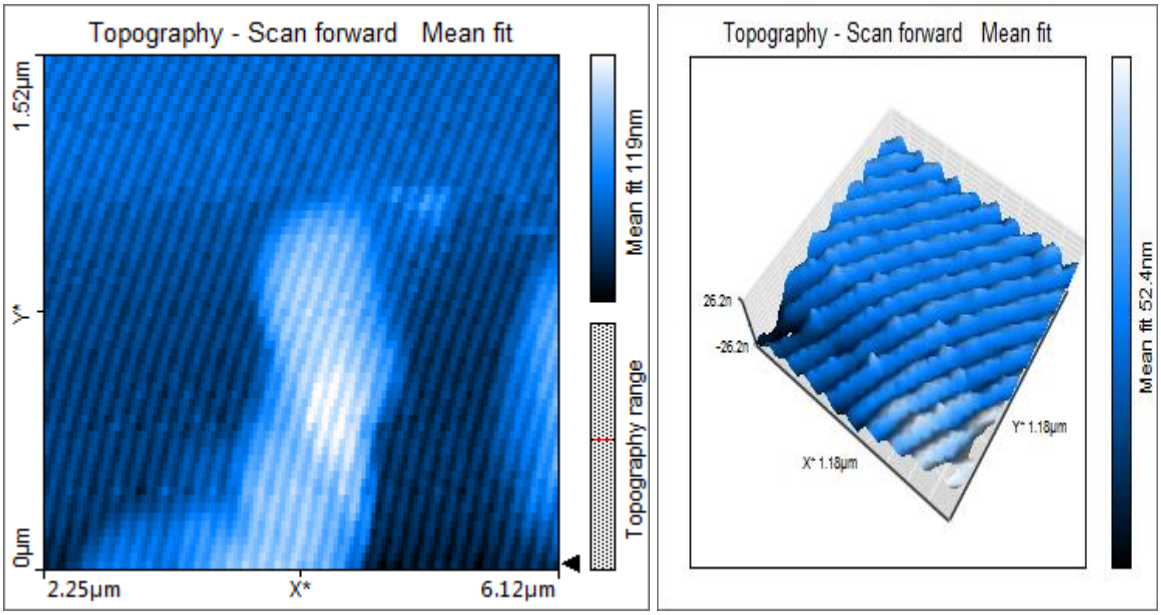

(c)

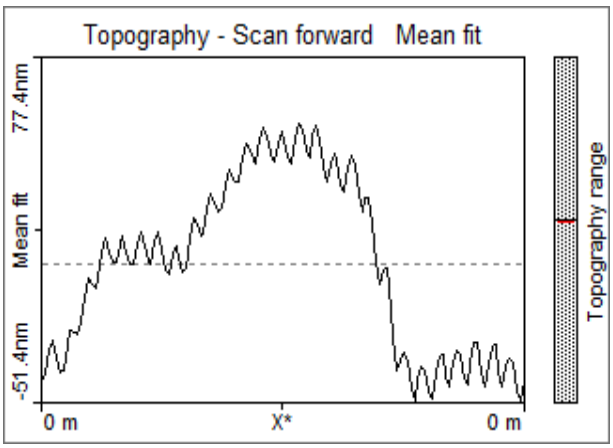

Figure (3.89): AFM photomicrograph of MWCNTs, (a): scan topography, b: 3D topography, & (c): line graph topography

3.1.7.3 Surface Morphology/ AFM Analysis of Nanocomposite

Some of composite hydrogel like (CPG/PANI) & nanocomposite were synthesized like (CPG/Fe_3O_4), (CPG/Fe_3O_4/PANI), (CPG/G), & (CPG/ MWCNTs) were investigated by (AFM). Picture of topography are shown in figures (3.90-3.95). AFM of coating Fe_3O_4 MNPs form (CPG/Fe_3O_4/PANI) is shown in figures (3.92 & 3.93). From figure (3.92) is shown the accumulation of magnetite nanoparticles coating with conductive hydrogel. Figure (3.93) is shows the little of magnetite nanoparticles coated and with nanoparticles size about (23.9-35.3nm), this size was nearly corresponding to XRD analysis.

(a) (b)

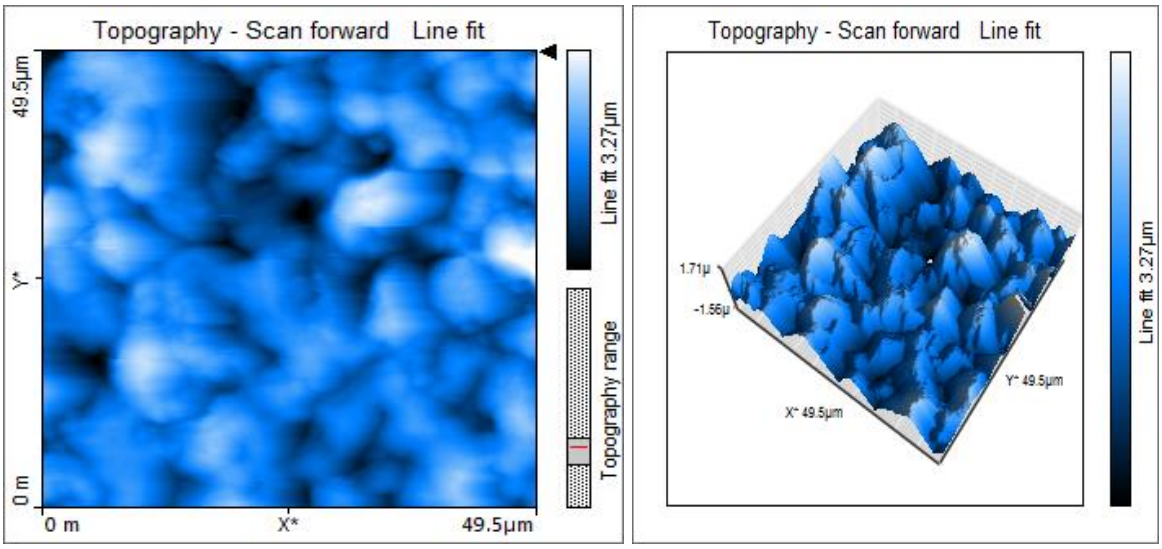

(c)

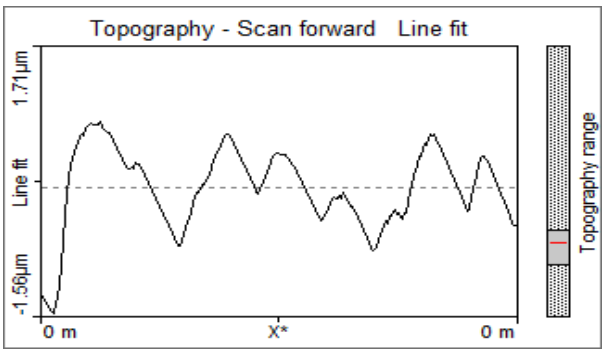

Figure (3.90): AFM photomicrograph of (CPG/PANI), (a): scan topography, b: 3D topography, & (c): line graph topography

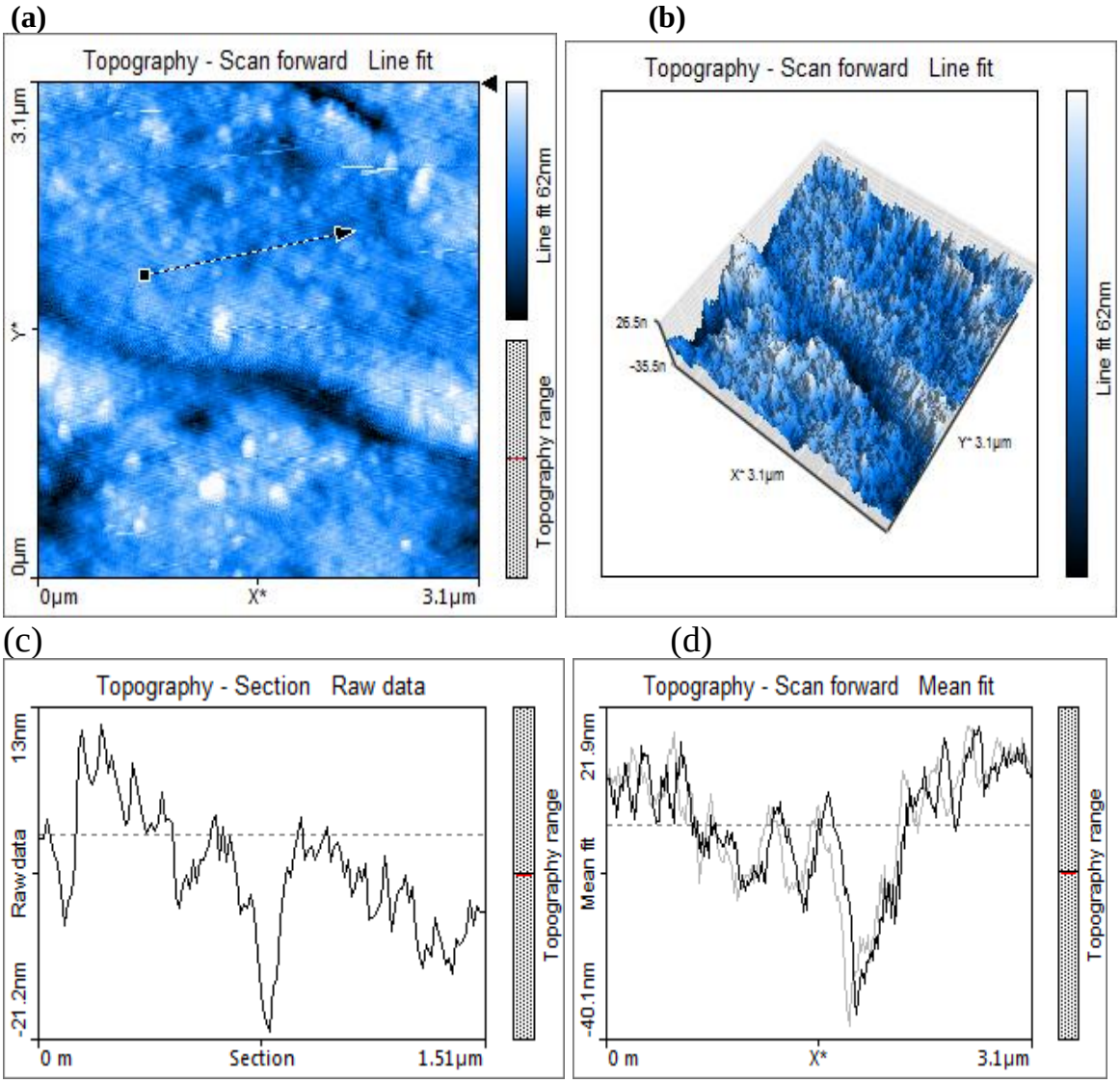

Figure (3.91): AFM photomicrograph of (CPG/Fe_3O_4), (a): scan topography, b: 3D topography, (c): cross-section topography, & (d): line graph topography

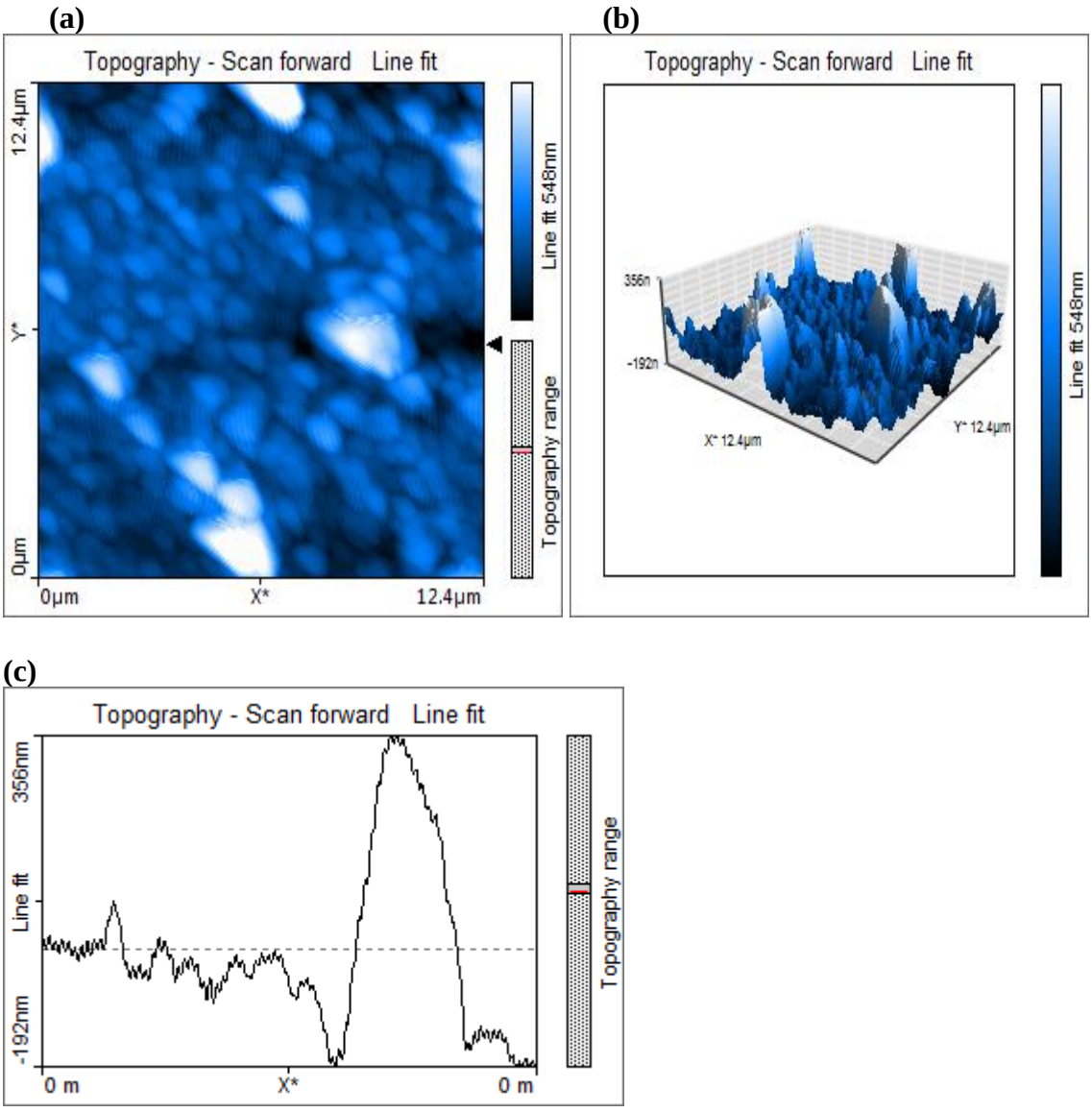

Figure (3.92): AFM photomicrograph of accumulation of (CPG/Fe_3O_4/PANI), (a): scan topography, (b): 3D topography, & (c): line graph topography

(a) **(b)**

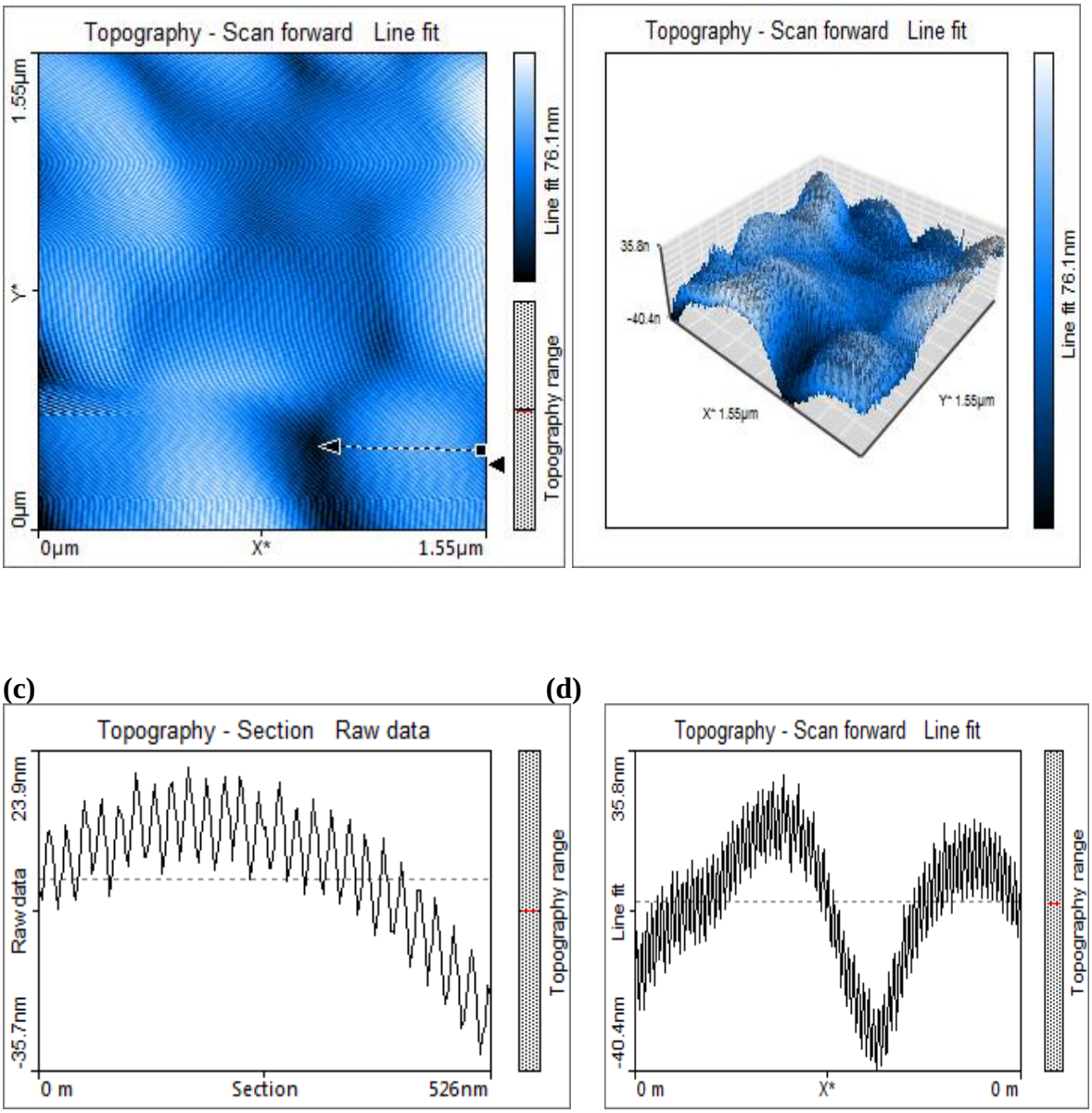

Figure (3.93): AFM photomicrograph of coated Fe_3O_4 form (CPG/Fe_3O_4/PANI) , (a): scan topography, b: 3D topography, (c): cross-section topography, & (d): line graph topography

(a) (b)

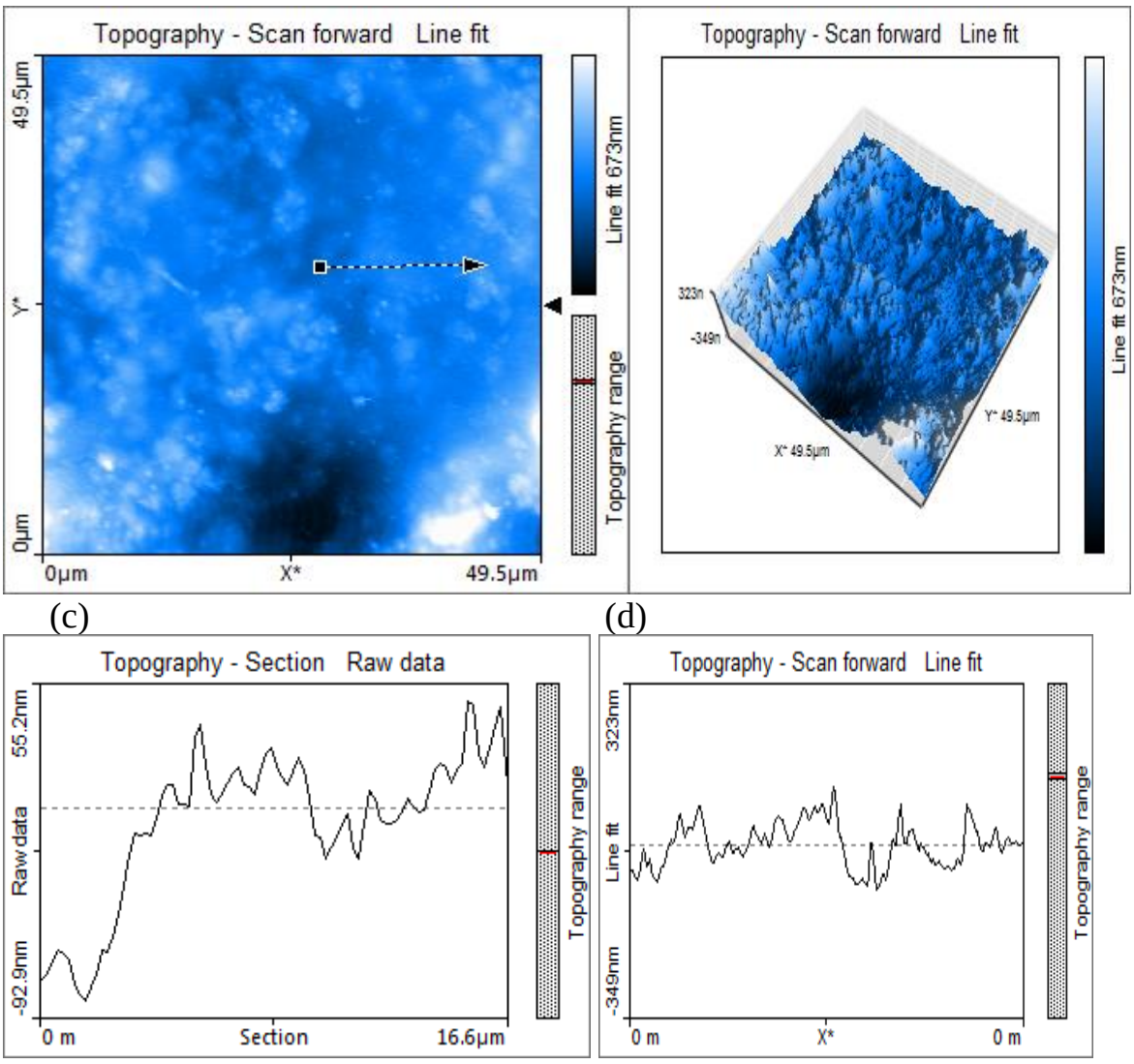

Figure (3.94): AFM photomicrograph of (CPG/G) , (a): scan topography, b: 3D topography, (c): cross-section topography, & (d): line graph topography

(a) (b)

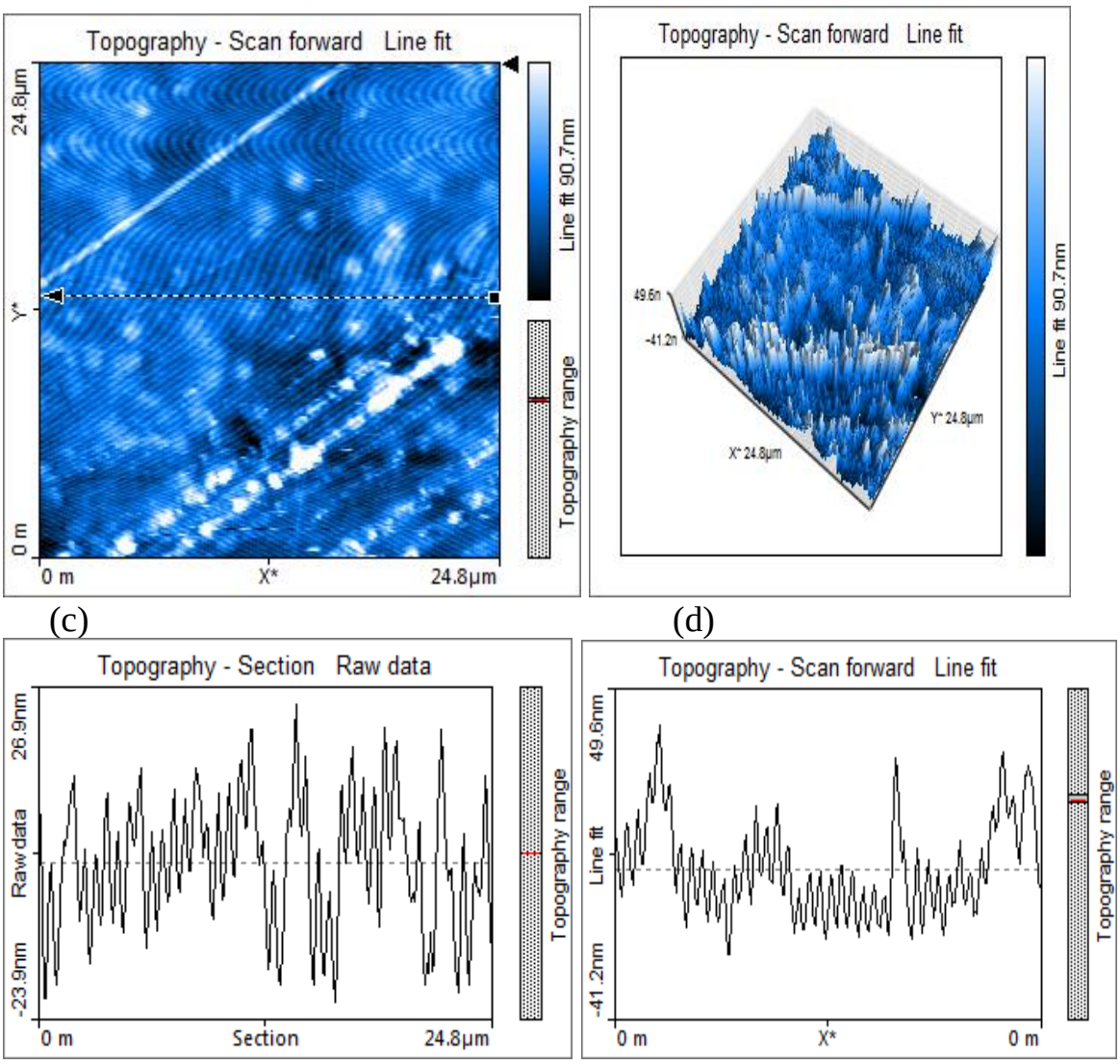

Figure (3.95): AFM photomicrograph of (CPG/MWCNTs) , (a): scan topography, b: 3D topography, (c): cross-section topography, & (d): line graph topography

3.1.8 Magnetic properties of Fe_3O_4 & coating form (CPG/Fe_3O_4/PANI)

Superparamagneticity of the uncoated and coated magnetite was proved using vibrating sample magnetometry (VSM) with an applied magnetic field with the field range of -10000 to + 10000 Oersted at room temperature. As shown in (Fig. 3.96 & 3.97), the hysteresis loop is completely reversible, the hysteresis has an "S" shape where both the descending and ascending loops coincide and yield zero coercivity, indicating that the magnetite nanoparticles are superparamagnetic[191]. Saturation magnetization of (CPG/Fe_3O_4/PANI) was (17.53514 emu g^{-1} at applied field 8499.915 Oe) which has been

significantly decreased compared to that of the pure Fe_3O_4 (59.79764 emu g-1 at applied field 8500.56 Oe) which can be assigned to hydrogel coating magnetite.

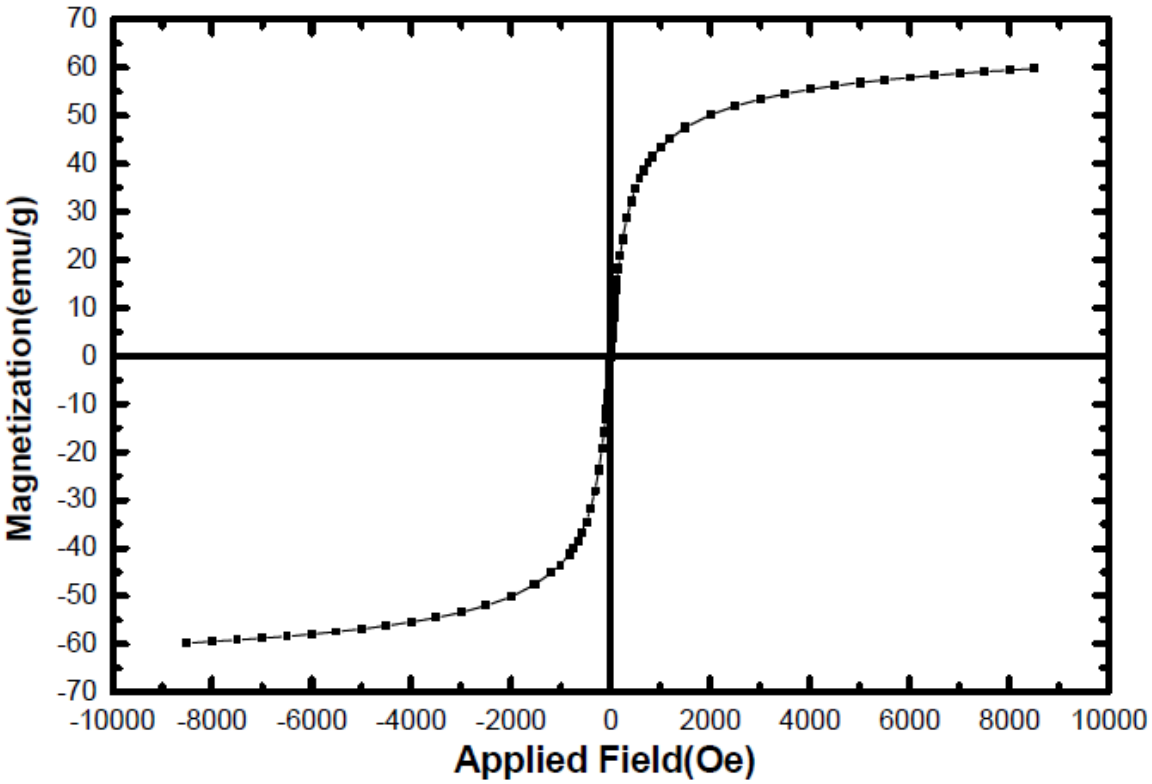

Figure (3.96): Hysteresis loop of uncoated Fe_3O_4

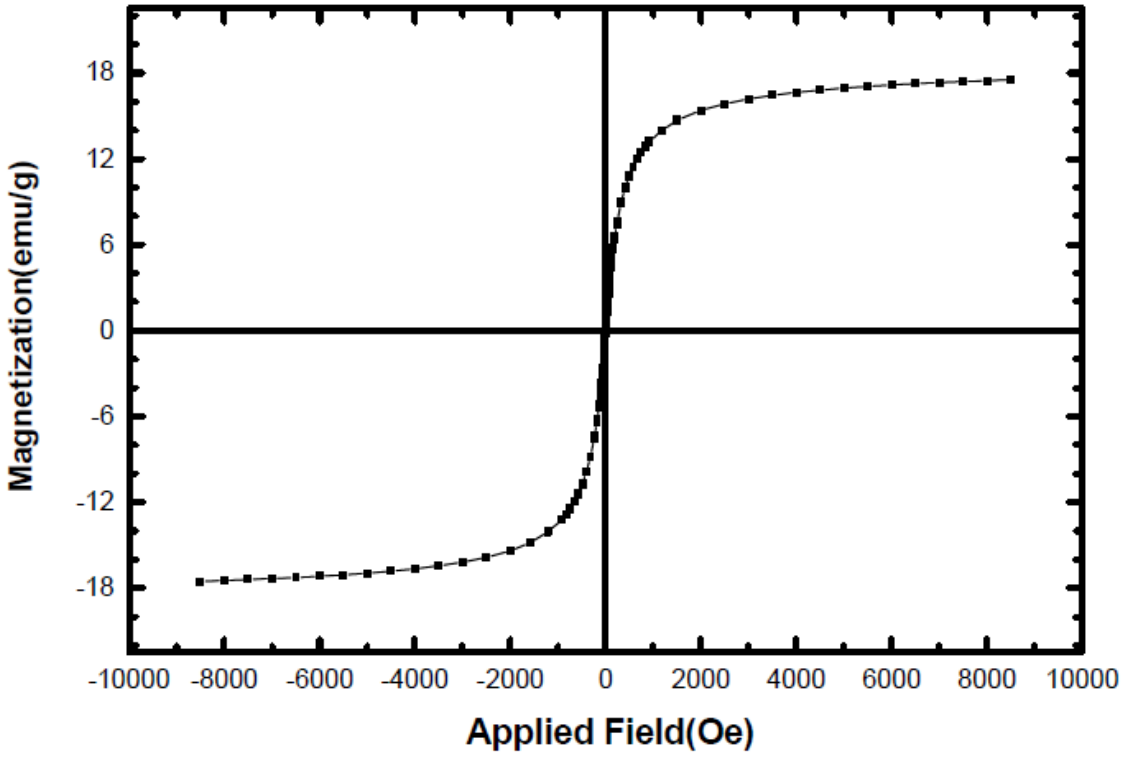

Figure (3.97): Hysteresis loop of coated form (CPG/Fe_3O_4/PANI)

3.2 Swelling properties of hydrogels and hydrogel composites

3.2.1 Swelling of hydrogel

The good properties of hydrogels are their ability to swell when placed in contact with a solvent thermodynamically compatible. When the hydrogel in its original state in connection with solvent molecules, the solvent to penetrate the hydrogel surface and penetrate into the polymeric network. In this case, the region rubber hydrogel be separated from the glassy phase unsolvated with moving boundary. The regular mesh network in the rubber phase starts to expand, allowing other solvent molecules to penetrate inside the hydrogel network [215].

The swelling properties, which typically use degree of swelling to define hydrogels, depend on many factors such as network density, solvent nature, polymer solvent interaction parameter [216].

The degree of the swelling changed with time and usually represent (S), the relation with the time coefficient in figure (3.98). From this figure it is obvious that the swelling increase with the time until it reaches the equilibrium state, at this point, the swelling stops, in the other word, reaches maximum of swelling.

Different hydrogels take various periods to reach point of equilibrium, this property is very important, thus we observe that maximum swelling for the (PgA) hydrogel in figure(3.98),is greater than the (CPM) hydrogel and the hydrogel of (PgA) was the greatest degree of swelling comparison with other hydrogel, this can be related to the network architecture of hydrogel. This hydrogel is consisting of PVA backbone was grafted by acrylic acid (see mechanism in chapter two). The molecular weight of repeating unit for PVA backbone was smaller than molecular weight of repeating unit for sugar polymers such as chitosan and pectin, subsequently the free space between the chitosan molecules or pectin molecules and crosslinker molecules was very closer, this caused be increased in density crosslinking which was reduced penetration the solvent molecules to hydrogel network. The reason other, the number of functional groups in chitosan or pectin backbone was greater than PVA

backbone subsequently the probability access the crosslinking from different sides, so the density of crosslinking in these hydrogel was greater than density of crosslinking in (PgA) hydrogel [217].

Also from (fig. 3.98) is shows the degree of swelling for CPM hydrogel was greater than CPG may be because difference by crosslinker. crosslinking between chitosan and PVA by glutaraldehyde was stronger than crosslinking between chitosan and PVA by maleic anhydride because different types of linkage (see mechanism in chapter two), the chitosan molecules was linked together on one hand by glutaraldehyde that explained disappeared the functional group of chitosan in FTIR spectra with appeared just (C=N) of Schiff base in spectra and other hand was linked with PVA by glutaraldehyde , so the crosslinking in CPM is weaker than CPG hydrogel, so the degree of swelling of CPM was greater than CPG[218]. This result was similar to literature [219]. The value of degree of swelling of hydrogel was recorded in tables (3.7, 3.8).

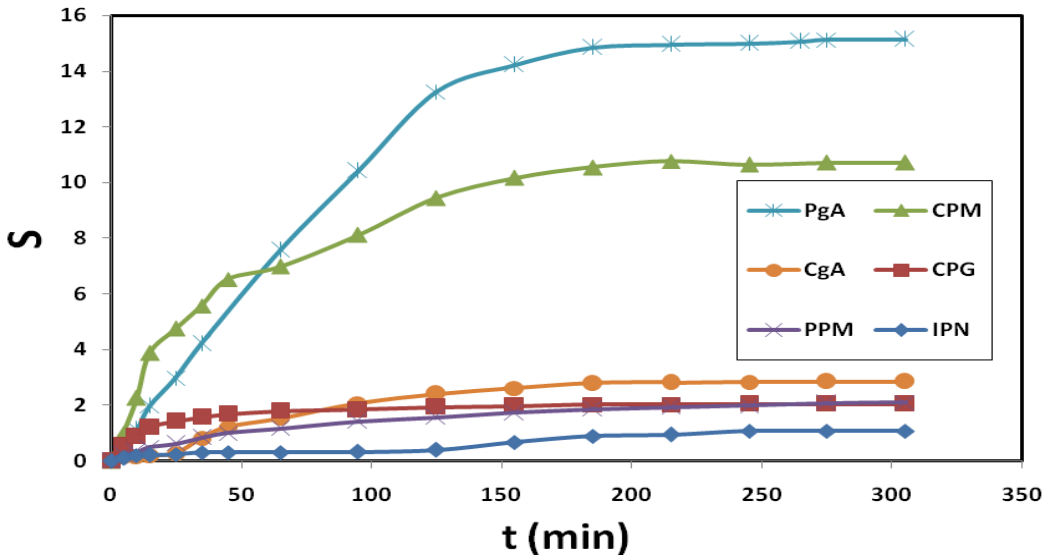

Figure (3.98): Degree of swelling for hydrogel

Table (3.7): Swelling studies in water of CPG (Wd =0.2561 g), CPM (Wd=0.0441 g), and PPM (Wd=0.3280) hydrogels

	CPG		CPM		PPM	
Time (min)	Ws (g)	S	Ws (g)	S	Ws (g)	S
5	0.3973	0.5513	0.0884	1.0045	0.4025	0.2271
10	0.4822	0.8829	0.1440	2.2653	0.4337	0.3223
15	0.5671	1.2144	0.2148	3.8707	0.4907	0.4960
25	0.6191	1.4174	0.2533	4.7438	0.5329	0.6247
35	0.6568	1.5646	0.2903	5.5828	0.6046	0.8433
45	0.6867	1.6814	0.3321	6.5306	0.6577	1.0052
65	0.7162	1.7966	0.3522	6.9864	0.7131	1.1741
95	0.7262	1.8356	0.4023	8.1224	0.7920	1.4146
125	0.7518	1.9356	0.4606	9.4444	0.8441	1.5735
155	0.7601	1.9680	0.4921	10.1587	0.8944	1.7268
185	0.7745	2.0242	0.5090	10.5420	0.9375	1.8582
215	0.7751	2.0266	0.5190	10.7687	0.9601	1.9271
245	0.7791	2.0422	0.5132	10.6372	0.9826	1.9957
275	0.7793	2.0430	0.5163	10.7075	1.0112	2.0829
305	0.7795	2.0437	0.5169	10.7211	1.0193	2.1076
day	0.8117	2.1695	0.7946	17.0181	1.1993	2.6564

Table (3.8): Swelling studies in water of PgA (Wd=0.0601 g), CgA (Wd=1.9394 g), and IPN (Wd=0.1432 g) hydrogels

	PgA		CgA		IPN	
Time (min)	Ws (g)	S	Ws (g)	S	Ws (g)	S
5	0.0896	0.4908	2.2153	0.1423	0.1592	0.1117
10	0.1276	1.1231	2.2506	0.1605	0.1711	0.1948
15	0.1783	1.9667	2.3350	0.2040	0.1745	0.2186
25	0.2394	2.9834	2.4534	0.2650	0.1774	0.2388
35	0.3134	4.2146	3.5352	0.8228	0.1870	0.3059
45	0.5150	7.5691	4.3070	1.2208	0.1877	0.3108
65	0.6862	10.4176	4.9293	1.5417	0.1880	0.3128
95	0.8570	13.2596	5.9580	2.0721	0.1886	0.3170
125	0.9152	14.2280	6.5987	2.4024	0.2010	0.4036
155	0.9521	14.8419	6.9989	2.6088	0.2390	0.6690
185	0.9588	14.9534	7.3456	2.7876	0.2716	0.8966
215	0.9608	14.9867	7.4108	2.8212	0.2793	0.9504
245	0.9652	15.0599	7.4321	2.8322	0.2972	1.0754
275	0.9692	15.1265	7.4492	2.8410	0.2975	1.0775
305	0.9695	15.1314	7.4518	2.8423	0.2979	1.0803
Day	1.0507	16.4825	9.1758	3.7313	0.2995	1.0915

3.2.2 Swelling of hydrogel composites

3.2.2.1 Swelling of hydrogels/PANI composite

The degree of swelling of hydrogels/PANI composites is shows in figure (3.99). In this figure was observed the degree of swelling of PgA and CPM hydrogel were very decreased comparison with pure hydrogels. This can be increased of density crosslinking with presence of poly aniline. This result is expected due to the fact that the conducting poly aniline was polymerized inside the hydrogel pores and the entanglement of the polyaniline chains in PgA & CPM hydrogels would reduce the hydrogel elasticity and the swelling degree.

The other hydrogels were almost maintained on the degree of swelling, may be caused the density of crosslinking of these hydrogel was prevented the poly aniline to polymerized inside the hydrogel pores but can't prevent small molecules of water to fill the pores and therefore maintained on degree of swelling of these hydrogels. This result was similar to literature [220]. The values of degree of swelling of hydrogel were recorded in table (3.9, 3.10).

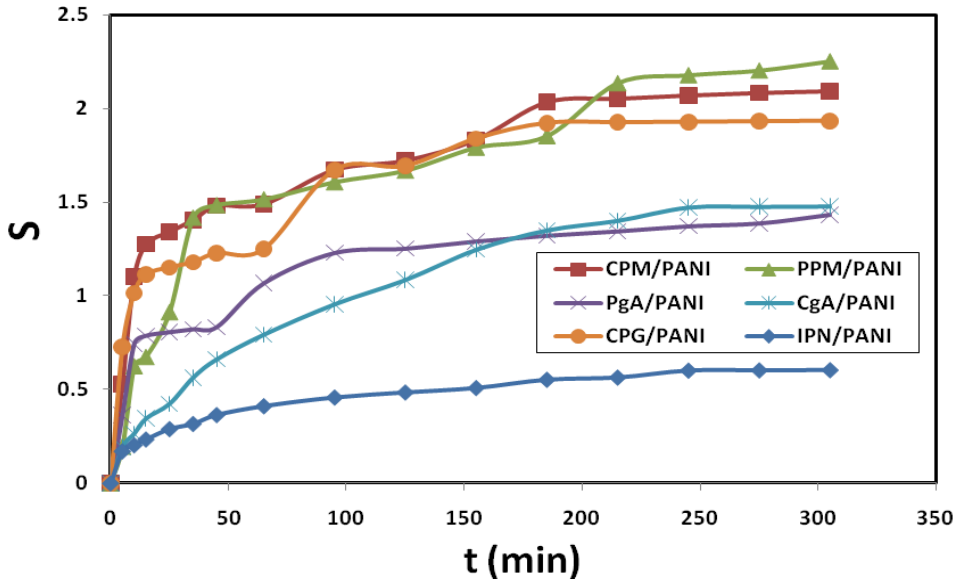

Figure (3.99): Degree of swelling for PANI composites

Table (3.9): Swelling studies in water of CPG/PANI (Wd=0.0895 g), CPM/PANI (Wd=0.0224 g), and PPM/PANI (Wd=0.0163) hydrogels

	CPG/PANI		CPM/PANI		PPM/PANI	
Time (min)	Ws (g)	S	Ws (g)	S	Ws (g)	S
5	0.1547	0.7285	0.0343	0.5313	0.0195	0.1963
10	0.1805	1.0168	0.0471	1.1027	0.0265	0.6258
15	0.1894	1.1162	0.0510	1.2768	0.0273	0.6748
25	0.1927	1.1531	0.0525	1.3438	0.0312	0.9141
35	0.1952	1.1810	0.0539	1.4063	0.0394	1.4172
45	0.1995	1.2291	0.0556	1.4821	0.0405	1.4847
65	0.2015	1.2514	0.0558	1.4911	0.0410	1.5153
95	0.2393	1.6737	0.0599	1.6741	0.0425	1.6074
125	0.2412	1.6950	0.0610	1.7232	0.0435	1.6687
155	0.2543	1.8413	0.0635	1.8348	0.0455	1.7914
185	0.2617	1.9240	0.0680	2.0357	0.0465	1.8528
215	0.2620	1.9274	0.0684	2.0536	0.0511	2.1350
245	0.2622	1.9296	0.0688	2.0714	0.0518	2.1779
275	0.2625	1.9330	0.0691	2.0848	0.0522	2.2025
305	0.2627	1.9352	0.0693	2.0938	0.0530	2.2515
Day	0.2880	2.2179	0.0732	2.2679	0.0580	2.5583

Table (3.10): Swelling studies in water of PgA/PANI (Wd=0.0260 g), CgA/PANI (Wd=0.2072 g), and IPN/PANI (Wd=0.2820 g) hydrogels

	PgA/PANI		CgA/PANI		IPN/PANI	
Time (min)	Ws (g)	S	Ws (g)	S	Ws (g)	S
5	0.0355	0.3654	0.2472	0.1931	0.3301	0.1706
10	0.0454	0.7462	0.2622	0.2654	0.3393	0.2032
15	0.0465	0.7885	0.2789	0.3460	0.3479	0.2337
25	0.0470	0.8077	0.2952	0.4247	0.3635	0.2890
35	0.0474	0.8231	0.3242	0.5647	0.3712	0.3163
45	0.0477	0.8346	0.3443	0.6617	0.3846	0.3638
65	0.0538	1.0692	0.3716	0.7934	0.3978	0.4106
95	0.0580	1.2308	0.4052	0.9556	0.4108	0.4567
125	0.0586	1.2538	0.4321	1.0854	0.4184	0.4837
155	0.0596	1.2923	0.4655	1.2466	0.4251	0.5074
185	0.0604	1.3231	0.4869	1.3499	0.4375	0.5514
215	0.0610	1.3462	0.4975	1.4011	0.4408	0.5631
245	0.0617	1.3731	0.5122	1.4720	0.4512	0.6000
275	0.0621	1.3885	0.5130	1.4759	0.4516	0.6014
305	0.0633	1.4346	0.5134	1.4778	0.4519	0.6025
Day	0.0699	1.6885	0.5669	1.7360	0.4602	0.6319

3.2.2.2 Swelling of hydrogels/G composite

Difference behavior of (hydrogels / G) composites is show in fig (3.100). As is clearly apparent in (Fig. 3.100), the swelling of the PgA and CPM hydrogel composites were much decreased in comparison of pure hydrogels. This is may be caused of interaction between functional groups of hydrogel network with functional group of graphene nanosheets and therefore increased of density of crosslinking. This was caused to decrease of swelling for two hydrogels; this result is similar to literature [221].

Conversely, as can be seen from the Figure (3.100), swelling behavior of the (CPG) and (IPN) hydrogel composite not particularly influenced by the presence of the graphene. On the contrary, degree of swelling of (PPM) and (CgA) hydrogel composite undergoes a drastic enhancement with presence of graphene. This finding might be attributed to the presence of graphene sheets that separate close macromolecular chains, thus reducing the cross-linking extent [222]. The values of degree of swelling of hydrogel were recorded in table (3.11, 3.12).

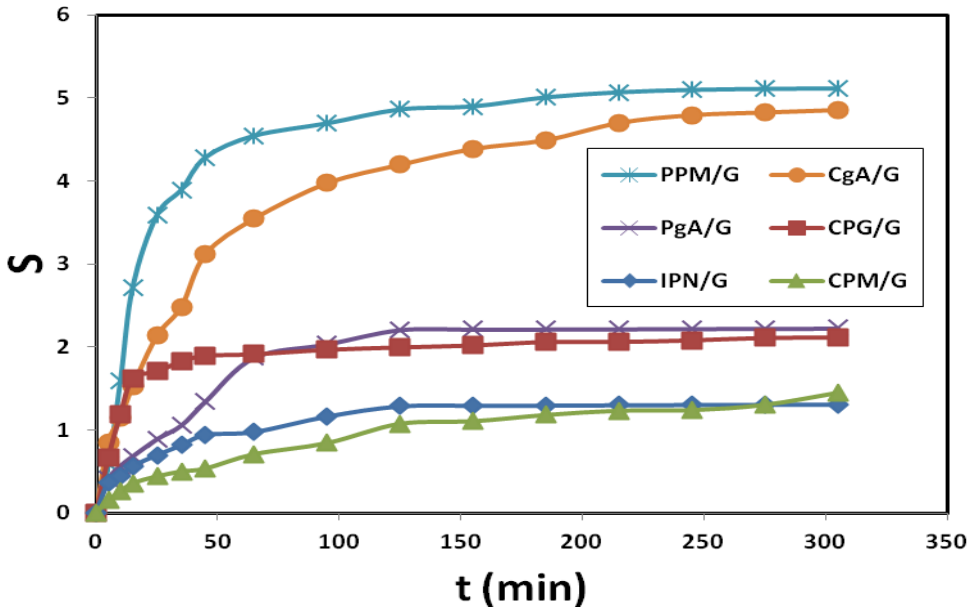

Figure (3.100): Degree of swelling for G composites

Table (3.11): Swelling studies in water of CPG/G (Wd=0.1122 g), CPM/G (Wd=0.0433 g), and PPM/G (Wd=0.2206) hydrogels

	CPG/G		CPM/G		PPM/G	
Time (min)	Ws (g)	S	Ws (g)	S	Ws (g)	S
5	0.1865	0.6622	0.0499	0.1524	0.3498	0.5857
10	0.2457	1.1898	0.0545	0.2587	0.5718	1.5920
15	0.2939	1.6194	0.0588	0.3580	0.8207	2.7203
25	0.3034	1.7041	0.0624	0.4411	1.0129	3.5916
35	0.3173	1.8280	0.0650	0.5012	1.0796	3.8939
45	0.3248	1.8948	0.0665	0.5358	1.1661	4.2860
65	0.3269	1.9135	0.0740	0.7090	1.2233	4.5453
95	0.3330	1.9679	0.0798	0.8430	1.2563	4.6949
125	0.3361	1.9955	0.0899	1.0762	1.2933	4.8626
155	0.3388	2.0196	0.0912	1.1062	1.3012	4.8985
185	0.3435	2.0615	0.0945	1.1824	1.3255	5.0086
215	0.3436	2.0624	0.0967	1.2333	1.3389	5.0694
245	0.3457	2.0811	0.0970	1.2402	1.3452	5.0979
275	0.3490	2.1105	0.0998	1.3048	1.3478	5.1097
305	0.3494	2.1141	0.1061	1.4503	1.3490	5.1151
Day	0.3501	2.1203	0.1102	1.5450	1.3713	5.2162

Table (3.12): Swelling studies in water of PgA/G (Wd=0.1981 g), CgA/G (Wd=0.6828 g), and IPN/G (Wd=0.0862 g) hydrogels

	PgA/G		CgA/G		IPN/G	
Time (min)	Ws (g)	S	Ws (g)	S	Ws (g)	S
5	0.2780	0.4033	1.2642	0.8515	0.1179	0.3677
10	0.3104	0.5669	1.4634	1.1432	0.1246	0.4455
15	0.3331	0.6815	1.7231	1.5236	0.1349	0.5650
25	0.3743	0.8894	2.1402	2.1344	0.1464	0.6984
35	0.4070	1.0545	2.3791	2.4843	0.1566	0.8167
45	0.4644	1.3443	2.8133	3.1202	0.1675	0.9432
65	0.5693	1.8738	3.1047	3.5470	0.1704	0.9768
95	0.6012	2.0348	3.3966	3.9745	0.1865	1.1636
125	0.6355	2.2080	3.5482	4.1965	0.1971	1.2865
155	0.6366	2.2135	3.6788	4.3878	0.1977	1.2935
185	0.6370	2.2155	3.7512	4.4938	0.1979	1.2958
215	0.6375	2.2181	3.8933	4.7020	0.1982	1.2993
245	0.6380	2.2206	3.9567	4.7948	0.1985	1.3028
275	0.6385	2.2231	3.9790	4.8275	0.1987	1.3051
305	0.6390	2.2256	3.9987	4.8563	0.1988	1.3063
Day	0.6613	2.3382	4.0190	4.8861	0.2173	1.5209

3.2.2.3 Swelling of hydrogels/MWCNTs composite

Swelling behavior of (hydrogel /MWCNTs) composites was approximately similar to (hydrogel/G) composites. As is clearly apparent in (Fig. 3.101), the swelling of the PgA and CPM hydrogel composite also was very decreased in comparison of pure hydrogels, swelling behavior of the CgA hydrogel composite not particularly influenced by the presence of the carbon nanotube and degree of swelling of PPM, CPG and IPN hydrogel composite undergoes a drastic enhancement with presence of carbon nanotubes for same reasons. The values of degree of swelling of hydrogel were recorded in table (3.13, 3.14).

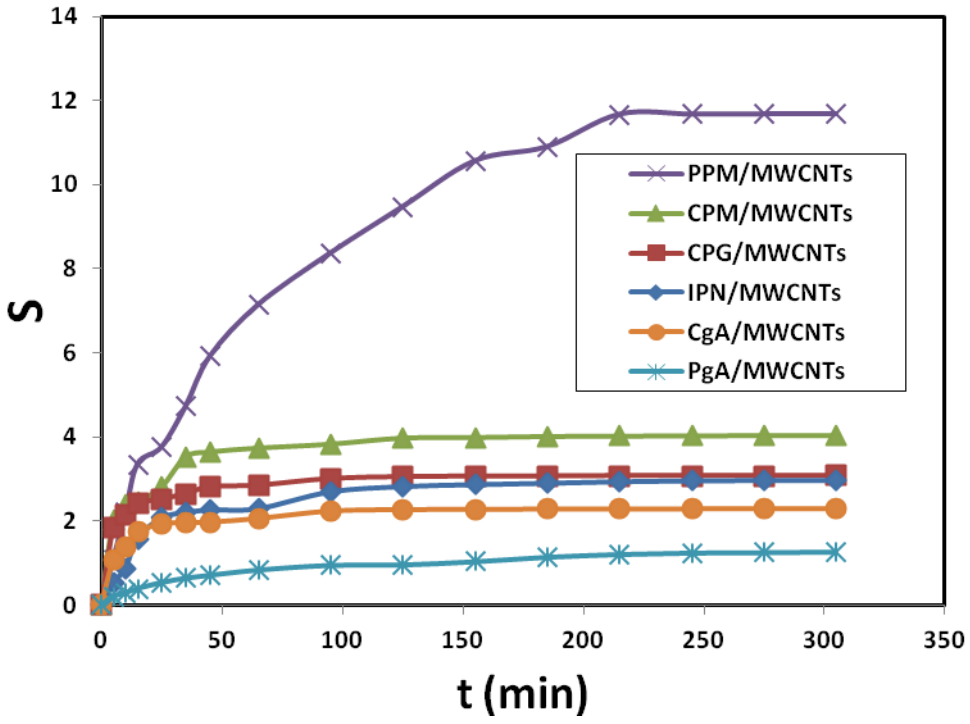

Figure (3.101): Degree of swelling for MWCNTs composites

Table (3.13): Swelling studies in water of CPG/MWCNTs (Wd=0.1174 g), CPM/MWCNTs (Wd=0.0891 g), and PPM/MWCNTs (Wd=0.0918) hydrogels

	CPG/MWCNTs		CPM/MWCNTs		PPM/MWCNTs	
Time (min)	Ws (g)	S	Ws (g)	S	Ws (g)	S
5	0.3337	1.8424	0.2691	2.0202	0.1918	1.0893
10	0.3693	2.1457	0.3010	2.3782	0.2942	2.2048
15	0.4001	2.4080	0.3077	2.4534	0.3991	3.3475
25	0.4131	2.5187	0.3396	2.8114	0.4366	3.7560
35	0.4271	2.6380	0.4031	3.5241	0.5255	4.7244
45	0.4470	2.8075	0.4136	3.6420	0.6343	5.9096
65	0.4510	2.8416	0.4219	3.7351	0.7469	7.1362
95	0.4698	3.0017	0.4303	3.8294	0.8597	8.3649
125	0.4750	3.0460	0.4431	3.9731	0.9609	9.4673
155	0.4766	3.0596	0.4443	3.9865	1.0613	10.5610
185	0.4770	3.0630	0.4466	4.0123	1.0922	10.8976
215	0.4781	3.0724	0.4473	4.0202	1.1628	11.6667
245	0.4783	3.0741	0.4478	4.0258	1.1632	11.6710
275	0.4784	3.0750	0.4484	4.0325	1.1636	11.6754
305	0.4786	3.0767	0.4487	4.0359	1.1638	11.6776
Day	0.4863	3.1422	0.4552	4.1089	1.1702	11.7473

Table (3.14): Swelling studies in water of PgA/ MWCNTs (Wd=0.1438 g), CgA/ MWCNTs (Wd=0.1078 g), and IPN/ MWCNTs (Wd=0.2286 g) hydrogels

	PgA/ MWCNTs		CgA/MWCNTs		IPN/MWCNTs	
Time (min)	Ws (g)	S	Ws (g)	S	Ws (g)	S
5	0.1723	0.1982	0.2235	1.0733	0.3490	0.5267
10	0.1849	0.2858	0.2560	1.3748	0.4267	0.8666
15	0.1997	0.3887	0.2950	1.7365	0.5897	1.5796
25	0.2206	0.5341	0.3158	1.9295	0.7024	2.0726
35	0.2354	0.6370	0.3192	1.9610	0.7312	2.1986
45	0.2455	0.7072	0.3206	1.9740	0.7456	2.2616
65	0.2637	0.8338	0.3300	2.0612	0.7523	2.2909
95	0.2797	0.9451	0.3491	2.2384	0.8438	2.6912
125	0.2812	0.9555	0.3528	2.2727	0.8734	2.8206
155	0.2925	1.0341	0.3534	2.2783	0.8833	2.8640
185	0.3081	1.1426	0.3540	2.2839	0.8912	2.8985
215	0.3174	1.2072	0.3545	2.2885	0.8996	2.9353
245	0.3223	1.2413	0.3547	2.2904	0.9043	2.9558
275	0.3239	1.2524	0.3551	2.2941	0.9067	2.9663
305	0.3259	1.2663	0.3554	2.2968	0.9072	2.9685
Day	0.3306	1.2990	0.3921	2.6373	0.9572	3.1872

3.3 Dielectric constant value measurements

3.3.1 Dielectric constant value measurements for hydrogels

It can be seen from figure (3.102) and figure (3.103) the real & imaginary permittivity versus log frequency of hydrogels, respectively, increase with decreasing frequency. The measurement performed at room temperature; hence, its influence on the permittivity actions can be neglected. The hydrogel constituent of permittivity is governed by the number of orientable dipoles present in the system and their ability to orient under un-applied electric field. At lower frequencies of applied voltage, all the free dipolar functional groups in the hydrogel can orient themselves resulting in a higher permittivity value at these frequencies. As the electric field frequency increases, the bigger dipolar groups find it hard to orient the same speed as the alternating field, therefore the contributions of these dipolar groups to the permittivity goes on reducing resulting in a continuously decreasing permittivity of the hydrogel system at higher frequencies[223].

The electrical conductivity depends on the number of charge carriers and frequency of the applied electric field on the hydrogels. From figure (3.104) was appeared all hydrogel are insulator.

Tables (3.15-3.17) are show measurement values of real, imaginary permittivity and electric conductivity of hydrogels.

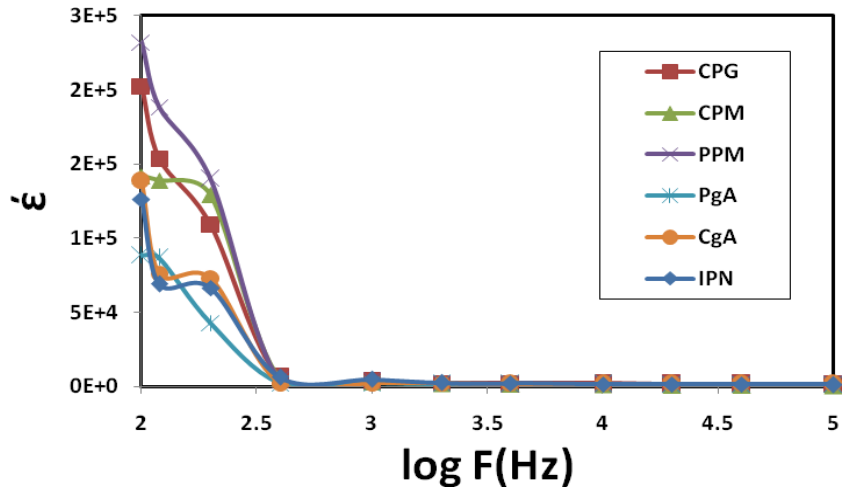

Figure (3.102): Real permittivity versus log frequency for hydrogels

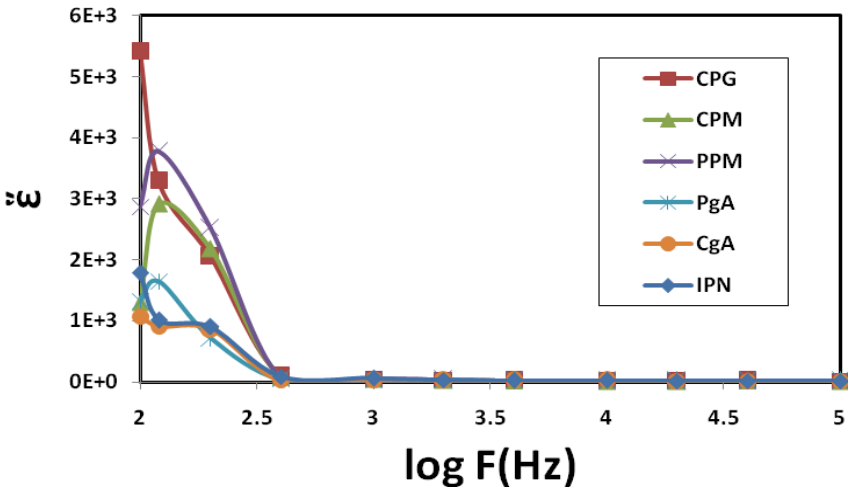

Figure (3.103): Imaginary permittivity versus log frequency for hydrogels

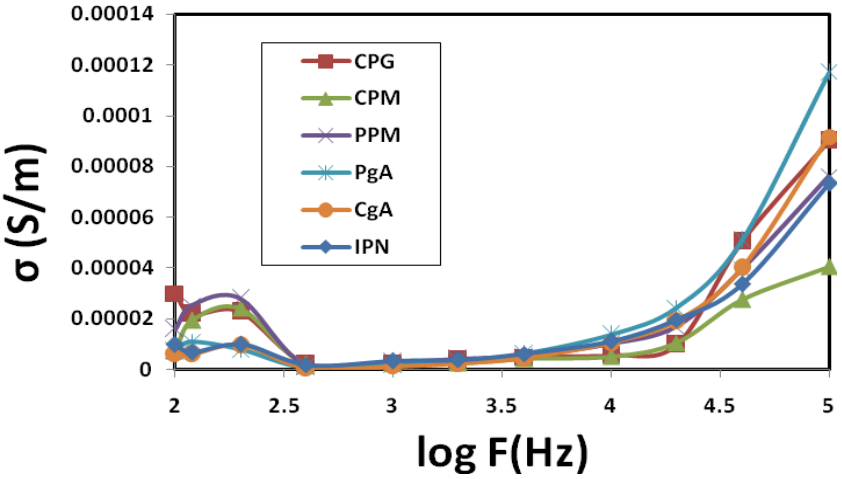

Figure (3.104): AC conductivity versus log frequency for hydrogel

3.3.2 Electric properties measurements of hydrogel composites

Figures (3.105, 3.108, & 3.111) were depicted the variation of real part of dielectric permittivity (ε') with frequency for (hydrogel/PANI), (hydrogels/G) & (hydrogels/MWCNTs) composites, respectively at room temperature. At low frequencies, permittivity reached higher values, in all cases, which decreased rapidly with frequency increasing. This is logical since in the low frequency region the alternation of the field is slow, providing thus enough time to permanent and induced dipoles to align themselves in relation to the applied field, leading to enhanced polarization. Enhanced values of (ε') particularly at low frequencies can be returned to interfacial polarization, and/or electrode polarization. Electrode polarization is associated to the buildup of space charges at the specimen-electrode interfaces and is describing by very high values of both real and imaginary part of dielectric permittivity [224-227]. Checking samples were tested under identical experimental conditions, having similar geometrical characteristics and composition. Thus, if electrode polarization was the predominant effect in a certain type of nanocomposite, should be also the predominant tendency to all other types. Under this point of think, the higher values of (ε') could be attributed to improved conductivity and interfacial polarization (IP). IP results from the collection of unbounded charges at the interfaces of the constituents, where they form large dipoles; its intensity is connected to the extent of the existing interfacial area within the composite system, giving thus indirect evidence of the achieved distribution of nano inclusions [228]. Dielectric loss (ε''), (Figures 3.106, 3.109, 3.112) were also increased with decrease of the frequency. The variation of σ (AC conductivity) was studied with frequency for hydrogel and hydrogel composite. The hydrogels were showed typical insulating behavior with a frequency-dependent conductivity. While the (hydrogels/PANI), (hydrogels/G) & (hydrogels/MWCNTs) were typical semiconductor with a frequency-dependent conductivity. They were transition from an insulator to semiconductor. This explained as percolation threshold associated with the formation of conducting network. [229] so it can be seen that the change in the electrical conductivity depends on presence (PANI, G, & MWCNTs) in the composites. The conductivity of the (PANI, G, & MWCNTs) composites increases with increasing frequency (fig. 3.107, 3.110, & 3.113), when the PANI or G or MWCNTs distributed in the hydrogel matrix to form conductive composite, it creates a lot of interfaces a large dominate of travelling electron could provide with large π-orbital of the PANI or G or MWCNTs, this is considered as a strong indication for charge migration via the hopping mechanism [230, 231].

The interface polarization can take place when electrons oriented under electric field. Furthermore, for (CPG/Fe_3O_4/ PANI), iron oxide increase the charge carries and the free volume increases and more vacant sites are created for the motion of ions, which in turn enhances the conductivity [232].

Tables (3.18-3.28) are show the real, imaginary permittivity and electric conductivity of PANI, G, MWCNTs and theirs composites.

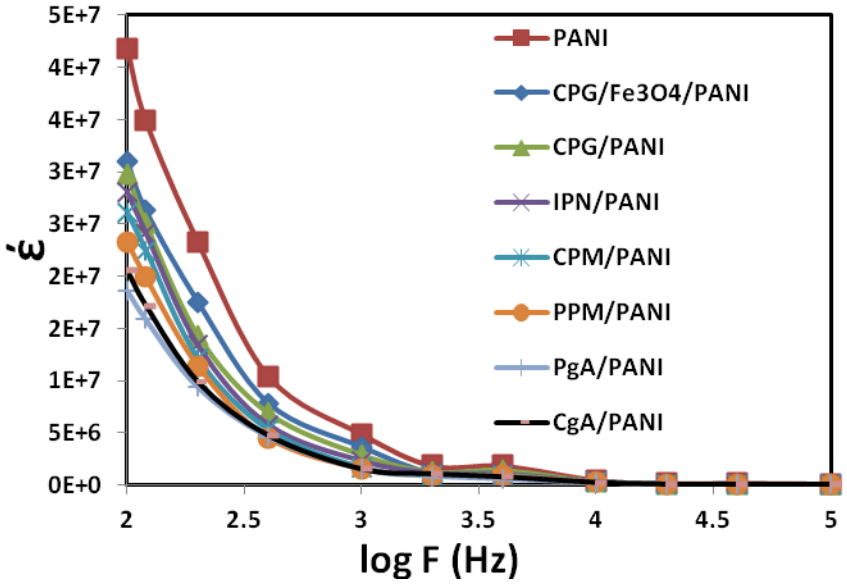

Figure (3.105): Real permittivity versus log frequency for PANI and composites

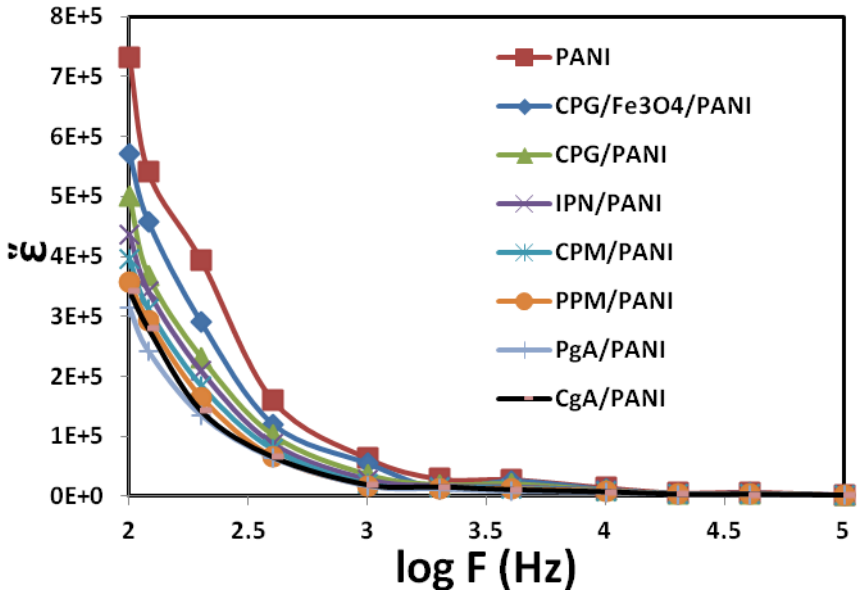

Figure (3.106): Imaginary permittivity versus log frequency for PANI and composites

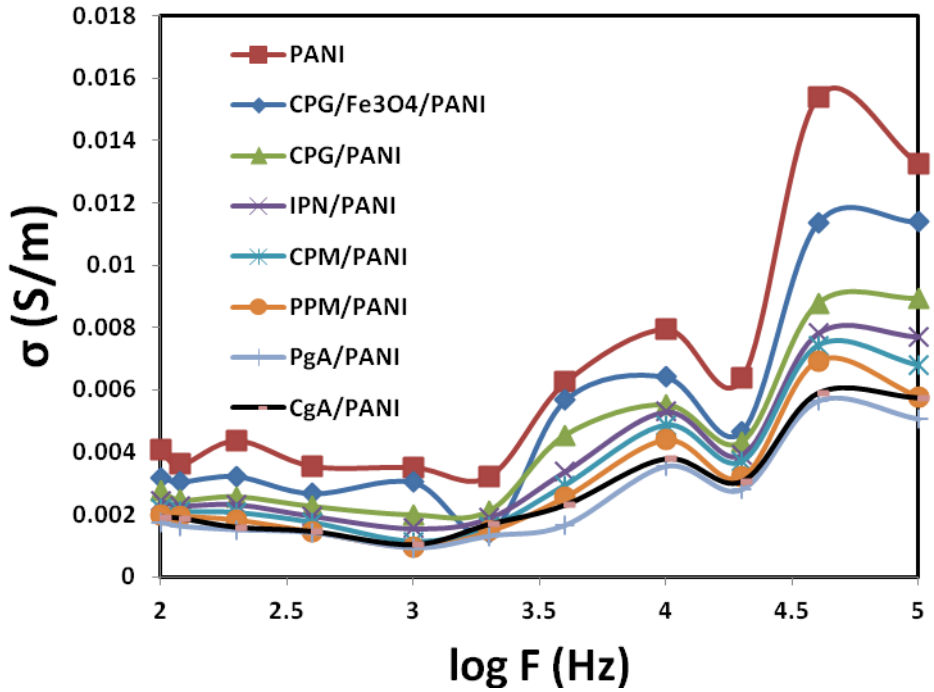

Figure (3.107): AC conductivity versus log frequency for PANI and composites

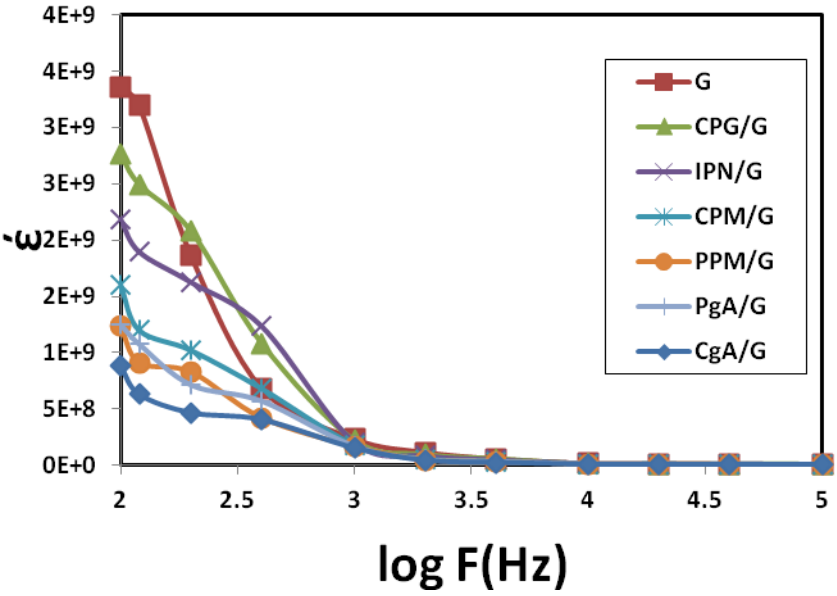

Figure (3.108): Real permittivity versus log frequency for G and composites

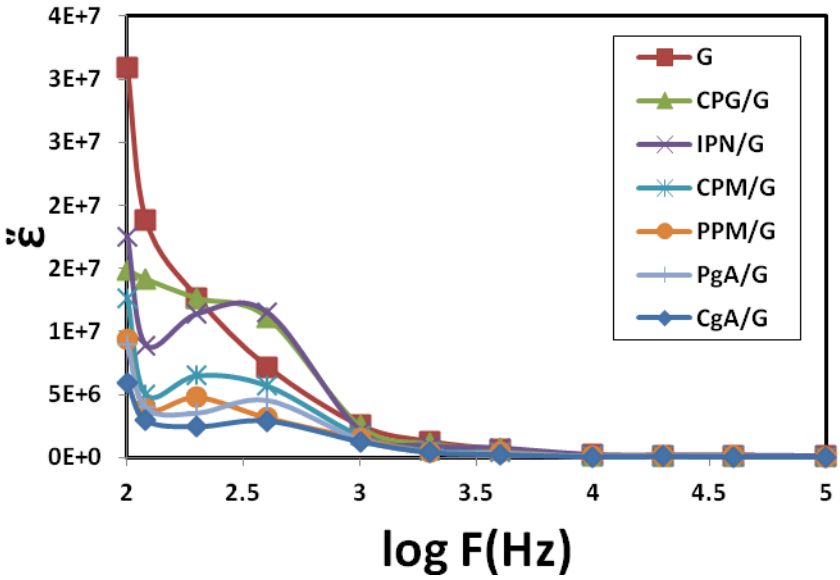

Figure (3.109): Imaginary permittivity versus log frequency for G and composites

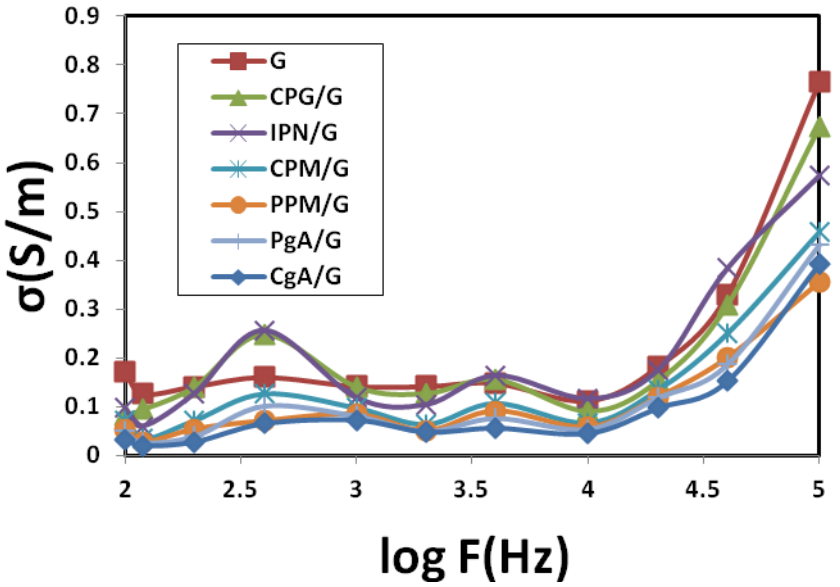

Figure (3.110): AC conductivity versus log frequency for G and composites

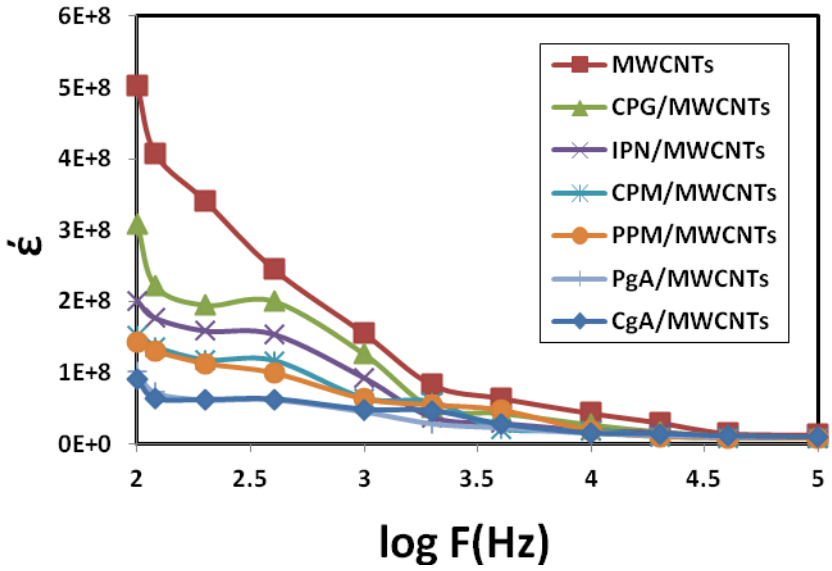

Figure (3.111): Real permittivity versus log frequency for MWCNTs and composites

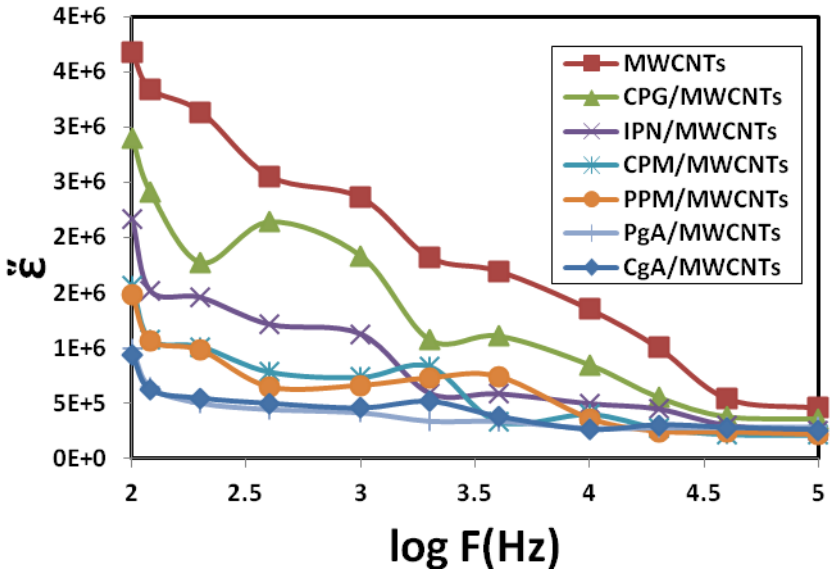

Figure (3.112): Imaginary permittivity versus log frequency for MWCNTs and composites

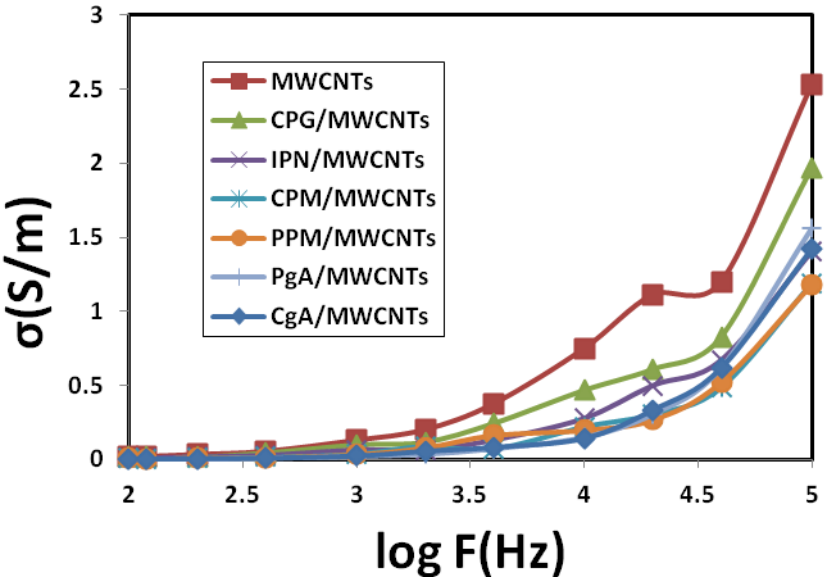

Figure (3.113): AC conductivity versus log frequency for MWCNTs and composites

Table (3.15): LCR measurements of CPG and CPM hydrogels at R.T.

	F (Hz)	**C (F)**	ε'	ε''	σ **(S/m)**
CPG	**100**	4.884E-06	2.0235E+05	5.4028E+03	3.0027E-05
	120	3.7112E-06	1.5376E+05	3.2858E+03	2.1914E-05
	200	2.638E-06	1.0930E+05	2.0515E+03	2.2803E-05
	400	1.511E-07	6.2603E+03	1.0065E+02	2.2375E-06
	1000	7.788E-08	3.2267E+03	5.1046E+01	2.8370E-06
	2000	5.504E-08	2.2804E+03	3.4605E+01	3.8465E-06
	4000	5.022E-08	2.0807E+03	2.2367E+01	4.9725E-06
	10000	4.925E-08	2.0405E+03	1.0121E+01	5.6250E-06
	20000	4.275E-08	1.7712E+03	8.8736E+00	9.8636E-06
	40000	4.265E-08	1.7670E+03	2.2636E+01	5.0322E-05
	100000	3.2016E-08	1.3265E+03	1.6196E+01	9.0015E-05
CPM	**100**	2.5080E-06	1.4169E+05	1.2979E+03	7.2136E-06
	120	2.4560E-06	1.3876E+05	2.9168E+03	1.9453E-05
	200	2.2900E-06	1.2938E+05	2.1736E+03	2.4160E-05
	400	9.9200E-08	5.6045E+03	9.0569E+01	2.0135E-06
	1000	5.0420E-08	2.8486E+03	4.5179E+01	2.5109E-06
	2000	3.0730E-08	1.7362E+03	2.3664E+01	2.6304E-06
	4000	2.7910E-08	1.5768E+03	1.8764E+01	4.1715E-06
	10000	1.7330E-08	9.7910E+02	9.1154E+00	5.0661E-06
	20000	1.5760E-08	8.9040E+02	9.4204E+00	1.0471E-05
	40000	1.4230E-08	8.0395E+02	1.2381E+01	2.7524E-05
	100000	9.8900E-09	5.5876E+02	7.2806E+00	4.0464E-05

Table (3.16): LCR measurements of PgA and CgA hydrogels at R.T.

	F (Hz)	C (F)	ε'	ε''	σ (S/m)
PgA	**100**	2.3450E-06	8.8324E+04	1.3275E+03	7.3780E-06
	120	2.2990E-06	8.6591E+04	1.6461E+03	1.0978E-05
	200	1.1340E-06	4.2712E+04	7.1671E+02	7.9666E-06
	400	6.0580E-08	2.2817E+03	3.7033E+01	8.2328E-07
	1000	5.5070E-08	2.0742E+03	3.2233E+01	1.7914E-06
	2000	5.2440E-08	1.9751E+03	3.0220E+01	3.3591E-06
	4000	4.8030E-08	1.8090E+03	2.7496E+01	6.1126E-06
	10000	4.5170E-08	1.7013E+03	2.4907E+01	1.3843E-05
	20000	4.1510E-08	1.5635E+03	2.1935E+01	2.4383E-05
	40000	3.9990E-08	1.5062E+03	2.2875E+01	5.0854E-05
	100000	3.8720E-08	1.4584E+03	2.1044E+01	1.1696E-04
CgA	**100**	2.4500E-06	1.3842E+05	1.0769E+03	5.9852E-06
	120	1.3490E-06	7.6215E+04	9.0848E+02	6.0590E-06
	200	1.2960E-06	7.3220E+04	8.6034E+02	9.5632E-06
	400	4.0120E-08	2.2667E+03	2.5183E+01	5.5984E-07
	1000	3.8820E-08	2.1932E+03	2.3577E+01	1.3104E-06
	2000	3.6660E-08	2.0712E+03	2.1540E+01	2.3943E-06
	4000	3.5140E-08	1.9853E+03	2.0032E+01	4.4533E-06
	10000	3.4010E-08	1.9215E+03	1.9099E+01	1.0615E-05
	20000	3.2060E-08	1.8113E+03	1.7153E+01	1.9067E-05
	40000	3.1590E-08	1.7847E+03	1.8062E+01	4.0153E-05
	100000	2.9880E-08	1.6881E+03	1.6493E+01	9.1665E-05

Table (3.17): LCR measurements of PPM and IPN hydrogels at R.T.

	F (Hz)	C (F)	ε'	ε''	σ (S/m)
PPM	**100**	5.9760E-06	2.3184E+05	2.8655E+03	1.5926E-05
	120	4.8520E-06	1.8823E+05	3.7765E+03	2.5187E-05
	200	3.6120E-06	1.4013E+05	2.5181E+03	2.7990E-05
	400	1.0219E-07	3.9644E+03	6.9179E+01	1.5379E-06
	1000	8.0460E-08	3.1214E+03	5.1628E+01	2.8694E-06
	2000	6.0980E-08	2.3657E+03	3.7903E+01	4.2132E-06
	4000	4.0430E-08	1.5685E+03	2.3919E+01	5.3175E-06
	10000	3.3090E-08	1.2837E+03	1.7985E+01	9.9956E-06
	20000	3.0150E-08	1.1697E+03	1.5358E+01	1.7071E-05
	40000	2.8400E-08	1.1018E+03	1.7713E+01	3.9378E-05
	100000	2.5630E-08	9.9431E+02	1.3692E+01	7.6095E-05
IPN	**100**	2.5790E-06	1.2628E+05	1.7843E+03	9.9169E-06
	120	1.4120E-06	6.9137E+04	1.0149E+03	6.7690E-06
	200	1.3550E-06	6.6347E+04	8.9900E+02	9.9929E-06
	400	1.2831E-07	6.2826E+03	8.3370E+01	1.8534E-06
	1000	1.0010E-07	4.9013E+03	6.2786E+01	3.4895E-06
	2000	4.9670E-08	2.4321E+03	3.4584E+01	3.8442E-06
	4000	4.3190E-08	2.1148E+03	2.7703E+01	6.1588E-06
	10000	3.3260E-08	1.6285E+03	2.0096E+01	1.1169E-05
	20000	3.0120E-08	1.4748E+03	1.7639E+01	1.9606E-05
	40000	2.8060E-08	1.3739E+03	1.5134E+01	3.3644E-05
	100000	2.6830E-08	1.3137E+03	1.3203E+01	7.3378E-05

Table (3.18): LCR measurements of MWCNTs and G at R.T.

	F (Hz)	C (F)	ε'	ε''	σ (S/m)
MWCNTs	**100**	2.9680E-03	5.0305E+08	3.6723E+06	2.0410E-02
	120	2.4040E-03	4.0746E+08	3.3412E+06	2.2283E-02
	200	2.0100E-03	3.4068E+08	3.1342E+06	3.4839E-02
	400	1.4470E-03	2.4525E+08	2.5506E+06	5.6704E-02
	1000	9.1600E-04	1.5525E+08	2.3599E+06	1.3116E-01
	2000	4.9000E-04	8.3051E+07	1.8188E+06	2.0217E-01
	4000	3.8000E-04	6.4407E+07	1.6939E+06	3.7657E-01
	10000	2.5600E-04	4.3390E+07	1.3494E+06	7.4998E-01
	20000	1.7800E-04	3.0169E+07	1.0016E+06	1.1134E+00
	40000	9.0000E-05	1.5254E+07	5.4000E+05	1.2005E+00
	100000	7.5670E-05	1.2825E+07	4.5530E+05	2.5305E+00
G	**100**	1.7850E-02	3.3616E+09	3.0927E+07	1.7188E-01
	120	1.6990E-02	3.1996E+09	1.8878E+07	1.2590E-01
	200	9.9000E-03	1.8644E+09	1.2678E+07	1.4092E-01
	400	3.6400E-03	6.8550E+08	7.1977E+06	1.6001E-01
	1000	1.2400E-03	2.3352E+08	2.5454E+06	1.4147E-01
	2000	6.1300E-04	1.1544E+08	1.2699E+06	1.4115E-01
	4000	3.1200E-04	5.8757E+07	6.6395E+05	1.4761E-01
	10000	8.9600E-05	1.6874E+07	2.0080E+05	1.1160E-01
	20000	6.7700E-05	1.2750E+07	1.6319E+05	1.8140E-01
	40000	6.0090E-05	1.1316E+07	1.4824E+05	3.2957E-01
	100000	5.3847E-05	1.0141E+07	1.3791E+05	7.6649E-01

Table (3.19): LCR measurements of PANI, CPG/Fe_3O_4/PANI at R.T.

	F (Hz)	C (F)	ε'	ε''	σ (S/m)
PANI	**100**	8.8800E-05	4.1808E+07	7.3164E+05	4.0663E-03
	120	7.4100E-05	3.4887E+07	5.4075E+05	3.6064E-03
	200	4.9490E-05	2.3300E+07	3.9378E+05	4.3771E-03
	400	2.2190E-05	1.0447E+07	1.5984E+05	3.5535E-03
	1000	1.0420E-05	4.9058E+06	6.3285E+04	3.5173E-03
	2000	4.0100E-06	1.8879E+06	2.9074E+04	3.2318E-03
	4000	4.0070E-06	1.8865E+06	2.8109E+04	6.2491E-03
	10000	1.0700E-06	5.0377E+05	1.4307E+04	7.9515E-03
	20000	4.0180E-07	1.8917E+05	5.7319E+03	6.3713E-03
	40000	4.6720E-07	2.1996E+05	6.9288E+03	1.5404E-02
	100000	3.2470E-07	1.5287E+05	2.3848E+03	1.3254E-02
CPG/Fe_3O_4/PANI	**100**	8.3200E-05	3.1024E+07	5.7084E+05	3.1726E-03
	120	7.0600E-05	2.6325E+07	4.5806E+05	3.0550E-03
	200	4.7120E-05	1.7570E+07	2.8991E+05	3.2225E-03
	400	2.1080E-05	7.8603E+06	1.2026E+05	2.6736E-03
	1000	9.9000E-06	3.6915E+06	5.4635E+04	3.0365E-03
	2000	3.1900E-06	1.1895E+06	1.2609E+04	1.4015E-03
	4000	3.0300E-06	1.1298E+06	2.5534E+04	5.6766E-03
	10000	1.0663E-06	3.9760E+05	1.1530E+04	6.4084E-03
	20000	3.9970E-07	1.4904E+05	4.2029E+03	4.6718E-03
	40000	3.7980E-07	1.4162E+05	5.1125E+03	1.1366E-02
	100000	2.8940E-07	1.0791E+05	2.0503E+03	1.1395E-02

Table (3.20): LCR measurements of CPG/MWCNTs and CPM/MWCNTs hydrogels at R.T

	F (Hz)	**C (F)**	ε'	ε''	σ **(S/m)**
CPG/MWCNTs	**100**	1.9500E-03	3.0847E+08	2.8997E+06	1.6116E-02
	120	1.4000E-03	2.2147E+08	2.4140E+06	1.6100E-02
	200	1.2300E-03	1.9458E+08	1.7706E+06	1.9682E-02
	400	1.2650E-03	2.0011E+08	2.1412E+06	4.7602E-02
	1000	7.9900E-04	1.2640E+08	1.8327E+06	1.0186E-01
	2000	3.2100E-04	5.0780E+07	1.0715E+06	1.1910E-01
	4000	2.7300E-04	4.3186E+07	1.1056E+06	2.4578E-01
	10000	1.7200E-04	2.7209E+07	8.4402E+05	4.6909E-01
	20000	1.1000E-04	1.7401E+07	5.4988E+05	6.1122E-01
	40000	7.3670E-05	1.1654E+07	3.7293E+05	8.2906E-01
	100000	6.5800E-05	1.0409E+07	3.5391E+05	1.9669E+00
CPM/MWCNTs	**100**	9.8000E-04	1.5134E+08	1.5588E+06	8.6633E-03
	120	8.8000E-04	1.3589E+08	1.0736E+06	7.1600E-03
	200	7.6000E-04	1.1736E+08	1.0093E+06	1.1219E-02
	400	7.5520E-04	1.1662E+08	7.8137E+05	1.7371E-02
	1000	4.1315E-04	6.3801E+07	7.3371E+05	4.0778E-02
	2000	3.7890E-04	5.8512E+07	8.3087E+05	9.2356E-02
	4000	1.3370E-04	2.0647E+07	3.3448E+05	7.4358E-02
	10000	1.2190E-04	1.8824E+07	4.0096E+05	2.2285E-01
	20000	6.7900E-05	1.0485E+07	2.7577E+05	3.0653E-01
	40000	5.0450E-05	7.7908E+06	2.1970E+05	4.8842E-01
	100000	4.6890E-05	7.2410E+06	2.1361E+05	1.1872E+00

Table (3.21): LCR measurements of PgA/MWCNTs and CgA/MWCNTs hydrogels at R.T.

	F (Hz)	**C (F)**	ε'	ε''	σ **(S/m)**
PgA/MWCNTs	**100**	6.7800E-04	1.0215E+08	9.9082E+05	5.5068E-03
	120	4.7800E-04	7.2015E+07	6.4093E+05	4.2746E-03
	200	4.1200E-04	6.2072E+07	4.9657E+05	5.5197E-03
	400	4.1250E-04	6.2147E+07	4.4124E+05	9.8094E-03
	1000	2.9970E-04	4.5153E+07	4.1089E+05	2.2836E-02
	2000	1.8830E-04	2.8369E+07	3.3476E+05	3.7210E-02
	4000	1.5070E-04	2.2704E+07	3.3375E+05	7.4197E-02
	10000	9.9700E-05	1.5021E+07	2.7187E+05	1.5110E-01
	20000	8.0400E-05	1.2113E+07	2.7618E+05	3.0699E-01
	40000	7.0500E-05	1.0621E+07	2.7934E+05	6.2102E-01
	100000	6.6200E-05	9.9736E+06	2.8126E+05	1.5632E+00
CgA/MWCNTs	**100**	5.8300E-04	9.0030E+07	9.3631E+05	5.2038E-03
	120	4.0900E-04	6.3160E+07	6.1897E+05	4.1281E-03
	200	3.9900E-04	6.1616E+07	5.4222E+05	6.0271E-03
	400	4.0550E-04	6.2620E+07	4.9469E+05	1.0998E-02
	1000	3.1230E-04	4.8227E+07	4.5333E+05	2.5195E-02
	2000	2.9940E-04	4.6235E+07	5.1321E+05	5.7046E-02
	4000	1.8050E-04	2.7874E+07	3.7630E+05	8.3655E-02
	10000	9.7300E-05	1.5026E+07	2.5844E+05	1.4364E-01
	20000	9.0800E-05	1.4022E+07	3.0007E+05	3.3354E-01
	40000	7.0800E-05	1.0933E+07	2.7771E+05	6.1738E-01
	100000	6.0200E-05	9.2964E+06	2.5565E+05	1.4209E+00

Table (3.22): LCR measurements of PPM/MWCNTs and IPN/MWCNTs hydrogels at R.T.

	F (Hz)	**C (F)**	ε'	ε''	σ **(S/m)**
PPM/MWCNTs	**100**	9.0300E-04	1.4285E+08	1.4856E+06	8.2567E-03
	120	8.2300E-04	1.3019E+08	1.0676E+06	7.1200E-03
	200	7.1200E-04	1.1263E+08	9.7991E+05	1.0892E-02
	400	6.2800E-04	9.9345E+07	6.4574E+05	1.4356E-02
	1000	3.9810E-04	6.2976E+07	6.6125E+05	3.6751E-02
	2000	3.4427E-04	5.4461E+07	7.2977E+05	8.1119E-02
	4000	2.9840E-04	4.7205E+07	7.4111E+05	1.6476E-01
	10000	1.1800E-04	1.8667E+07	3.6027E+05	2.0023E-01
	20000	6.3500E-05	1.0045E+07	2.4209E+05	2.6910E-01
	40000	5.5400E-05	8.7638E+06	2.3487E+05	5.2215E-01
	100000	4.8100E-05	7.6090E+06	2.1229E+05	1.1799E+00
IPN/MWCNTs	**100**	1.3300E-03	2.0038E+08	2.1641E+06	1.2027E-02
	120	1.1700E-03	1.7627E+08	1.5159E+06	1.0110E-02
	200	1.0500E-03	1.5819E+08	1.4554E+06	1.6177E-02
	400	1.0190E-03	1.5352E+08	1.2128E+06	2.6962E-02
	1000	6.1280E-04	9.2324E+07	1.1264E+06	6.2600E-02
	2000	2.4500E-04	3.6911E+07	5.9058E+05	6.5647E-02
	4000	1.8970E-04	2.8580E+07	5.8589E+05	1.3025E-01
	10000	1.2270E-04	1.8486E+07	4.9727E+05	2.7637E-01
	20000	1.0350E-04	1.5593E+07	4.4908E+05	4.9918E-01
	40000	6.4600E-05	9.7326E+06	3.0171E+05	6.7074E-01
	100000	5.0900E-05	7.6685E+06	2.5306E+05	1.4065E+00

Table(3.23) LCR measurements of CPG/G and CPM/G hydrogels at R.T.

	F (Hz)	**C (F)**	ε'	ε''	σ **(S/m)**
CPG/G	**100**	1.5280E-02	2.7625E+09	1.4917E+07	8.2908E-02
	120	1.3790E-02	2.4931E+09	1.4211E+07	9.4776E-02
	200	1.1500E-02	2.0791E+09	1.2682E+07	1.4097E-01
	400	5.9900E-03	1.0829E+09	1.1154E+07	2.4797E-01
	1000	1.2200E-03	2.2056E+08	2.5365E+06	1.4097E-01
	2000	5.2890E-04	9.5620E+07	1.1474E+06	1.2755E-01
	4000	3.1570E-04	5.7076E+07	7.0203E+05	1.5607E-01
	10000	7.8400E-05	1.4174E+07	1.6442E+05	9.1381E-02
	20000	6.2340E-05	1.1271E+07	1.3750E+05	1.5284E-01
	40000	5.4890E-05	9.9236E+06	1.3893E+05	3.0886E-01
	100000	5.0320E-05	9.0974E+06	1.2100E+05	6.7247E-01
CPM/G	**100**	9.9000E-03	1.6034E+09	1.2667E+07	7.0399E-02
	120	7.4000E-03	1.1985E+09	5.0337E+06	3.3571E-02
	200	6.3000E-03	1.0203E+09	6.5302E+06	7.2587E-02
	400	4.2000E-03	6.8023E+08	5.7139E+06	1.2703E-01
	1000	1.1110E-03	1.7994E+08	1.7634E+06	9.8005E-02
	2000	3.5090E-04	5.6831E+07	5.7968E+05	6.4435E-02
	4000	2.1650E-04	3.5064E+07	4.8388E+05	1.0757E-01
	10000	6.0400E-05	9.7823E+06	1.2130E+05	6.7416E-02
	20000	5.5010E-05	8.9093E+06	1.2117E+05	1.3468E-01
	40000	4.8700E-05	7.8874E+06	1.1279E+05	2.5074E-01
	100000	4.5900E-05	7.4339E+06	8.2516E+04	4.5861E-01

Table (3.24): LCR measurements of PgA/G and CgA/G hydrogels at R.T.

	F (Hz)	C (F)	ε'	ε''	σ (S/m)
PgA/G	**100**	7.9000E-03	1.2497E+09	8.9980E+06	5.0009E-02
	120	6.8000E-03	1.0757E+09	3.9801E+06	2.6545E-02
	200	4.5000E-03	7.1186E+08	3.5593E+06	3.9564E-02
	400	3.6000E-03	5.6949E+08	4.5559E+06	1.0128E-01
	1000	1.0550E-03	1.6689E+08	1.4520E+06	8.0697E-02
	2000	3.0890E-04	4.8866E+07	4.4468E+05	4.9428E-02
	4000	1.9890E-04	3.1464E+07	3.4296E+05	7.6245E-02
	10000	5.4300E-05	8.5898E+06	9.7065E+04	5.3947E-02
	20000	4.9300E-05	7.7989E+06	1.0606E+05	1.1790E-01
	40000	4.4200E-05	6.9921E+06	8.3905E+04	1.8653E-01
	100000	3.9600E-05	6.2644E+06	7.7679E+04	4.3172E-01
CgA/G	**100**	5.9000E-03	8.8889E+08	5.9556E+06	3.3100E-02
	120	4.2000E-03	6.3277E+08	2.9740E+06	1.9835E-02
	200	3.1000E-03	4.6704E+08	2.4753E+06	2.7515E-02
	400	2.7000E-03	4.0678E+08	2.9288E+06	6.5111E-02
	1000	1.0120E-03	1.5247E+08	1.2960E+06	7.2027E-02
	2000	2.8820E-04	4.3420E+07	4.2986E+05	4.7781E-02
	4000	1.6030E-04	2.4151E+07	2.5117E+05	5.5837E-02
	10000	4.8200E-05	7.2618E+06	8.0606E+04	4.4799E-02
	20000	4.5900E-05	6.9153E+06	8.7132E+04	9.6853E-02
	40000	3.9100E-05	5.8908E+06	6.8333E+04	1.5191E-01
	100000	3.6300E-05	5.4689E+06	7.0549E+04	3.9210E-01

Table (3.25): LCR measurements of PPM/G and IPN/G hydrogels at R.T.

	F (Hz)	C (F)	ε'	ε''	σ (S/m)
PPM/G	**100**	8.2200E-03	1.2384E+09	9.4120E+06	5.2310E-02
	120	6.0400E-03	9.0998E+08	3.9129E+06	2.6097E-02
	200	5.5000E-03	8.2863E+08	4.8060E+06	5.3422E-02
	400	2.8000E-03	4.2185E+08	3.1638E+06	7.0336E-02
	1000	1.0890E-03	1.6407E+08	1.5094E+06	8.3891E-02
	2000	3.1280E-04	4.7126E+07	4.5241E+05	5.0288E-02
	4000	2.1020E-04	3.1669E+07	4.0852E+05	9.0820E-02
	10000	5.7200E-05	8.6177E+06	1.0341E+05	5.7475E-02
	20000	5.1900E-05	7.8192E+06	1.0712E+05	1.1907E-01
	40000	4.8100E-05	7.2467E+06	8.9859E+04	1.9977E-01
	100000	4.0700E-05	6.1318E+06	6.3771E+04	3.5443E-01
IPN/G	**100**	1.2900E-02	2.1864E+09	1.7492E+07	9.7214E-02
	120	1.1200E-02	1.8983E+09	8.9220E+06	5.9504E-02
	200	9.6000E-03	1.6271E+09	1.1390E+07	1.2660E-01
	400	7.3000E-03	1.2373E+09	1.1507E+07	2.5581E-01
	1000	1.1990E-03	2.0322E+08	2.1135E+06	1.1746E-01
	2000	4.9890E-04	8.4559E+07	9.3015E+05	1.0339E-01
	4000	2.8850E-04	4.8898E+07	7.3347E+05	1.6306E-01
	10000	9.9600E-05	1.6881E+07	2.0764E+05	1.1540E-01
	20000	7.0500E-05	1.1949E+07	1.5653E+05	1.7400E-01
	40000	7.5900E-05	1.2864E+07	1.7238E+05	3.8323E-01
	100000	5.0300E-05	8.5254E+06	1.0316E+05	5.7333E-01

Table (3.26): LCR measurements of CPG/PANI and CPM/PANI hydrogels at R.T.

	F (Hz)	C (F)	ε'	ε''	σ (S/m)
CPG/PANI	**100**	8.3200E-05	2.9770E+07	5.0014E+05	2.7797E-03
	120	7.0050E-05	2.5065E+07	3.6846E+05	2.4574E-03
	200	4.0120E-05	1.4356E+07	2.3112E+05	2.5691E-03
	400	1.9300E-05	6.9058E+06	1.0152E+05	2.2568E-03
	1000	8.1200E-06	2.9055E+06	3.5737E+04	1.9862E-03
	2000	3.5780E-06	1.2803E+06	1.9076E+04	2.1204E-03
	4000	3.9990E-06	1.4309E+06	2.0462E+04	4.5489E-03
	10000	1.0200E-06	3.6497E+05	9.9272E+03	5.5174E-03
	20000	3.9580E-07	1.4162E+05	3.8946E+03	4.3291E-03
	40000	3.6490E-07	1.3057E+05	3.9431E+03	8.7660E-03
	100000	2.9715E-07	1.0632E+05	1.6055E+03	8.9231E-03
CPM/PANI	**100**	7.8560E-05	2.6039E+07	3.9579E+05	2.1997E-03
	120	6.7810E-05	2.2476E+07	3.1241E+05	2.0836E-03
	200	3.6600E-05	1.2131E+07	1.8439E+05	2.0496E-03
	400	1.6070E-05	5.3264E+06	7.7765E+04	1.7288E-03
	1000	5.1800E-06	1.7169E+06	2.0260E+04	1.1260E-03
	2000	3.0500E-06	1.0109E+06	1.4355E+04	1.5957E-03
	4000	2.9800E-06	9.8772E+05	1.3235E+04	2.9424E-03
	10000	1.0100E-06	3.3476E+05	8.7374E+03	4.8560E-03
	20000	3.7847E-07	1.2544E+05	3.3243E+03	3.6951E-03
	40000	3.5070E-07	1.1624E+05	3.3361E+03	7.4165E-03
	100000	2.6860E-07	8.9027E+04	1.2197E+03	6.7787E-03

Table (3.27): LCR measurements of PgA/PANI and CgA/PANI hydrogels at R.T.

	F (Hz)	**C (F)**	ε'	ε''	σ **(S/m)**
PgA/PANI	**100**	7.6190E-05	1.8653E+07	3.1337E+05	1.7416E-03
	120	6.4880E-05	1.5884E+07	2.4144E+05	1.6102E-03
	200	3.8320E-05	9.3815E+06	1.3416E+05	1.4912E-03
	400	1.8870E-05	4.6198E+06	6.2829E+04	1.3968E-03
	1000	6.2400E-06	1.5277E+06	1.6346E+04	9.0849E-04
	2000	3.5500E-06	8.6911E+05	1.1646E+04	1.2945E-03
	4000	2.4300E-06	5.9492E+05	7.3769E+03	1.6400E-03
	10000	1.0220E-06	2.5021E+05	6.3553E+03	3.5321E-03
	20000	3.7760E-07	9.2444E+04	2.5052E+03	2.7847E-03
	40000	3.4022E-07	8.3293E+04	2.5321E+03	5.6292E-03
	100000	2.7088E-07	6.6317E+04	9.0854E+02	5.0495E-03
CgA/PANI	**100**	7.7890E-05	2.0536E+07	3.4295E+05	1.9061E-03
	120	6.5190E-05	1.7188E+07	2.8016E+05	1.8685E-03
	200	3.7440E-05	9.8712E+06	1.4215E+05	1.5800E-03
	400	1.7990E-05	4.7431E+06	6.4981E+04	1.4446E-03
	1000	5.8600E-06	1.5450E+06	1.8386E+04	1.0218E-03
	2000	4.0900E-06	1.0783E+06	1.5097E+04	1.6781E-03
	4000	3.0200E-06	7.9623E+05	1.0351E+04	2.3012E-03
	10000	1.0080E-06	2.6576E+05	6.8035E+03	3.7813E-03
	20000	3.8028E-07	1.0026E+05	2.7472E+03	3.0537E-03
	40000	3.3844E-07	8.9231E+04	2.6502E+03	5.8916E-03
	100000	2.6633E-07	7.0219E+04	1.0322E+03	5.7369E-03

Table (3.28): LCR measurements of PPM/PANI and IPN/PANI hydrogels at R.T.

	F (Hz)	**C (F)**	ε'	ε''	σ **(S/m)**
PPM/PANI	**100**	7.7360E-05	2.3310E+07	3.5664E+05	1.9821E-03
	120	6.6090E-05	1.9914E+07	2.9274E+05	1.9524E-03
	200	3.7910E-05	1.1423E+07	1.6449E+05	1.8284E-03
	400	1.5050E-05	4.5348E+06	6.5302E+04	1.4517E-03
	1000	5.2400E-06	1.5789E+06	1.7368E+04	9.6528E-04
	2000	3.1700E-06	9.5518E+05	1.3181E+04	1.4652E-03
	4000	2.9500E-06	8.8889E+05	1.1556E+04	2.5689E-03
	10000	1.0160E-06	3.0614E+05	7.8984E+03	4.3898E-03
	20000	3.6610E-07	1.1031E+05	2.8792E+03	3.2004E-03
	40000	3.4750E-07	1.0471E+05	3.1203E+03	6.9368E-03
	100000	2.6978E-07	8.1290E+04	1.0405E+03	5.7829E-03
IPN/PANI	**100**	8.0050E-05	2.8040E+07	4.3743E+05	2.4311E-03
	120	6.8890E-05	2.4131E+07	3.4266E+05	2.2853E-03
	200	3.8270E-05	1.3405E+07	2.0912E+05	2.3245E-03
	400	1.6540E-05	5.7937E+06	8.7484E+04	1.9449E-03
	1000	6.6800E-06	2.3399E+06	2.7845E+04	1.5476E-03
	2000	3.3900E-06	1.1875E+06	1.6981E+04	1.8875E-03
	4000	3.1500E-06	1.1034E+06	1.5227E+04	3.3851E-03
	10000	1.0150E-06	3.5554E+05	9.5284E+03	5.2957E-03
	20000	3.7623E-07	1.3179E+05	3.5187E+03	3.9113E-03
	40000	3.4507E-07	1.2087E+05	3.5174E+03	7.8195E-03
	100000	2.7690E-07	9.6993E+04	1.3870E+03	7.7087E-03

3.4 Study of drug release

3.4.1 Study of drug release of PANI composite at 8V and room temperature

The indigo carmine was used in this study as drug model. Indigo carmine loading on (hydrogels/ PANI) formulations were immersed in 65 mL of PBS (pH 7.4; R.T). A 5cm gold electrode was used as the cathode and a 5 cm gold electrode was used as the anode. The conductive hydrogels are placed directly on the two electrodes and the potential difference is kept between the two electrodes. In this study, (hydrogels / PANI) formulations were synthesized and loaded it with dye, (8V) is potential applied to each shape respectively. The potential difference was kept for measurement times and 3 mL PBS was measured by UV-Vis analysis for intervals time with replacement of fresh PBS medium after the applied of the electrical stimulation to maintain sink conditions. The amount of drug release was obtained in (fig 3. 114).

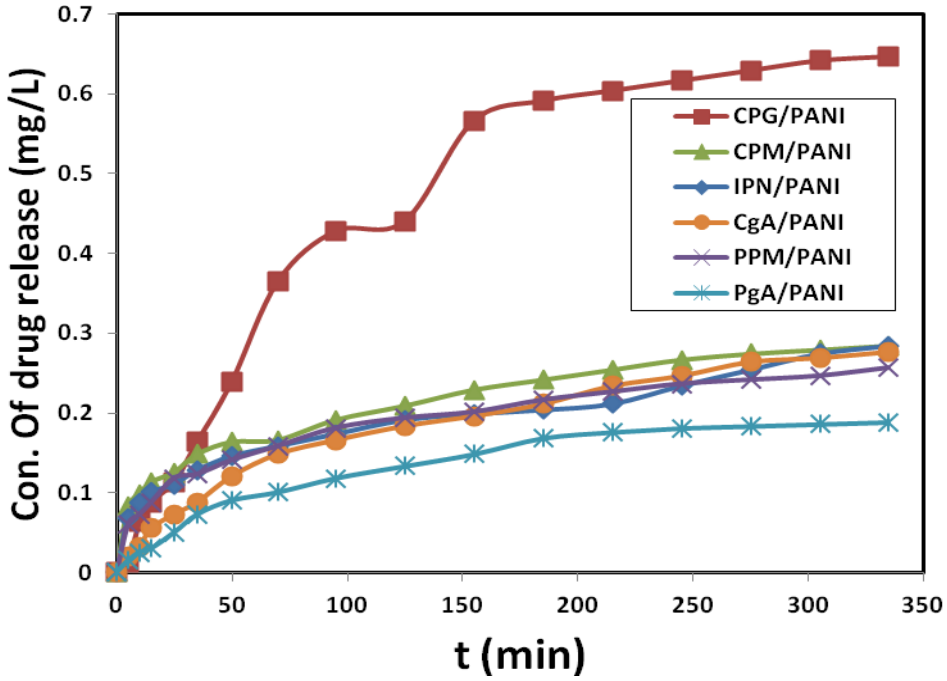

Figure (3.114): Indigo release from PANI composites at R.T. and Voltage=8

From figure (3.114) is a show the drug release for (hydrogels/PANI) was increased with time. The CPG/PANI composite was greater than other hydrogels, unlike results of swelling for (hydrogels/PANI) composite. This was explained by conductivity of this hydrogel which obtained from LCR measurements comparison with other hydrogel (see table 3.26). Also may be returned to difference medium from

distilled water (pH=6.5) to PBS (pH=7.4), the polycationic nature of native chitosan. Chitosan pKa is (6.2-7), [233, 234], so that its amino terminations are protonated in distilled water (pH 6.5), while they are likely neutralized in PBS (0.01 M, pH 7.4). This effect is reduced in crosslinked chitosan and inversely-related to the network crosslinking density because when immersed hydrogel in indigo carmine aqueous solution for one day, where in aqueous solution , sulfonic acid groups of drug will be able to mediate additional electrostatic crosslinks with free, protonated amino groups, and when placed in electro cell which contained to PBS solution . At this time, the electrostatic interactions may be disappears in (PBS), since the free amino groups hydrogel are neutralized in these conditions. Consequently, the hydrogel expelled the drug out, because the electrostatic repulsion between negatively-charged sulfonic acid moieties of drug.

Drug release concentration was obtained from calibration curve while the percentage of drug release was measured by equation (3.2):

$$\%Drug\ Rlease = [1 - \frac{A_0 - A_t}{A_0}] \times 100 \text{-----------} (3.2)$$

Where, A_0 indicates absorbance of the model drug solution before loading on hydrogel sample, while A_t, describes the absorbance of drug release from hydrogel which stimulated by electric voltage [219].The concentration and percentage of indigo release from (PANI) composite was recorded in table (3.29, 3.30).

Table (3.29): Indigo release from CPG/PANI, CPM/PANI , and PPM/PANI composites in 65ml of phosphate buffer solution (0.01M),Initial concentration of indigo solution (5mg/L)at R.T ,voltage=8Volt

	CPG/PANI		CPM/PANI		PPM/PANI	
Time (min)	**Conc. of indigo release (mg/L)**	**%Drug release**	**Conc. of indigo release (mg/L)**	**%Drug release**	**Conc. of indigo release (mg/L)**	**%Drug release**
5	0.013	0.253	0.083	1.673	0.060	1.216
10	0.063	1.267	0.098	1.977	0.073	1.470
15	0.088	1.774	0.113	2.281	0.088	1.774
25	0.113	2.281	0.126	2.534	0.118	2.382
35	0.164	3.294	0.148	2.990	0.123	2.484
50	0.239	4.815	0.164	3.294	0.141	2.838
70	0.365	7.349	0.166	3.345	0.159	3.193
95	0.428	8.616	0.191	3.852	0.181	3.649
125	0.440	8.870	0.209	4.207	0.194	3.903
155	0.566	11.404	0.229	4.612	0.201	4.055
185	0.591	11.911	0.242	4.866	0.216	4.359
215	0.604	12.164	0.254	5.119	0.226	4.562
245	0.617	12.418	0.267	5.373	0.237	4.764
275	0.629	12.671	0.274	5.525	0.242	4.866
305	0.642	12.924	0.279	5.626	0.247	4.967
335	0.647	13.026	0.284	5.727	0.257	5.170

Table (3.30): Indigo release from PgA/PANI, CgA/PANI , and IPN/PANI composites in 65ml of phosphate buffer solution (0.01M),Initial concentration of indigo solution (5mg/L)at R.T ,voltage=8Volt

	PgA/PANI		CgA/PANI		IPN/PANI	
Time (min)	**Conc. of indigo release (mg/L)**	**%Drug release**	**Conc. of indigo release (mg/L)**	**%Drug release**	**Conc. of indigo release (mg/L)**	**%Drug release**
5	0.015	0.304	0.020	0.405	0.068	1.368
10	0.025	0.507	0.033	0.659	0.088	1.774
15	0.030	0.608	0.055	1.115	0.101	2.027
25	0.050	1.014	0.073	1.470	0.111	2.230
35	0.073	1.470	0.088	1.774	0.128	2.585
50	0.091	1.825	0.121	2.433	0.146	2.940
70	0.101	2.027	0.148	2.990	0.159	3.193
95	0.118	2.382	0.166	3.345	0.174	3.497
125	0.133	2.686	0.184	3.700	0.191	3.852
155	0.148	2.990	0.196	3.953	0.199	4.004
185	0.169	3.396	0.211	4.257	0.204	4.105
215	0.176	3.548	0.234	4.714	0.211	4.257
245	0.181	3.649	0.247	4.967	0.234	4.714
275	0.184	3.700	0.264	5.322	0.254	5.119
305	0.186	3.751	0.269	5.423	0.274	5.525
335	0.189	3.801	0.277	5.575	0.284	5.727

3.4.2 Study of drug release of G composite at 2V and room temperature

The indigo carmine also used in this study as drug model. The drug release of hydrogels/G composite is shows in (fig. 3.115); the same method for procedure previous was used. Also the CPG/G composite was greater than other hydrogels, unlike results of swelling for (hydrogels/G) composite. This was explained by conductivity of this hydrogel which obtained from LCR measurements comparison with other hydrogel (see table 3.23), and other reasons was previously reported.

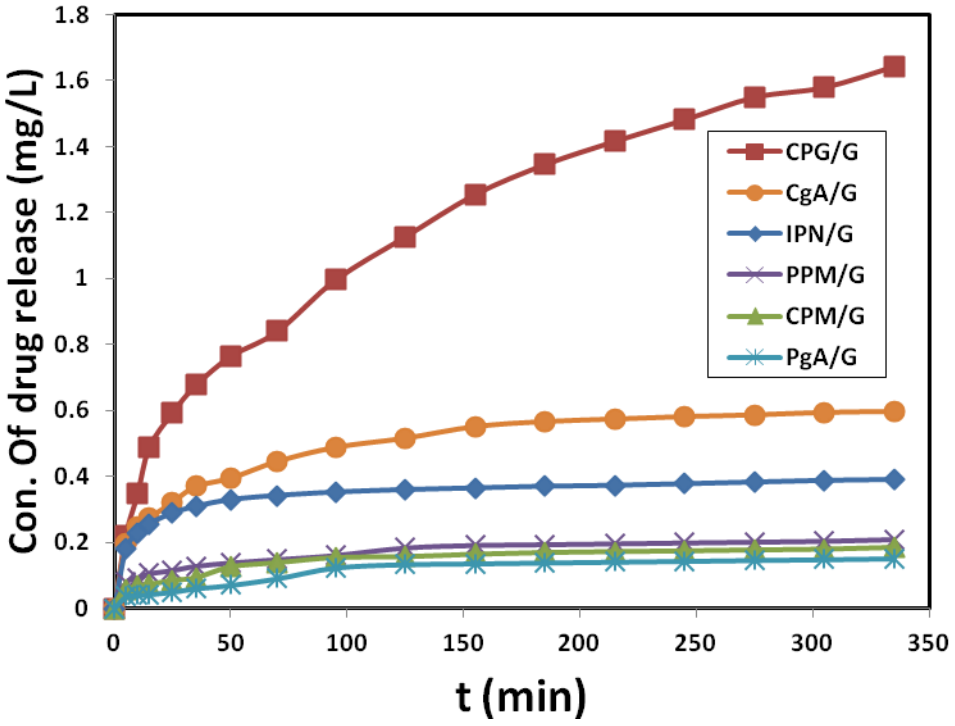

Figure (3.115): Indigo release from G composites at R.T. and Voltage=2

From figure above was observed the drug release ratio from hydrogel/G composite was greater than the drug release ratio from (hydrogels/PANI) composite. This was explained by difference of electric conductivity values for G and PANI, where from measurements of LCR was observed the electrical conductivity of G was greater than PANI (see table3.18, 3.19).

The concentration and percentage of indigo release from hydrogel /G composite were recorded in table (3.31, 3.32).

Table (3.31): Indigo release from CPG/G, CPM/G , and PPM/G composites in 65ml of phosphate buffer solution (0.01M),Initial concentration of indigo solution (5mg/L)at R.T ,voltage=2Volt

	CPG/G		CPM/G		PPM/G	
Time (min)	**Conc. of indigo release (mg/L)**	**%Drug release**	**Conc. of indigo release (mg/L)**	**%Drug release**	**Conc. of indigo release (mg/L)**	**%Drug release**
5	0.221	4.460	0.055	1.115	0.078	1.571
10	0.347	6.994	0.068	1.368	0.093	1.875
15	0.488	9.833	0.073	1.470	0.106	2.129
25	0.594	11.961	0.086	1.723	0.116	2.331
35	0.677	13.634	0.093	1.875	0.128	2.585
50	0.765	15.408	0.126	2.534	0.138	2.788
70	0.840	16.929	0.138	2.788	0.148	2.990
95	0.996	20.071	0.153	3.092	0.161	3.244
125	1.127	22.707	0.156	3.142	0.184	3.700
155	1.256	25.291	0.164	3.294	0.191	3.852
185	1.346	27.116	0.169	3.396	0.194	3.903
215	1.417	28.535	0.171	3.447	0.196	3.953
245	1.482	29.853	0.174	3.497	0.199	4.004
275	1.550	31.221	0.176	3.548	0.201	4.055
305	1.580	31.830	0.179	3.599	0.204	4.105
335	1.643	33.097	0.184	3.700	0.209	4.207

Table (3.32): Indigo release from PgA/G, CgA/G , and IPN/G composites in 65ml of phosphate buffer solution (0.01M),Initial concentration of indigo solution (5mg/L)at R.T ,voltage=2Volt

	PgA/G		CgA/G		IPN/G	
Time (min)	**Conc. of indigo release (mg/L)**	**%Drug release**	**Conc. of indigo release (mg/L)**	**%Drug release**	**Conc. of indigo release (mg/L)**	**%Drug release**
5	0.035	0.710	0.196	3.953	0.181	3.649
10	0.040	0.811	0.247	4.967	0.229	4.612
15	0.043	0.862	0.274	5.525	0.257	5.170
25	0.050	1.014	0.322	6.488	0.289	5.829
35	0.060	1.216	0.370	7.451	0.310	6.234
50	0.070	1.419	0.395	7.957	0.330	6.640

70	0.091	1.825	0.445	8.971	0.342	6.893
95	0.123	2.484	0.488	9.833	0.352	7.096
125	0.133	2.686	0.516	10.390	0.360	7.248
155	0.136	2.737	0.551	11.100	0.365	7.349
185	0.138	2.788	0.566	11.404	0.370	7.451
215	0.141	2.838	0.574	11.556	0.372	7.501
245	0.143	2.889	0.581	11.708	0.377	7.603
275	0.146	2.940	0.586	11.809	0.382	7.704
305	0.148	2.990	0.594	11.961	0.388	7.805
335	0.151	3.041	0.596	12.012	0.390	7.856

3.4.3 Study of drug release of MWCNTs composite at 2V and room temperature

The indigo carmine also used in this study as drug model. The drug release of hydrogels/MWCNTs composite is shows in (fig 3.116); the same method for procedure previous was used. Also the CPG/MWCNTs composite was greater than other hydrogels, unlike results of swelling for (hydrogels/MWCNTs) composite. This was explained by conductivity of this hydrogel which obtained from LCR measurements comparison with other hydrogel (see table 3.20), and other reasons was previously reported.

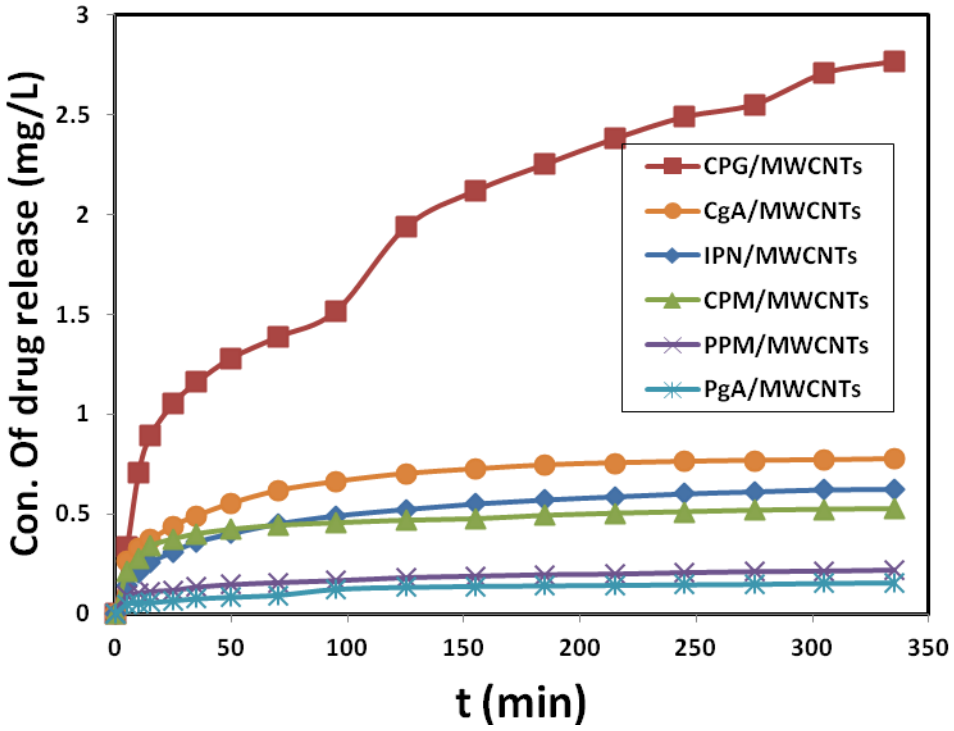

Figure (3.116): Indigo release from MWCNTs composites at R.T. and Voltage=2

From figure above was observed the drug release ratio from (hydrogel/MWCNTs) composite was greatest the drug release ratio from (hydrogels/PANI) and (hydrogels/G) composites. This was explained by difference of electric conductivity values for MWCNTs, G and PANI, where from measurements of LCR was observed the electrical conductivity of MWCNTs was greatest the electrical conductivity of G and PANI (see table 3.18, 3.19).

The concentration and percentage of indigo release from hydrogel/MWCNTs composite were recorded in tables (3.33, & 3.34).

Table (3.33): Indigo release from CPG/MWCNTs, CPM/MWCNTs, and PPM/MWCNTs composites in 65ml of phosphate buffer solution (0.01M),Initial concentration of indigo solution (5mg/L)at R.T ,voltage=2Volt

	CPG/MWCNTs		CPM/MWCNTs		PPM/MWCTs	
Time (min)	**Conc. of indigo release (mg/L)**	**%Drug release**	**Conc. of indigo release (mg/L)**	**%Drug release**	**Conc. of indigo release (mg/L)**	**%Drug release**
5	0.332	6.690	0.211	4.257	0.088	1.774
10	0.707	14.242	0.279	5.626	0.101	2.027
15	0.891	17.942	0.340	6.842	0.111	2.230
25	1.054	21.237	0.375	7.552	0.118	2.382
35	1.160	23.365	0.400	8.059	0.133	2.686
50	1.281	25.798	0.423	8.515	0.146	2.940
70	1.387	27.927	0.443	8.920	0.156	3.142
95	1.517	30.563	0.455	9.174	0.166	3.345
125	1.938	39.027	0.468	9.427	0.181	3.649
155	2.119	42.676	0.476	9.579	0.189	3.801
185	2.252	45.362	0.493	9.934	0.196	3.953
215	2.380	47.947	0.503	10.137	0.199	4.004
245	2.489	50.127	0.511	10.289	0.206	4.156
275	2.552	51.394	0.518	10.441	0.211	4.257
305	2.708	54.536	0.523	10.542	0.214	4.308
335	2.765	55.702	0.526	10.593	0.219	4.410

Table (3.34): Indigo release from PgA/MWCNTs, CgA/MWCNTs , and IPN/MWCNTs composites in 65ml of phosphate buffer solution (0.01M),Initial concentration of indigo solution (5mg/L)at R.T. ,voltage=2Volt

	PgA/MWCNTs		CgA/MWCNTs		IPN/MWCNTs	
Time (min)	**Conc. of indigo release (mg/L)**	**%Drug release**	**Conc. of indigo release (mg/L)**	**%Drug release**	**Conc. of indigo release (mg/L)**	**%Drug release**
5	0.048	0.963	0.262	5.271	0.141	2.838
10	0.053	1.064	0.327	6.589	0.209	4.207
15	0.055	1.115	0.370	7.451	0.257	5.170
25	0.065	1.318	0.440	8.870	0.312	6.285
35	0.075	1.521	0.491	9.883	0.360	7.248
50	0.083	1.673	0.554	11.151	0.403	8.109
70	0.093	1.875	0.617	12.418	0.450	9.072
95	0.123	2.484	0.662	13.330	0.491	9.883
125	0.133	2.686	0.702	14.141	0.523	10.542
155	0.138	2.788	0.725	14.597	0.551	11.100
185	0.141	2.838	0.745	15.003	0.571	11.505
215	0.143	2.889	0.755	15.205	0.586	11.809
245	0.146	2.940	0.762	15.357	0.601	12.114
275	0.148	2.990	0.767	15.459	0.611	12.316
305	0.153	3.092	0.770	15.509	0.622	12.519
335	0.156	3.142	0.775	15.611	0.624	12.570

3.4.4 Voltage Optimization of Indigo Release from conductive hydrogel (CPG/PANI) & (CPG/Fe_3O_4/PANI)

(CPG/PANI) & (CPG/Fe_3O_4/PANI) formulations were synthesized and Indigo carmine loading on it with a potential difference ranging from (3 V, 5 V and 8 V) was applied to each formulation respectively using an Ac transformer. The external magnet placed on conductive composite when studying drug release from (CPG/Fe_3O_4/PANI). The amount of drug release was obtained in (fig 3.117, 3.118).

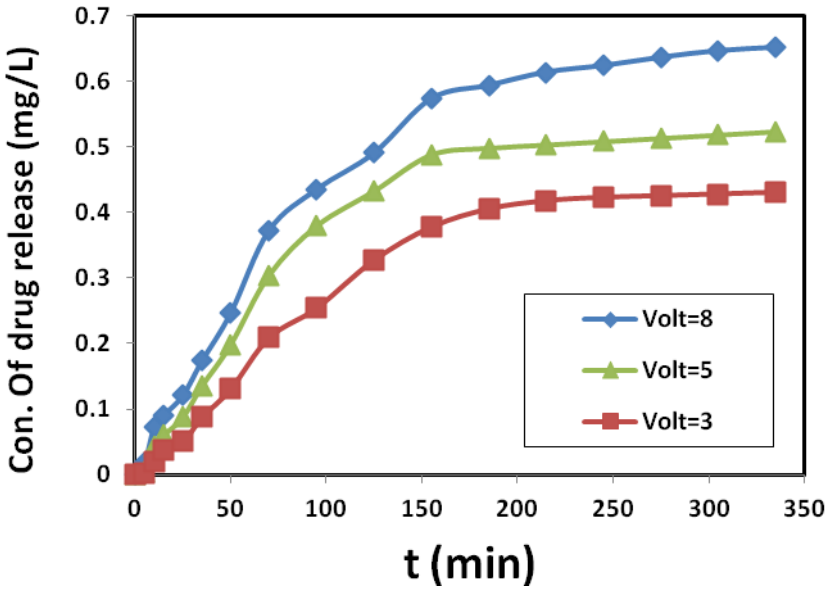

Figure (3.117): Indigo release from (CPG/PANI) composite at 37ºC and difference voltages

From figures (3.117, 3.118) are showing amount of drug release from (CPG/PANI) & (CPG/Fe_3O_4/PANI) hydrogel composites increases with voltages this can be attributed to three forces driving: electrostatic force between electrons of composite hydrogel and drug, the route of modified hydrogel, and expansion of hydrogel composite. Because of electric field application was, the electrons of hydrogel composite push anion drug produced small paths in the hydrogel. So at higher electric field strength, higher amount of indigo release will be occurred. The third driving power, expanding hydrogels, is given a direct result of expanding hydrogel conductive composite pore size after using electric field. When a conductive hydrogel chains expanding, and free space in the hydrogel matrix is being created, thereby electric field pushing ionic drug by electrostatic force. Moreover, the electric field created in the hydrogel micro path while at the same time expanding the mesh size of hydrogel. As a result, amount and rate of drug released increases with applied external electric field.
Also was observed the drug release from (CPG/PANI) greater than from of (CPG/Fe_3O_4/PANI) hydrogel this can be explained by nature of

(CPG/Fe_3O_4/PANI) hydrogel matrix, the presence of magnetite in the matrix of hydrogel was filled some pores of hydrogel matrix, so, the amount of drug release was decreased[235, 236].

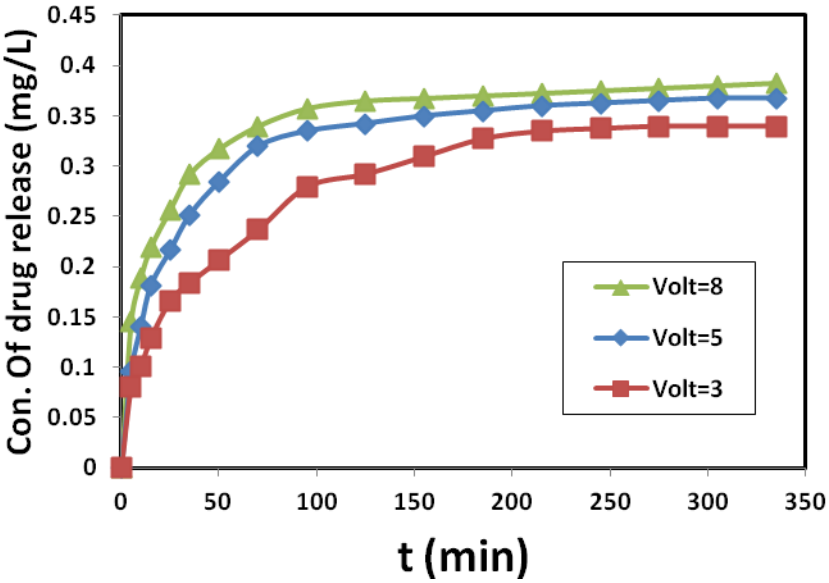

Figure (3.118): Indigo release from (CPG/Fe_3O_4/PANI) composite at 37ºC and difference voltages

The concentration and percentage of indigo release from CPG/PANI and CPG/Fe_3O_4/PANI under voltage effect were recorded in table (3.32) and (3.33), respectively.

Table (3.35): Indigo release from CPG/PANI composite in 65ml of phosphate buffer solution (0.01M),Initial concentration of indigo solution (5mg/L)at 37ºC ,voltage(3,5, and 8)Volt

CPG/PANI						
	Voltage=3		Voltage=5		Voltage=8	
Time (min)	**Conc. of indigo release (mg/L)**	**%Drug release**	**Conc. of indigo release (mg/L)**	**%Drug release**	**Conc. of indigo release (mg/L)**	**%Drug release**
5	0.003	0.051	0.005	0.101	0.018	0.355
10	0.020	0.405	0.043	0.862	0.073	1.470
15	0.038	0.760	0.060	1.216	0.091	1.825
25	0.050	1.014	0.088	1.774	0.121	2.433
35	0.088	1.774	0.136	2.737	0.174	3.497
50	0.131	2.636	0.199	4.004	0.247	4.967
70	0.209	4.207	0.304	6.133	0.372	7.501
95	0.254	5.119	0.380	7.653	0.435	8.768
125	0.327	6.589	0.433	8.718	0.491	9.883
155	0.377	7.603	0.488	9.833	0.574	11.556
185	0.405	8.160	0.498	10.035	0.594	11.961
215	0.418	8.414	0.503	10.137	0.614	12.367
245	0.423	8.515	0.508	10.238	0.624	12.570
275	0.425	8.566	0.513	10.340	0.637	12.823
305	0.428	8.616	0.518	10.441	0.647	13.026
335	0.430	8.667	0.523	10.542	0.652	13.127

Table (3.36): Indigo release from CPG/Fe_3O_4/PANI composite in 65ml of phosphate buffer solution (0.01M),Initial concentration of indigo solution (5mg/L)at 37ºC ,voltage(3,5, and 8)Volt

CPG/Fe_3O_4/PANI						
	Voltage=3		Voltage=5		Voltage=8	
Time (min)	**Conc. of indigo release (mg/L)**	**%Drug release**	**Conc. of indigo release (mg/L)**	**%Drug release**	**Conc. of indigo release (mg/L)**	**%Drug release**
5	0.081	1.622	0.096	1.926	0.146	2.940
10	0.101	2.027	0.141	2.838	0.189	3.801
15	0.128	2.585	0.181	3.649	0.219	4.410
25	0.166	3.345	0.216	4.359	0.257	5.170
35	0.184	3.700	0.252	5.068	0.292	5.879
50	0.206	4.156	0.284	5.727	0.317	6.386
70	0.237	4.764	0.320	6.437	0.340	6.842
95	0.279	5.626	0.335	6.741	0.357	7.197
125	0.292	5.879	0.342	6.893	0.365	7.349
155	0.310	6.234	0.350	7.045	0.367	7.400
185	0.327	6.589	0.355	7.146	0.370	7.451
215	0.335	6.741	0.360	7.248	0.372	7.501
245	0.337	6.792	0.362	7.299	0.375	7.552
275	0.340	6.842	0.365	7.349	0.377	7.603
305	0.340	6.842	0.367	7.400	0.380	7.653
335	0.340	6.842	0.367	7.400	0.382	7.704

3.4.5 Effective of temperature on the indigo Release from conductive hydrogel (CPG/PANI) & (CPG/Fe_3O_4/PANI)

The same work previous re-work done for studying the effect of temperature changes on the drug release from conductive hydrogel (CPG/PANI) & (CPG/Fe_3O_4/PANI) at constant voltage, different temperatures and using external magnet placed on conductive composite when studying drug release from (CPG/Fe_3O_4/PANI). Indigo carmine loading on hydrogel with best potential (8V) and temperature difference ranging along (35.5, 37, & 38.5) ˚C was applied to each formulation respectively. The amount of drug release was obtained in (fig 3.119, 3.120).

From figures (3.119, 3.120) are shows the highest value of amount of the drug release from (CPG/PANI) & (CPG/Fe_3O_4/PANI) hydrogels at 38, and 37˚C, respectively then arrange to order as in figures above. This means at this temperature the hydrogel chains have a higher flexibility than at other temperatures. Thus, drug will be released more easily and consequently nanocarriers can behave specific matrices as thermosensitive [237].

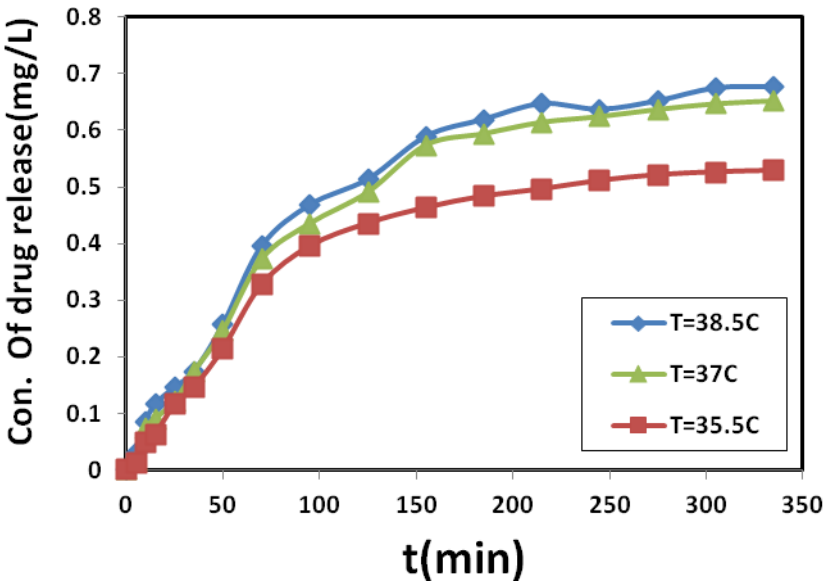

Figure (3.119): Indigo release from (CPG/ PANI) composite at different temperature and 8V

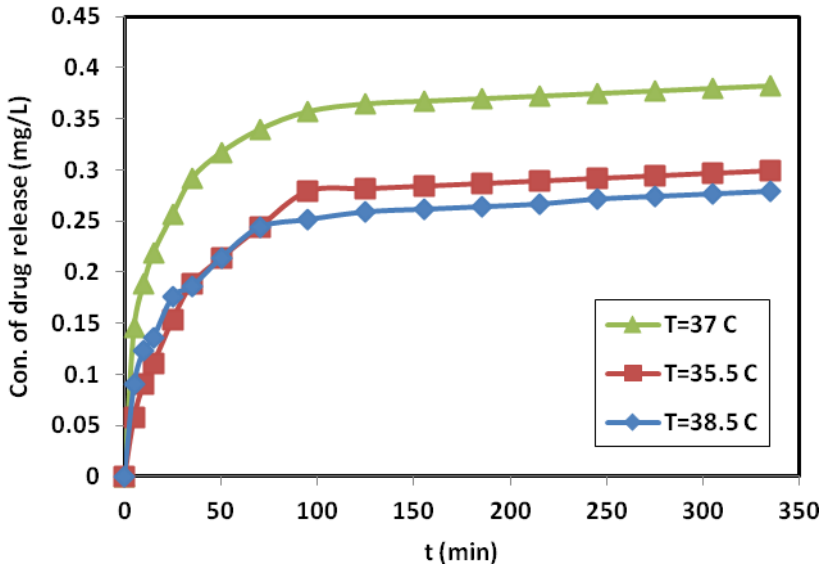

Figure (3.120): Indigo release from (CPG/Fe_3O_4/ PANI) composite at different temperature and 8V

The concentration and percentage of indigo release from CPG/PANI and CPG/Fe_3O_4/PANI under temperature effect were recorded in table (3.37) and (3.38), respectively.

Table (3.37): Indigo release from CPG/PANI composite in 65ml of phosphate buffer solution (0.01M),Initial concentration of indigo solution (5mg/L)at (35.5,37, and 38.5)ºC ,voltage=8Volt

CPG/PANI						
	T=35.5ºC		T=37ºC		T=38.5ºC	
Time (min)	**Conc. of indigo release (mg/L)**	**%Drug release**	**Conc. of indigo release (mg/L)**	**%Drug release**	**Conc. of indigo release (mg/L)**	**%Drug release**
5	0.013	0.253	0.018	0.355	0.030	0.608
10	0.048	0.963	0.073	1.470	0.086	1.723
15	0.063	1.267	0.091	1.825	0.116	2.331
25	0.116	2.331	0.121	2.433	0.146	2.940
35	0.146	2.940	0.174	3.497	0.174	3.497
50	0.214	4.308	0.247	4.967	0.257	5.170
70	0.327	6.589	0.372	7.501	0.395	7.957
95	0.395	7.957	0.435	8.768	0.468	9.427
125	0.435	8.768	0.491	9.883	0.513	10.340
155	0.463	9.326	0.574	11.556	0.589	11.860
185	0.483	9.731	0.594	11.961	0.619	12.468
215	0.496	9.985	0.614	12.367	0.647	13.026
245	0.511	10.289	0.624	12.570	0.637	12.823
275	0.521	10.492	0.637	12.823	0.652	13.127
305	0.526	10.593	0.647	13.026	0.674	13.583
335	0.528	10.644	0.652	13.127	0.677	13.634

Table (3.38): Indigo release from CPG/ Fe_3O_4 /PANI composite in 65ml of phosphate buffer solution (0.01M),Initial concentration of indigo solution (5mg/L)at (35.5,37, and 38.5)ºC ,voltage=8Volt

CPG/Fe_3O_4/PANI						
	T=35.5ºC		T=37ºC		T=38.5ºC	
Time (min)	**Conc. of indigo release (mg/L)**	**%Drug release**	**Conc. of indigo release (mg/L)**	**%Drug release**	**Conc. of indigo release (mg/L)**	**%Drug release**
5	0.058	1.166	0.146	2.940	0.091	1.825
10	0.091	1.825	0.189	3.801	0.123	2.484
15	0.111	2.230	0.219	4.410	0.136	2.737
25	0.153	3.092	0.257	5.170	0.176	3.548
35	0.189	3.801	0.292	5.879	0.186	3.751
50	0.214	4.308	0.317	6.386	0.214	4.308
70	0.244	4.916	0.340	6.842	0.244	4.916
95	0.279	5.626	0.357	7.197	0.252	5.068
125	0.282	5.677	0.365	7.349	0.259	5.220
155	0.284	5.727	0.367	7.400	0.262	5.271
185	0.287	5.778	0.370	7.451	0.264	5.322
215	0.289	5.829	0.372	7.501	0.267	5.373
245	0.292	5.879	0.375	7.552	0.272	5.474
275	0.294	5.930	0.377	7.603	0.274	5.525
305	0.297	5.981	0.380	7.653	0.277	5.575
335	0.299	6.031	0.382	7.704	0.279	5.626

3.4.6 Voltage Optimization of Indigo Release from conductive hydrogel (CPG/G), (CPG/MWCNTs)

The same work previous was used to study the optimization voltage for Indigo release from (CPG/G), (CPG/MWCNTs) composites. The figures (3.121, 3.122) are shows the drug release form (CPG/G), (CPG/MWCNTs) hydrogel composites at different voltages, 37 ºC, the similar behavior of previously composite was observed in the study. The concentration and percentage of indigo release from (CPG/G), (CPG/MWCNTs) hydrogel composites were recorded in tables (3.39, 3.40).

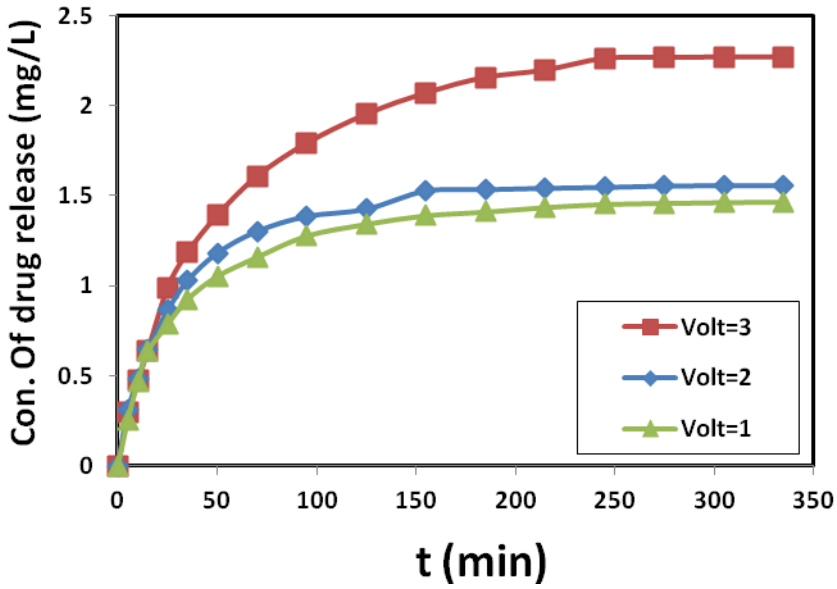

Figure (3.121): Indigo release from (CPG/G) composite at 37ºC and difference voltages

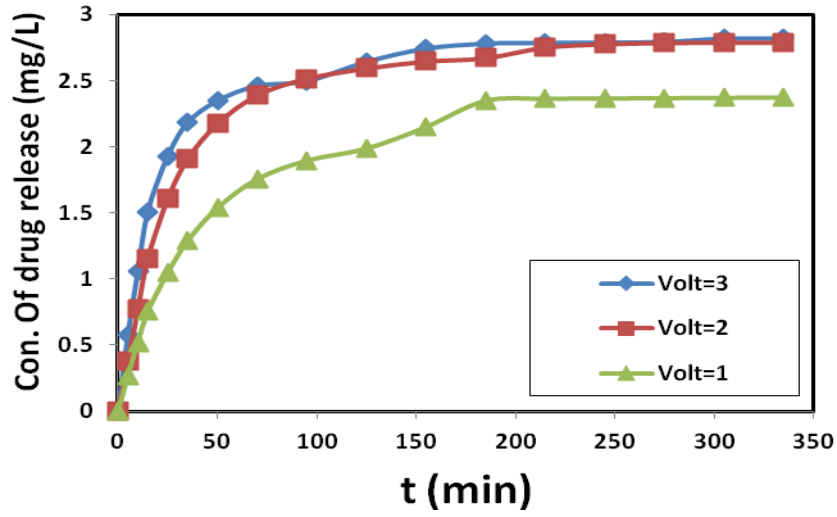

Figure (3.122): Indigo release from (CPG/MWCNTs) composite at different Voltages and 37ºC

Table(3.39): Indigo release from CPG/G hydrogel composite in 65ml of phosphate buffer solution (0.01M),Initial concentration of indigo solution (5mg/L)at 37ºC ,voltage(1,2, and 3)Volt

CPG/G						
	Voltage=1		Voltage=2		Voltage=3	
Time (min)	**Conc. of indigo release (mg/L)**	**%Drug release**	**Conc. of indigo release (mg/L)**	**%Drug release**	**Conc. of indigo release (mg/L)**	**%Drug release**
5	0.257	5.170	0.307	6.183	0.297	5.981
10	0.466	9.377	0.481	9.681	0.476	9.579
15	0.637	12.823	0.642	12.924	0.639	12.874
25	0.788	15.864	0.863	17.385	0.989	19.919
35	0.926	18.652	1.029	20.730	1.185	23.872
50	1.054	21.237	1.183	23.822	1.392	28.028
70	1.160	23.365	1.303	26.254	1.608	32.387
95	1.278	25.748	1.387	27.927	1.792	36.087
125	1.344	27.065	1.427	28.738	1.953	39.331
155	1.392	28.028	1.527	30.765	2.071	41.713
185	1.412	28.434	1.535	30.917	2.157	43.436
215	1.437	28.941	1.543	31.069	2.197	44.247
245	1.454	29.295	1.548	31.171	2.262	45.565
275	1.459	29.397	1.555	31.323	2.267	45.666
305	1.465	29.498	1.558	31.374	2.270	45.717
335	1.467	29.549	1.558	31.374	2.270	45.717

Table(3.40): Indigo release from CPG/MWCNTs hydrogel composite in 65ml of phosphate buffer solution (0.01M),Initial concentration of indigo solution (5mg/L)at 37ºC ,voltage(1,2, and 3)Volt

CPG/MWCNTs						
	Voltage=1		Voltage=2		Voltage=3	
Time (min)	**Conc. of indigo release (mg/L)**	**%Drug release**	**Conc. of indigo release (mg/L)**	**%Drug release**	**Conc. of indigo release (mg/L)**	**%Drug release**
5	0.272	5.474	0.377	7.603	0.579	11.657
10	0.521	10.492	0.773	15.560	1.057	21.287
15	0.755	15.205	1.155	23.264	1.510	30.411
25	1.047	21.085	1.605	32.337	1.928	38.824
35	1.288	25.950	1.907	38.419	2.182	43.943
50	1.537	30.968	2.174	43.791	2.348	47.288
70	1.756	35.378	2.391	48.150	2.461	49.569
95	1.897	38.216	2.516	50.684	2.496	50.279
125	1.988	40.041	2.594	52.255	2.642	53.218
155	2.151	43.335	2.647	53.320	2.743	55.246
185	2.350	47.339	2.672	53.827	2.781	56.006
215	2.365	47.643	2.753	55.449	2.786	56.107
245	2.368	47.694	2.778	55.955	2.788	56.158
275	2.370	47.745	2.788	56.158	2.793	56.260
305	2.373	47.795	2.791	56.209	2.818	56.766
335	2.375	47.846	2.791	56.209	2.818	56.766

3.4.7 Effective of temperature on Indigo Release from conductive hydrogel (CPG/G), (CPG/MWCNTs)

The same work previous re-work done for studying the effect of temperature changes on the drug release from conductive hydrogel (CPG/G),(CPG/MWCNTs). The same behavior previously of composite was observed (see figures 3.123, 3.124). The drug loading values for (CPG/G), (CPG/MWCNTs) under temperature effect were recorded in table (3.41, 3.42).

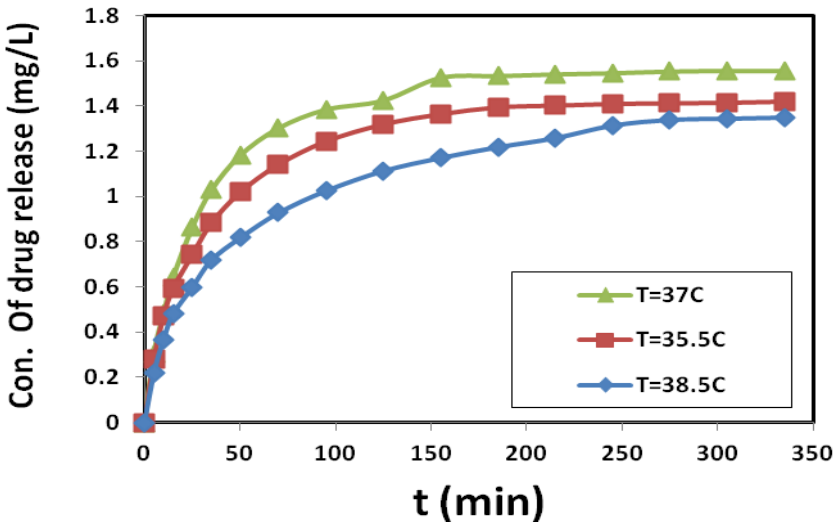

Figure (3.123): Indigo release from (CPG/G) composite at different temperature and 2 V

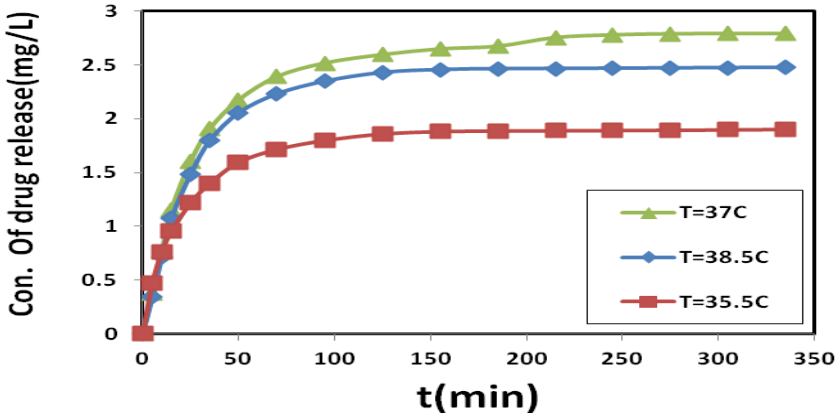

Figure (3.124): Indigo release from (CPG/MWCNTs) composite at different temperature and 2 V

Table (3.41): Indigo release from CPG/G hydrogel composite in 65ml of phosphate buffer solution (0.01M),Initial concentration of indigo solution (5mg/L)at (35.5,37, and 38.5)ºC ,voltage=2Volt

CPG/G						
	T=35.5ºC		T=37ºC		T=38.5ºC	
Time (min)	**Conc. of indigo release (mg/L)**	**%Drug release**	**Conc. of indigo release (mg/L)**	**%Drug release**	**Conc. of indigo release (mg/L)**	**%Drug release**
5	0.279	5.626	0.307	6.183	0.219	4.410
10	0.471	9.478	0.481	9.681	0.367	7.400
15	0.594	11.961	0.642	12.924	0.481	9.681
25	0.742	14.952	0.863	17.385	0.599	12.063
35	0.883	17.790	1.029	20.730	0.720	14.496
50	1.019	20.527	1.183	23.822	0.818	16.472
70	1.142	23.011	1.303	26.254	0.929	18.702
95	1.246	25.089	1.387	27.927	1.027	20.679
125	1.321	26.609	1.427	28.738	1.115	22.453
155	1.366	27.522	1.527	30.765	1.173	23.619
185	1.397	28.130	1.535	30.917	1.220	24.582
215	1.404	28.282	1.543	31.069	1.261	25.393
245	1.412	28.434	1.548	31.171	1.316	26.508
275	1.414	28.485	1.555	31.323	1.341	27.015
305	1.417	28.535	1.558	31.374	1.346	27.116
335	1.422	28.637	1.558	31.374	1.351	27.217

Table (3.42): Indigo release from CPG/MWCNTs hydrogel composite in 65ml of phosphate buffer solution (0.01M),Initial concentration of indigo solution (5mg/L)at (35.5,37, and 38.5)ºC ,voltage=2Volt

CPG/MWCNTs						
	T=35.5ºC		T=37ºC		T=38.5ºC	
Time (min)	**Conc. of indigo release (mg/L)**	**%Drug release**	**Conc. of indigo release (mg/L)**	**%Drug release**	**Conc. of indigo release (mg/L)**	**%Drug release**
5	0.471	9.478	0.377	7.603	0.342	6.893
10	0.765	15.408	0.773	15.560	0.722	14.546
15	0.956	19.260	1.155	23.264	1.077	21.693
25	1.218	24.531	1.605	32.337	1.485	29.904
35	1.402	28.231	1.907	38.419	1.797	36.189
50	1.595	32.134	2.174	43.791	2.053	41.358
70	1.716	34.567	2.391	48.150	2.229	44.906
95	1.799	36.239	2.516	50.684	2.348	47.288
125	1.860	37.456	2.594	52.255	2.428	48.910
155	1.882	37.912	2.647	53.320	2.456	49.468
185	1.887	38.013	2.672	53.827	2.464	49.620
215	1.890	38.064	2.753	55.449	2.466	49.671
245	1.892	38.115	2.778	55.955	2.469	49.721
275	1.895	38.165	2.788	56.158	2.471	49.772
305	1.897	38.216	2.791	56.209	2.474	49.823
335	1.902	38.317	2.791	56.209	2.476	49.873

3.4.8 Voltage Optimization of Doxorubicin hydrochloride Release from conductive hydrogels

In this study, Doxorubicin hydrochloride was used as drug. The same behavior was obtained in previous studies; the drug release for hydrogel composite was increased with increase voltage. The amount of Doxorubicin release from (CPG/PANI), (CPG/Fe_3O_4/PANI), (CPG/G) & (CPG/MWCNTs) are shows in figures (3.125, 3.126, 3.127, 3.128) respectively.

Tables (3.43, 3.44, 3.45, 3.46) are shows the concentration and percentage from (CPG/PANI), (CPG/Fe_3O_4/PANI), (CPG/G) &(CPG/MWCNTs) under difference voltages effect , respectively.

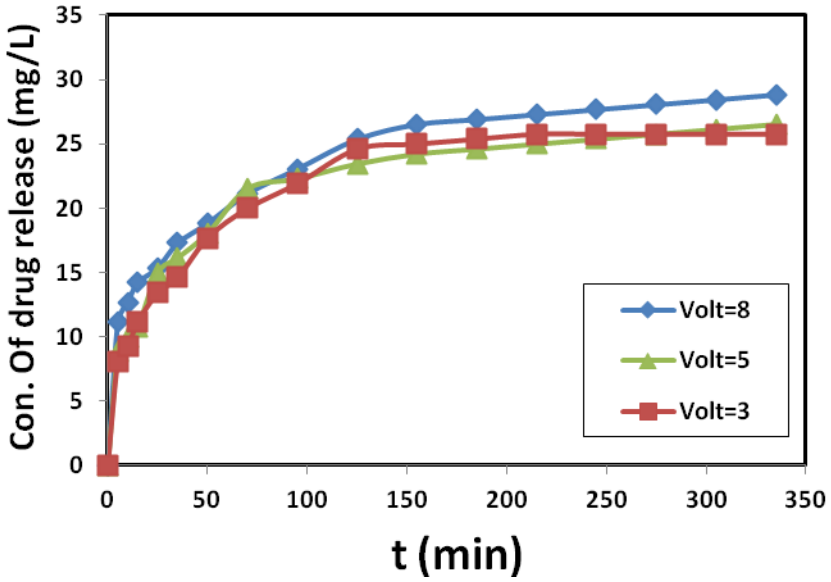

Figure (3.125): Doxorubicin hydrochloride release from (CPG/PANI) composite at different voltages and 37ºC

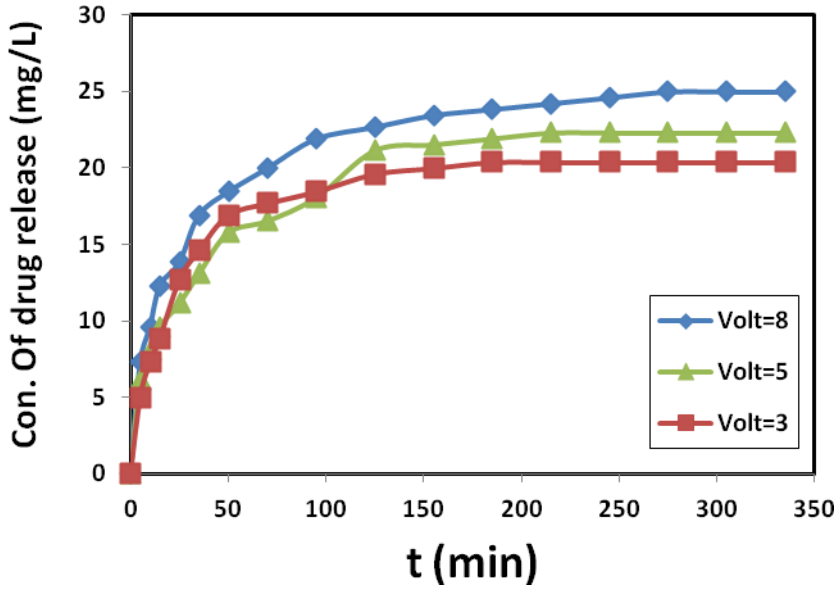

Figure (3.126): Doxorubicin hydrochloride release from (CPG/ Fe_3O_4/PANI) composite at different voltages and 37ºC

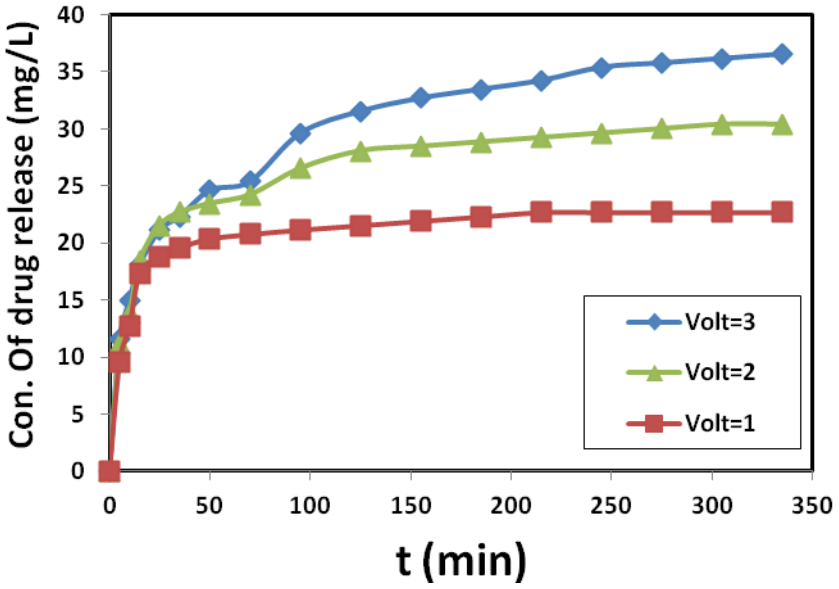

Figure (3.127): Doxorubicin hydrochloride release from (CPG/G) composite at different voltages and 37ºC

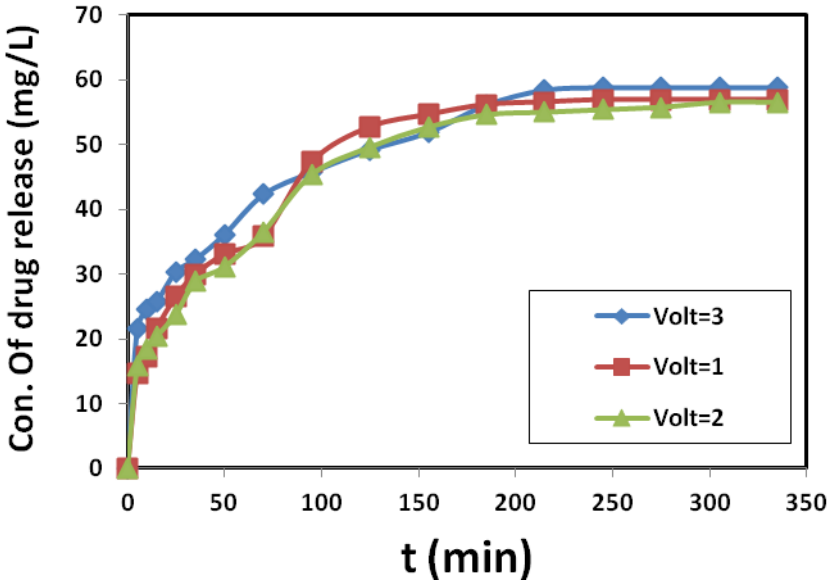

Figure (3.128): Doxorubicin hydrochloride release from (CPG/MWCNTs) composite at different voltages and 37ºC

Table (3.43): Doxorubicin release from CPG /PANI hydrogel composite in 65ml of phosphate buffer solution (0.01M),Initial concentration of Doxorubicin solution (100mg/L)at 37ºC ,voltage(3,5, and 8)Volt

CPG/PANI						
	Voltage=3		Voltage=5		Voltage=8	
Time (min)	**Conc. of doxorubicin release (mg/L)**	**%Drug release**	**Conc. of doxorubicin release (mg/L)**	**%Drug release**	**Conc. of doxorubicin release (mg/L)**	**%Drug release**
5	8.077	8.171	8.846	8.949	11.154	11.284
10	9.231	9.339	10.000	10.117	12.692	12.840
15	11.154	11.284	10.769	10.895	14.231	14.397
25	13.462	13.619	15.000	15.175	15.385	15.564
35	14.615	14.786	16.154	16.342	17.308	17.510
50	17.692	17.899	18.077	18.288	18.846	19.066
70	20.000	20.233	21.538	21.790	21.154	21.401
95	21.923	22.179	22.308	22.568	23.077	23.346
125	24.615	24.903	23.462	23.735	25.385	25.681
155	25.000	25.292	24.231	24.514	26.538	26.848
185	25.385	25.681	24.615	24.903	26.923	27.237
215	25.769	26.070	25.000	25.292	27.308	27.626
245	25.769	26.070	25.385	25.681	27.692	28.016
275	25.769	26.070	25.769	26.070	28.077	28.405
305	25.769	26.070	26.154	26.459	28.462	28.794
335	25.769	26.070	26.538	26.848	28.846	29.183

Table (3.44): Doxorubicin release from CPG /Fe3O4/PANI hydrogel composite in 65ml of phosphate buffer solution (0.01M),Initial concentration of Doxorubicin solution (100mg/L)at 37ºC ,voltage(3,5, and 8)Volt

CPG /Fe_3O_4/PANI						
	Voltage=3		Voltage=5		Voltage=8	
Time (min)	**Conc. of doxorubicin release (mg/L)**	**%Drug release**	**Conc. of doxorubicin release (mg/L)**	**%Drug release**	**Conc. of doxorubicin release (mg/L)**	**%Drug release**
5	5.000	5.058	6.154	6.226	7.308	7.393
10	7.308	7.393	8.077	8.171	9.615	9.728
15	8.846	8.949	9.615	9.728	12.308	12.451
25	12.692	12.840	11.154	11.284	13.846	14.008
35	14.615	14.786	13.077	13.230	16.923	17.121
50	16.923	17.121	15.769	15.953	18.462	18.677
70	17.692	17.899	16.538	16.732	20.000	20.233
95	18.462	18.677	18.077	18.288	21.923	22.179
125	19.615	19.844	21.154	21.401	22.692	22.957
155	20.000	20.233	21.538	21.790	23.462	23.735
185	20.385	20.623	21.923	22.179	23.846	24.125
215	20.385	20.623	22.308	22.568	24.231	24.514
245	20.385	20.623	22.308	22.568	24.615	24.903
275	20.385	20.623	22.308	22.568	25.000	25.292
305	20.385	20.623	22.308	22.568	25.000	25.292
335	20.385	20.623	22.308	22.568	25.000	25.292

Table (3.45): Doxorubicin release from CPG /G hydrogel composite in 65ml of phosphate buffer solution (0.01M),Initial concentration of Doxorubicin solution (100mg/L)at 37ºC ,voltage(1,2, and 3)Volt

CPG /G						
	Voltage=1		Voltage=2		Voltage=3	
Time (min)	**Conc. of doxorubicin release (mg/L)**	**%Drug release**	**Conc. of doxorubicin release (mg/L)**	**%Drug release**	**Conc. of doxorubicin release (mg/L)**	**%Drug release**
5	9.615	9.728	11.154	11.284	11.538	11.673
10	12.692	12.840	13.846	14.008	15.000	15.175
15	17.308	17.510	18.462	18.677	18.077	18.288
25	18.846	19.066	21.538	21.790	21.154	21.401
35	19.615	19.844	22.692	22.957	22.308	22.568
50	20.385	20.623	23.462	23.735	24.615	24.903
70	20.769	21.012	24.231	24.514	25.385	25.681
95	21.154	21.401	26.538	26.848	29.615	29.961
125	21.538	21.790	28.077	28.405	31.538	31.907
155	21.923	22.179	28.462	28.794	32.692	33.074
185	22.308	22.568	28.846	29.183	33.462	33.852
215	22.692	22.957	29.231	29.572	34.231	34.630
245	22.692	22.957	29.615	29.961	35.385	35.798
275	22.692	22.957	30.000	30.350	35.769	36.187
305	22.692	22.957	30.385	30.739	36.154	36.576
335	22.692	22.957	30.385	30.739	36.538	36.965

Table (3.46): Doxorubicin release from CPG /MWCNTs hydrogel composite in 65ml of phosphate buffer solution (0.01M),Initial concentration of Doxorubicin solution (100mg/L)at 37ºC ,voltage(1,2, and 3)Volt

CPG /MWCNTs						
	Voltage=1		Voltage=2		Voltage=3	
Time (min)	**Conc. of doxorubicin release (mg/L)**	**%Drug release**	**Conc. of doxorubicin release (mg/L)**	**%Drug release**	**Conc. of doxorubicin release (mg/L)**	**%Drug release**
5	14.615	14.786	15.769	15.953	21.538	21.790
10	17.308	17.510	18.462	18.677	24.615	24.903
15	21.538	21.790	20.385	20.623	25.769	26.070
25	26.538	26.848	23.846	24.125	30.385	30.739
35	30.000	30.350	28.846	29.183	32.308	32.685
50	33.077	33.463	31.154	31.518	36.154	36.576
70	35.769	36.187	36.538	36.965	42.308	42.802
95	47.308	47.860	45.385	45.914	45.769	46.304
125	52.692	53.307	49.615	50.195	49.231	49.805
155	54.615	55.253	52.692	53.307	51.923	52.529
185	56.154	56.809	54.615	55.253	56.154	56.809
215	56.538	57.198	55.000	55.642	58.462	59.144
245	56.923	57.588	55.385	56.031	58.846	59.533
275	56.923	57.588	55.769	56.420	58.846	59.533
305	56.923	57.588	56.538	57.198	58.846	59.533
335	56.923	57.588	56.538	57.198	58.846	59.533

3.4.9 Effective of temperature on Doxorubicin hydrochloride Release from conductive hydrogel

The figures (3.129, 3.130, 3.131, and 3.132) are observing Doxorubicin hydrochloride release from (CPG/PANI), (CPG/Fe_3O_4/PANI), (CPG/G), (CPG/MWCNTs) under differences temperatures, respectively. The behavior similar previous studies, the temperature at 38.5˚C was given the largest rate of Doxorubicin release. Tables (3.47, 3.48, 3.49, & 3.50) are shows the concentration and percentage of doxorubicin hydrochloride release from (CPG/PANI), (CPG/Fe_3O_4/PANI), (CPG/G), & (CPG/MWCNTs) under different temperature, respectively.

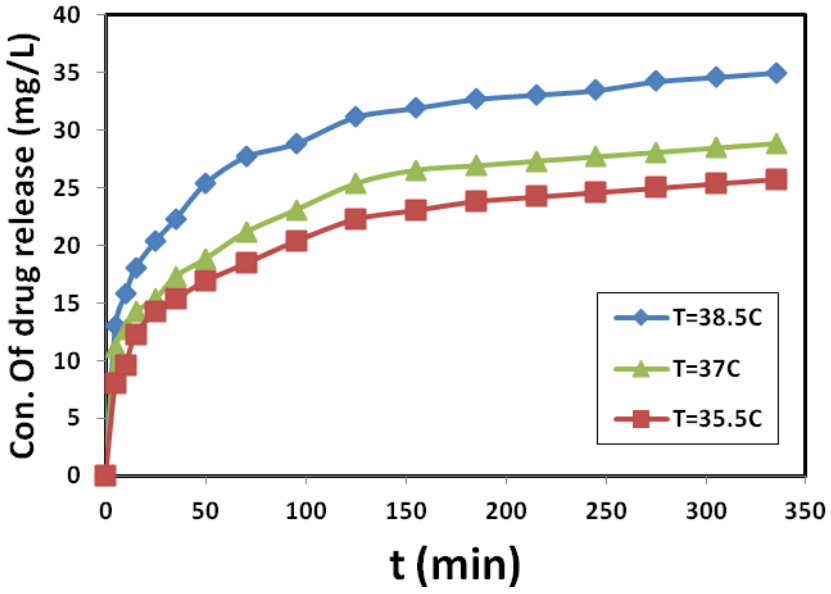

Figure (3.129): Doxorubicin hydrochloride release from (CPG/PANI) composite at different temperatures and 8V

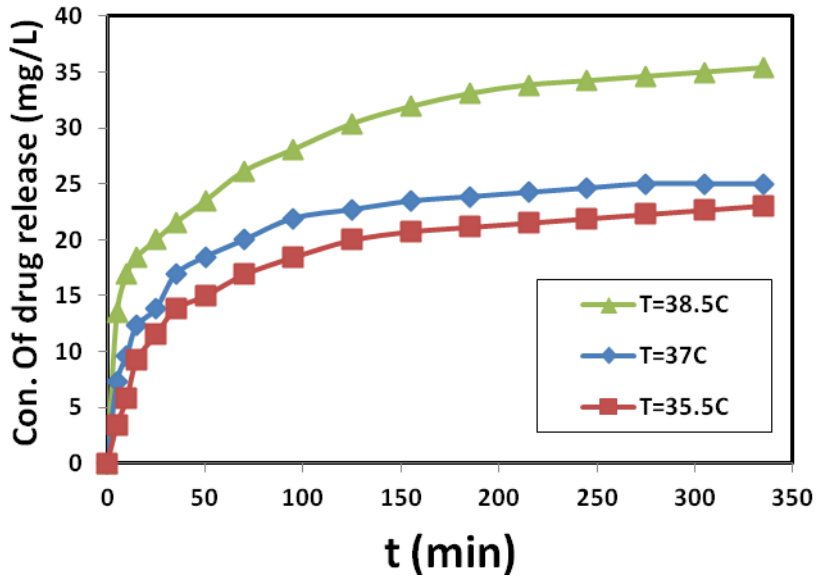

Figure (3.130): Doxorubicin hydrochloride release from (CPG/Fe_3O_4/PANI) composite at different temperatures and 8V

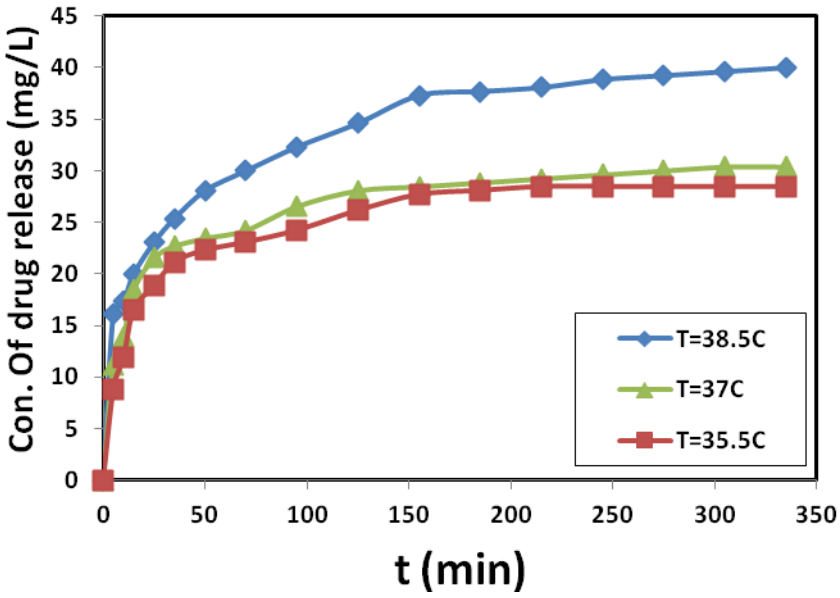

Figure (3.131): Doxorubicin hydrochloride release from (CPG/G) composite at different temperatures and 2V

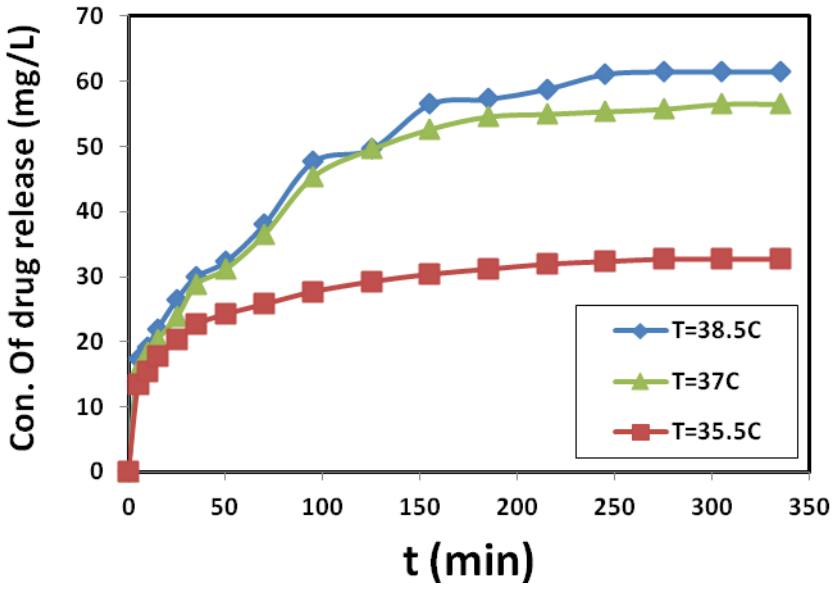

Figure (3.132): Doxorubicin hydrochloride release from (CPG/MWCNTs) composite at different temperatures and 2V

Table (3.47): Doxorubicin release from CPG/PANI hydrogel composite in 65ml of phosphate buffer solution (0.01M),Initial concentration of Doxorubicin solution (100mg/L)at (35.5,37, and 38.5)ºC ,voltage=8Volt

CPG/PANI						
	T=35.5ºC		T=37ºC		T=38.5ºC	
Time (min)	**Conc. of doxorubicin release (mg/L)**	**%Drug release**	**Conc. of doxorubicin release (mg/L)**	**%Drug release**	**Conc. of doxorubicin release (mg/L)**	**%Drug release**
5	8.077	8.171	11.154	11.284	13.077	13.230
10	9.615	9.728	12.692	12.840	15.769	15.953
15	12.308	12.451	14.231	14.397	18.077	18.288
25	14.231	14.397	15.385	15.564	20.385	20.623
35	15.385	15.564	17.308	17.510	22.308	22.568
50	16.923	17.121	18.846	19.066	25.385	25.681
70	18.462	18.677	21.154	21.401	27.692	28.016
95	20.385	20.623	23.077	23.346	28.846	29.183
125	22.308	22.568	25.385	25.681	31.154	31.518
155	23.077	23.346	26.538	26.848	31.923	32.296
185	23.846	24.125	26.923	27.237	32.692	33.074
215	24.231	24.514	27.308	27.626	33.077	33.463
245	24.615	24.903	27.692	28.016	33.462	33.852
275	25.000	25.292	28.077	28.405	34.231	34.630
305	25.385	25.681	28.462	28.794	34.615	35.019
335	25.769	26.070	28.846	29.183	35.000	35.409

Table (3.48): Doxorubicin release from CPG/Fe_3O_4/PANI hydrogel composite in 65ml of phosphate buffer solution (0.01M),Initial concentration of Doxorubicin solution (100mg/L)at (35.5,37, and 38.5)ºC ,voltage=8Volt

CPG/ Fe_3O_4/PANI						
	T=35.5ºC		T=37ºC		T=38.5ºC	
Time (min)	**Conc. of doxorubicin release (mg/L)**	**%Drug release**	**Conc. of doxorubicin release (mg/L)**	**%Drug release**	**Conc. of doxorubicin release (mg/L)**	**%Drug release**
5	3.462	3.502	7.308	7.393	13.462	13.619
10	5.769	5.837	9.615	9.728	16.923	17.121
15	9.231	9.339	12.308	12.451	18.462	18.677
25	11.538	11.673	13.846	14.008	20.000	20.233
35	13.846	14.008	16.923	17.121	21.538	21.790
50	15.000	15.175	18.462	18.677	23.462	23.735
70	16.923	17.121	20.000	20.233	26.154	26.459
95	18.462	18.677	21.923	22.179	28.077	28.405
125	20.000	20.233	22.692	22.957	30.385	30.739
155	20.769	21.012	23.462	23.735	31.923	32.296
185	21.154	21.401	23.846	24.125	33.077	33.463
215	21.538	21.790	24.231	24.514	33.846	34.241
245	21.923	22.179	24.615	24.903	34.231	34.630
275	22.308	22.568	25.000	25.292	34.615	35.019
305	22.692	22.957	25.000	25.292	35.000	35.409
335	23.077	23.346	25.000	25.292	35.385	35.798

Table (3.49): Doxorubicin release from CPG/G hydrogel composite in 65ml of phosphate buffer solution (0.01M), Initial concentration of Doxorubicin solution (100mg/L)at (35.5,37, and 38.5)ºC ,voltage=2Volt

CPG/ G						
	T=35.5ºC		T=37ºC		T=38.5ºC	
Time (min)	**Conc. of doxorubicin release (mg/L)**	**%Drug release**	**Conc. of doxorubicin release (mg/L)**	**%Drug release**	**Conc. of doxorubicin release (mg/L)**	**%Drug release**
5	8.846	8.949	11.154	11.284	16.154	16.342
10	11.923	12.062	13.846	14.008	17.308	17.510
15	16.538	16.732	18.462	18.677	20.000	20.233
25	18.846	19.066	21.538	21.790	23.077	23.346
35	21.154	21.401	22.692	22.957	25.385	25.681
50	22.308	22.568	23.462	23.735	28.077	28.405
70	23.077	23.346	24.231	24.514	30.000	30.350
95	24.231	24.514	26.538	26.848	32.308	32.685
125	26.154	26.459	28.077	28.405	34.615	35.019
155	27.692	28.016	28.462	28.794	37.308	37.743
185	28.077	28.405	28.846	29.183	37.692	38.132
215	28.462	28.794	29.231	29.572	38.077	38.521
245	28.462	28.794	29.615	29.961	38.846	39.300
275	28.462	28.794	30.000	30.350	39.231	39.689
305	28.462	28.794	30.385	30.739	39.615	40.078
335	28.462	28.794	30.385	30.739	40.000	40.467

Table (3.50): Doxorubicin release from CPG/MWCNTs hydrogel composite in 65ml of phosphate buffer solution (0.01M),Initial concentration of Doxorubicin solution (100mg/L)at (35.5,37, and 38.5)ºC ,voltage=2Volt

CPG/ MWCNTs						
	T=35.5ºC		T=37ºC		T=38.5ºC	
Time (min)	**Conc. of doxorubicin release (mg/L)**	**%Drug release**	**Conc. of doxorubicin release (mg/L)**	**%Drug release**	**Conc. of doxorubicin release (mg/L)**	**%Drug release**
5	13.462	13.619	15.769	15.953	17.308	17.510
10	15.385	15.564	18.462	18.677	19.231	19.455
15	17.692	17.899	20.385	20.623	21.923	22.179
25	20.385	20.623	23.846	24.125	26.538	26.848
35	22.692	22.957	28.846	29.183	30.000	30.350
50	24.231	24.514	31.154	31.518	32.308	32.685
70	25.769	26.070	36.538	36.965	38.077	38.521
95	27.692	28.016	45.385	45.914	47.692	48.249
125	29.231	29.572	49.615	50.195	49.615	50.195
155	30.385	30.739	52.692	53.307	56.538	57.198
185	31.154	31.518	54.615	55.253	57.308	57.977
215	31.923	32.296	55.000	55.642	58.846	59.533
245	32.308	32.685	55.385	56.031	61.154	61.868
275	32.692	33.074	55.769	56.420	61.538	62.257
305	32.692	33.074	56.538	57.198	61.538	62.257
335	32.692	33.074	56.538	57.198	61.538	62.257

3.4.10 Voltage Optimization of Methotrexate Release from conductive hydrogel

In this study, Methotrexate was used as drug. Same behavior was obtained in previous studies; the drug release for hydrogel composite was increased with increase voltage. The amount of Methotrexate release from (CPG/PANI), (CPG/Fe_3O_4/PANI), (CPG/G) & (CPG/MWCNTs) are showing in figures (3.133, 3.134, 3.135, 3.136) respectively. Tables (3.51, 3.52, 3.53, 3.54) are observing concentration and percentage of methotrexate release from (CPG/PANI), (CPG/Fe_3O_4/PANI), (CPG/G) & (CPG/MWCNTs) under difference voltages effect, respectively.

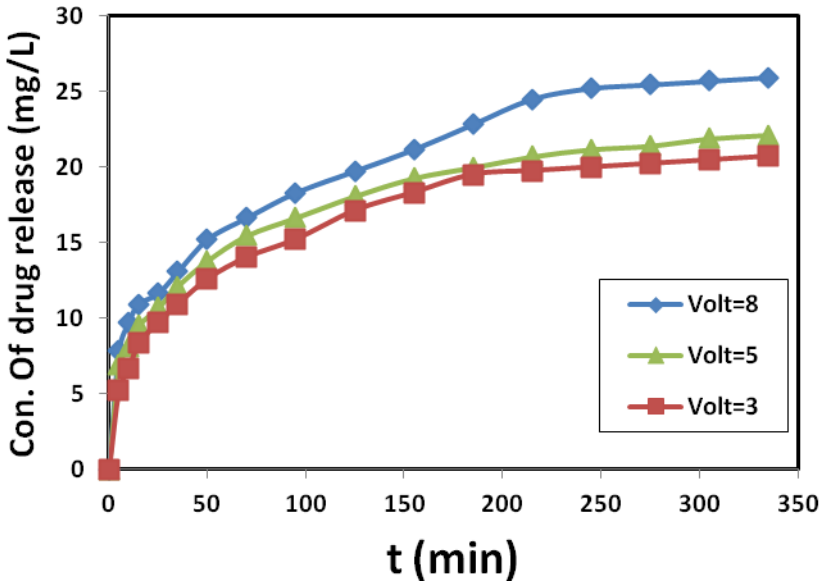

Figure (3.133): Methotrexate release from (CPG/PANI) composite at different Voltages and 37ºC

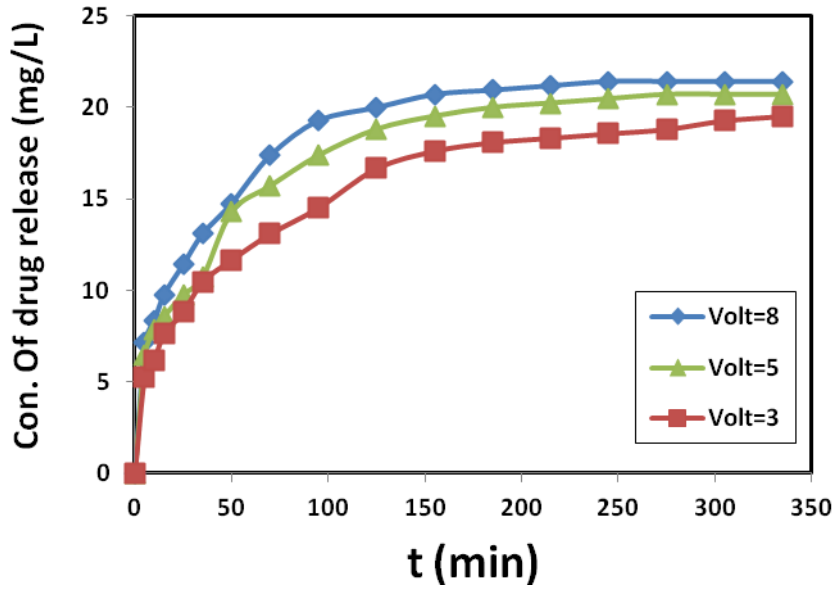

Figure (3.134): Methotrexate release from (CPG/Fe_3O_4/PANI) composite at different Voltages and 37ºC

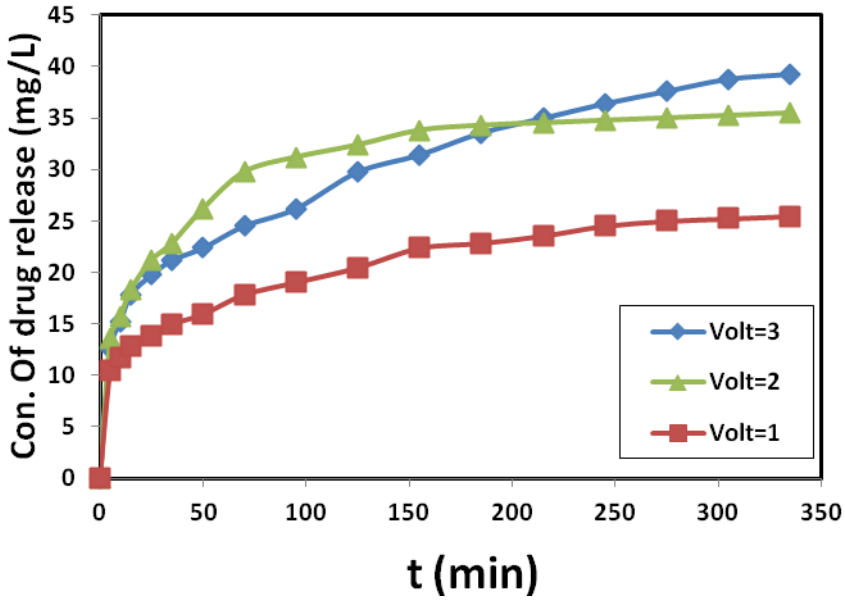

Figure (3.135): Methotrexate release from (CPG/G) composite at different Voltages and 37ºC

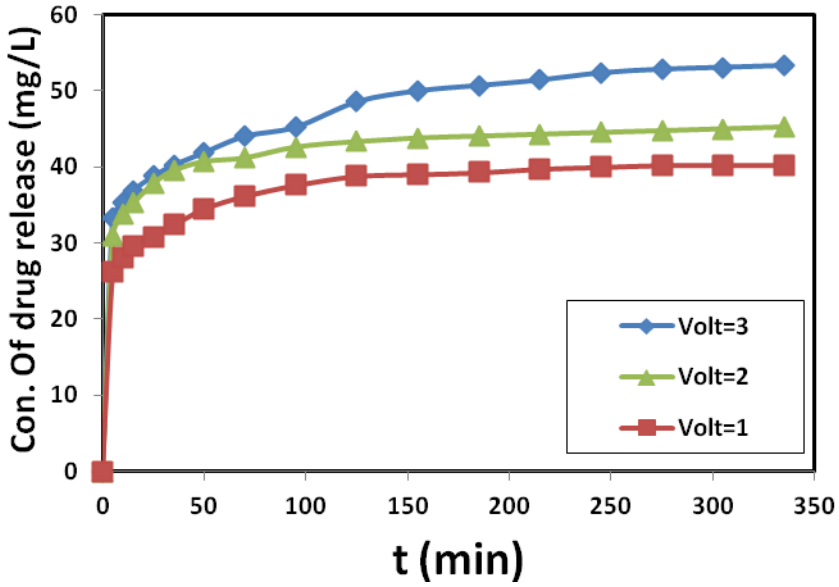

Figure (3.136): Methotrexate release from (CPG/MWCNTs) composite at different Voltages and 37ºC

Table (3.51): Methotrexate release from CPG /PANI hydrogel composite in 65ml of phosphate buffer solution (0.01M),Initial concentration of methotrexate solution (100mg/L)at 37ºC ,voltage(3,5, and 8)Volt

CPG/ PANI						
	Voltage=3		Voltage=5		Voltage=8	
Time (min)	**Conc. of methotrex. release (mg/L)**	**%Drug release**	**Conc. of methotrex. release (mg/L)**	**%Drug release**	**Conc. of methotrex. release (mg/L)**	**%Drug release**
5	5.238	4.803	6.905	6.332	7.857	7.205
10	6.667	6.114	8.095	7.424	9.762	8.952
15	8.333	7.642	9.524	8.734	10.952	10.044
25	9.762	8.952	10.714	9.825	11.667	10.699
35	10.952	10.044	12.143	11.135	13.095	12.009
50	12.619	11.572	13.810	12.664	15.238	13.974
70	14.048	12.882	15.476	14.192	16.667	15.284
95	15.238	13.974	16.667	15.284	18.333	16.812
125	17.143	15.721	18.095	16.594	19.762	18.122
155	18.333	16.812	19.286	17.686	21.190	19.432
185	19.524	17.904	20.000	18.341	22.857	20.961
215	19.762	18.122	20.714	18.996	24.524	22.489
245	20.000	18.341	21.190	19.432	25.238	23.144
275	20.238	18.559	21.429	19.651	25.476	23.362
305	20.476	18.777	21.905	20.087	25.714	23.581
335	20.714	18.996	22.143	20.306	25.952	23.799

Table (3.52): Methotrexate release from CPG /Fe_3O_4/PANI hydrogel composite in 65ml of phosphate buffer solution (0.01M),Initial concentration of Methotrexate solution (100mg/L)at 37ºC ,voltage(3,5, and 8)Volt

CPG/Fe_3O_4/ PANI						
	Voltage=3		Voltage=5		Voltage=8	
Time (min)	**Conc. of methotrex. release (mg/L)**	**%Drug release**	**Conc. of methotrex. release (mg/L)**	**%Drug release**	**Conc. of methotrex. release (mg/L)**	**%Drug release**
5	5.238	4.803	6.429	5.895	7.143	6.550
10	6.190	5.677	7.857	7.205	8.333	7.642
15	7.619	6.987	8.571	7.860	9.762	8.952
25	8.810	8.079	9.762	8.952	11.429	10.480
35	10.476	9.607	10.714	9.825	13.095	12.009
50	11.667	10.699	14.286	13.100	14.762	13.537
70	13.095	12.009	15.714	14.410	17.381	15.939
95	14.524	13.319	17.381	15.939	19.286	17.686
125	16.667	15.284	18.810	17.249	20.000	18.341
155	17.619	16.157	19.524	17.904	20.714	18.996
185	18.095	16.594	20.000	18.341	20.952	19.214
215	18.333	16.812	20.238	18.559	21.190	19.432
245	18.571	17.031	20.476	18.777	21.429	19.651
275	18.810	17.249	20.714	18.996	21.429	19.651
305	19.286	17.686	20.714	18.996	21.429	19.651
335	19.524	17.904	20.714	18.996	21.429	19.651

Table (3.53): Methotrexate release from CPG /G hydrogel composite in 65ml of phosphate buffer solution (0.01M),Initial concentration of methotrexate solution (100mg/L)at 37ºC ,voltage(1,2, and 3)Volt

CPG /G						
	Voltage=1		Voltage=2		Voltage=3	
Time (min)	**Conc. of methotrex. release (mg/L)**	**%Drug release**	**Conc. of methotrex. release (mg/L)**	**%Drug release**	**Conc. of methotrex. release (mg/L)**	**%Drug release**
5	10.476	9.607	13.571	12.445	12.619	11.572
10	11.667	10.699	15.714	14.410	15.238	13.974
15	12.857	11.790	18.333	16.812	17.857	16.376
25	13.810	12.664	21.190	19.432	19.762	18.122
35	15.000	13.755	22.857	20.961	21.190	19.432
50	15.952	14.629	26.190	24.017	22.381	20.524
70	17.857	16.376	29.762	27.293	24.524	22.489
95	19.048	17.467	31.190	28.603	26.190	24.017
125	20.476	18.777	32.381	29.694	29.762	27.293
155	22.381	20.524	33.810	31.004	31.429	28.821
185	22.857	20.961	34.286	31.441	33.571	30.786
215	23.571	21.616	34.524	31.659	35.000	32.096
245	24.524	22.489	34.762	31.878	36.429	33.406
275	25.000	22.926	35.000	32.096	37.619	34.498
305	25.238	23.144	35.238	32.314	38.810	35.590
335	25.476	23.362	35.476	32.533	39.286	36.026

Table (3.54): Methotrexate release from CPG /MWCNTs hydrogel composite in 65ml of phosphate buffer solution (0.01M),Initial concentration of methotrexate solution (100mg/L)at 37ºC ,voltage(1,2, and 3)Volt

CPG /MWCNTs						
	Voltage=1		Voltage=2		Voltage=3	
Time (min)	**Conc. of methotrex. release (mg/L)**	**%Drug release**	**Conc. of methotrex. release (mg/L)**	**%Drug release**	**Conc. of methotrex. release (mg/L)**	**%Drug release**
5	26.190	24.017	30.952	28.384	33.333	30.568
10	28.095	25.764	33.810	31.004	35.238	32.314
15	29.524	27.074	35.238	32.314	36.905	33.843
25	30.714	28.166	37.857	34.716	38.810	35.590
35	32.381	29.694	39.524	36.245	40.238	36.900
50	34.524	31.659	40.714	37.336	41.905	38.428
70	36.190	33.188	41.190	37.773	44.048	40.393
95	37.619	34.498	42.619	39.083	45.238	41.485
125	38.810	35.590	43.333	39.738	48.571	44.541
155	39.048	35.808	43.810	40.175	50.000	45.852
185	39.286	36.026	44.048	40.393	50.714	46.507
215	39.762	36.463	44.286	40.611	51.429	47.162
245	40.000	36.681	44.524	40.830	52.381	48.035
275	40.238	36.900	44.762	41.048	52.857	48.472
305	40.238	36.900	45.000	41.266	53.095	48.690
335	40.238	36.900	45.238	41.485	53.333	48.908

3.4.11 Effective of temperature on the Methotrexate Release from conductive hydrogel

The figures (3.137, 3.138, 3.139, and 3.140) are showing the Methotrexate release from (CPG/PANI), (CPG/Fe_3O_4/PANI), (CPG/G), (CPG/MWCNTs) under differences temperatures, respectively. The behavior similar previous studies, the temperature at 38.5℃ was given the largest rate of Methotrexate release.

Tables (3.55, 3.56, 3.57, & 3.58) are showing the concentration and percentage of methotrexate release from (CPG/PANI), (CPG/Fe_3O_4/PANI), (CPG/G), & (CPG/MWCNTs) under different temperature, respectively.

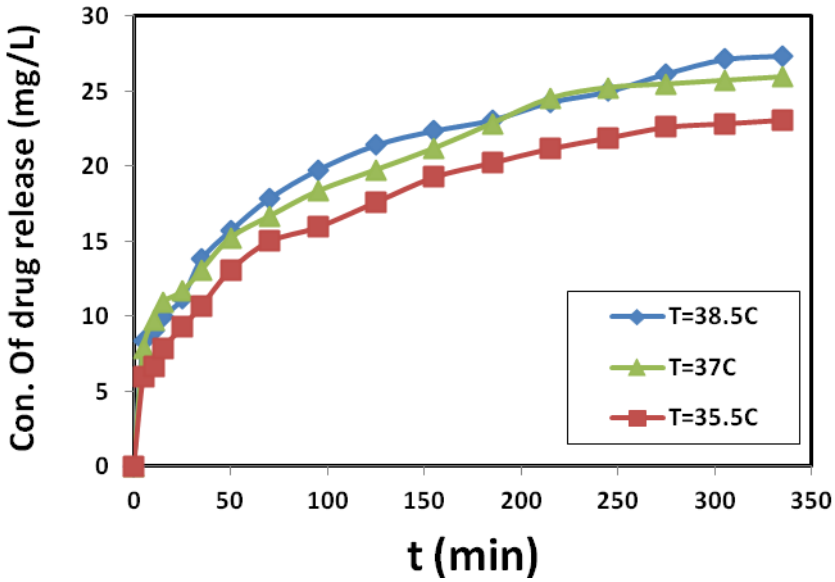

Figure (3.137): Methotrexate release from (CPG/PANI) composite at different temperatures and 8V

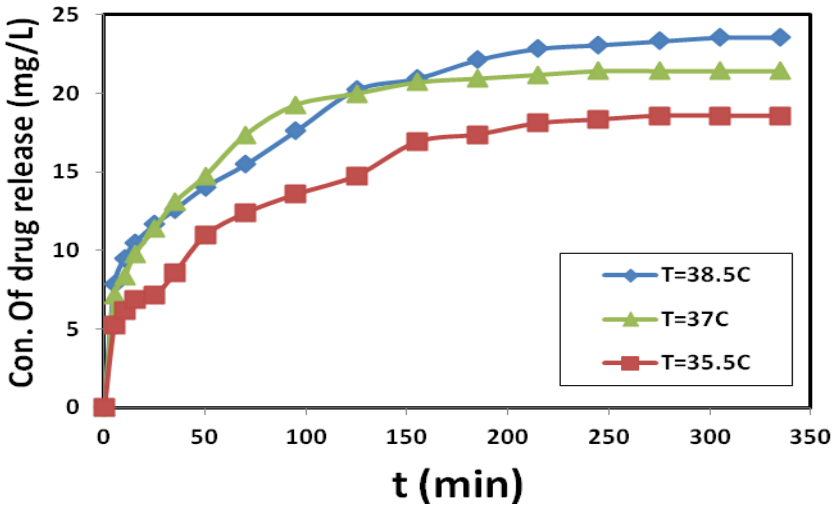

Figure (3.138): Methotrexate release from (CPG/Fe_3O_4/PANI) composite at different temperatures and 8V

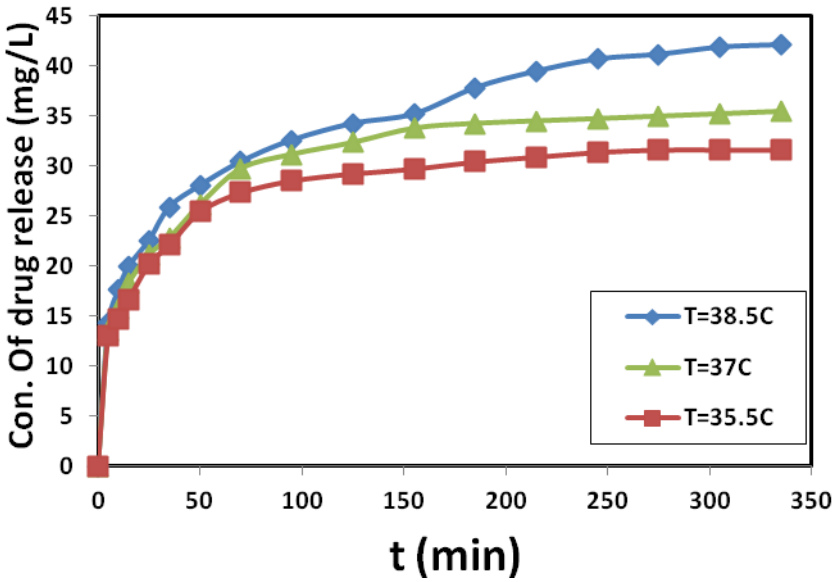

Figure (3.139): Methotrexate release from (CPG/G) composite at different temperatures and 2V

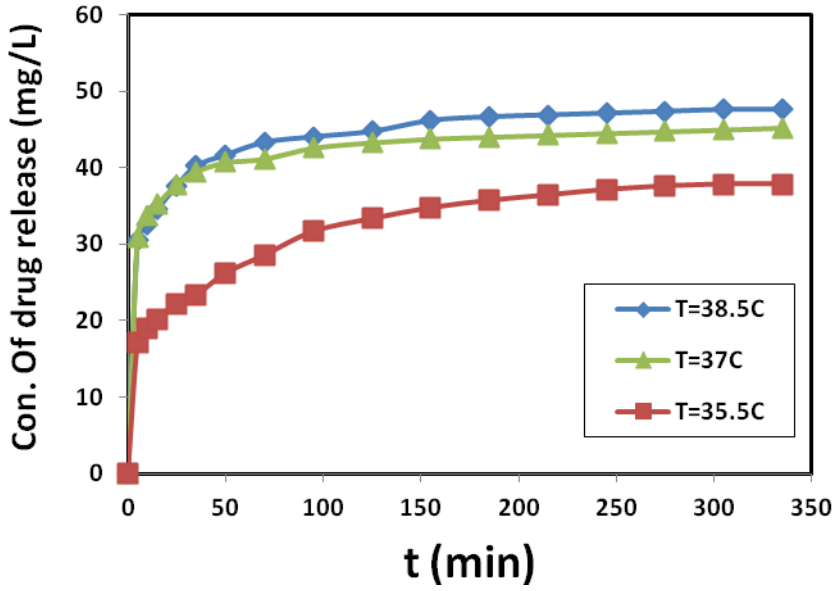

Figure (3.140): Methotrexate release from (CPG/MWCNTs) composite at different temperatures and 2V

Table(3.55): Methotrexate release from CPG/PANI hydrogel composite in 65ml of phosphate buffer solution (0.01M),Initial concentration of methotrexate solution (100mg/L)at (35.5,37, and 38.5)ºC ,voltage=8Volt

CPG /PANI						
	T=35.5ºC		T=37ºC		T=38.5ºC	
Time (min)	**Conc. of methotrex. release (mg/L)**	**%Drug release**	**Conc. of methotrex. release (mg/L)**	**%Drug release**	**Conc. of methotrex. release (mg/L)**	**%Drug release**
5	5.952	5.459	7.857	7.205	8.333	7.642
10	6.667	6.114	9.762	8.952	9.048	8.297
15	7.857	7.205	10.952	10.044	10.000	9.170
25	9.286	8.515	11.667	10.699	11.190	10.262
35	10.714	9.825	13.095	12.009	13.810	12.664
50	13.095	12.009	15.238	13.974	15.714	14.410
70	15.000	13.755	16.667	15.284	17.857	16.376
95	15.952	14.629	18.333	16.812	19.762	18.122
125	17.619	16.157	19.762	18.122	21.429	19.651
155	19.286	17.686	21.190	19.432	22.381	20.524
185	20.238	18.559	22.857	20.961	23.095	21.179
215	21.190	19.432	24.524	22.489	24.286	22.271
245	21.905	20.087	25.238	23.144	25.000	22.926
275	22.619	20.742	25.476	23.362	26.190	24.017
305	22.857	20.961	25.714	23.581	27.143	24.891
335	23.095	21.179	25.952	23.799	27.381	25.109

Table (3.56): Methotrexate release from CPG/Fe_3O_4/PANI hydrogel composite in 65ml of phosphate buffer solution (0.01M),Initial concentration of methotrexate solution (100mg/L)at (35.5,37, and 38.5)ºC ,voltage=8Volt

CPG /Fe_3O_4/PANI						
	T=35.5ºC		T=37ºC		T=38.5ºC	
Time (min)	**Conc. of methotrex. release (mg/L)**	**%Drug release**	**Conc. of methotrex. release (mg/L)**	**%Drug release**	**Conc. of methotrex. release (mg/L)**	**%Drug release**
5	5.238	4.803	7.143	6.550	7.857	7.205
10	6.190	5.677	8.333	7.642	9.524	8.734
15	6.905	6.332	9.762	8.952	10.476	9.607
25	7.143	6.550	11.429	10.480	11.667	10.699
35	8.571	7.860	13.095	12.009	12.619	11.572
50	10.952	10.044	14.762	13.537	14.048	12.882
70	12.381	11.354	17.381	15.939	15.476	14.192
95	13.571	12.445	19.286	17.686	17.619	16.157
125	14.762	13.537	20.000	18.341	20.238	18.559
155	16.905	15.502	20.714	18.996	20.952	19.214
185	17.381	15.939	20.952	19.214	22.143	20.306
215	18.095	16.594	21.190	19.432	22.857	20.961
245	18.333	16.812	21.429	19.651	23.095	21.179
275	18.571	17.031	21.429	19.651	23.333	21.397
305	18.571	17.031	21.429	19.651	23.571	21.616
335	18.571	17.031	21.429	19.651	23.571	21.616

Table(3.57): Methotrexate release from CPG/G hydrogel composite in 65ml of phosphate buffer solution (0.01M),Initial concentration of methotrexate solution (100mg/L)at (35.5,37, and 38.5)ºC ,voltage=2Volt

CPG /G						
	T=35.5ºC		T=37ºC		T=38.5ºC	
Time (min)	**Conc. of methotrex. release (mg/L)**	**%Drug release**	**Conc. of methotrex. release (mg/L)**	**%Drug release**	**Conc. of methotrex. release (mg/L)**	**%Drug release**
5	13.095	12.009	13.571	12.445	14.286	13.100
10	14.762	13.537	15.714	14.410	17.619	16.157
15	16.667	15.284	18.333	16.812	20.000	18.341
25	20.238	18.559	21.190	19.432	22.619	20.742
35	22.143	20.306	22.857	20.961	25.952	23.799
50	25.476	23.362	26.190	24.017	28.095	25.764
70	27.381	25.109	29.762	27.293	30.476	27.948
95	28.571	26.201	31.190	28.603	32.619	29.913
125	29.286	26.856	32.381	29.694	34.286	31.441
155	29.762	27.293	33.810	31.004	35.238	32.314
185	30.476	27.948	34.286	31.441	37.857	34.716
215	30.952	28.384	34.524	31.659	39.524	36.245
245	31.429	28.821	34.762	31.878	40.714	37.336
275	31.667	29.039	35.000	32.096	41.190	37.773
305	31.667	29.039	35.238	32.314	41.905	38.428
335	31.667	29.039	35.476	32.533	42.143	38.646

Table (3.58): Methotrexate release from CPG/MWCNTs hydrogel composite in 65ml of phosphate buffer solution (0.01M),Initial concentration of methotrexate solution (100mg/L)at (35.5,37, and 38.5)ºC ,voltage=2Volt

CPG /MWCNTs						
	T=35.5ºC		T=37ºC		T=38.5ºC	
Time (min)	**Conc. of methotrex. release (mg/L)**	**%Drug release**	**Conc. of methotrex. release (mg/L)**	**%Drug release**	**Conc. of methotrex. release (mg/L)**	**%Drug release**
5	17.143	15.721	30.952	28.384	30.476	27.948
10	19.048	17.467	33.810	31.004	32.619	29.913
15	20.238	18.559	35.238	32.314	34.524	31.659
25	22.143	20.306	37.857	34.716	37.619	34.498
35	23.333	21.397	39.524	36.245	40.238	36.900
50	26.190	24.017	40.714	37.336	41.667	38.210
70	28.571	26.201	41.190	37.773	43.333	39.738
95	31.667	29.039	42.619	39.083	44.048	40.393
125	33.333	30.568	43.333	39.738	44.762	41.048
155	34.762	31.878	43.810	40.175	46.190	42.358
185	35.714	32.751	44.048	40.393	46.667	42.795
215	36.429	33.406	44.286	40.611	46.905	43.013
245	37.143	34.061	44.524	40.830	47.143	43.231
275	37.619	34.498	44.762	41.048	47.381	43.450
305	37.857	34.716	45.000	41.266	47.619	43.668
335	37.857	34.716	45.238	41.485	47.619	43.668

Conclusion

The main object of the present work was to explore the possibility of using conductive nanocomposite as carrier of drugs (Indigo carmine, Doxorubicin hydrochloride, Methotrexate). For this work, different hydrogels (CPG, CPM, PPM, PgA, CgA, & IPN), and different nano materials (Fe_3O_4 MNPs, GO nanosheets, G nanosheets) were synthesized by different methods. Also it was used MWCNTs from CheapTubes for same purpose.

The most of nano and nanocomposite materials was characterization by FTIR, XRD, SEM, EDS, TEM, & AFM, while TGA, DSA technique was used to study thermal properties for hydrogel only.

The swelling of hydrogel and composite was studied in distilled water (pH=6.5) with interval times and after day. The maximum of degree of swelling was returned to PgA for hydrogel at 305 min and after day equal to S=15.1314, & S=16.4825. The maximum of degree of swelling for hydrogel composite was returned to PPM/MWCNTs at 305 min and after day equal to S=11.6776, & S=11.7473.

The electrical properties of hydrogel and hydrogel nanocomposite were study with LCR meter with frequencies (100Hz-100 KHz). The real & imaginary permittivity was found an increase with decreased of frequency, while electric conductivity was increased with increasing voltages. The maximum electrical conductivity was returned to MWCNTs and its composite form (CPG/MWCNTs), the value is equal to σ=2.5305 S/m & σ=1.9669 S/m, respectively.

The Indigo carmine release from all hydrogel composites was studied by UV-Visible spectrophotometer in PBS (pH=7.4), room temperature and voltage=8 for PANI composite, 2 for MWCNTs& G composite. From this study was found that the CPG/MWCNTs composite has the best ratio for drug release equal to 55.702%.

The effected of voltage and temperature changes on the amount of drug (Indigo carmine, Doxorubicin hydrochloride, Methotrexate) release from the best hydrogel composites (CPG/PANI, CPG/Fe_3O_4/PANI, CPG/G, &CPG/MWCNTs) were studied. The change of voltages has huge effect in most studies which was carried out for drug release. The highest ratio for Doxorubicin hydrochloride release on CPG/MWCNTs at 38.5C, 2volt was found equal to 62.257% while highest ratio for Methotrexate release on same nanocomposite (CPG/MWCNTs) at 38.5C, 2volt was found equal to 43.668%. The percentage ratio of drugs release from all nanocomposite hydrogels was found to have the following order:

(CPG/MWCNTs) > (CPG/G) >(CPG/PANI) >(CPG/Fe_3O_4/PANI).

Recommendation:

1. This studying can be applied in vivo on experimental rats, rabbits, etc. to examine the efficiency of drugs release from conductive nanocomposite hydrogel to target site. By injecting the solution of this hydrogel loaded with the drug to the infected cells and stimulated release of drug with external specific electric voltage, to control drug release especially anticancer drugs.
2. The electro-magnetic nanocomposite which was synthesized form (CPG/Fe_3O_4/PANI) has sensitive electro-magnetic field can be used to delivery drugs system. The drugs loading on this hydrogel will be injected in infected site by using stimulated electric voltage. The release of drug can be controlled using magnetic field, in other words to avoid drugs diffusion to healthy cells, subsequently drug will be arrived to target site (infected cells only) as much as possible.

References:

1- G. Ciofani, C. Riggio, V. Raffa, A. Menciassi, & A. Cuschieri, “A bi-modal approach against cancer: Magnetic alginate nanoparticles for combined chemotherapy and hyperthermia” **Medical Hypotheses, 73**, 80-82 (2009).

2- T. Hoare, & D. S. Kohane., “Hydrogels in drug delivery: progress and challenges”**, Polymer, 49,** 1993-2007(2008).

3- A. S. Hoffman, “Hydrogels for biomedical applications”, **Advanced Drug Delivery Reviews, 64,** 18- 23(2012).

4- M. Patenaude, N. M. Smeets, & T. Hoare., “Designing Injectable, Covalently Cross-Linked Hydrogels for Biomedical Applications”, **Macromol Rapid Commun, 35 (6)**, 598-617(2014).

5- Y. Masayuki, “Drug targeting with nano-sized carrier systems”, **J Artif Organs, 8**, 77–84(2005).

6- D. K. Jackson, S. B. Leeb, A. H. Mitwalli, P. Narvaez, D. Fusco, & E.C. Lupton., “Power Electronic Drives for Magnetically Triggered Gels”, **IEEE Transactions on Industrial Electronics, 44 (2),** 217-225(1997).

7- T. Hoare, J. Santamaria, G. F. Goya, S. Irusta, D. Lin, S. Lau, R. Padera, R. Langer, & D. S. Kohane, “A magnetically triggered composite membrane for on-demand drug delivery”, **Nano Lett. , 9 (10),** 3651-3657(2009).

8- W. M. Saltzman, **"Drug Delivery: Engineering Principles for Drug Therapy"**, Oxford University Press, New York, (2001).

9- C. D. Klaassen," **Casarett and Doull's toxicology: the basic science of poisons",** 8th ed, McGraw-Hill Education, New York, (2013).

10- S. Laurent, D. Forge, M. Port, A. Roch, C. Robic, L. Vander Elst, & R. N. Muller., “Magnetic iron oxide nanoparticles: synthesis,

stabilization, vectorization, physicochemical characterizations, and biological applications", **Chem. Rev., 108 (6),** 64-110(2008).

11- J. Kreuter, Nanoparticles, in: J. Kreuter (Ed.)," **Colloidal Drug Delivery Systems"**, Marcel Dekker, New York 219–342(1994).

12- C. G. Knight "**Liposomes From Physical Structure To Therapeutic Applications**", Elsevier, Amsterdam (1981).

13- H. Hezaveh, & I. I. Muhamad, "Impact of metal oxide nanoparticles on oral release properties of pH-sensitive hydrogel nanocomposites", **International Journal of Biological Macromolecule, 50**, 1334-1340(2012).

14- R. Langer, "Biomaterials in drug delivery and tissue engineering: One laboratory's experience", **Acc. Chem. Res., 33,** 94–101 (2000).

15- S. Sershen & J. West, "Implantable, polymeric systems for modulated drug delivery", **Adv. Drug Deliv. Rev., 54**, 1225–1235 (2002).

16- G. Crini, "Non-coventional low cost adsorbent for dye removal: a review", **Bioresour Technol., 97(9)**, 1061-1085(2006).

17- A. Borzacchielo, L. Ambrosias, P. Netter, L. Nicholais, A. Balard & P. Sam, "Chitosan – based hydrogels: synthesis and characterization", **Journal of Material Sciences: Materials in Medicine. 12**, 861-864(2001).

18- A. Zhu, S. Wang, D. Cheng, Q. Chen, C. Lin, J. Shen, & S. Lin, "Attachment and growth of cultured fibroblast cells on chitosan / PHEA – blended hydrogel", **Sheugwu Gongcheng Xuebao, 18**, 109-111(2002).

19- S. R. Jameela, A. Misra, & A. Jayakrishnan, "Cross-linked chitosan microspheres as carriers for prolonged delivery of macromolecular drugs", **Journal of Biomaterial Science. Poylmer Education**, **6**, 621-631(1994).

20- Julie Nilsen-Nygaard, Sabina P. Strand , Kjell M. Vårum, Kurt I. Draget and Catherine T. Nordgård, "Chitosan: Gels and Interfacial Properties"**, Polymers, 7**, 552-579(2015).

21- A. Pourjavadi, G. R. Mahdavinia & M. J. Zohuriaan-Mehr, " Modified chitosan. II. H-chitoPAN, a novel pH-responsive superabsorbent hydrogel", **J. Appl. Polym. Sci.**, **90**, 3115-3121(2003).

22- M. Ashford, J. T. Fell, D. Attwood, H. Sharma, & P. Woodhead, "An evaluation of pectin as a carrier for drug targeting to the colon", **J Control Release, 26,** 213-220(1993).

23- Z. Warkley, J. T. Fell, D. Attwood, & D. Parkins, "Studies on drug release from Pectin/ethyl cellulose filmcoated tablets: a potential colonic delivery system", **Int. J. Pharm, 153**, 219-224(1997).

24- Pornsak Sriamornsak, "Chemistry of pectin and its pharmaceutical uses: A review", **Silpakorn University International Journal, 3,** Issue 1-2, 206-228 (2003).

25- J. A. De Vries, "Distribution of methoxyl groups in pectins" **Carbohydrate Polymers, 6(1)**: 65-176(1986).

26- K. G. H. Desai, "Preparation and Characteristics of high-amylose corn starch/pectin blend microparticles", **AAPS Pharm Sci. Tech., 6,** 136-701(2005).

27- R. K. Tubbs, "Sequence distribution of partially hydrolyzed poly (vinylacetate)", **J. Polym. Sci. Part A-1: Polym. Chem., 4,** 623–629(1966).

28- S. M. Shaheen & K. Yamaura, "preparation of theophylline hydrogels of atactic poly (vinyl alcohol) NaCl/H_2O system for drug delivery system", **J. Control. Release, 81**, 367-377(2002).

29- J. M. Rosiak & F. Yoshii, "Hydrogels and their medical applications", **Nuclear Instruments and Methods in Physics Research, B 151**, 56-64(1999).

30- W. E. Hennink, & C. F. VanNostrum, "Novel crosslinking methods to design hydrogels", **Advanced Drug Delivery Reviews, 54(1)**, 13–36, (2002).

31- T. Funami, M. Hiroe, S. Noda, I. Asai, S. Ikeda, & K. Nishimari, "Influence of molecular structure imaged with atomic force microscopy on the rheological behavior of carrageenan aqueous systems in the presence or absence of cations", **Food Hydrocolloids 21,** 617-629(2007).

32- C. Esteban, & D. Severian, "Polyionic hydrogels based on xanthan and chitosan for stabilising and controlled release of vitamins", **Vol. WO0004086 (A1)** (ed. U. United States Patent), Kemestrie Inc [CA], USA(2000).

33- M. Takigami, H. Amada, N. Nagasawa, T. Yagi, T. Kasahara, S. Takigami, & M. Tamada, "Preparation and properties of CMC gel", **Transactions of the Materials Research Society of Japan, Vol .32, No. 3,** 713-716(2007).

34- P. A. Williams & G. O. Phillips, "Physicochemical characterisation of gum Arabic arabinogalactan protein complex", **Food and Food Ingredients Journal of Japan, 211,** 181- 188(2006).

35- A. M. Islam, G. O. Phillips, A. Sljivo, M. J. Snowden, & P. A. Williams, "A review of recent developments on the regulatory, structural and functional aspects of gum Arabic", **Food Hydrocolloids 11,** 493-505(1997).

36- P. J. Willcox, D. W. Howie, K. Schmidt-Rohr, D. A. Hoagland, S. P. Gido, S. Pudjijanto, L. W. Kleiner, & S. Venkatraman, "Microstructure of poly(vinyl alcohol) hydrogels produced by freeze/thaw cycling", **Journal of Polymer Science Part BPolymer Physics, 37(24)**: 3438-3454(1999).

37- P. Giannouli, & E. R. Morris, "Cryogelation of xanthan", **Food Hydrocolloids, 17(4)**: 495-501(2003).

38- Kunal Pal, A. K. Banthia, & D. K. Majumdar, "Starch Based Hydrogel with Potential Biomedical Application as Artificial Skin"**, African Journal of Biomedical Research, Vol. 9, No. 1**, 23-29(2006).

39- A. S. Waldman, L. Schechinger, G. Govindarajoo, J. S. Nowick, & L. H. Pignolet, "The alginate demonstration: polymers, food science, and ion exchange". **Journal of Chemical Education 75(11)**: 1430-1431(1998).

40- A. Pourjavadi, & M. J. Zohuriaan-Mehr, "Modification of carbohydrate polymers via grafting in air. 2. Ceric-initiated graft copolymerization of acrylonitrile onto natural and modified polysaccharides", **Starch-Starke 54,** 482-488(2002).

41- Fangfang Song, Xiaoqiong, Qun Wang, Liqiong Liao, & Chao Zhang, "Nanocomposite Hydrogels and Their Applications in Drug Delivery and Tissue Engineering", **Journal of Biomedical Nanotechnology, 10,** 1–13, (2014).

42- D. Stauffer, & A. Aharony, **"Introduction to Percolation Theory",** Taylor and Francis, London (1992).

43- P. L. McEuen, M. S. Fuhrer, & H. Park, "Single-walled Carbon Nanotube Electronics", **IEEE Transactions On Nanotechnology, 1**, **1,** 78-85 (2002).

44- F. Hennrich, R. Krupke, K. Arnold, J. A. Rojas Stutz, S. Lebedkin, T.Koch, T. Schimmel, & M. M. Kappes, "The mechanism of cavitation-induced scission of single-walled carbon nanotubes", **J. Phys. Chem. B ,111(8),** 1932-1937(2007).

45- M. Endo, T. Hayashi, Y. A. Kim, M. Terrones, & M. S. Dresselhaus, "Application of carbon nanotubes in the twenty- first century", **Phil. Trans. R. Soc. Lond. A, 362,** 2223–2238(2004).

46- D. Galpaya, M. Wang, M. Liu, N. Motta, E. Waclawik, & C. Yan, "Recent advances in fabrication and characterization of graphene-polymer nanocomposites", **Graphene, 1**, 30–49(2012).

47- T. Kuilla, S. Bhadrab, D. Yao, N. H. Kim, S. Bose, & J. H. Lee, "Recent advances in graphene based polymer composites", **Progress in Polymer Science 35**, 1350–1375(2010).

48- S. H. Xie, Y. Y. Liu, & J. Y. Li, "Comparison of the effective conductivity between composites reinforced by graphene nanosheets and carbon nanotubes", **Applied Physics Letters 92** : 243121(2008).

49- R. S. Ruoff, S. Stankovich, D. A. Dikin, G. H. B. Dommett, K. M. Kohlhaas, E. J. Zimney, E. A. Stach, R. D. Piner, & S. T. Nguyen, "Graphene-based composite materials", **Nature, 442**,282–286(2006).

50- N. H. Alamusi, F. Hisao, A. Satoshi, L. Yaolu, & L. Jinhua, "Piezoresistive strain sensors made from carbon nanotubes based polymer nanocomposites", **Sensor 11**: 10691–10723(2011).

51- Alain Nouailhat, **"An Introduction to Nanoscience and Nanotechnology"** ISTE Ltd, UK, London and John Wiley & Sons, Inc., USA, Hoboken, 1-206(2008).

52- W. Fu, H. Yang, H. Bala, S. Liu, M. Li, & G. Zou , "Preparation and magnetic characterization of core-shell structure stainless steel/silica nanoparticles", **Mater. Lett., 60,** 1728-1732(2006).

53- B. Mishra, B. B. Patel, & S. Tiwari , "Colloidal nanocarriers: a review on formulation technology, types and applications toward targeted drug delivery", **Nanomedicine , 6(1),** 9-24(2010).

54- W. H. Suh, K.S. Suslick, G.D. Stucky, & Y. H. Suh, "Nanotechnology, nanotoxicology, and neuroscience", **Progress in Neurobiology 87,** 133–170 (2009).

55- P. Stepp, F. Thomas, P. R. Lockman, H. Chen, & A. J. Rosengart, " In vivo interactions of magnetic nanoparticles with the blood–brain barrier", **J. Magn. Magn. Mater., 321,** 1591–1593(2009).

56- V. Mailander & K. Landfester, "Interaction of nanoparticles with cells", **Biomacromolecules, 10,** 2379–2400(2009).

57- V. Kral, J. Sotola, P. Neuwirth, Z. Kejik, K. Zaruba, & P. Martasek, "Nanomedicine—current status and perspectives: a big potential or just a catchword?", **Chemicke Listy, 100**, 4–9 (2006).

58- J. Corchero & A. Villaverde, "Biomedical applications of distally controlled magnetic nanoparticles", **Trends Biotechnol, 27,** 468–476(2009).

59- A. K. Gupta & M. Gupta , "Synthesis and surface engineering of iron oxide nanoparticles for biomedical applications"**, Biomaterials, 26**, 3995-4021 (2005).

60- P. Tartaj, M. P. Morales, S. Veintemillas-Verdaguer, Teresita Gonzalez –Carreno, & Carlos J. Serna, "The preparation of magnetic nanoparticles for applications in biomedicine", **J. Phys. D: Appl. Phys., 36**, R182-R197(2003).

61- D. M. Souza, A. L. Andrade, J. D. Fabris, P. Valério, A. M. Goes, M. F. Leite, & R. Z. Domingus, "Synthesis and in vitro evaluation of toxicity of silica-coated magnetite nanoparticles", **Journal of Non-Crystalline Solids, Vol. 354, No. 42-44**, 4894-4897(2008).

62- R. V. Ferreira, I. L. S. Pereira, L. C. D. Cavalcante, L. F. Gamarra, , S. M. Carneiro, E. Amaro, J. D. Fabris, R. Z. Domingues, & A. L. Andrade, "Synthesis and characterization of silica-coated nanoparticles of magnetite", **Hyperfine Interactions, 195,** 265-274(2009).

63- C. C. Berry & A. S. G. Curtis, "Functionalisation of magnetic nanoparticles for applications in biomedicine" **Journal of Physics D: Applied Physics, Vol. 36, No. 13**, R198-R206 (2003).

64- A. L. Andrade, D. M. Souza, M.C. Pereira , J. D. Fabris & R.Z. Domingues, “Magnetic properties of nanoparticles obtained by different chemical routes”, **Journal of Nanoscience and Nanotechnology, Vol. 9, No. 3,** 2081-2087(2003).

65- A. L. Higginbotham, J. R. Lomeda, A. B. Morgan, & J. M. Tour, “Graphite oxide flame retardant polymer nanocomposites”, **Appl. Mater. Interfaces, 1**, 2256-2261(2009).

66- A. Lerf, J. Klinowski, H. He, & M. Forster, “Structure of graphite oxide revisited”, **J. Phys. Chem., B 102,** 4477-4482(1998).

67- J. Klinowski, H. He, & M. Forster, “A new structural model for graphite oxide”, **Chem. Phys. Lett., 287**, 53-56(1998).

68- F. Uhl, & C. Wilkie, “preparation of nanocomposites from styrene and modified graphite oxides”, **Polym. Degrad. Stab., 84,** 215-226(2004).

69- C. Hontoria- Lucas, A. Lo´ pez-Peinado, J. Lo´pez-Gonza´lez, M. Rojas-Cervantes, & R. Martı´n-Aranda, “Study of oxygen- containing groups in a series of graphite oxides: Physical and chemical characterization”, **Carbon, 33,** 1585-1592(1995).

70- B. C. Brodie, “On the atomic weight of graphite” , **Philos. Trans. R. Soc. London, 14,** 249–259(1859).

71- L. Staudenmaier, “Verfahren zur Darstellung der Graphitsa¨ure. Ber. Dtsch”, **Chem. Ges., 31**, 1481-1487(1898).

72- W. S. Hummers, & R. E. Offeman, “Preparation of graphitic oxide” **J. Am. Chem. Soc., 80,** 1339-1339(1958).

73- T. Ishikawa, T. Nagaoki, & Shin tanso kogyo, **"New Carbon Industry"**. 2nd ed.; Kindai hensyusya: Tokyo, 125-36(1986).

74- T. Szabo´, O. Berkesi, P. Forgo´, K. Josepovits, Y. Sanakis, D. Petridis, & I. Dekany, “Evolution of surface functional groups in a series of progressively oxidized graphite oxides”, **Chem. Mater**., **18(11)**, 2740–2749(2006).

75- N. Savage, “Super carbon”, **Nature, 483**, S30–S31(2012).

76- H. Wang, X. Yuan, Y. Wu, H. Huang, X. Peng, G. Zeng, H. Zhong, J. Liang, & M. Ren, “Graphene-based materials: fabrication, characterization and application for the decontamination of wastewater and wastegas and hydrogen storage/generation” **Adv. Colloid Interface Sci.**, **195–196**, 19–40(2013).

77- A. H. Castro Neto, F. Guinea, N. M. R. Peres, K. S. Novoselov, & A. K. Geim, “The electronic properties of graphene” **Rev. Mod. Phys.**, **81,** 109–162(2009).

78- K. S. Novoselov, A. K. Geim , S. V. Morozov, D. Jiang, Y. Zhang, S. V. Dubonos, I. V. Grigorieva, & A. A. Firsov, “Electric field effect in atomically thin carbon films” **Science**, **306**, 666–669(2004).

79- R. R. Nair, P. Blake, A. N. Grigorenko, K. S. Novoselov, T. J. Booth, T. Stauber, N. M. R. Peres, & A. K. Geim, “Fine structure constant defines visual transparency of graphene” **Science**, **320**, 1308 (2008).

80- Sasha Stankovich, Dmitriy A. Dikin, Geoffrey H. B. Dommett, Kevin M. Kohlhaas, Eric J. Zimney, Eric A. Stach, Richard D. Piner, SonBinh T. Nguyen & Rodney S. Ruoff, “Graphene-based composite materials” **Nature**, **442**, 282–286(2006).

81- X. Li, X. Wang, L. Zhang, S. Lee, & H. Dai, “Chemically derived, ultrasmooth graphene nanoribbon semiconductors” **Science**, **319**, 1229–1232(2008).

82- S. Mao, K. Yu, J. Chang, D. A. Steeber, L. E. Ocola, & J. Chen, “Direct growth of vertically-oriented graphene for field effect transistor biosensor”, **Sci. Rep., 3,** 1696–1702(2013).

83- W. Li, C. Tan, M. A. Lowe, H. D. Abruna, & D. C. Ralph, “Electrochemistry of individual monolayer graphene sheets” **ACS Nano**, **5**, 2264–2270(2011).

84- T. Ramanathan, A. A. Abdala, S. Stankovich, D. A. Dikin, M. Herrera-Alonso, R. D. Piner, D. H. Adamson, H. C. Schniepp, X. Chen, R. S. Ruoff, S. T. Nguyen, I. A. Aksay, R. K. Prud'Homme & L. C. Brinson, "Functionalized graphene sheets for polymer nanocomposites" **Nature Nanotechnol., 3**, 327– 331(2008).

85- M. D. Stoller, S. Park, Y. Zhu, J. An, & R. S. Ruoff, "Graphene-based ultracapacitors" **Nano Lett., 8**, 3498–3502(2008).

86- M. Pumera, "Graphene in biosensing", **Mater. Today**, **14**, 308–315(2011).

87- M. F. El-Kady, V. Strong, S. Dubin, & R. B. Kaner, "Laser scribing of high-performance and flexible graphene-based electrochemical capacitors" **Science, 335**, 1326–1330(2012).

88- A. Bianco, "Graphene: safe or toxic? The two faces of the medal" **Angew. Chem., Int. Engl., 52**, 4986–4997(2013).

89- Gregg P. Kotchey, Brett L. Allen, Harindra Vedala, Naveena Yanamala, Alexander A. Kapralov, Yulia Y. Tyurina, Judith Klein-Seetharaman, Valerian E. Kagan, & Alexander Star, "The enzymatic oxidation of graphene oxide", **ACS Nano, 5(3)**, 2098–2108(2011).

90- S. Iijima, & T. Ichihashi, "Single-Shell Carbon Nanotubes of 1-nm Diameter", **Nature, vol. 363**, 603-605(1993).

91- S. Iijima, "Helical Microtubules of Graphitic Carbon", **Nature**, **vol. 354,** 56-58(1991).

92- P. J. F. Harris, **"Carbon Nanotube Science"**, Cambridge University Press, Cambridge, (2009).

93- M. M. J. Treacy, T. W. Ebbesen, & J. M. Gibson, "Exceptionally high Young's modulus observed for individual carbon nanotubes", **Nature**, **381**, 678-680(1996).

94- O. Lourie, D. M. Cox, & H. D. Wagner, "Buckling and collapse of embedded carbon nanotubes", **Phys. Rev. Lett. 81,** 1638-1641(1998).

95- R. A. Vaia, & H. D. Wagner, "Framework for nanocomposites", **Mater. Today , 7,** 32-37(2004).

96- M. Magnuson, J. H. Guo, S. M. Butorin, A. Agui, C. Såthe & J. Nordgren, **"**The electronic structure of polyaniline and doped phases studied by soft X-ray absorption and emission spectroscopies", **Journal of Chemical Physics, 111**, 4756(1999).

97- Kerileng M. Molapo, Peter M. Ndangili, Rachel F. Ajayi, Gcineka Mbambisa, Stephen M. Mailu, Njagi Njomo, Milua Masikini, Priscilla Baker & Emmanuel I. Iwuoha, " Electronics of Conjugated Polymers (I): Polyaniline", **Int. J. Electrochem. Sci., 7,** 11859 – 11875(2012).

98- Faris Yilmaz**,"Polyaniline: Synthesis, Characterization, Solution Properties and Composites"**, Ph.D. thesis reported in Graduate School of Natural and Applied Sciences of Middle East Technical University, Ankara, Turkey (2007).

99- A. J. Epstein & A.G. MacDiarmid, "Structure, Order, and the Metallic State in Polyaniline and Its Derivatives", **Synthetic Metals 41,** 601-606 (1991).

100- B. S. Fey Lin, **"Electrical studies of metal-insulator-semiconductor structures"** MSC. Thesis Submitted to the Graduate Faculty of Texas Tech University, USA, Texas(1988).

101- D. Jiles, **"Introduction to the Electronic Properties of Materials",** Chapman & Hall, London, UK (1994).

102- M. R .Aguilar, C. Elvira, A. Gallardo, B. Vázquez, & J.S. Román, **"Smart Polymers and their Applications as Biopolymers"** Topics in Tissue Engineering, Eds. N Ashammakhi, R Reis & E Chiellini, Vol. 3, ch.6(2007).

103- N. A. Peppas, P. Bures, & W. Leobandung, “Hydrogels in pharmaceutical formulations”, **Eur. J. Pharm. Biopharm., 50 (1**), 27- 46(2000).

104- E. S. Gil, & S. M. Hudson, “Stimuliresponsive polymers and their bioconjugates”, **Progress in Polymer Sciences, 29 (12**), 1173-222(2004).

105- N. Ohnishi, K. Aoshima, & K. Kataoka, “Stimuli-responsive polymer utilizing ketoenol tautomerization for pharmaceutical and medical use”, patent number **US 6852819B2**(2005).

106- Garima Singh, Alka Lohani, & Shiv Sankar Bhattacharya, “Hydrogel as a novel drug delivery system: a review”, **J. Fundam. Pharm. res. 2(1),** 35-48(2014).

107- X. Liu, H. Guo, & L. Zha, “Study of pH/temperature dual stimuli-responsive nanogel with interpenetrating polymer network structure”, **Plym. Int. 61(7),** 1144-1150(2012).

108- R. E. Rosenweig**," Ferrohydrodynamics",** Cambridge University Press, Cambridge, London, New York, New Rochelle, Melburne, Sydney, (1985).

109- J. E. Mark, “Bimodal networks and networks reinforced by in situ precipitation of silica”, **British Polymer Journal 17(2)**, 144-148 (1985).

110- W. Haas, M. Zrínyi, H.- G. Kilian, & B. Heise, “**Colloid and Polymer Science”, 271,** 1024 (1993).

111- C. J. Sunderland, M. Steiert, J. E. Talmadge, A. M. Derfus, & S. E. Barry , “Targeted nanoparticles for detecting and treating cancer”, **Drug Dev Res 67(1):**70–93(2006).

112- L. M. Luiz, & S. I. C. de Torresi, “Conducting polymer-hydrogel composites for electrochemical release devices: Synthesis and characterization of semi-interpenetrating polyaniline-polyacrylamide networks”, **Electrochem. Commun., 7,** 717-723(2005).

113- S. Geetha, C. R. K. Rao, M. Vijayan, & D. C. Trivedi, "Biosensing and drug delivery by polypyrrole" **Anal. Chim. Acta, 568,** 119-125(2006).

114- D. Posadas, & M. I. Florit, "The redox switching of electroactive polymers"**, J. Phys. Chem. B**, **108,** 15470-15476 (2004).

115- S. Richardson-Burns, J. L. Hendricks, B. Foster, L. K. Povlich, D. Kim, & D.C. Martin, "Polymerization of the conducting polymer poly(3,4-ethylenedioxythiophene) (PEDOT) around living neural cells", **Biomaterials, 28,** 1539-1552 (2007).

116- P. J. Kinlen, B. G. Frushour, Y. Ding, & V. Menon, "Synthesis and characterization of organically soluble polyaniline and polyaniline block copolymer", **Synth. Met., 101,** 758-761(1999).

117- J. L. Breads, & R. Silbey, **"Conjugated Polymers"** Kluwer Academic: Amsterdam, The Netherlands(1991).

118- J. Y. Wong, R. Langer, & D. E. Ingberi, "Electrically Conducting Polymers Can Noninvasively Control the Shape and Growth of Mammalian Cells", **Proc Natl Acad Sci USA, 91,** 3201-3204(1994).

119- G. B. Street**, "Polypyrrole: from Powders to Plastics"** In: T. A. Skotheim, editor. *Handbook of conducting polymers*, vol. I. New York: Marcel Dekker, 265-291(1986).

120- G. M. Spinks, V. Mottaghitalab, M. Bahrami-Samani, P. G. Whitten, & G. G. Wallace, "Carbon-Nanotube-Reinforced Polyaniline Fibres for high-strength artificial muscle", **Adv. Mater., 18,** 637-640(2006).

121- G. Ćirić-Marjanović, L. Dragičević, M. Milojević, M. Mojović, S. Mentus, B. Dojčinović, B. Marjanović, & J. Stejskal, "Synthesis and characterization of self-assembled polyaniline nanotubes/silica nanocomposites", **J. Phys. Chem., 113,** 7116-7127(2009).

122- G. G. Wallace, M. Smyth, & H. Zhao, "Conducting electroactive polymer-based biosensors", **Trends Anal. Chem., 18,** 245-251(1999).

123- Y. H. Park, & C. R. Park, "Preparation of conducting polyacrylonitrile/polyaniline composite films by electrochemical synthesis and their electroactivity", **Synth. Met., 118,** 187-192(2001).

124- S. Jayanty, G .K. Prasad, B. Sreedhar, & T. P. Radhakrishnan, "Polyelectrolyte template polyaniline-film morphology and conductivity"**, Polymer, 44,** 7265-7270(2003).

125- P. R. Bidez, S. Li, A. G. MacDiarmid, E. C. Venancio, Y. Wei, & P. I. Lelkes, "Polyaniline, an electroactive polymer, supports adhesion and proliferation of cardiac myoblasts" **J. Biomater. Sci. Polym. Ed., 17,** 199-212(2006).

126- S. Brahim, & A. Guiseppi-Elie, "Electroconductive hydrogels: Electrical and electrochemical properties of polypyrrole-poly(HEMA) composite", **Electroanalysis, 17,** 556-570(2004).

127- William G. Pitt, Ghaleb A. Husseini, & Bryant J. Staples, "Ultrasonic Drug Delivery – A General Review", **Expert Opin Drug Deliv.,1(1),** 37-56(2004).

128- C. Barrett, & O. Mermut, "Polymer multilayer films with azobenzene for photoactive biosurfaces", **PMSE Preprints, 92,** 51-52(2005).

129- Krishna Vamshi Allam, & Gannu Praveen Kumar, " Colorants the cosmetics for the pharmaceutical dosage forms", **International Journal of Pharmacy and Pharmaceutical Sciences, 3,** (2011).

130- J. D. Craik & D. K. Afifi " The safety of intravenous indigo carmine to assess ureteric patency during transvaginal uterosacral suspension of the vaginal vault", **Journal of Pelvic Medicine and Surgery, 15,** 11-15, (2009).

131- D. P. Hurlstone, D.S. Sanders, S. S. Cross, I. Adam, A. J. Shorthouse, S. Brown, K. Drew, & A. J. Lodo, "Colonoscopic resection of lateral

spreading tumours: a prospective analysis of endoscopic mucosal resection", **Gut, 53**, 1334-1339 (2004).

132- S. Kudo, S. Tamura, T. Nakajima, H. Yamano, H. Kusaka, & H. Watanabe, " Diagnosis of colorectal timorous lesions by magnifying endoscopy" **Gastrointest Endosc, 44(1),** 8-14(1996).

133- A. J. Klein-Szanto, "Carcinogenic effects of chemotherapeutic compounds", **Prog Clin Biol Res**, **374** :167–174(1992).

134- A. Jemal, F. Bray, M. M. Center, J. Ferlay, E. Ward, & D. Forman, "Global cancer statistics" **CA Cancer J Clin, 61**, 69-90(2011).

135- S. J. Duthie, "Folic-acid-mediated inhibition of human colon-cancer cell growth", **Nutrition, 17**: 736-737(2001).

136- Yoon S-A, Choi JR, Kim J-O, Shin J-Y, Zhang X, & Kang J-H., "Influence of reduced folate carrier and dihydrofolate reducatse genes on methotrexate-induced cytotoxicity", **Cancer Res Treat, 42** :163-171(2010).

137- M. Das, & S. K. Sahoo , "Epithelial cell adhesion molecule targeted nutlin-3a loaded immunonanoparticles for cancer therapy", **Acta Biomater, 7 :**355-369(2011).

138-D. Banerjee, P. Mayer-Kuckuk, G. Capiaux, T. Budak-Alpdogan, R. Gorlick, & J. R. Bertino, "Novel aspects of resistance to drugs targeted to dihydrofolate reductase and thymidylate synthase", **Biochim Biophys Acta;1587**:164-173(2002).

139- S. Murdan, "Electro-Responsive Drug Delivery from Hydrogels" **J. Controlled Release, 92,** 1–17(2003).

140- Y. Yang, & J. B. F. N. Engberts, "Stimuli Response of Poly soap Hydrogels in Aqueous Solution and DC Electric Fields", **Colloids Surf., A , 169,** 85–94(2000).

141- K. Sutani, I. Kaetsu, & K. Uchida, "The Synthesis and the Electric-Responsiveness of Hydrogels Entrapping Natural Polyelectrolyte", **Radiat. Phys. Chem.**, **61,** 49–54(2001).

142- W. C. Huang, T. J. Lee, C. S. Hsiao, S. Y. Chen, & D. M. Liu "Characterization and Drug Release Behavior of Chip-Like Amphiphilic Chitosan-Silica Hybrid Hydrogel for Electrically Modulated Release of Ethosuximide: An in Vitro Study", **J. Mater. Chem., 21,** 16077–16085(2011).

143- H. W. Liu, S. H. Hu, Y. W. Chen, & S. Y. Chen , "Characterization and Drug Release Behavior of Highly Responsive Chip-Like Electrically Modulated Reduced Graphene Oxide-Poly(vinyl alcohol) Membranes" **J. Mater. Chem., 22,** 17311–17320(2012).

144-S . Ramanathan, & L. H. Block, "The use of chitosan gels as matrices for electrically-modulated drug delivery", **J. Control Release 70** 109–123(2001).

145- K. Sutani, I. Kaetsu, & K. Uchida, "The synthesis and the electric-responsiveness of hydrogels entrapping natural polyelectrolyte", **Radiation Physics and Chemistry, 61(1),** 49–54(2001).

146- T. Tanaka, I. Nishio, S.T. Sun, & S. Ueno-Nishio, "Collapse of gels in an electric field", **Science 218**, 467–469(1982).

147-S. H. Gehrke, "Synthesis, equilibrium swelling, kinetics, permeability and applications of environmentally-responsive gels", **Adv. Polym. Sci. 110,** 81–144(1993).

148-K. Laursen, S. Murdan, D. Dimitrijevic, & A. T. Florence, "The formation and swelling behaviour of chondroitin", **Pharm. Sci. 3 (3)** (2001).

149- M. Jensen, P. B. Hansen, S. Murdan, S. Frokjaer, & A. T. Florence, "The Florence, Loading into and electro-stimulated release of peptides and proteins from chondroitin-4-sulphate hydrogels", **Eur. J. Pharm. Sci. 15,** 139–148(2002).

150- R. Tomer, D. Dimitrijevic, & A. T. Florence, "Electrically controlled release of macromolecules from cross-linked hyaluronic acid hydrogels", **J. Control. Release, 33,** 405– 413(1995).

151- K. Sawahata, M. Hara, H. Yasunaga, & Y. Osada, "Electrically controlled drug delivery system using polyelectrolyte gels", **J. Control. Release 14,** 253–262(1990).

152- I .C. Kwon, Y. H. Bae, T. Okano, & S. W. Kim, "Drug release from electric current sensitive polymers", **J. Control. Release 17,** 149–156(1991).

153- I. C. Kwon, Y. H. Bae, & S. W. Kim, "Electrically erodible polymer gel for controlled release of drugs", **Nature, 354**, 291–293(1991).

154- S. Mohammadi-Samani, R. Miri, M. Salmanpour, N. Khalighian, S. Sotoudeh & N. Erfani, "preparation and assessment of chitosan-coated superparamagnetic Fe_3O_4 nanoparticles for controlled delivery of methotrexate", **Research in Pharmaceutical Sciences, 8(1):** 25-33(2013).

155- Doina Hritcu, Marcel I. Popa, Niculina Popa, Vasile Badescu, & Vera Balan, "Preparation and characterization of magnetic chitosan nanospheres", **Turk J. Chem. 33,** 785 – 796(2009).

156- Dena Dorniani , Mohd Zobir Bin Hussein , Aminu Umar Kura , Sharida Fakurazi , Abdul Halim Shaari, & Zalinah Ahmad, "Sustained release of prindopril erbumine from Its chitosan-coated magnetic nanoparticles for biomedical applications"**, Int. J. Mol. Sci., 14,** 23639-23653(2013).

157- S. Asgari, Z. Fakhari, & S. Berijani, "Synthesis and characterization of Fe_3O_4 magnetic nanoparticles coated with carboxymethyl chitosan grafted sodium methacrylate", **Journal of NanoStructures, 4,** 55-63 (2014).

158- Jude Namanga, Josepha Foba, Derek Tantoh Ndinteh, Divine Mbom Yufanyi, & Rui Werner Maçedo Krause, "Synthesis and magnetic properties of a superparamagnetic nanocomposite (pectin-magnetite nanocomposite)", **Journal of Nanomaterials , Volume 2013,** Article ID 137275, 8 pages(2013).

159- Foba-Tendo J. Ngenefeme, Namanga J. Eko, Yufanyi D. Mbom, Ndinteh D. Tantoh, & Krause W. M. Rui, "A one pot green synthesis and characterisation of iron oxide-pectin hybrid nanocomposite", **Open Journal of Composite Materials, 3,** 30-37(2013).

160- Reyhan Omidirad, Farzaneh Hosseinpour Rajabi & Bahman Vashechani Farahani, "Preparation and in vitro drug delivery response of doxorubicin loaded poly(acrylic acid)-coated magnetite nanoparticles"**, J. Serb. Chem. Soc. 78 (10),** 1609–1616 (2013).

161- S. Kayal, & R.V. Ramanujan, "doxorubicin loaded PVA coated iron oxide nanoparticles for targeted drug delivery", **Materials Science and Engineering C 30,** 484–490(2010).

162- Xing-ping Qiua & Francoise Winnikb, "Preparation and characterization of PVA coated magnetic nanoparticles", **Chinese Journal of Polymer Science Vol. 18, No. 6,** 535-539 (2000).

163- Hailong Fan, Lili Wang, Keke Zhao, Nan Li, Zujin Shi, Zigang Ge, & Zhaoxia Jin, "Fabrication, mechanical properties, and biocompatibility of graphene-reinforced chitosan composites", **Biomacromolecules, 11,** 2345–2351(2010).

164- Lulu Ren, Tianxi Liu, Juan Guo, Shuzhong Guo, Xiaoyan Wang & Weizhi Wang, "A smart pH responsive graphene/polyacrylamide complex via noncovalent interaction", **Nanotechnology, 21,** 335701 (7pp) (2010).

165- I. Tantis, G. C. Psarras, & D. Tasis, "Functionalized graphene – poly(vinyl alcohol) nanocomposites: Physical and dielectric

properties”, **eXPRESS Polymer Letters, Vol.6, No.4** 283–292(2012).

166- Jangho Kim, Yang-Rae Kim, Yeonju Kim, Ki Taek Lim, Hoon Seonwoo, Subeom Park, Sung-Pyo Cho, Byung Hee Hong, Pill-Hoon Choung, Taek Dong Chung, Yun-Hoon Choung, & Jong Hoon Chung, “Graphene-incorporated chitosan substrata for adhesion and differentiation of human mesenchymal stem cells”, **J. Mater. Chem. B, 1**, 933–938(2013).

167- Yeon-Yi Kim, Jumi Yun, Young-Seak Lee & Hyung-Il Kim, “Electro-responsive transdermal drug release of MWCNT/PVA nanocomposite hydrogels”, **Carbon Letters, Vol. 11, No. 3**, 211-215(2010).

168- Sajjad Sedaghat, “Synthesis and characterization of new biocompatible copolymer: chitosan-graft-polyaniline”, **International Nano Letters, 4, 2,** 1-6(2014).

169- Tong-Sheng Tsai, Viness Pillay, Yahya E. Choonara , Lisa C. du Toit , Girish Modi , Dinesh Naidoo & Pradeep Kumar, “A polyvinyl alcohol-polyaniline based electro-conductive hydrogel for controlled stimuli-actuable release of indomethacin”, **Polymers, 3,** 150-172 (2011).

170- A. K. Bajpai, J. Bajpai, & S. N. Soni, “Preparation and characterization of electrically conductive composites of poly(vinyl alcohol)-g-poly(acrylic acid) hydrogels impregnated with polyaniline (PANI)”, **eXPRESS Polymer Letters Vol.2, No.1,** 26–39(2008).

171- Reetu Prabhakar & D. Kumar, “Investigation on poly(acrylate-co-acrylamide)/polyaniline conducting hydrogel”, **American Journal of Polymer Science & Engineering, 3:** 14 (2015).

172- Sungjin Park , Jinho An , Jeffrey R. Potts , Aruna Velamakanni , Shanthi Murali , & Rodney S. Ruoff, “Hydrazine-reduction of graphite- and graphene oxide”, **Carbon ,49 ,**3019 –3023(2011).

173- J. Liu, J. Shi, L. Jiang, F. Zhang, L. Wang, & S. Yamamoto, "Segmented magnetic nanofibers for single cell manipulation", **Appl. Surf. Sci., Vol. 258,** 7530–7535(2012).

174- J. Stejskal & R. G. Gilbert, "Polyaniline. Preparation of a conducting Polymer (IUPAC Technical Report)" , **Pure Appl. Chem., Vol. 74, No. 5,** 857–867, (2002).

175- Parimal Maji, Arijit Gandhi, Sougata Jana, & Nirmal Maji, "Preparation and characterization of maleic anhydride cross-Linked chitosan-polyvinyl alcohol hydrogel matrix transdermal patch", **Journal of PharmaSciTech, 2(2)**:62-67(2013).

176- Katarzyna Lewandowska , Aldona Dąbrowska, and Halina Kaczmarek, "Rheological properties of pectin, poly(vinyl alcohol) and their blends in aqueous solutions", **e-Polymers., 12, Issue 1,** 160–172, (2013).

177- T. Jamnongkan, & S. Kaewpirom, "Controlled-Release Fertilizer Based on Chitosan Hydrogel: Phosphorus Release Kinetics", **Sci. J. UBU, Vol. 1, No. 1,** 43-50(2010).

178- P. Ramakrishna, B. Mallikarjuna, A. Chandra Babu, P. Sudhakar, K. Chowdoji Rao and M.C.S. Subha, "Interpenetrating polymer network of crosslinked blend microspheres for controlled release of Acebutolol HCl", **Journal of Applied Pharmaceutical Science 01 (06)**, 212-219 (2011).

179-Long Xu , Yun-An Huang , Qiu-Jin Zhu , & Chun Ye, "Chitosan in Molecularly-Imprinted Polymers: Current and Future Prospects", **Int. J. Mol. Sci. 16**, 18328-18347(2015).

180-P. Rama Subba Reddy, S. Eswaramma, K. S. V. Krishna Rao, & Yong Ill Lee, "Dual Responsive Pectin Hydrogels and Their Silver Nanocomposites: Swelling Studies, Controlled Drug Delivery and Antimicrobial Applications", **Bull. Korean Chem. Soc., Vol. 35, No. 8**, 2391(2014).

181-J. M. Gohil, A. Bhattacharya, & P. Ray, "Studies on the cross-linking of poly(vinyl alcohol)", **Journal of Polymer Research 13**,161-169(2006).

182- Ali Pourjavadi, & Gholam Reza Mahdavinia, "Superabsorbency, pH-sensitivity and swelling kinetics of partially hydrolyzed chitosan-g-poly(acrylamide) hydrogels", **Turk J. Chem., 30,** 595 – 608(2006).

183-Michel Bocourt Povea, Waldo Argüelles Monal, Juan Valerio Cauich Rodríguez, Alejando May Pat, Nancy Badas Rivero, & Carlos Peniche Covas, "Interpenetrated chitosan-poly(acrylic acid-Co-acrylamide) hydrogels. synthesis, characterization and sustained protein release studies", **Materials Sciences and Applications, 2,** 509-520, (2011).

184-G.R. Mahdavinia, A. Pourjavadi, H. Hosseinzadeh, and M.J. Zohuriaan, "Superabsorbent hydrogels from poly(acrylic acid-co-acrylamide) grafted chitosan with salt- and pH-responsiveness properties", **European Polymer Journal, 40** 1399–1407(2004).

185- M. Efentakis, M. Vlachou, & N. H. Choulis, " Effects of excipients on swelling and drug release from compressed matrices" **Drug Development and Industrial Pharmacy, 23(1),** 107- 112(1997).

186- Chunxiao Wu, Seong Loong Lo, Jerome Boulaire, Michelle Li Wen Hong, Hui Min Beh, Doreen Siu Yi Leung, & Shu Wang, "A peptide-based carrier for intracellular delivery of proteins into malignant glial cells in vitro", **Journal of Controlled Release, 130,** 140–145(2008).

187- Seyfullah Madakbas, Kadir Esmer, Ersin Kayahan, & Mehmet Yumak, "Synthesis and Dielectric Properties of Poly(aniline)/Na-bentonite Nanocomposite", **Science and Engineering of Composite Materials 17,** 145-153 (2010).

188- S. R. Elliott**, "The Physics and Chemistry of Solids"**, Chichester: John Wiley & Sons, 630(1998).

189- Hilda W. F. Sung & Czeslaw Rudowicz, **"A closer look at the hysteresis loop for ferromagnets: A survey of misconceptions and misinterpretations in textbooks",** City University of Hong Kong, Department of Physics and Materials Science, (2002).

190-William Lowrie, **"Fundamentals of Geophysics",** 2nd Edition, University Printing House, Cambridge CB2 8BS, United Kingdom (2007).

191- Guozhong Cao, & C. Jeffrey Brinker, **" Annual review of nano research. Volume 2",** Hackensack, NJ: World Scientific, (2008).

192-A. Pawlak, & M. Mucha, "Thermogravimetric and FTIR studies of chitosan blends", **Thermochimica Acta 396**: 153-166(2003).

193-H. Zheng, Y. M. Du, J. H. Yu, R. H. Huang & L. N. Zhang, "Preparation and charecterization of chitson/polyvinyl alcohol blend fibres", **J. Appl. Polym. Sci. 80(13**): 2558–2565(2001).

194-H. Y. Kweon, I. C. Um & Y. H. Park, "Structural and thermal characteristics of Antheraea pernyi silk fibroin/chitosan blend film", **Polymer 42**: 6651-6656(2001).

195-A. Sinitsya, J. Copikova, P. Matejka & V. Machovic, "Fourier transform raman and infrared spectroscopy of pectins" , **Carbohy. Polym., 54(1)**: 97-106(2003).

196-M. A. Coimbra, A. Barros, M. Barros, D. N. Rutledge, & I. Delgadillo, "Multivaliate of uronic acid and neutral sugars in whole pectin samples by FT-IR spectroscopy", **Carbohy. Polym., 37**: 241(1998).

197-T. Wang, M. Turhan, & S. Gunasekaran, " Selected properties of pH-sensitive, biodegradable chitosan-poly(vinyl alcohol) hydrogel", **Polym Int. ;53(7):**911–918(2004).

198-H. S. Mansur, C. M. Sadahira, A. N. Souza, & A. A. P. Mansur,

"FTIR spectroscopy characterization of poly (vinyl alcohol) hydrogel with different hydrolysis degree and chemically crosslinked with glutaraldehyde", **Mater. Sci. Eng. C.; 28(4):**539–548(2008).

199-D. Sahoo, S. Sahoo, J. Das, T. K. Dangar & P. L. Na- yak, "Antibacterial Activity of Chitosan Crosslinked with Aldehydes and Blended with Cloisite 30B," **NanoTrends , 10,** 1-9(2011).

200-L. M. Manocha, Hasmukh Gajera, Vishal Mankadia, & S. Manocha, "Oxidation-Reduction of Natural Graphite - A step Towards Synthesis of Graphene", **Journal of Pure and Applied Sciences, 18**: 92 – 97 (2010).

201-Z. Y. Lin, Y. G. Yao, Z. Li, Y. Liu, Z. Li, & C. P. Wong, "Solvent-assisted thermal reduction of graphite oxide", **Journal of Physical Chemistry C 114** , 14819–14825(2010).

202-Anupama Chaturvedi1, Ashutosh Tiwari2, & Atul Tiwari1, "Spectroscopic and morphological analysis of graphene vinylester nanocomposites", **Adv. Mat. Lett.**, **4(9),** 656-661(2013).

203-Muhammad Ali Turgunov1, Jin Oh Oh, & Sung Ho Yoon, "Surface Modification of Multiwall Carbon Nanotubes by Sulfuric Acid and Nitric Acid", **Advanced Science and Technology Letters , 64**, 22-25(2014).

204-Karina Donadel, Marcos D. V. Felisberto, Valfredo T. Fávere, Mauricio Rigoni, Nelson Jhoe Batistela, & Mauro C.M. Laranjeira, "Synthesis and characterization of the iron oxide magnetic particles coated with chitosan biopolymer", **Materials Science and Engineering C 28** , 509–514(2008).

205-Liang Guo , Guang Liu , Ruo-Yu Hong , & Hong-Zhong Li, "Preparation and Characterization of Chitosan Poly(acrylic acid) Magnetic Microspheres", **Mar. Drugs, 8,** 2212-2222(2010).

206-S. Tripathi, G. K. Mehrotra, & P. K. Dutta, "Physicochemical and bioactivity of cross-linked chitosan–PVA film for food packaging

applications", **International Journal of Biological Macromolecules, 45,** 372–376(2009).

207-Liu L, Xiao L, Zhu HY, & Shi XW, " Preparation of magnetic and fluorescent bifunctional chitosan nanoparticles for optical determination of copper ion", **Microchim Acta 178**(3–4):413–419(2012).

208-Q. Du, M. Zheng, L. Zhang, Y. Wang, J. Chen, L. Xue, W. Dai, G. Ji, & J. Cao, "Preparation of functionalized graphene sheets by a low-temperature thermal exfoliation approach and their electrochemical supercapacitive behaviors", **Electrochim. Acta 55**, 3897-3903(2010).

209-S. Park, J. An, J. Potts, A. Velamakanni, S. Murali, & S. Ruoff Rodney "Hydrazine-reduction of graphite- and graphene oxide" **Carbon 49**, 3019–3023 (2011).

210-S. Dubin, S. Gilje, K. Wang, V. Tung, K. Cha, A. Hall, J. Farrar, R. Varshneya, Y. Yang, & R. Kaner, "A one-step, solvothermal reduction method for producing reduced graphene oxide dispersions in organic solvents" **ACS Nano 4,** 3845–3852 (2010).

211-K. Moon In, J. Lee, S. Ruoff Rodney, & H. Lee, "Reduced graphene oxide by chemical graphitization" **Nat. Commun., 1(6):** 73 (2010).

212-M. Endo, K. Takeuchi, T. Hiraoka, T. Furuta, T. Kasai, X. Sun, C. H. Kiang, & M. S. Dresselhaus**,** "Stacking Nature of Graphene Layers in Carbon Nanotubes and Nanofibres"**, J. Phys. Chem. Solids,58**, 1707-1712(1997).

213-A. R. Subrahmanyam, V. Geetha, Atul kumar, A. Alakanandana, & J. Siva Kumar, "Mechanical and Electrical Conductivity Studies of PANI-PVA and PANI-PEO Blends", **International Journal of Material Science, 2(1)**, 27-30(2012).

214-S. Raghunadh Acharyulu, T. Gomathi and P. N. Sudha, "Synthesis and characterization of cross linked chitosan-polystyrene polymer

blends", **Der Pharmacia Lettre, 5 (4),** 74-83(2013).

215-E. C. Achilleos, R. K. Prud'homme , K. N. Christodoulou, K. R. Gee , & I. G. Kevrekidis, "Dynamic deformation visualization in swelling of polymer gels", **Chem Eng Sci, 55**, 3335-3340, (2000).

216-Raphael M. Ottenbrite, Kinam Park, & Teruo Okano, **"Biomedical Applications of Hydrogels Handbook"** Springer (2010).

217-Giuseppe Tronci, Hiroharu Ajiro, Stephen J. Russell, David J. Wood, & Mitsuru Akashi, "Tunable drug-loading capability of chitosan hydrogels with varied network architectures", **Acta Biomaterialia, Volume 10, Issue 2,** Pages 821–830(2014).

218-N. A. Peppas, & C. T. Reinhart, "Solute diffusion in swollen membranes. Part I. A new theory", **J. Membr. Sci. 15**, 275–287(1983).

219-Lei Shang , Sam Zhang , Hejun Du , & Subbu S. Venkatraman, "A novel approach for the control of drug release rate through hydrogel membrane: I. Effect of drug immobilization on drug release rate by copolymerization method", **European Journal of Pharmaceutics and Biopharmaceutics , 68(3): 715-723** (2008).

220-Suelen H. Takahashi, Luiz M. Lira, & Susana I. Córdoba de Torresi, "Zero-Order Release Profiles from a Multistimuli Responsive Electro-Conductive Hydrogel", **Journal of Biomaterials and Nanobiotechnology**, **3**, 262-268(2012).

221-S. Sayyar, E. Murray, B. C. Thompson, J. Chung, D. L. Officer, S. Gambhir, G. M. Spinks & G. G. Wallace, "Processable conducting graphene/chitosan hydrogels for tissue engineering" **Journal of Materials Chemistry B, 3 (3),** 481-490(2015).

222-Valeria Alzari, Daniele Nuvoli, Sergio Scognamillo, Massimo Piccinini, Emilia Gioffredi, Giulio Malucelli, Salvatore Marceddu, Mario Sechi, VannaSanna & Alberto Mariani, "Graphene-containing thermoresponsive nanocomposite hydrogels of poly(*N*-

isopropylacrylamide) prepared by frontal polymerization", **J. Mater. Chem.**, **21**, 8727-8733(2011).

223-Rahna K Shamsudeen, Shiny Nair & V G Jayakumari, "Equilibrium swelling, conductivity and electroactive characteristics of poly acrylamide hydrogels", **Indian Journal of Engineering & Materials Sciences, 13,** 62-68(2006).

224-G. M. Tsangaris, G. C. Psarras, & N. Kouloumbi "Polyurethane latex/water dispersible boehmite alumina nanocomposites: Thermal, mechanical and dielectrical properties", **Journal of Materials Science, , vol. 33, No. 8,** 2027-2037, (1998).

225-K. G. Gatos, J. G. Martinez Alcazar, G. C. Psarras, R. Thomann, & J. Karger-Kocsis, "Polyurethane latex/water dispersible boehmite alumina nanocomposites: thermal mechanical and dielectrical properties", **Composites Science and Technology 67 (2)** 157–167(2007).

226-G. C. Psarras, K. G. Gatos, P. K. Karahaliou, S. N. Georga , C. A. Krontiras, & J. Karger-Kocsis, "Relaxation phenomena in rubber/ layered silicate nanocomposites", **Springer, Express Polymer Letters, vol. 1**, 837-845(2007).

227-A. Kalini A, K. G. Gatos, P. K. Karahaliou, S. N. Georga, C. A. Krontiras, & G. C. Psarras, "Probing the dielectric response of polyurethane/alumina nanocomposites"**, Journal of Polymer Science Part B: Polymer Physics, vol. 48,** 2346-2354 (2010).

228-Y. C. Li, R. K. Y. Li, & S. C. Tjong, "Frequency and temperature dependences of dielectric dispersion and electrical properties of polyvinylidene fluoride/expanded graphite composites" javascript:; Springer, **Journal of Nanomaterials**, no vol., and pp. given, (2010).

229-S. C. Tjong, & Y. W. Mai, **"Conductivity and dielectric characterization of polymer nanocomposites. in 'Physical properties of polymer nanocomposites",** Woodhead, Cambridge,

31–69 (2010).

230-G. C. Psarras, “Hopping conductivity in polymer matrix– metal particles composites”, **Composites Part A, Applied Science and Manufacturing**, **37**, 1545–1553 (2006).

231-Z. Dang, L. Wang, Y. Yin, Q. Zhang, & Q. Lei, “Giant dielectric permittivities in functionalized carbonnanotube/ electroactive - polymer nanocomposites”, **Advanced Materials, 19**, 852-857 (2007).

232-S. Devikala, P. Kamaraj & M. Arthanareeswari, “Conductivity and Dielectric Studies of PMMA Composites”, **Chem. Sci. Trans., 2(S1),** S129-S134 (2013).

233-B. Guo, A. Finne-Wistrand, & A. C. Albertsson, “Facile synthesis of degradable and electrically-conductive polysaccharide hydrogels” **Biomacromolecules, 12** , 2601-2609(2011).

234-M. A. Pujiana, L. Perez-Alvarez, L. C. C. Iturbe, & I. Katime, “Water-dispersible pH-responsive chitosan nanogels modified with biocompatible crosslinking-agents”, **Polymer, 53**, 3107-3116(2012).

235-A. K. Bajpai, S. K. Shukla, S. Bhanu, & S. Kankane, “Responsive polymers in controlled drug delivery”. **Prog. Polym. Sci., 33**, 1088–1118(2008).

236-Y. Li, K. G. Neoh, & E. T. Kang, “Controlled release of heparin from polypyrrole-poly(vinyl alcohol) assembly by electrical stimulation”, **J. Biomed. Mater. Res., 73A**, 171–181(2005).

237-M. Filippousi, T. Altantzis, G. Stefanou, M. Betsiou, D. N. Bikiaris, M. Angelakeris, E. Pavlidou, D. Zamboulis & G. Van Tendeloo, “Polyhedral iron oxide core–shell nanoparticles in a biodegradable polymeric matrix: preparation, characterization and application in magnetic particle hyperthermia and drug delivery”, **RSC Adv., 3**, 24367–24377(2013).